Nr 3 (51)/2011

ISSN 1507-2711

Cena: 25 zł (w tym 5% VAT)

EKSPLOATACJA I NIEZAWODNOŚĆ

MAINTENANCE AND RELIABILITY

Polskie Naukowo-Techniczne Towarzystwo Eksploatacyjne (Warszawa)

POLISH MAINTENANCE SOCIETY (WARSAW)

Co-financed by the Minister of Science and Higher Education

The Journal is indexed and abstracted in the Journal Citation Reports (JCR Science Edition), Scopus, Science Citation Index Expanded (SciSearch®) and Index Copernicus International.
The Quarterly appears on the list of journals credited with a high impact factor by the Polish Ministry of Science and Higher Education and is indexed in the Polish Technical Journal Contents database – BAZTECH and the database of the Digital Library Federation.

All the scientific articles have received two positive reviews from independent reviewers.

Editorial staff:	Dariusz Mazurkiewicz, PhD Eng (Editor-in-Chief, Secretary of the Scientific Board) Anna Rudawska, PhD Eng (Editorial secretary) Leszek Semotiuk, PhD Eng (Typesetting and text makeup) Krzysztof Olszewski, PhD Eng (Webmaster)
Publisher:	Polish Maintenance Society, Warsaw
Scientific patronage:	Polish Academy of Sciences Branch in Lublin
Address for correspondence:	"Eksploatacja i Niezawodność" - Editorial Office 20-618 Lublin, ul. Nadbystrzycka 36, Poland e-mail: office@ein.org.pl http://www.ein.org.pl
Circulation:	550 copies

Spis treści

LV W., WANG W.: **Modelling Preventive maintenance based on the delay time concept in the context of a case study;** Eksploatacja i Niezawodność - Maintenance and Reliability 2011; 3: 5-11.

Using the delay time concept and associated models, this paper presents a modelling study of optimising the preventive maintenance (PM) interval of a production plant within the context of a case study. To establish the relationship between the PM interval and expected downtime per unit time, we need the data of both failure times and the number of defects identified and removed at PM epochs. However, the available data to us was only the recorded times of failures. To overcome this problem, we obtained an estimated mean number of the defects identified at the PM epoch by the plant maintenance technicians. Based on these two types of data, we first establish a likelihood function of the observed times to failure and then a squared function of the difference between the number of defect identification estimated by the technician and the corresponding expected value from the model is mixed with the likelihood function to estimate the unknown model parameters. We test by simulation to show the validity of the above parameter estimation method. Once the parameters of the model are known, a PM model is proposed to optimize the expected downtime per unit time with respect to the PM interval. The modeling process is demonstrated by the case study presented.

LV W., WANG W.: **Modelowanie konserwacji zapobiegawczej w oparciu o pojęcie czasu zwłoki w kontekście studium przypadku;** Eksploatacja i Niezawodność - Maintenance and Reliability 2011; 3: 5-11.

Wykorzystując pojęcie czasu zwłoki oraz modele stowarzyszone, w artykule przedstawiono badania modelowe optymalizacji przerwy konserwacyjnej w zakładzie produkcyjnym w oparciu o studium przypadku. Aby ustalić związek pomiędzy przerwą konserwacyjną a oczekiwanym czasem przestoju na jednostkę czasu, potrzebne są dane dotyczące zarówno czasów uszkodzeń jak i liczby usterek wykrytych i usuniętych w okresach konserwacji zapobiegawczej. Niestety, w badanym przez nas przypadku jedynymi dostępnymi danymi były czasy uszkodzeń. Aby obejść ten problem, wykorzystaliśmy szacunkową średnią liczbę usterek wykrytych w okresie konserwacji zapobiegawczej przez obsługę techniczną zakładu. W oparciu o wspomniane dwa typy danych, ustaliliśmy, w pierwszej kolejności, funkcję wiarygodności dla obserwowanych czasów do uszkodzenia. Następnie, w celu określenia niewiadomych parametrów modelu, funkcję tę połączyliśmy z funkcją najmniejszych kwadratów dla różnicy pomiędzy liczbą wykrytych usterek oszacowaną przez pracownika obsługi technicznej a odpowiadającą jej oczekiwaną wartością wyprowadzoną z modelu. Wiarygodność powyższej metody oceny parametrów sprawdzono za pomocą symulacji. Znając wartości parametrów modelu, zaproponowano model konserwacji zapobiegawczej pozwalający na optymalizację oczekiwanego czasu przestoju na jednostkę czasu w odniesieniu do przerwy konserwacyjnej. Proces modelowania przedstawiono za pomocą studium przypadku..

HUK M., SZCZEPANIK M.:**Multiple classifier error probability for multi-class problems;** Eksploatacja i Niezawodność - Maintenance and Reliability 2011; 3: 12-16.

In this paper we consider majority voting of multiple classifiers systems in the case of two-valued decision support for many-class problem. Using an explicit representation of the classification error probability for ensemble binomial voting and two class problem, we obtain general equation for classification error probability for the case under consideration. Thus we are extending theoretical analysis of the given subject initially performed for the two class problem by Hassen and Salamon and still used by Kuncheva and other researchers. This allows us to observe important dependence of maximal posterior error probability of base classifier allowable for building multiple classifiers from the number of considered classes. This indicates the possibility of improving the performance of multiple classifiers for multiclass problems, which may have important implications for their future applications in many fields of science and industry, including the problems of machines diagnostic and systems reliability testing.

HUK M., SZCZEPANIK M.:**Prawdopodobieństwo błędu klasyfikatorów złożonych dla problemów wieloklasowych;** Eksploatacja i Niezawodność - Maintenance and Reliability 2011; 3: 12-16.

W niniejszym artykule rozważamy systemy złożonych klasyfikatorów z głosowaniem większościowym dla przypadku problemów wieloklasowych, wykorzystujące wielowartościowe klasyfikatory bazowe. Stosując bezpośrednią reprezentację prawdopodobieństwa błędnej klasyfikacji dla analogicznych systemów w problemach dwuklasowych, otrzymujemy ogólny wzór na prawdopodobieństwo błędu klasyfikacji w przypadku wieloklasowym. Tym samym rozszerzamy teoretyczne analizy tego zagadnienia pierwotnie przeprowadzone dla problemów dwuklasowych przez Hansena i Salomona i ciagle wykorzystywane przez Kuncheve i innych badaczy. Pozwala nam to zaobserwować istotną zależność maksymalnego dopuszczalnego poziomu prawdopodobieństwa błędów klasyfikatorów bazowych od liczby rozważanych przez nie klas. Wskazuje to na możliwość poprawy parametrów klasyfikatorów złożonych dla problemów wieloklasowych, co może mieć niebagatelne znaczenie dla dalszych ich zastosowań w licznych dziedzinach nauki i przemysłu, z uwzględnieniem zagadnień diagnostyki maszyn oraz badania niezawodności systemów.

GŁADYSIEWICZ L., KRÓL R., BUKOWSKI J.: **Tests of belt conveyor resistance to motion;** Eksploatacja i Niezawodność - Maintenance and Reliability 2011; 3: 17-25.

The modern of belt conveyor calculations are based upon the advanced computational methods, mostly multivariate simulations. Dimensioning of a conveyor drive depends on the identification of belt conveyor resistance to motion which can be identified with the biggest accuracy after adopting the exact methods of calculation the components of the main resistance force. The development of these methods requires verification of theoretical algorithms. Various tests of the belt conveyor resistance to motion, from the laboratory individual idler rotational resistance to motion, through the combined idler rotational and indentation resistances with the use of a special test rig up to the in-situ tests of an idler subjected to typical operational conditions have been presented. The obtained results have been used both for the verification of calculation methods and the comparison of idlers with alternative steel or polyurethane coating.

GŁADYSIEWICZ L., KRÓL R., BUKOWSKI J.: **Eksperymentalne badania oporów ruchu przenośnika taśmowego;** Eksploatacja i Niezawodność - Maintenance and Reliability 2011; 3: 17-25.

Podstawą projektowania przenośników taśmowych są zaawansowane metody obliczeniowe oraz wielowariantowe symulacje różnych stanów pracy. Kluczowym zadaniem projektowym jest wymiarowanie napędu głównego w oparciu wyznaczone opory ruchu przenośnika, Najlepsze oszacowanie oporów ruchu przynoszą metody oporów jednostkowych rozwijane różnych środkach badawczych. Doskonalenie metod obliczeniowych wymaga prowadzenia badań w celu weryfikacji opracowanych zależności. W artykule przedstawiono eksperymentalne metody badań wybranych składowych oporów ruchu przenośnika taśmowego, obejmujące pomiary na stanowisku do badań krążników, pomiary toczącego się wózka z dwoma krążnikami na bieżni wyłożonej taśmą przenośnikową oraz pomiary oporów ruchu pojedynczego zestawu krążnikowego na przenośniku kopalnianym. Uzyskane wyniki pomiarów posłużyły nie tylko do weryfikacji metod obliczeniowych, ale również do porównania krążników z płaszczem stalowym z krążnikami z płaszczem poliuretanowym.

LATA S., KUMAR A.: **Mehar's method for analyzing the fuzzy reliability of piston manufacturing system;** Eksploatacja i Niezawodność - Maintenance and Reliability 2011; 3: 26-39.

To the best of our knowledge till now there are only two analytical methods for finding the exact solution of fuzzy differential equations. In this paper, the shortcoming of one of these existing methods is pointed out. To overcome the shortcoming of the existing method, a new method, named as Mehar's method, is proposed for solving fuzzy differential equations. To show the advantage of Mehar's method over existing method the fuzzy Kolmogorov's differential equations, developed by using fuzzy Markov model of piston manufacturing system, are solved by using the existing and Mehar's method and it is shown that the results, obtained by using the existing method, may or may not be fuzzy number while the results, obtained by using Mehar's method, are always fuzzy number.

LATA S., KUMAR A.: **Metoda Mehar do analizy rozmytej niezawodności systemu produkcji tłoków;** Eksploatacja i Niezawodność - Maintenance and Reliability 2011; 3: 26-39.

Wedle naszej najlepszej wiedzy, do tej pory stworzono jedynie dwie metody analityczne precyzyjnego rozwiązywania rozmytych równań różniczkowych. W artykule wskazano wady jednej z istniejących metod oraz zaproponowano nową metodę rozwiązywania równań różniczkowych, nazwaną metodą Mehar, w której wady te zostały wyeliminowane. Aby wykazać przewagę metody Mehar nad istniejącą metodą, rozwiązano za pomocą obu tych metod rozmyte równania różniczkowe Kołmogorowa wyprowadzone przy użyciu rozmytego markowowskiego modelu systemu produkcji tłoków. Wykazano, że wyniki otrzymane z wykorzystaniem istniejącej metody, mogą ale nie muszą być liczbami rozmytymi, natomiast wyniki otrzymane przy pomocy metody Mehar zawsze stanowią liczbę rozmytą.

KOSZAŁKA G.: **Predicting the durability of the piston-rings-cylinder assembly of a diesel engine using a piston ring pack model;** Eksploatacja i Niezawodność - Maintenance and Reliability 2011; 3: 40-44.

The article presents a new method for predicting the durability of an internal combustion engine, which uses results of wear measurements of components of the piston-rings-cylinder system and computer simulations of the piston ring pack. In contrast to traditional methods, the method proposed here does not require previous knowledge of wear limits, which, though crucial for precise prediction, are difficult to determine reliably in modern structures. In the method presented here, wear limits are determined on the basis of an analytical model of the piston ring pack. The article shows an example of the application of the proposed method for predicting the durability of a motor-vehicle compression-ignition engine.

MUCHA J.: **The analysis of rectangular clinching joint in the shearing test;** Eksploatacja i Niezawodność - Maintenance and Reliability 2011; 3: 45-50.

This paper presents the results of experimental researches on effect of clinching joint's load direction change on its characteristics and the maximum shearing force value. The single-folded clinching joints made of aluminum sheet AW1050A have been the subject of researches. Properly prepared specimens of rectangle clinching joints with material notch have been shear tested on the tensile testing machine UTS 100. The extreme joint destruction have been analyzed for the layout angle $\beta = 0°, 90°$. The separation mechanism has been described for all angle values $\beta = 0^o, 30^o, 45^o, 90^o$. The total separation work by joint shearing has also been mentioned.

SKOTNICKA-ZASADZIEŃ B., BIAŁY W.: **An analysis of possibilities to use a Pareto chart for evaluating mining machines' failure frequency;** Eksploatacja i Niezawodność - Maintenance and Reliability 2011; 3: 51-55.

The article presents a general classification of quality management tools applied in different industry branches. From among these tools the authors have chosen a pareto chart to present an analysis of mining machines participating in the mining process. The analysis covers mining machines such as: a roadheader, chain conveyor, belt conveyer, crusher and a support.

PANG Y., HUANG H-Z., HE L., WANG Z., XIAO N-C.: **Convex sublattice based reliability theory;** Eksploatacja i Niezawodność - Maintenance and Reliability 2011; 3: 56-61.

Classical probability theory has been widely used in reliability analysis; however, it is hard to handle when the system is lack of adequate and sufficient data. Nowadays, alternative approaches such as possibility theory and fuzzy set theory have also been proposed to analyze vagueness and epistemic uncertainty regarding reliability aspects of complex and large systems. The model presented in this paper is based upon possibility theory and multistate assumption. Convex sublattice is addressed on congruence relation regarding the complete lattice of structure functions. The relations between the equivalence classes on the congruence relation and the set of all structure functions are established. Furthermore, important reliability bounds can be derived under the notion of convex sublattice. Finally, a numerical example is given to illustrate the results.

GRONOSTAJSKI Z., HAWRYLUK M., KASZUBA M., SADOWSKI P., WALCZAK S., JABŁOŃSKI D.: **Measuring & control systems in industrial die forging processes;** Eksploatacja i Niezawodność - Maintenance and Reliability 2011; 3: 62-69.

The paper presents portable measuring & control systems, designed and built by the authors, and their application to the analysis of two industrial processes: the precision hot forging of CV universal joint casings in closed dies in the crank press (GKN Driveline Oleśnica) and the forging of concrete slab carrying handles in a TR device in the eccentric press (INOP Poznań). The systems enable the measurement, archiving and analysis of forging force-time/displacement traces correlated with tool temperature, as well as the measurement of production speed and the quantity of produced forgings. Recently an acoustic emission (AE) signal registration capacity has been incorporated into the system to investigate the changes occurring during the forging process, especially progressive tool wear. The information obtained in this way is to be used to improve the operating conditions of the forging presses and to optimize the whole forging

KOSZAŁKA G.: **Prognozowanie trwałości układu tłok-pierścienie-cylinder silnika o zapłonie samoczynnym z wykorzystaniem modelu uszczelnienia TPC;** Eksploatacja i Niezawodność - Maintenance and Reliability 2011; 3: 40-44.

W artykule przedstawiono nową metodę prognozowania trwałości tłokowego silnika spalinowego, wykorzystującą wyniki pomiarów zużycia elementów układu tłok-pierścienie-cylinder oraz komputerową symulację uszczelnienia TPC silnika. W przeciwieństwie do tradycyjnych metod, proponowana metoda nie wymaga wyprzedzającej znajomości zużycia granicznego, kluczowego dla dokładności prognozy, a którego wiarygodne określenie dla nowych konstrukcji jest trudne. W prezentowanej metodzie zużycie graniczne wyznaczane jest na podstawie analitycznego modelu uszczelnienia TPC. W artykule przedstawiono przykład wykorzystania metody do prognozowania trwałości samochodowego silnika o zapłonie samoczynnym.

MUCHA J.: **Analiza zniszczenia prostokątnego złącza przetłoczeniowego w próbie ścinania;** Eksploatacja i Niezawodność - Maintenance and Reliability 2011; 3: 45-50.

W pracy zawarto wyniki badań eksperymentalnych dotyczących wpływu zmiany kierunku obciążenia przetłoczeniowego złącza na przebieg charakterystyki i maksymalną wartość siły ścinania. Przedmiotem badań były jednozakładkowe połączenia przetłoczeniowe blach z aluminium AW1050A. Odpowiednio wykonane próbki prostokątnych połączeń przetłoczeniowych z nacięciem materiału poddano testom ścinania na maszynie wytrzymałościowej UTS 100. Przeanalizowano skrajne przypadki zniszczenia złącza dla kąta ułożenia $\beta = 0^o, 90^o$. Opisano mechanizm rozdzielenia połączenia dla wszystkich wartości kąta $\beta = 0^o, 30^o, 45^o, 90^o$. Zwrócono również uwagę na wielkość całkowitej pracy rozdzielenia przez ścinanie złącza.

SKOTNICKA-ZASADZIEŃ B., BIAŁY W.: **Analiza możliwości wykorzystania narzędzia Pareto-Lorenza do oceny awaryjności urządzeń górniczych;** Eksploatacja i Niezawodność - Maintenance and Reliability 2011; 3: 51-55.

W artykule przedstawiono ogólną klasyfikację narzędzi zarządzania jakością stosowanych w różnych gałęziach przemysłu. Spośród tych narzędzi został wybrany diagram Pareto-Lorenza, za pomocą którego przestawiono analizę awaryjności urządzeń górniczych biorących udział w procesie wydobywczym kopalni. Analizie poddano kombajn, przenośnik zgrzebłowy, przenośnik taśmowy, kruszarkę oraz obudowę.

PANG Y., HUANG H-Z., HE L., WANG Z., XIAO N-C.: **Teoria niezawodności oparta na pojęciu podkraty wypukłej;** Eksploatacja i Niezawodność - Maintenance and Reliability 2011; 3: 56-61.

Klasyczna teoria prawdopodobieństwa ma szerokie zastosowanie w analizie niezawodności, jednak trudno jest się nią posługiwać, kiedy brak jest wystarczających i odpowiednich danych na temat systemu. Obecnie, proponuje się alternatywne podejścia, takie jak teoria możliwości czy teoria zbiorów rozmytych, za pomocą których można analizować niepewność epistemiczną oraz nieostrość w odniesieniu do aspektów niezawodności złożonych i dużych systemów. Model przedstawiony w niniejszym artykule oparto na teorii możliwości oraz na założeniu wielostanowości. Podkratę wklęsłą opisano na relacji kongruencji, odnoszącej się do całej kraty funkcji struktury. Ustalono relacje pomiędzy klasami równoważności na relacji kongruencji a zbiorem wszystkich funkcji struktury. Ponadto posługując się pojęciem podkraty wypukłej można wyprowadzać istotne kresy niezawodności. Wyniki zilustrowano przykładem numerycznym..

GRONOSTAJSKI Z., HAWRYLUK M., KASZUBA M., SADOWSKI P., WALCZAK S., JABŁOŃSKI D.: **Systemy kontrolno-pomiarowe w przemysłowych procesach kucia matrycowego;** Eksploatacja i Niezawodność - Maintenance and Reliability 2011; 3: 62-69.

W pracy przedstawiono zastosowania autorskich, przenośnych systemów pomiarowo-kontrolnych do analizy dwóch przemysłowych procesów: kucia na ciepło obudowy przegubów homokinetycznych na prasie korbowej w matrycach zamkniętych (GKN Driveline Oleśnica) oraz kucia zaczepów do przenoszenia płyt betonowych na prasie mimośrodowej w przyrządzie TR (INOP Poznań). Zbudowane przez autorów systemy pozwalają na pomiar, archiwizację i analizę przebiegów sił kucia w funkcji czasu/przemieszczenia skorelowane z pomiarem temperatury narzędzi, pomiary prędkości procesu oraz ilości wykutych odkuwek. Ostatnio wzbogacono je o rejestrację sygnału akustycznego AE w celu określenia zachodzących zamian podczas procesu a szczególnie postępującego zużycia narzędzi. Uzyskane informacje mają posłużyć również do poprawy warunków eksploatacji pras oraz do optymalizacji całego procesu kucia wyprocess by means of CAD/CAM/CAE software based on FEM. The measuring & control systems consist of an industrial computer (comprising a real-time controller, a multi-speed measurement card, RAM memory, large capacity hard disks and a set of amplifiers and transducers) and sensors (force, displacement, pyrometers, thermocouples, linear and angular encoders, accelerometers and AE). Two applications (based on LabView) have been developed for each of the systems. One of the applications is installed on the industrial computer and is used to control the system as well as to record and process the voltage signals received from the individual sensors. The other application enables the analysis of the processed signals.

korzystując narzędzia CAD/CAM/CAE oparte o MES. Prezentowane systemy zbudowane są z komputera przemysłowego (kontrolera czasu rzeczywistego, wielokanałowej szybkiej karty pomiarowej, kości pamięci operacyjnej, dysków twardych o dużej pojemności, zestawu wzmacniaczy i przetworników) oraz odpowiednich czujników pomiarowych (siły, przemieszczenia, pirometrów, termopar, enkoderów liniowych i kątowych, akcelerometrów, czujników AE). Do każdego z systemów opracowano po 2 aplikacje (na bazie programu LabView). Pierwsza aplikacja jest zainstalowana w komputerze przemysłowym i służy do sterowania systemem oraz zapisem i przetwarzaniem sygnałów napięciowych uzyskiwanych z poszczególnych czujników. Druga przeznaczona jest do analizy zarejestrowanych sygnałów.

MAZUR Z., HERNANDEZ-ROSSETTE A.: **Service problems of an axial compressors of a land based, high power, reaction gas turbines;** Eksploatacja i Niezawodność - Maintenance and Reliability 2011; 3: 70-76.

A compressor blade failure was experienced at the 69 MW gas turbine of a combined cycle (C.C.) unit after four years operation since the last overhaul. Three unit failure events occurred at small periods, which caused forced outage. Visual examination carried out after the failure events indicated that the compressor vanes (diaphragms) had cracks in their airfoils initiating at blade tenons welded to the diaphragm outer shroud at some stages. Also, many stationary vanes and moving blades showed foreign object damage (FOD), rubbing and bending. A compressor failure evaluation was completed including cracked vane metallographic analysis, unit operation parameter analysis, history-of-events analysis, and crack initiation and propagation analysis. This paper provides an overview of the compressor failure investigation, which led to identification of the vane high cycle fatigue (HCF) failure mechanism generated by rotating stall during unit start-ups, highly accelerated by corrosion generated by the fogging system and influenced by high stationary vane and moving blade brittleness as the primary contribution to the observed failure. They are provided recommendations to avoid similar failure of the compressor blades in the future.

MAZUR Z., HERNANDEZ-ROSSETTE A.: **Problemy eksploatacyjne osiowych sprężarek reakcyjnych stacjonarnych silników turbinowych dużych mocy;** Eksploatacja i Niezawodność - Maintenance and Reliability 2011; 3: 70-76.

W sprężarce turbiny gazowej o mocy 69 MW, pracującej w cyklu kombinowanym wystąpiły uszkodzenia łopatek po czterech latach eksploatacji od ostatniego remontu głównego. Zarejestrowano trzy przypadki uszkodzeń w krótkim odstępie czasu, które spowodowały potrzebę zatrzymania i remontu turbiny. Badania wzrokowe przeprowadzone po każdym stwierdzeniu uszkodzeń, ujawniły pęknięcia w łopatkach niektórych stopni palisad kierowniczych zlokalizowane w piórach łopatek. Pęknięcia zaczynały sie w stopach łopatek spawanych do bandaża zewnętrznego palisad kierowniczych. Znaczna liczba łopatek kierowniczych i wirnikowych miała również uszkodzenia spowodowane przez obce ciała, przytarcia i były pogięte. Przeprowadzono badania i analizę uszkodzeń sprężarki włączając w to badania metalograficzne pękniętych łopatek, analizę parametrów operacyjnych turbiny, analizę historii zarejestrowanych przypadków uszkodzeń i analizę inicjacji i propagacji pęknięć. W niniejszym artykule opisuje sie badania uszkodzeń palisad łopatkowych sprężarki, które doprowadziły do konkluzji końcowej, ze pęknięcia łopatek palisad kierowniczych były rezultatem zmęczenia wysokocyklicznego materiału łopatek, spowodowanego przez oderwania wirow w czasie uruchomienia turbiny, przyspieszone przez korozje wywołaną chłodzeniem mieszankowym. Uszkodzenia ułatwiła znaczna kruchość materiału łopatek sprężarki. Zostały sformułowane zalecenia aby uniknąć podobnych uszkodzeń łopatek sprężarki w przyszłości.

HUANG N., HOU D., CHEN Y., XING L., KANG R.: **A Network Reliability Evaluation Method based on Applications and Topological Structure;** Eksploatacja i Niezawodność - Maintenance and Reliability 2011; 3: 77-83.

Applications play an important role in the reliability evaluation of communication networks. In other words, the reliability of a network can be totally different when different applications are considered for the same network. However existing reliability evaluation methods, which are mostly based on the graph theory, give no or little consideration to applications. This paper proposes a concept of network application reliability and a Markov-based method for analyzing the proposed network application reliability measure. Furthermore, based on the reliability of each individual application, a method is proposed to evaluate the overall network reliability that incorporates effects of different applications running on the network. Both a case study and experiments are performed to illustrate the proposed concept and methods.

HUANG N., HOU D., CHEN Y., XING L., KANG R.: **Metoda oceny niezawodności sieci oparta na aplikacjach i strukturze topologicznej;** Eksploatacja i Niezawodność - Maintenance and Reliability 2011; 3: 77-83.

Aplikacje odgrywają ważną rolę w ocenie niezawodności sieci komunikacyjnych. Innymi słowy, niezawodność sieci może być całkowicie różna dla różnych aplikacji tej samej sieci. Niestety, istniejące metody oceny niezawodności, w większości oparte na teorii grafów, poświęcają niewiele lub nie poświęcają wcale uwagi aplikacjom. W niniejszym artykule przedstawiono koncepcję niezawodności aplikacji sieciowych oraz opartą na modelu Markowa metodę analizy proponowanej miary niezawodności aplikacji sieciowych. Ponadto, na podstawie niezawodności poszczególnych aplikacji, zaproponowano metodę oceny ogólnej niezawodności sieci, która łączy efekty różnych aplikacji działających w danej sieci. Zaproponowaną koncepcję i metody omówiono na podstawie studium przypadku oraz badań eksperymentalnych..

JURECKI R., STAŃCZYK T.L.: **The test methods and the reaction time of drivers;** Eksploatacja i Niezawodność - Maintenance and Reliability 2011; 3: 84-91.

The paper presents issues related to determination of the driver's reaction time. A brief review of methods for determining the reaction time of drivers has been conducted. The results of own researches on the reaction time of drivers in pre-accident situations have been presented. The scenario of an accident situation according to which they were conducted has been presented. The presentation includes results of measurements of the reaction time set in the three test environments: on a test track, in a driving simulator and on the psychological aptitude test stand. A comparison of the obtained reaction time values has been conducted and the correlation between them has been determined.

JURECKI R., STAŃCZYK T.L.: **Metody badań a czas reakcji kierowców;** Eksploatacja i Niezawodność - Maintenance and Reliability 2011; 3: 84-91.

W artykule przedstawiono zagadnienia związane z wyznaczaniem czasu reakcji kierowcy. Przeprowadzono krótki przegląd metod wyznaczania czasu reakcji kierowców. Zaprezentowano wyniki własnych badań dotyczących czasu reakcji kierowców w sytuacjach przedwypadkowych. Omówiono scenariusz sytuacji wypadkowej, według którego zostały one przeprowadzone. Przedstawiono wyniki pomiarów czasu reakcji wyznaczone w trzech środowiskach badawczych: na torze badawczym, w symulatorze jazdy samochodem oraz na stanowisku do badań psychotechnicznych. Dokonano porównania otrzymanych wartości czasu reakcji i wyznaczono korelacje pomiędzy nimi.

Wenyuan LV
Wenbin WANG

MODELLING PREVENTIVE MAINTENANCE BASED ON THE DELAY TIME CONCEPT IN THE CONTEXT OF A CASE STUDY

MODELOWANIE KONSERWACJI ZAPOBIEGAWCZEJ W OPARCIU O POJĘCIE CZASU ZWŁOKI W KONTEKŚCIE STUDIUM PRZYPADKU

Using the delay time concept and associated models, this paper presents a modelling study of optimising the preventive maintenance (PM) interval of a production plant within the context of a case study. To establish the relationship between the PM interval and expected downtime per unit time, we need the data of both failure times and the number of defects identified and removed at PM epochs. However, the available data to us was only the recorded times of failures. To overcome this problem, we obtained an estimated mean number of the defects identified at the PM epoch by the plant maintenance technicians. Based on these two types of data, we first establish a likelihood function of the observed times to failure and then a squared function of the difference between the number of defect identification estimated by the technician and the corresponding expected value from the model is mixed with the likelihood function to estimate the unknown model parameters. We test by simulation to show the validity of the above parameter estimation method. Once the parameters of the model are known, a PM model is proposed to optimize the expected downtime per unit time with respect to the PM interval. The modeling process is demonstrated by the case study presented.

Keywords: *delay time, Preventive Maintenance (PM), parameter estimation, modelling.*

Wykorzystując pojęcie czasu zwłoki oraz modele stowarzyszone, w artykule przedstawiono badania modelowe optymalizacji przerwy konserwacyjnej w zakładzie produkcyjnym w oparciu o studium przypadku. Aby ustalić związek pomiędzy przerwą konserwacyjną a oczekiwanym czasem przestoju na jednostkę czasu, potrzebne są dane dotyczące zarówno czasów uszkodzeń jak i liczby usterek wykrytych i usuniętych w okresach konserwacji zapobiegawczej. Niestety, w badanym przez nas przypadku jedynymi dostępnymi danymi były czasy uszkodzeń. Aby obejść ten problem, wykorzystaliśmy szacunkową średnią liczbę usterek wykrytych w okresie konserwacji zapobiegawczej przez obsługę techniczną zakładu. W oparciu o wspomniane dwa typy danych, ustaliliśmy, w pierwszej kolejności, funkcję wiarygodności dla obserwowanych czasów do uszkodzenia. Następnie, w celu określenia niewiadomych parametrów modelu, funkcję tę połączyliśmy z funkcją najmniejszych kwadratów dla różnicy pomiędzy liczbą wykrytych usterek oszacowaną przez pracownika obsługi technicznej a odpowiadającą jej oczekiwaną wartością wyprowadzoną z modelu. Wiarygodność powyższej metody oceny parametrów sprawdzono za pomocą symulacji. Znając wartości parametrów modelu, zaproponowano model konserwacji zapobiegawczej pozwalający na optymalizację oczekiwanego czasu przestoju na jednostkę czasu w odniesieniu do przerwy konserwacyjnej. Proces modelowania przedstawiono za pomocą studium przypadku.

Słowa kluczowe: *czas zwłoki, konserwacja zapobiegawcza, ocena parametrów, modelowanie.*

1. Introduction

The delay time concept proposed by Christer has been extensively applied to maintenance problems of plant inspection practice[9, 13, 16]. The period from the first point at which a defect can be identified at a PM inspection to the time when a repair is essential is called the delay time, denoted by h. The objective of most delay time based studies is to either minimize a cost function or a down time function subject to a preventive inspection interval [16].

A major task in modelling the above inspection practice based upon the delay time concept is the estimation of parameters which describe (1) $\lambda(u)$, the rate of occurrence of defects at time u, (2) $F(h)$, the cumulative probability function of delay time h. (3) the probability of perfect defects identification at PM. In general, there are two established methods to estimate model parameters, namely the subjective method [2, 11, 12, 17] and the objective method, see Akbarov [11], Aven [3], Christer and Wang [6, 8], Jones *et at* [10], Wang [15]. The former is based on the subjective data obtained from maintenance engineers' experience. The latter is based on the observed data of recorded failure times and the number of defects identified at each PM epoch.

If the maintenance records of failures and the number of defects identified at PM are available and sufficient in quantity and quality, the delay time model parameters can be estimated by the objective method, generally the classical statistical method of maximum likelihood. If however, such a data set does not exist, or is insufficient in quantity and quality for the purposed of estimation, the alternative is to use expert judgment for obtaining those parameters [6].

In many cases, there are some objective data available, but those data are insufficient to estimate by merely the objective data, so more recent development in delay time modelling has established that these parameters can also be estimated using limited PM data and selective repair at PM [5, 7]. Wang and Jia [14] presented an empirical Bayesian based approach to estimate the delay time model parameters using both subjective and objective data. This approach starts with subjective data first, and then updates the estimates when objective data become available.

In this paper, because of the operating practice of PM and data constraints of the case we studied, we present an estimation procedure which is different from previous delay time models of complex plant. Here historic data exist for failure time points and PM times, but the interval of PMs is not equal, and no records exist for the number of the defects identified and removed at PM. However, we obtained latter a subjective estimate of the mean number of the defects identified and removed at PM from the factory technicians who maintained the plant. In this case a mixture of both objective data of failures and subjective PM data will be utilized in order to estimate model parameters. A mixed likelihood function with a least squared function (take the negative) is proposed and maximized to obtain the estimated values of the model parameters. Simulated data based upon imperfect inspections are generated to test whether the above mixed likelihood method can recover the underlying model parameters within a required accuracy. Finally an inspection model as a function of the PM interval is proposed and an optimal PM interval is obtained for the plant concerned. The modelling objective is to minimize the total downtime per unit time in terms of the PM interval.

The paper is organized as follows. Section 1 presents a basic introduction to the problem and a brief literature review. Section 2 outlines the modeling assumptions and notation, the modeling developments, and the test of this developed model using simulation. Section 3 proposes a downtime model. Section 4 presents a numerical example and section 5 concludes the paper.

2. The statistical model for model parameter estimation

2.1. Assumptions

Based upon the observation of the plant maintenance practice and referring to the published delay time papers [9, 13, 16], the following modeling assumptions are proposed to characterize the operation of the plant over the period of data collection.

1) Defects arise according to a Homogeneous Poisson Process (HPP).
2) Defects are assumed to arise independently of each other.
3) The delay time h of a random defect is independent of its time origin and has a $pdf,\ f(\bullet)$, and a $cdf,\ F(\bullet)$, common to all defects.
4) Inspections carried out at a PM are assumed to be imperfect in the sense that a defect present will be identified with a known probability.
5) All identified defects are rectified by repairs or replacements during the PM period.
6) Failures are identified immediately, and repairs or replacements are made as soon as possible.

2.2. Notation and likelihood formulation

We shall adopt the following notation:

λ	The rate of occurrence of defects.
$v(t)$	The rate of occurrence of failures at time t.
r	The probability of detecting a defect at PM, if it is present.
h	delay time of a random defect with pdf $f(*)$ and cdf $F(*)$.
T_i	The time of the ith PM from new.
$t_{(i-1)j}$	The time of the jth failure occurring in (T_{i-1}, T_i), $j=1,2,\ldots,k_{i-1}$, and $t_{(i-1)k_{i-1}}$ is the time of the last failure in (T_{i-1}, T_i).
Δt	A small time interval sufficiently small that only one failure event at most can arise within it.
n_i	The number of the defects identified at the ith PM.
$EN_f(T_{i-1},T_i)$	The expected number of the failures over the inspection interval (T_{i-1},T_i).
$EN_p(T_i)$	The expected number of the defects identified and rectified at T_i.

Consider all observations in (T_{i-1},T_i), namely the number of the defects identified at T_i, and the failure times in (T_{i-1},T_i), $i=1,2, \ldots ,n$, and $T_0=0$, see Fig. 1. The likelihood function is the product of the probabilities of these observations arising. At T_i, we need to formulate the probability of the number of the defects identified and rectified. Also, for each failure time in (T_{i-1},T_i), we need to formulate the probability of a failure arising at times $t_{(i-1)j}$ $j=1,2,\ldots,k_{i-1}$, and of having no other failures between recorded consecutive failure times. Therefore, the likelihood function L is given by:

$$L = \prod_{i=1}^{n} \left\{ p(n_i \text{defects identified at } T_i) \prod_{j=1}^{k_{i-1}} \Big[p(\text{a failure at time } t_{(i-1)j}) \cdot \right.$$
$$\left. \cdot\, p(\text{no further failure between } t_{(i-1)(j-1)} \text{and } t_{(i-1)j}) \Big] \right\} \qquad (1)$$

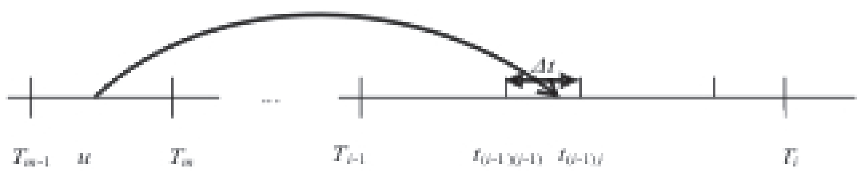

Fig. 1. The failure process in (T_{i-1}, T_i) due to a defect arising at u in (T_{m-1}, T_m)

The log likelihood function is given by:

$$\ell = \sum_{i=1}^{n} \Big\{ \log p(n_i \text{ defects identified at } T_i) + $$
$$+ \sum_{j=1}^{k_{i-1}} \Big[\log p(\text{a failure at time } t_{(i-1)j}) + $$
$$+ \log p(\text{no further failure between } t_{(i-1)(j-1)} \text{and } t_{(i-1)j}) \Big] \Big\} \quad (2)$$

In equation (2), the term P (no further failure between $t_{(i-1)j}$ and $t_{(i-1)(j+1)}$) is necessary because of the use of an HPP for the defect arrival so that the interval between failures has to be modeled. Equation (2) assumes that the necessary objective data are available from both PMs and failures.

To compute the above likelihood function, firstly, we consider the probability of a failure in $(t, t+\Delta t)$, namely $P(t, t+\Delta t|u)$, see Fig. 2, where, $T_{n-1} < t \le T_n$, $T_{i-1} < u \le T_i$.

$$p(t, t+\Delta t \mid u) = \begin{cases} (1-r)^{n-i}(F(t+\Delta t-u) - F(t-u)) & T_{i-1} < u < T_i, i=1,...,n-1 \\ F(t+\Delta t-u) - F(t-u) & T_{n-1} < u < t \\ F(t+\Delta t-u) & t < u < t+\Delta t \\ 0 & u > t+\Delta t \end{cases} \quad (3)$$

So the rate of occurrence of failures, $v(t)$, is derived below:

$$v(t) = \int_0^t \lambda \lim_{\Delta t \to 0} \frac{P(t, t+\Delta t)}{\Delta t} du$$
$$= \lambda \left\{ \sum_{i=1}^{n-1} (1-r)^{n-i} \int_{T_{i-1}}^{T_i} f(t-u)du + \int_{T_{n-1}}^{t} f(t-u)du \right\} \quad (4)$$
$$= \lambda \left\{ \sum_{i=1}^{n-1} (1-r)^{n-i} \big[\big(F(t-T_{i-1}) - F(t-T_i) \big) \big] + F(t-T_{n-1}) \right\}$$

where, $T_{n-1} < t \le T_n$. For The derivation of Equation (4), see Christer and Wang [6]. So the expected number of failures over the inspection interval (T_{n-1}, T_n) is as follows:

$$EN_f(T_{n-1}, T_n) = \int_{T_{n-1}}^{T_n} v(t)dt = \lambda \int_{T_{n-1}}^{T_n} \sum_{i=1}^{n-1} (1-r)^{n-i}$$
$$\big[\big(F(t-T_{i-1}) - F(t-T_i) \big) \big] dt + \lambda \int_{T_{n-1}}^{T_n} F(t-T_{n-1})dt \quad (5)$$

Using equation (4), we obtain the probability of a failure arising in time interval $(t_{(i-1)j}, t_{(i-1)j}+\Delta t)$, for sufficiently small Δt,

$$P(\text{a failure in } (t_{(i-1)j}, t_{(i-1)j}+\Delta t)) = v(t_{(i-1)j})\, \Delta t \quad (6)$$

Since the failure process is NHPP, it is straightforward that:

$$p(\text{no failure in } (t_{(i-1)(j-1)}, t_{(i-1)j})) = e^{-\int_{t_{(i-1)(j-1)}}^{t_{(i-1)j}} v(t)dt} \quad (7)$$

If failure durations are negligible, the logged probability of no further failure between recorded failures within (T_{i-1}, T_i) is simply given by

$$\sum \log p(\text{no further failure in } (t_{(i-1)(j-1)}, t_{(i-1)j})) =$$
$$= \sum_{j=1}^{k_{i-1}} \Big(-\int_{t_{(i-1)(j-1)}}^{t_{(i-1)j}} v(t)dt \Big) - \int_{t_{(i-1)k(i-1)}}^{T_i} v(t)dt = \int_{T_{i-1}}^{T_i} v(t)dt \quad (8)$$

From equation (3), we obtain the expected number of the defects found at T_n, namely $EN_p(T_n)$, given by Christer *et al.* [6].

$$EN_p(T_n) = \lambda \sum_{i=1}^{n-1} (1-r)^{n-i} r \int_{T_{i-1}}^{T_i} [1 - F(T_n - u)]\, du + \lambda r \int_{T_{n-1}}^{T_n} [1 - F(T_n - u)]\, du \quad (9)$$

Because the number of defects identified at PMs follows a Poisson distribution with the mean defined by equation (9), [6], the probability of n_n defects identified at T_n is

$$p(n_n \text{defects identified at } T_n) = \frac{(EN_{\mathrm{p}}(T_n))^{n_n} e^{-EN_p(T_n)}}{n_n!} \quad (10)$$

Dividing equation (6) by Δt and taking the log of equation (10). The log likelihood function for the problem described becomes:

$$\log L = \sum_{i=1}^{n} \left\{ (n_i \log EN_p(T_i) - EN_p(T_i) - \log n_i!) + \sum_{j=1}^{k_{i-1}} \log v(t_{(i-1)j}) - \int_{T_{i-1}}^{T_i} v(t)dt \right\} \quad (11)$$

In this case, PM inspection data are not available, so the first part of the right hand side of equation (11) cannot be computed, but the estimated mean number of the defects identified and rectified at PMs are provided by the maintenance technicians. So we used the likelihood of the failure events (the second part of the right hand side of equation (11)) and a least square function and the function, Z, to be maximized is given by:

$$Z = \sum_{i=1}^{n} \left\{ \left[\sum_{j=1}^{k_{i-1}} \log v(t_{(i-1)j}) - \int_{T_{i-1}}^{T_i} v(t)dt \right] - \big[EN_p(T_i) - ES_p(T) \big]^2 \right\} \quad (12)$$

where $ES_p(T)$ denotes the subjective estimate of the mean number of the defects identified and rectified given T where T is the average PM interval length. This equation has not been used before in delay time based models. Maximizing equation (12), we may obtain the estimated parameters of the model, namely λ ,r and those in $f(h)$ from actual failure records and subjective PM data.

2.3. The assessment of the model

2.3.1. The simulation test

We have run a simulation experiment to test the validity and feasibility of equation (12). The failure processes with imperfect inspection of r=0.2, 0.5 and 0.8 are simulated respectively.

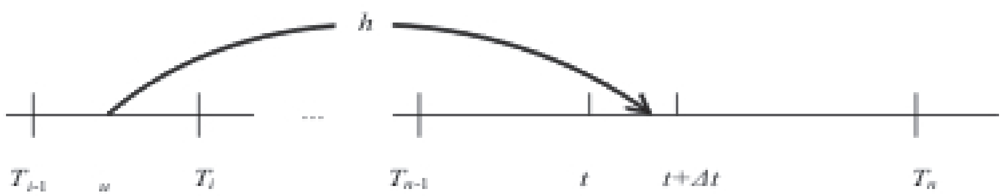

Fig. 2 The failure process of a defect arising in (T_{i-1}, T_i)

We then averaged the observed number of the defects identified at PM to be used as an assumed estimate from the technicians. Table 1 shows that fitted parameter values, in which the rate of occurrence of faults is λ=1.1528 and the scale parameter of the exponential delay time α=0.0288, and the inspection interval is 7 days. The full data likelihood is also run to compare with that from equation (11). From table 1 it can be seen that the estimates from using equation (12) are not far from the true parameter values and validate our approach. Though they are not as good as the estimate using the full data, but the method is a good approximate way for model parameter estimates.

2.3.2. Choice of possible candidates for model

Before fitting a model to the data, the functional form of the delay time distribution must be specified. The best choice of the distribution from a family of distributions for h is chosen, using the criterion of minimum Akaike information criterion (AIC) [4]. Possible candidates for $F(.)$ are 1) Exponential distribution $F(x)=1-e^{-ax}$; 2) Mix delta-exponential distribution $F(x)=1-(1-p)e^{-ax}$; and 3) Weibull distribution $F(x)=1-e^{-(\alpha x)^{\beta}}$. Exponential distribution is usually selected first. If there is any defect with zero delay time, model (2) is preferred, where p is the proportion of defects with zero delay time and a is the scale parameter of the exponential distribution. This mixed distribution can be used for Weibull as well.

3. Downtime model

The relationship between the PM frequency and the total downtime is established as shown below, [16]:

$$ED(T)=\frac{d_f . EN_f(T)+d_p}{T} \tag{13}$$

where: $ED(T)$ - the total expected downtime per unit time over an infinite horizon with PM interval T, d_f - the average downtime per failure, $EN_f(T)$ - the expected number of failures over PM interval T, d_p - the average downtime per PM, where since we assume that the plant is already operated very long to be in a steady state so, $EN_f(T_{n-1},T_n) = EN_f(T)$ for sufficient large n.

4. Case study

This case study involves an important machine in Harbin Turbine Co Ltd. The machine is called the NC Gantry-type Milling Machine which is an advanced numerical controlled machine which is key plant item within the company with over 80% of products being processed on it at some stages of their production. This machine is operated 22 hours a day (three shifts), 7 days a week, excluding public holidays. At the time of the study, in order to reduce the downtime, preventive maintenance was performed 4 times per year, namely on Spring Festival, 1st May, 1st October and New Year. The company's objective is to reduce the downtime caused both by failures and PM activities, and thereby increase the availability of the plant. The key issue of concern is: How long the PM interval should be the best for the machine?

4.1. Data collection and Analysis of failure data

Through collecting records for this milling machine over a period of two years, we obtain some valuable information including the time of failures, causes of failures, or the failure mode, the length of the downtime for each failure and repair actions to the failures.

Based on the failure data, the following analysis is carried out, 1) Frequency analysis of failure modes; 2) Analysis of the causes of failures.

The number of failures occurred in different subsystem of NC Gantry-type Milling Machine is shown in table 2. From table 2, the number of failures occurred over past two years total to 77.

The frequency of failure modes for different main components with each subsystem of the machine is shown in Figures 3, 4 and 5 respectively.

The main failure modes are shown in table 3. It can be seen that the downtime due to the main shaft electric motor in the electric system, totaling 817 hours, accounts for 27 percent total downtime. Next is the brake controller of girder, its downtime reaches 611 hours and accounts for 20 percent total downtime. Others failure modes influencing the availability include the cooler system and attachments for the cutting tool.

Table 1 Estimation result for an exponential delay-time distribution via various r values

r	PM cycle	Sample data	Use failure data and actual PM data			Use failure data and mean PM data		
			$\hat{\lambda}$	$\hat{a}$	$\hat{r}$	$\hat{\lambda}$	$\hat{a}$	$\hat{r}$
r=0.2	10	58	1.1530	0.0245	0.1340	0.9780	0.0555	0.3000
	50	372	1.1040	0.0330	0.2040	1.0480	0.0560	0.3000
	100	792	1.1600	0.0270	0.1920	1.2090	0.0410	0.3000
r=0.5	10	69	1.1110	0.0235	0.4020	1.0830	0.0415	0.6000
	50	381	1.1040	0.0340	0.4860	1.1040	0.0455	0.6000
	100	798	1.1460	0.0350	0.6000	1.2370	0.0320	0.6000
r=0.8	10	74	1.0970	0.0295	0.7019	1.0620	0.0440	0.8999
	50	391	1.1180	0.0425	0.8999	1.0690	0.0450	0.8999
	100	805	1.1530	0.0355	0.8959	1.0480	0.0400	0.8999

True parameter values are λ=1.1528, α=0.0288, an d the PM period is 7days.

Table 2. Failures number of different subsystems of NC Gantry-type Milling Machine and its percentage

Subsystems	Failures number	Percentage
Mechanical system	12	15.6
Hydraulic system	23	29.9
Electric system	42	55.5
Total	77	100

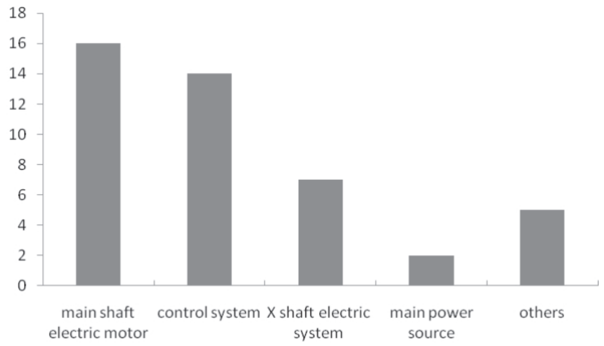

Fig. 3 Frequency analysis of electric system failures over two years

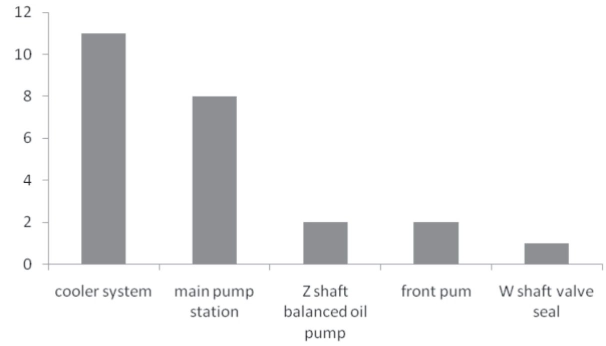

Fig.4 Frequency analysis of hydraulic system failures over two years

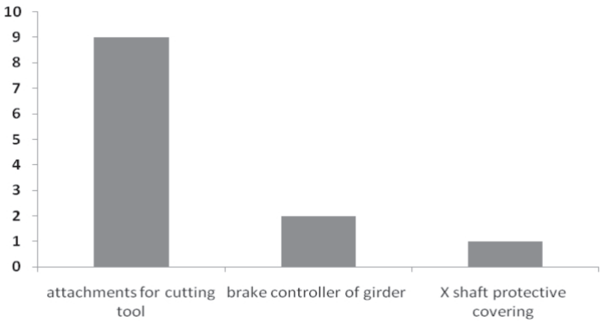

Fig. 5. Frequency analysis of mechanical system failures over two years

Table 3. Main failure modes influencing NC Gantry-type Milling Machine's downtime

Failure mode	Downtime (hr)	Percent %
Main shaft electric motor	817	27
Brake controller of girder	611	20
Cooler system	220	7
Attachments for cutting tool	215	7
Main pump station	150	5
Control system	149	5
Others	881	29
Total downtime	3043	100

Discussion with the company maintenance technicians revealed that the main reasons for the failures are as follows: 1) Inadequate maintenance lead to the frequently failure occurrence of the main shaft electric motor, the cooler system and the main pump station as well. 2) Poor design for the attachments for the cutting tool resulted in its frequent failure occurrence. 3) Too much time waiting for the repair parts lead to the long downtime of the failure of the brake controller of girder. Some advices are proposed as follows: 1) Enhancing the preventive maintenance activity, e.g. determining an optimal PM interval is expected to reduce the failure number occurred for the main shaft electric motor, the cooler system and the main pump station. 2) Redesigning the attachments for the cutting tools, will help to reduce the failure downtime resulting from the bad system design. 3) Enhancing the supply chain management and avoiding the long waiting for repair parts, will increase greatly the availability of the system. In this paper we pay attention to first item.

4.2. The calculation of interval of PM

Now we focus on the determination of the optimal interval of PM for the whole system since a PM is usually scheduled for the whole system. The available data is as follows: the time of each failure happened, the length of downtime per failure. However, we have not had the number of the defects identified and identified at PM. According the experience of the chief technician who has been responsible for the maintenance of this machine for years, the estimate of the number of defects identified at PM is about 3-5, so we take its mean value, namely 4.

Using equation (12), the fitted values of parameters are shown in Table 4. From Table 4, the mixed exponential distribution is selected as having the lowest AIC value.

Using the mixed exponential delay time, from equation (5), we have [5]:

$$EN_f(T) = \lambda\, T - \frac{\lambda r\,(e^{\alpha T}-1)(1-p)}{\alpha(\,e^{\alpha T}-1+r)} \tag{14}$$

Table 4. Models and fitted values of parameters from the real data

Models	$F(x)=1-e^{-ax}$	$F(x)=1-(1-p)e^{-ax}$	$F(x)=1-e^{-(\alpha x)^{\beta}}$
$\hat{\lambda}$	0.1283	0.1233	0.1294
$\hat{\alpha}$ (scale parameter)	0.0321	0.0301	0.0341
$\hat{\beta}$ (shape parameter)	-	-	0.8844
$\hat{p}$	-	0.10	-
$\hat{r}$	0.8521	0.8411	0.8023
Maximum log-likelihood	-73.3779	-72.2862	-73.1773
AIC	152.7558	152.5724	154.3546

p is the proportion of zero delay time. λ is the rate of occurrence of faults.
AIC=-2*logmaxlikelihood+2*(number of parameters)

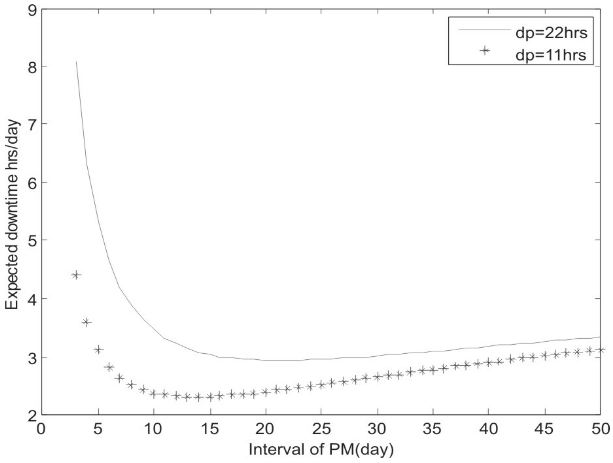

Fig. 6. Expected downtime (hour) per day against PM cycle length (day)

From tables 2 and 3, we obtain d_f=3043/77=39.5195 hours, and d_p=22 hours from the PM schedule. Substituting equation (14) into equation (13), we obtain the model output shown in Figure 3. From Figure 3, it can be seen that the optimal PM interval should be around 19 days. Since the expected downtime per unit time, when T=14 days, T=30 days, is increased less 5% than that when T=19 days, the suitable PM interval range is from 2 weeks to a month.

If the interval of PM is changed to 19 days, the expected downtime per day for this machine is 2.9340 hours, and the observed average downtime when T=3 months is 3043/(2*340)=4.4750 hours per day. So with the optimal PM interval, the expected downtime of this machine will be reduced to （4.4750-2.9340）hour/day×340 days/year＝524 hours/year. Since the average loss for this machine is 500 RMB/hour, so the decision made by the above optimal model will help the company to save at least 262,000 RMB per year. When T=90 days, the output of the model is 3.8907 hours per day, so it is not far from 4.4750 hours per day from the data.

If improving the skills of maintenance technicians and strengthening the management of maintenance activity, the inspection time could be reduced to d_p=11 hours, then the optimal inspection interval is 12 days from equation (13), and the expected downtime per day is 2.2981 hour per day, so the expected gain will be the (4.4750-2.2981）hour/day×340 days/year ×500yuan/hour=370,000 RMB.

5. Conclusion

In this paper, we propose a model to determine the optimal PM interval. The model is based upon the delay-time concept. A mixed likelihood and lease squared method based upon actual failures and the subjectively estimated PM data has been used to obtain the estimated values of the model parameters. A PM inspection model has then been used to find the optimal PM inspection interval which minimizes the total expected downtime per day caused by failures and PMs. The model shows that if the machine can be checked up every 19 days, the expected downtime is minimized. Of course, some important factors such as production schedule, maintenance manpower, and spare parts should also be considered together before making the final decision of the PM inspection interval.

****

This research is supported by National Natural Science Foundation of China under grant No.71071097, Specialized Research Fund for the Doctoral Program of Higher Education 3309303004, also supported by Shanghai Leading Academic Discipline Project, Project Number: S30504.

****

6. References

1. Akbarov A, Wang W, Christer AH. Problem identification in the frame of maintenance modelling: a case study. Int J Prod Res 2008; 46(4): 1031–46.
2. Apeland S, Scarf P A. A fully subjective approach to modeling inspection maintenance. European Journal of Operational Research 2003; 148: 410-425.
3. Aven T, Castro IT. A delay time model with safety constraint. Reliab Eng & Syst Saf 2009; 94:261–267.
4. Bozdogan H. Model selection and Akaike's Information Criterion (AIC): The general theory and its analytical extensions. Psychometrika 1987; 52(3): 345-370.
5. Christer A H, Lee C, Wang W. A data deficiency based parameter estimating problem and case study in delay-time PM modelling. Int J. Production Economics 2000; 67: 63-76.
6. Christer A H, Wang W, Baker R.D., Sharp J. Modelling maintenance practice of production plant using the delay time concept. IMA Journal of Mathematics Applied in Business & Industry 1995; 6: 67-83.
7. Christer A H, Wang W, ChoI K, Sharp J. The delay-time modelling of preventive of preventive maintenance of plant given limited PM data and selective repair at PM. IMA Journal of Mathematics Applied in Medicine and Biology 1998; 15: 355-379.
8. Christer A H, Wang W. A delay-time-based maintenance model of a multi-component system. IMA Journal of Mathematics Applied in Business & Industry 1995; 6: 205-222.
9. Christer A H. Developments in delay time analysis for modelling plant maintenance. Journal of the Operational Research Society 1999; 50: 1120-1137.
10. Jones B, Jenkinson I, Wang J. Methodology of using delay-time analysis for a manufacturing industry. Reliability Engineering and System Safety 2009; 94: 111-124.
11. Jones B, Jenkinson I, Yang Z, Wang J. The use of Bayesian net work modeling for maintenance planning in a manufacturing industry. Reliability Engineering and System Safety 2010; 95: 267–277.

12. Pillay A, Wang J, Wall A. Optimal inspection period for fishing vessel equipment: a cost and down time model using delay time analysis. Mar Technol SNAME N 2001; 38(2): 122–9.
13. Wang W, Carr M. Scheduling asset maintenance and technology insertions, to appear in complex engineering service systems. In: NgI, Parry G, Wild P, McFarlane D, editors. Concepts and research. Amsterdam: Springer; 2010.
14. Wang W, Jia J. A Bayesian approach in delay time maintenance model parameters estimation using both subjective and objective data. Quality Maintenance and Reliability Int 2007; 23: 95-105.
15. Wang W. An inspection model for a process with two types of inspections and repairs. Reliab Eng & Syst Saf 2009; 94: 526–533.
16. Wang W. Delay time modelling. In: Murthy DNP, Kobbacy AKS, editors. Complex system maintenance handbook. Amsterdam: Springer 2008; 345–70.
17. Wang W. Subjective estimation of the delay time distribution in maintenance modeling. European Journal of Operational Research 1997; 99: 516-529.

Prof. Wenyuan LV
School of Business
University of Shanghai for Science & Technology
516 Jungogn Road
Shanghai, 200093, China
e-mail: lvy@usst.edu.cn

Prof. Wenbin WANG
Salford Business School
University of Salford, UK
School of Economics and Management
University of Science and Technology
Beijing, China
e-mail: w.wang@salford.ac.uk

Maciej HUK
Michał SZCZEPANIK

MULTIPLE CLASSIFIER ERROR PROBABILITY FOR MULTI-CLASS PROBLEMS

PRAWDOPODOBIEŃSTWO BŁĘDU KLASYFIKATORÓW ZŁOŻONYCH DLA PROBLEMÓW WIELOKLASOWYCH*

In this paper we consider majority voting of multiple classifiers systems in the case of two-valued decision support for many-class problem. Using an explicit representation of the classification error probability for ensemble binomial voting and two class problem, we obtain general equation for classification error probability for the case under consideration. Thus we are extending theoretical analysis of the given subject initially performed for the two class problem by Hassen and Salamon and still used by Kuncheva and other researchers. This allows us to observe important dependence of maximal posterior error probability of base classifier allowable for building multiple classifiers from the number of considered classes. This indicates the possibility of improving the performance of multiple classifiers for multiclass problems, which may have important implications for their future applications in many fields of science and industry, including the problems of machines diagnostic and systems reliability testing.

Keywords: *multiple classifiers, majority voting, multi-class problems.*

W niniejszym artykule rozważamy systemy złożonych klasyfikatorów z głosowaniem większościowym dla przypadku problemów wieloklasowych, wykorzystujące wielowartościowe klasyfikatory bazowe. Stosując bezpośrednią reprezentację prawdopodobieństwa błędnej klasyfikacji dla analogicznych systemów w problemach dwuklasowych, otrzymujemy ogólny wzór na prawdopodobieństwo błędu klasyfikacji w przypadku wieloklasowym. Tym samym rozszerzamy teoretyczne analizy tego zagadnienia pierwotnie przeprowadzone dla problemów dwuklasowych przez Hansena i Salomona i ciagle wykorzystywane przez Kunchevę i innych badaczy. Pozwala nam to zaobserwować istotną zależność maksymalnego dopuszczalnego poziomu prawdopodobieństwa błędów klasyfikatorów bazowych od liczby rozważanych przez nie klas. Wskazuje to na możliwość poprawy parametrów klasyfikatorów złożonych dla problemów wieloklasowych, co może mieć niebagatelne znaczenie dla dalszych ich zastosowań w licznych dziedzinach nauki i przemysłu, z uwzględnieniem zagadnień diagnostyki maszyn oraz badania niezawodności systemów.

Słowa kluczowe: *klasyfikatory złożone, głosowanie większościowe, problemy wieloklasowe.*

1. Introduction

Multiple classifiers systems, also known as ensembles or committees, were considered in many papers [5, 10, 13, 21, 23, 29, 34] and books [6, 8, 12, 18]. Committee approaches that learn and retain multiple hypotheses and combine their decisions during classification [3, 7] are frequently regarded as one of the major advances in inductive learning in the past decade [2, 12, 19, 20, 27]. In the effect, the ensemble methodology has been used to improve the predictive performance of single models, in many fields such as: finance [22], bioinformatics [32], medicine [24], manufacturing [28], geography [4], information security [16, 25], information retrieval [10] and recommender systems [17]. On this basis many solutions were proposed to the problems of machines and electronic systems diagnostic [31, 35] as well as testing systems reliability [14, 30]. Solutions of this type can be a valuable complement to other, previously used approaches [26, 33, 36].

In the present paper we extend theoretical analysis of the ensemble classification error probability initially performed for the two class problem by Hassen and Salamon [15] and still used by Kuncheva and other researchers [18-20, 29]. We consider the general case of multi-class classification problems for ensembles using classical majority voting. We will derive general formula for multiple classifier error probability for number of classes greater than two and for any number of base classifiers with mutually equal posterior error probabilities. In the process of this we also show, what is often omitted, how the well known formula for multiple classifier error probability for two-class problems is changing when the number of base classifiers is not restricted to odd values. Analysis of the results obtained indicate the possibility of using multivalue base classifiers to improve the performance of ensembles of classifiers, even for very difficult classification problems.

2. Multiple classifier error probability for two-class problems

Let $D=\{D_1,...D_L\}$ be a set of L classifiers such that $D_i : \Re^n \to \Omega$, where $\Omega=\{\omega_1,.., \omega_C\}$, assigning class label $\omega_j \in \Omega$ to input data vector $\mathbf{x} \in \Re^n$. It is assumed that classifiers from set D can be successfully used to form ensemble, if their mutual errors are uncorrelated or negatively correlated [1] and when for each base classifier D_i its posterior error probability P_S^i is less than 0.5. In the case of two-class problems (K=2) with use of the majority voting the situation is relatively easy and the ensemble error probability P_E of multiple classifier is then often presented to be:

(*) Tekst artykułu w polskiej wersji językowej dostępny w elektronicznym wydaniu kwartalnika na stronie ***www.ein.org.pl***

$$P_E = \sum_{j=j_0}^{L} \binom{L}{j} P_S^j [1-P_S]^{L-j} \quad (1)$$

where L is odd, all classifiers have equal posterior error probability P_S and initial value j_0 is the minimal number of classifiers giving wrong answer that leads to ensemble decision error.

But it should be remembered, that for many-class problems limiting the number of base classifiers L to odd values does not eliminate the possibility that base classifiers will draw. In such case the solution of random class label selection is often used - when no other class gains higher number of votes than the proper one but some of other classes tie with it, class label is randomly selected from this group, with equal posterior probabilities for each class. With this in mind the factor of ensemble error probability connected with ties can't be neglected. Thus looking for the guideline for further analysis of multi-class problems, we can omit the assumption that L is odd and extended the expression (1) to the form:

$$P_E = \sum_{j=j_0}^{L} \binom{L}{j} P_S^j [1-P_S]^{L-j} + \frac{1}{2}\delta(L \bmod 2, 0)\binom{L}{\frac{L}{2}} P_S^{L/2}[1-P_S]^{L/2} \quad (2)$$

where

$$j_0 = \begin{cases} (L+1)/2 & : L \bmod 2 > 0 \\ L/2+1 & : L \bmod 2 = 0 \end{cases} \quad (3)$$

and $\delta(x,y)$ is the Kronecker's delta:

$$\delta(x,y) = \begin{cases} 1 & : x = y \\ 0 & : x \neq y \end{cases} \quad (4)$$

The factor ½ before the Kronecker's delta in (2) is the probability of wrong random class selection when base classifiers draw and the Newton symbol $\binom{L}{\frac{L}{2}}$ determine the number of possible ties between base classifiers for two-class problem, when L is even.

3. Multiple classifier error probability for multi-class problems

The first step to find the general equation for multiple classifier error probability for multiclass problems can be rewriting the expression (2) to the form in which each component probability is explicite connected with votes assigned by base classifiers to individual classes.. Beacause without loosing the generality we can assume that the class with index 1 is the correct one, thus by simple algebraic transformations we can see that right side of (1) can take the form:

$$\sum_{k_1=0}^{L}\sum_{k_2=0}^{L}\left(\binom{L}{k_2} P_S^{k_2}\left(1-P_S\right)^{L-k_2} \cdot \delta(k_1+k_2, L) H(k_2-k_1)\right) \quad (5)$$

where k_1 and k_2 represent various numbers of votes that can be given by L base classifiers respectively for classes 1 and 2. The introduced Kronecker's delta ensures that only those combinations of votes are taken under consideration, for which the sum of votes for all classes equals the number of base classifiers:

$$k_1 + k_2 = L \quad (6)$$

and H is the Heaviside's step function used to select factors for which $k_2 > k_1$:

$$H(x) = \begin{cases} 1 & : x > 0 \\ 0 & : x \leq 0 \end{cases} \quad (7)$$

Finally, by further use of (6) for calculation of $L - k_2$, and by introducing that:

$$P_1 = 1 - P_S \quad \text{and} \quad P_2 = P_S \quad (8)$$

are probabilities of voting at the class 1 and 2 respectively, we can rewrite (5) in the form:

$$\sum_{k_1=0}^{L}\sum_{k_2=0}^{L}\left(\frac{L!}{k_1!k_2!} P_1^{k_1} P_2^{k_2} \delta(k_1+k_2, L) H(k_2-k_1)\right) \quad (9)$$

Similarly, the right part of the right side of expression (2) can be transformed to:

$$\sum_{k_2=0}^{L}\left(\frac{1}{2}\binom{L}{k_2} P_S^{k_2}[1-P_S]^{L-k_2}\,\delta(k_2, \frac{L}{2})\right) \quad (10)$$

Next, because in the case of a tie $k_1 = k_2 = L/2$, formula (10) can be rewritten as:

$$\sum_{k_1=0}^{L}\sum_{k_2=0}^{L}\left(\frac{1}{2}\delta(k_1+k_2, L)\delta(k_1,k_2)\frac{L!}{k_1!k_2!} P_1^{k_1} P_2^{k_2}\right) \quad (11)$$

In the result, after combining (5) and (11) and reorganizing, the formula for ensemble error probability for two-class problem (2) can be given by:

$$P_E = \sum_{k_1=0}^{L}\sum_{k_2=0}^{L}\left(\delta(k_1+k_2, L)\left[H(k_2-k_1) + \frac{1}{2}\delta(k_1,k_2)\right]\frac{L!}{k_1!k_2!} P_1^{k_1} P_2^{k_2}\right) \quad (12)$$

The expression (12) shows the natural method of determining the ensemble error probability for multi-class problems (K>2) – by adding further summations connected with other classes. It is easy to notice, that in such case only the part of (12) taken in square brackets require special analysis. The Heaviside's function gives information if the proper class received fewer votes than the wrong class. Thus for many classes it should be replaced by the form:

$$H_E = H(\sum_{i=2}^{K} H(k_i - k_1)) \quad (13)$$

which has value 1 if one or more classes received more votes form base classifiers than the correct class and zero in other cases. The second, right part in square brackets in (12) - the Kronecker's delta - can be identified as an element holding the number of classes that tie with the correct one, additionally multiplied by the probability of wrong random class selection. In the general case (K>2) the number of ties can be represented by the formula:

$$H_D = \sum_{i=2}^{K}\delta(k_1, k_i) \quad (14)$$

and due to that the probability of wrong random class selection during tie is given by:

$$\frac{H_D}{H_D+1} \quad (15)$$

Now it is easy to calculate that the ensemble error probability for multi-class problems is given by:

$$P_E = \sum_{k_1=0}^{L}\sum_{k_2=0}^{L}\cdots\sum_{k_K=0}^{L}\left(\delta(\sum_{i=1}^{K}k_i, L)\left[H_E + (1-H_E)\left(1-\frac{1}{1+H_D}\right)\right]L!\prod_{i=1}^{K}\frac{P_i^{k_i}}{k_i!}\right) \quad (16)$$

where the sum of the probabilities of assigning votes for each class:

$$\sum_{i=1}^{K} P_i = 1 \tag{17}$$

But it is noteworthy that factor:

$$L! \prod_{i=1}^{K} \frac{1}{k_i!} \tag{18}$$

is a multinomial coefficient P_{MF} of the multinomial probability distribution, thus the expression (16) can be written finally as:

$$P_E = \sum_{k_1=0}^{L} \sum_{k_2=0}^{L} \cdots \sum_{k_K=0}^{L} \left(P_{MF} \left[H_E + (1 - H_E) \left(1 - \frac{1}{1 + H_D} \right) \right] \right) \tag{19}$$

where:

$$P_{MF} = f(k_1, k_2, ..., k_K, L, P_1, P_2, ..., P_K) \tag{20}$$

is the probability mass function of the multinomial distribution for non-negative integers k_1, k_2,...,k_K.

4. Simulations and i discussion of results

Formula (19) derived in previous section was at first verified experimentally with the use of statistical simulations of the system with multiple base classifiers. Due to the high computational cost of such simulations, we considered only cases of classes numbers K from 2 to 10, numbers of base classifiers from 1 to 100 and selected values of base classifiers classification error probabilities P_S (0; 0,1; 0,3; 0,5; 0,7; 0,9 i 1). During simulations for each set of parameters 10^6 votings were performed where answers of individual base classifiers were generated randomly with use of standard random generator included in Borland Object Pascal System library.

Obtained results have shown high consistency between outcomes of conducted simulations and values of formula (19). For all considered values of parameters the difference between results of simulations and calculated error probabilities was not greater than 2,7% of computed values (average 0,043%). Additionally, for the case of two class problems both methods have given results consistent also with values of expression (2).

On the above basis, we observed how the multiple classifier error probability changes with increasing number of classes under consideration (see fig.1). For typical example of L = 21 and P_S = 0,3 for two classes the error probability is $P_E \approx$ 0,0264, but for three and five classes it amounts just to 0,00202 and 0,000126. This is the result of growing number of classes other than the correct one - missed votes are dispersed over all K - 1 wrong classes. In the effect the average cumulative number of votes for individual wrong class decreases with increase of K, which do not apply to the correct class.

It is also very interesting that for number of classes K greater than 2, the upper limit of base classifier posterior error probability, that allows successfull building of multiple classifier is greater than 0.5 (compare fig. 2a and fig. 2b). Due to practical difficulties in creating large sets of base classifiers with a low errors probabilities and also with a high degree of lack of correlation between errors committed by them, observed result suggests the possibility of easier ensembles of classifiers building for complex multiclass problems by admission to the considerations also base classifiers that commit errors more frequently than in the half the cases.

For example - when the number of classes K = 5 and the number of base classifiers L = 21, error probability of base

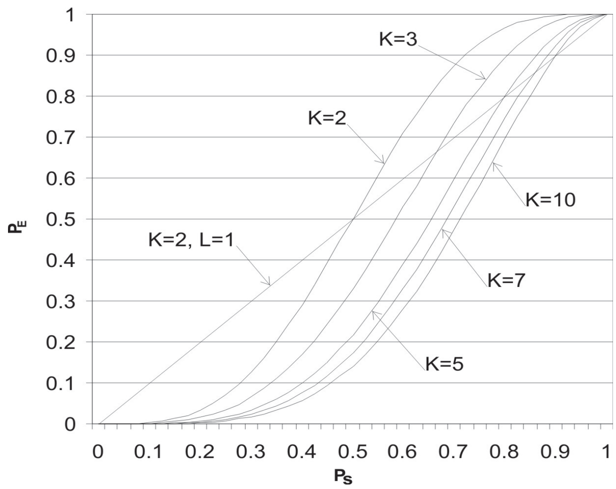

Fig. 1. Multiple classifier error probability P_E as a function of the error probability P_S of seven base classifiers (L=7), with negatively correlated mutual errors,for different numbers of classes K

a)

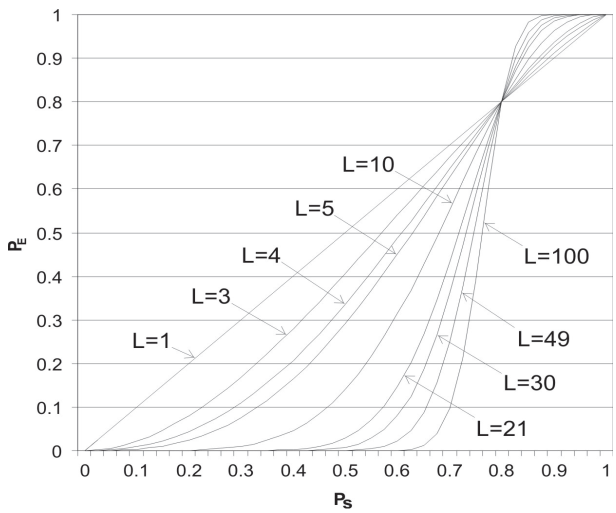

b)

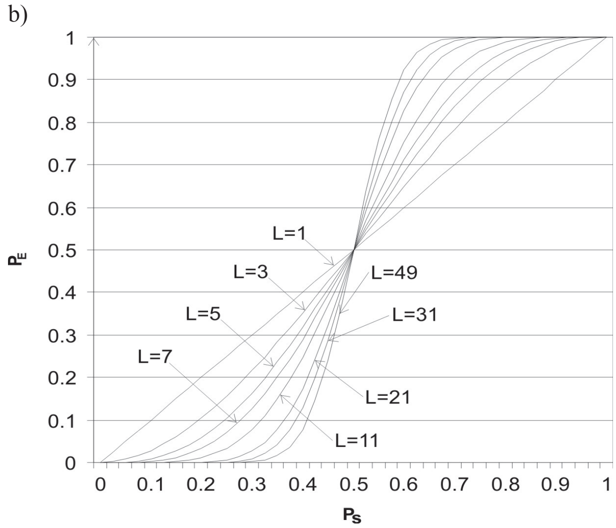

Fig. 2. Multiple classifier error probability P_E as a function of the error probability P_S for different numbers L of base classifiers, with negatively correlated mutual errors, for five a) and two b) classes

classifiers $P_S = 0,6$ results in an error probability of a multiple classifier $P_E \approx 0,146$, what is the better value than randomly guessing. In addition, by increasing the number of base classifiers to 100, the above probability of multiple classicier error can be reduced to just 0,000815. However, it should be remembered that presented results were obtained under the assumption that the underlying mutual errors of base classifiers are fully uncorrelated or negatively correlated, which is difficult to achieve in practice. Partial correlation of errors can cause changes in individual values of the above probabilities, however, should not affect the basic properties of the results.

5. Summary and future work

In this work the formula for multiple classifier error probability for multi-class problems was formally presented. Its detailed derivation was based on the widely known analogous formula for two-class problems, which was additionally extended for even numbers of base classifiers.

Simulations during analysis of obtained formula indicate that increasing the number of considered classes lowers ensemble error probability. But what is more interesting, under assumption that mutual errors of base classifiers are uncorrelated or negatively correlated, the upper limit of base classifier posterior error probability P_S that allows successfull building of multiple classifier is increasing with considered number of classes.

As a consequence, the transition from the schema of bivalued to multivalued hypotheses, facilitates the creation of large collections of diverse base classifiers, and thus - even finer ensembles of classifiers. This could be of great importance for further applications of such methods in many fields of science and industry - including the issues of machines maintenance and diagnostics and systems reliability testing.

In future works we will investigate how the partial correlation between errors of multivalued base classifiers modifies error probabilities of multiple classifiers for numbers of classes greater than 2. We will also try to find computationally efficient expressions for estimation of derived formula for number of classes above 100.

6. References

1. Ali K, Pazzani M. Error reduction through learning multiple descriptions. Machine Learning 1996; 24(3): 173-206.
2. Bian S, Wang W. On diversity and accuracy of homogeneous and heterogeneous ensembles. IOS Press Amsterdam: 2007, 4(2): 103-128.
3. Brown G, Wyatt J, Harris R, Yao X. Diversity creation methods: A survey and categorization. Journal of Information Fusion 2005; 6(1).
4. Bruzzone L, Cossu R, Vernazza G. Detection of land-cover transitions by combining multidate classifiers. IOS Press Amsterdam: 2007, 25(13): 1491-1500.
5. Buhlmann P, Hothorn T. Boosting algorithms: Regularization, Prediction and Model Fitting. Statistical Science 2007; 22(4): 477-505.
6. Claeskens G, Hjort N. Model Selection and Model Averaging. Volume 27 of Cambridge Series in Statistical and Probabilistic Mathematics. Cambridge University Press 2008.
7. Dietterich T. An experimental comparison of three methods for constructing ensembles of decision trees: Bagging, boosting, and randomization., Machine Learning 2000; 40(2): 139-157.
8. Dietterich T. (Ensemble learning, in M. ARBIB (Ed.)) The Handbook of Brain Theory and Neural Networks. Second ed., Cambridge: 2002, 405-408.
9. Elovici, Y, Shapira B, Kantor P. A decision theoretic approach to combining information filters: Analytical and empirical evaluation., Journal of the American Society for Information Science and Technology 2006; 57(3): 306-320.
10. Evgeniou T, Pontil M, Elisseef A. Leave one out error, stability, and generalization of voting combinations of classifiers, Machine Learning 2004; 55(1): 71-97.
11. Freund Y, Lu J, Schapire R. Boosting: Models, Applications and Extensions., Chapman and Hall/CRC 2010.
12. Freund Y, Schapire R. Experiments with a new boosting algorithm., Machine Learning: Proceedings of the Thirteenth International Conference (ICML 96). SanFrancisco: 1996, 148-156.
13. Fumera G, Roli F. A theoretical and experimental analysis of linear combiners for multiple classifier systems., IEEE Transactions on Pattern Analysis and Machine Intelligence 2005; 27(6): 942-956.
14. Halbiniak Z, Jóźwiak I.: Deterministic chaos in the processor load. Chaos, Solitons and Fractals 2007; 31(2): 409-416.
15. Hansen L, Salamon P. Neural network ensembles, IEEE Transactions on Pattern Analysis and Machine Intelligence 1990; 12(10): 993-1001.
16. Jacak J, Jóźwiak I, Jacak L.: Composite fermions in braid group terms. Open Systems and Information Dynamics 2010; 17(1): 53-71.
17. Jahrer M, Tscher A, Legenstein R. Combining predictions for accurate recommender systems, Proceedings of the 16th ACM SIGKDD international conference on Knowledge discovery and data mining, Washington, DC, USA: 2010, 693-702.
18. Kuncheva L. Combining Pattern Classifiers. Methods and Algorithms., Wiley 2004
19. Kuncheva L, Bezdek J, Sutton M. On combining multiple classifiers by fuzzy templates, Proceedings of the on combining multiple classifiers by fuzzy templates. Conference, Pensacola, Florida USA: 1990, 193-197.
20. Kuncheva L, Whitaker C, Shipp C, Duin R. Limits on the majority vote accuracy in classifier fusion, Pattern Analysis and Applications 2003; 6: 22-31.

21. Leapa N, Clemansa P, Bauer K, Oxley M. An investigation of the effects of correlation and autocorrelation on classifier fusion and optimal classifier ensembles, International Journal of General Systems 2008; 37(4): 475-498.
22. Leigh W, Purvis R, Ragusa J. Forecasting the nyse composite index with technical analysis, pattern recognizer, neural networks, and genetic algorithm: a case study in romantic decision support. Decision Support Systems 2002; 32(4): 361-377.
23. Liu Y, Yao X, Higuchi T. Evolutionary ensembles with negative correlation learning. IEEE Transactions on Evolutionary Computation 2000; 4(4): 380-387.
24. Mangiameli P, West D, Rampal R. Model selection for medical diagnosis decision support systems, Decision Support Systems 2004; 36(3): 247-259.
25. Menahem E, Shabtai A, Rokach L, Elovici Y. Improving malware detection by applying multi-inducer ensemble. Computational Statistics and Data Analysis 2009; 53(4): 1483-1494.
26. Niewczas A, Pieniak D, Bachanek T, Surowska B, Bieniaś J, Pałka K. Prognosing of functional degradation of bio-mechanical systems exemplified by the tooth-composite filling system. Eksploatacja i Niezawodnosc - Maintenance and Reliability 2010; 45(1): 23-34.
27. Opitz D, Shavlik J. Generating accurate and diverse members of a neural-network ensemble, Advances in Neural Information Processing Systems. MIT Press, Denver: 1996, 535-543.
28. Rokach L. Mining manufacturing data using genetic algorithm-based feature set decomposition. International Journal of Intelligent Systems Technologies and Applications 2008; 4(1): 57-78.
29. Rokach L. Taxonomy for characterizing ensemble methods in classification tasks: a review and annotated bibliography. Computational Statistics and Data Analysis 2009; 53(12): 4046-4072.
30. Santhanam P, Bassin K. Managing the maintenance of ported, outsourced, and legacy software via orthogonal defect classification. In proc. IEEE International Conference on Software Maintenance 2001; 726-734
31. Shahrtash S, Jamehbozorg A. A Decision-Tree-Based Method for Fault Classification in Single-Circuit Transmission Lines. IEEE Transactions on Power Delivery 2010; 25(4): 2190-2196.
32. Tan A, Gilbert D, Deville Y. Multi-class protein fold classification using a new ensemble machine learning approach. Genome Informatics 2003; 14: 206-217.
33. Tao J, Zhang Y, Chen X, Ming Z. Bayesian reliability growth model based on dynamic distribution parameters. Eksploatacja i Niezawodnosc - Maintenance and Reliability 2010; 46(2): 13-16.
34. Valentini G, Masulli F. Ensembles of learning machines. in M. M. and T. R. (Eds), Neural Nets: 13th Italian Workshop on Neural Nets, Vol. 2486 of Lecture Notes in Computer Science, Springer, Berlin: 2002, 3-19.
35. Xu D, Wu M, An J. Design of an expert system based on neural network ensembles for missile fault diagnosis. In Proc. IEEE International Conference on Robotics, Intelligent Systems and Signal Processing 2003, 2: 903-908.
36. Yu T, Cui W, Song B, Wang S. Reliability growth estimation for unmanned aerial vechicle during flight-testing phases. Eksploatacja i Niezawodnosc - Maintenance and Reliability 2010; 46(2): 43-47.

Dr inż. Maciej HUK
Mgr inż. Michał SZCZEPANIK
Instytut Informatyki
Politechnika Wrocławska
Ul. Wyb. Wyspiańskiego nr 27
50-370 Wrocław, Polska
e-mail: Maciej.Huk@pwr.wroc.pl
e-mail: Michal.Szczepanik@pwr.wroc.pl

Lech GŁADYSIEWICZ
Robert KRÓL
Jędrzej BUKOWSKI

TESTS OF BELT CONVEYOR RESISTANCE TO MOTION

EKSPERYMENTALNE BADANIA OPORÓW RUCHU PRZENOŚNIKA TAŚMOWEGO*

The modern of belt conveyor calculations are based upon the advanced computational methods, mostly multivariate simulations. Dimensioning of a conveyor drive depends on the identification of belt conveyor resistance to motion which can be identified with the biggest accuracy after adopting the exact methods of calculation the components of the main resistance force. The development of these methods requires verification of theoretical algorithms. Various tests of the belt conveyor resistance to motion, from the laboratory individual idler rotational resistance to motion, through the combined idler rotational and indentation resistances with the use of a special test rig up to the in-situ tests of an idler subjected to typical operational conditions have been presented. The obtained results have been used both for the verification of calculation methods and the comparison of idlers with alternative steel or polyurethane coating.

Keywords: *belt conveyor, idler, rotational resistance, loading, strain gauge.*

Streszczenie: *Podstawą projektowania przenośników taśmowych są zaawansowane metody obliczeniowe oraz wielowariantowe symulacje różnych stanów pracy. Kluczowym zadaniem projektowym jest wymiarowanie napędu głównego w oparciu wyznaczone opory ruchu przenośnika, Najlepsze oszacowanie oporów ruchu przynoszą metody oporów jednostkowych rozwijane różnych środkach badawczych. Doskonalenie metod obliczeniowych wymaga prowadzenia badań w celu weryfikacji opracowanych zależności. W artykule przedstawiono eksperymentalne metody badań wybranych składowych oporów ruchu przenośnika taśmowego, obejmujące pomiary na stanowisku do badań krążników, pomiary toczącego się wózka z dwoma krążnikami na bieżni wyłożonej taśmą przenośnikową oraz pomiary oporów ruchu pojedynczego zestawu krążnikowego na przenośniku kopalnianym. Uzyskane wyniki pomiarów posłużyły nie tylko do weryfikacji metod obliczeniowych, ale również do porównania krążników z płaszczem stalowym z krążnikami z płaszczem poliuretanowym.*

Słowa kluczowe: *przenośnik taśmowy, krążnik, opór obracania, obciążenie, tensometr.*

1. Introduction

A good machine (belt conveyor) design is based on calculations while a theory is based on experiments, which are an exhaustible source of knowledge. A theory and calculations are inseparably bound. Without a verified theory taking all the factors into account one cannot make accurate calculations and so one cannot optimally design a machine (belt conveyor). Currently, belt conveyor calculations are based on advanced computing methods, mostly multivariate simulations. This approach guarantees the best solutions at all the design stages. The identification of the effect of different factors on belt conveyor motion resistance is the basis for any measures taken to modernize existing transport systems. In most cases, solutions reducing energy consumption are sought.

2. Belt conveyor motion resistance components

Primary resistances – all the forces which occur along the belt conveyor's route in the zones of contact between the belt and the support elements (typically idlers, or sliding elements) – predominate in over 80 m long belt conveyors. Considering the energy conversion (dissipation) phenomena which accompany the motion of the belt, the primary resistances are divided into:

- idler rotational resistance W_k,
- belt-on-idler rolling (indentation) resistance W_e,
- belt bending resistance (flexure resistance of a belt) W_b,
- flexure resistance of bulk material W_f,
- sliding resistance of a belt on idlers W_r.

The effect of the conveyor's technical parameters and the properties of the belt and the transported bulk materal on the particular components of the primary resistances has been quite well explored (mainly theoretically and to a smaller degree, experimentally) [7]. Multivariate simulations have become possible thanks to the advanced computing methods. One of the key problems is the effect of the properties of the belt and the idlers on conveyor motion resistances. The problem has been the subject of numerous investigations [1,2,3,5,6,10]. Another major problem is the effect of the force in the belt on the magnitude of motion resistances. Knowledge in this regard is essential for designing and operating long and ascending belt conveyors since the belt and the idlers generate most of the primary resistances and the force in the top strand varies widely [4,9]. This is illustrated in figure 1 which shows all the primary resistance components for the whole range of force variation in the top strand for conveyor route length L=1100 m. When the conveyor is in steady motion, the force in the top strand grows from S=142 kN in the vicinity of the return station to S=638 kN near

(*) Tekst artykułu w polskiej wersji językowej dostępny w elektronicznym wydaniu kwartalnika na stronie ***www.ein.org.pl***

the stub-end drive station. Being independent of the force in the belt, idler rotational resistance and belt rolling (indentation) resistance along the conveyor's top strand remain constant. The proportions of the other three primary resistance components (flexure resistance of a belt, flexure resistance of bulk material and sliding resistance of a belt on idlers) significantly depend on the force in the belt. The motion resistance components shown in fig. 1 were calculated per single top-strand idler set.

The division of the primary resistances into the components shown in fig. 1 is based on the phenomena which accompany the motion of the belt (with transported material) on idlers. Knowing the conveyor specifications, the operating conditions, the belt and spoil influence parameters, the components can be quite accurately analytically determined, whereas experimentally they are not always separable. The only component which can be experimentally investigated on special measuring rigs is idler rotational resistance. Various methods of investigating conveyor motion resistances, aimed at identifying the phenomena and refining computing methods in order to reduce the energy consumption of the belt conveyor's main drive, are presented below.

3. Tests of idler rotational resistance

The rotational resistance of a single roller is defined as a tangential force applied to the roller shell in order to overcome the frictional resistance in the bearings and the seals. This component can be only experimentally determined. In accordance with Polish standard PN-91 M-46606 "*Belt Conveyors. Idlers*", idler rotational resistance is tested on a special measuring rig shown in fig. 2.

One end of the roller axle is fixed in rotary fixture (4) through which the rotations from motor (2) are transmitted via belt transmission (3). Its other end is clampwise supported in nonrotary fixture (5). The roller shell is fixed in a clamping ring whose arm rests on a balance (whereby the roller shell is immobilized). The motion of the axle motion relative to the stationary shell produces a torque which is transmitted by the arm (having a constant length) to the balance or a force gauge. The registered force is converted, using the condition torque equilibrium relative to the roller axle, into a rotational resistance value. The

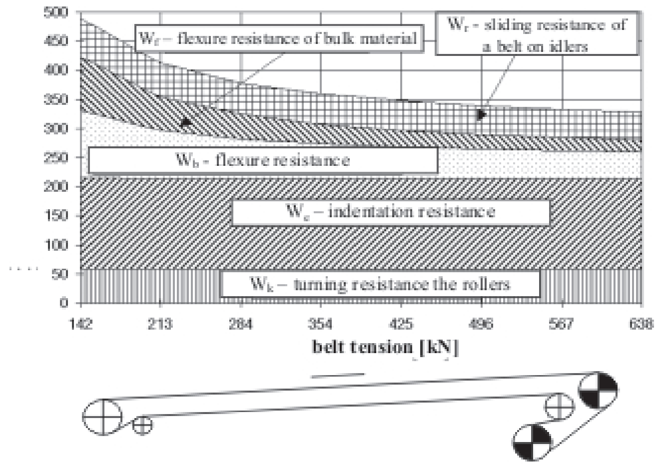

Fig. 1. *Proportions of primary resistance components along top strand of overburden conveyor with specifications: route length L=1100 m; load-lifting height H=10 m; route inclination angle δ=0.52°; belt width B=2.25 m; belt speed v_t=5.24m/s; top-strand idler set spacing l_g=1.0 m; mining spoil bulk density ρ=1600kg/m³; top strand trough angle λ=45°; ambient temperature T_C=0ºC; main stub-end station drive 4×1000kW, belt St 3150, idlers in good technical condition*

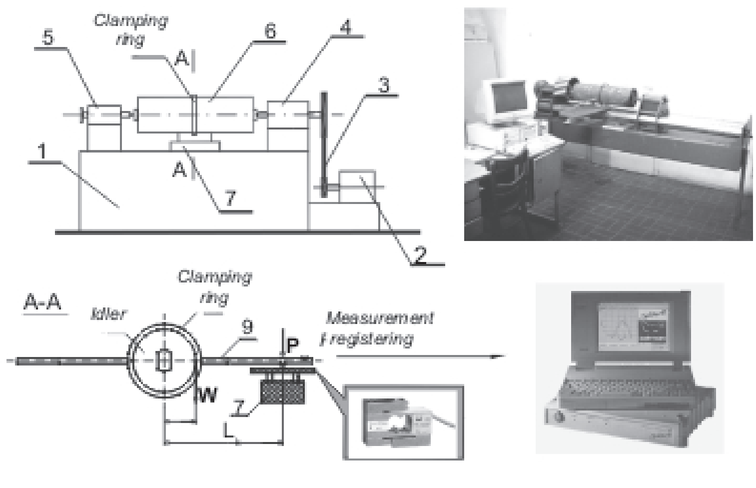

Fig. 2. *Rig for measuring rotational resistance of idler rollers: 1 – frame bearer, 2 – electric motor, 3 – belt transmission, 4 – rotary fixture support, 5 – nonrotary clamping fixture support, 6 – tested idler, 7 – force gauge, 8 – clamping ring, 9 – arm*

motor which drives the axle is equipped with a system of infinitely variable speed control through supply current frequency adjustment. The balance is coupled with a measuring laptop registering idler rotational resistance over time. Idler rotational resistance W_k is calculated from the formula:

$$W_k = P_w \cdot \frac{L_k}{r_p}[N] \quad (1)$$

where: P_w- balance readings, in N; L_k- the distance of clamp ring arm pressure on the balance pan from the roller axle, in m; r_p- the outer radius of the roller shell, in m.

According to standard PN-91 M-46606, prior to the proper measurements new idler rollers should be rotated with a rotational speed of 600 rpm for 4 hours. Then after stabilization (about 2000 seconds) one can start measuring the rotational speed. Figure 3 shows typical rotational resistance traces for an roller with a steel shell and an roller with a polyurethane shell.

From the point of view of comparisons and analyses of the influence of conveyor structural parameters on motion resistances the dependence between idler rotational speed and angular velocity is a key one. Results of the measurement of rotational resistance during starting at rotational speed growing from 0 to 500 rpm for 2 types of roller shell are compared in fig. 4.

Since the above method of determining idler rotational resistance is simple, its error is small. Its drawback is that the idler is not under load when its rotational resistance is measured. A new test rig enabling the measuring of idler rotational resistance under load has been developed in the Institute of Mining at Wrocław University of Technology in collaboration with the German idler manufacturer Artur Kuepper GmbH & Co AG. A schematic of the new test rig for measuring idler rotational resistance is shown in fig. 5. The axle of the tested idler is fixed in two supports (3). The idler shell is loaded with two wheels (6 and 7) one of which is connected via a drive shaft and a belt transmission (2) with an electric motor (1). This wheel drives the idler. The other wheel is put into motion directly by the rotating idler and it performs the role of the loading wheel. Through set screws (5) and a link mechanism the two wheels can exert pressure on the idler shell, generating radial force F_r of up to 20kN.

Two measuring bolts (2) registering radial force F_r acting perpendicularly to the roller axle are placed in holes in the supports (3) (fig. 6). Radial force F_r decomposes into reactions T_1, T_2 in the places where the largest shearing stresses occur in the measuring bolts. Force F_o which can act along the bolt axis is compensated by the measuring system whereby it does not disturb the measurement. If the roller shell remains stationary, bolt reactions T and T_2 are equal.

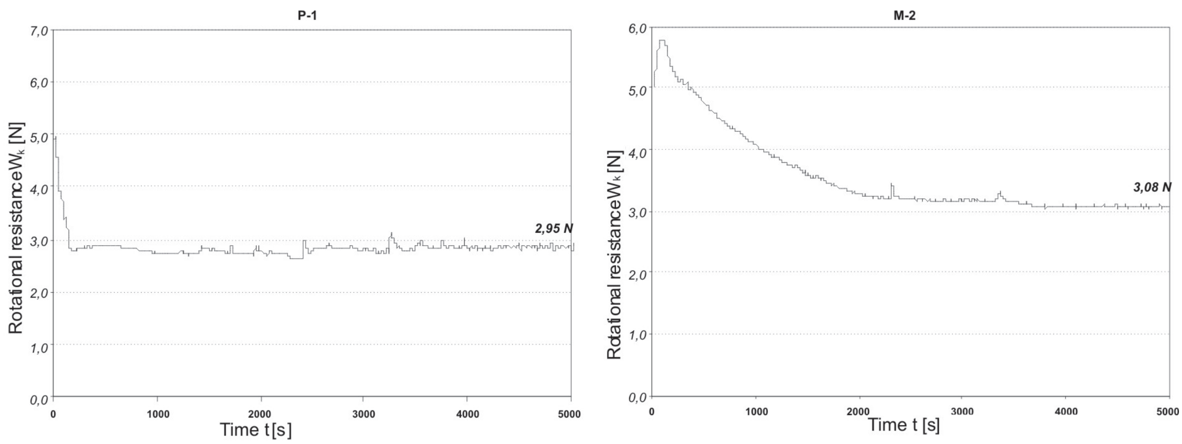

Fig. 3. Traces of rotational resistance for idler rollers with polyurethane shell (P-1) and with steel shell (M-2)

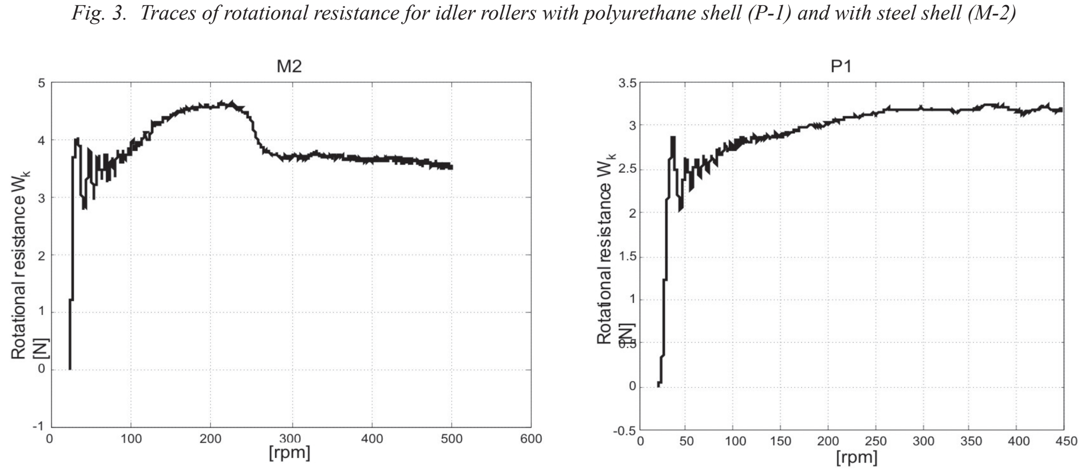

Fig. 4. Comparison of recorded rotational resistance traces for idler rollers with metal shell M-2 and with polyurethane shell P-1 in rotational speed range of 0-500 rpm

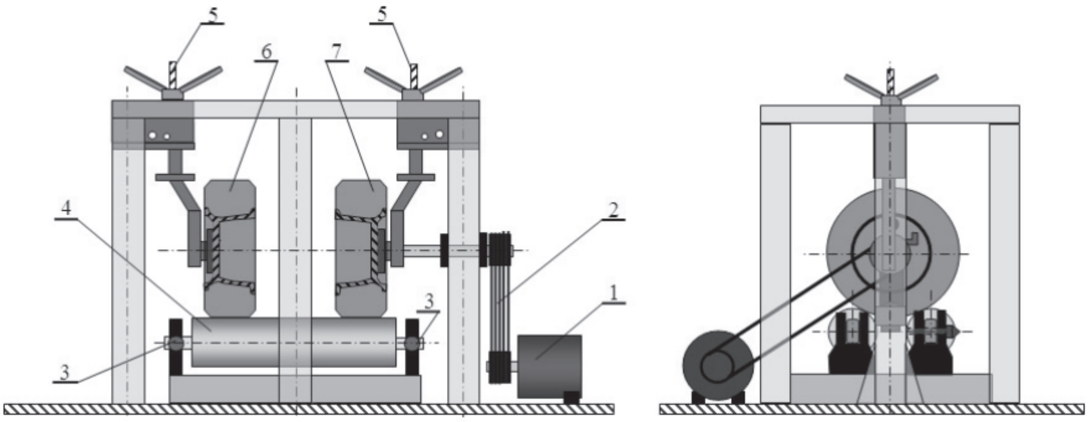

Fig. 5. Test rig for measuring idler rotational resistance

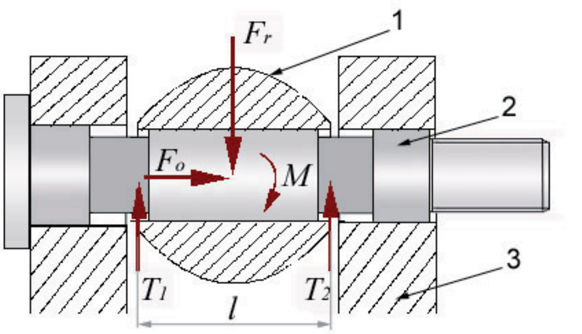

Fig. 6. Distribution of forces and torque on measuring bolt: **1** *axle of tested roller,* **2** *measuring bolt,* **3** *support*

When the idler is put in motion, a difference between reactions T_1 and T_2 appears. The difference is the larger, the greater the idler rotational resistance. Knowing the values of reactions T_1 and T_2 and length l of the arm on which the reactions act, one can determine torque M acting on the roller axle. Thus one gets the following relations:

$$M = T_1 \cdot \frac{l}{2} - T_2 \cdot \frac{l}{2} \tag{3}$$

$$M = (T_1 - T_2) \cdot \frac{l}{2} \tag{4}$$

where: M – the torque turning the roller axle, in Nm; T_1, T_2 – reactions arising on the bolt as a result of the action of radial force F_r, in N; l – the distance between the places where shearing forces T_1, T occur, in N.

Knowing torque M and roller radius r one can calculate idler rotational resistance W_k from the relation:

$$W_k = \frac{M}{r_p} \tag{5}$$

where: W_k – idler rotational resistance, in N; r_p – a radius equal to the half of the roller diameter, in m.

The tensometric technique was employed to measure idler rotational resistance W_k. The measuring bolt was so designed that two full strain gauge bridges could be stuck on in the places of the highest shearing stresses (T_1, T_2) (fig.7). The measuring bolts are made of highest quality spring steel whereby they can undergo elastic deformations from 0 to 12kN. Hottinger series Y 120Ω strain gauge rosettes for steel, 6-wire connected into three independent strain gauge bridges, were used in the measurements. Thanks to the 6-wire connection and the use of full bridges the measuring system is insensitive to changes in ambient temperature.

The measuring system enables the simultaneous registration of radial loads and idler rotational resistances. The rig is used for durability tests in which the (rotational resistance versus radial force) characteristic of the tested idlers is determined.

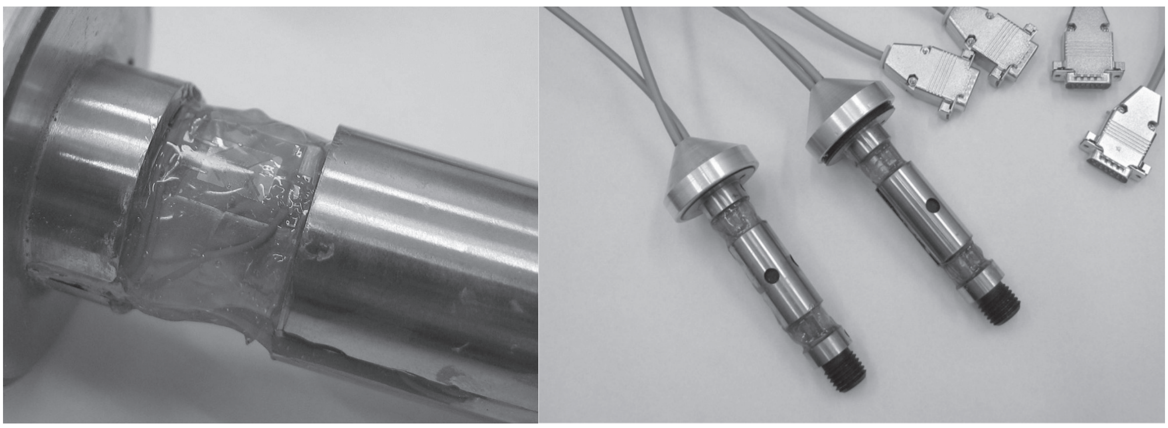

Fig.7. Measuring bolts and measuring point with stuck on strain gauges

For this purpose a series (usually six) idler rotational resistance over time measurements are performed for different idler load levels (ranging from 250 to 12000N). Figure 8a shows a trace of idler rotational resistance W_k over time t under radial load F_r of 1000N. Since the tested idler (Artur Kuepper GmbH & Co AG 219x1160mm with 6312-2Z C4 bearings) had worked in a mine for about 2 years rotational resistance stabilized after 20 minutes since the test start. Then on the basis of the results obtained from the series of measurements under the set load F_r (0.25 ÷ 12kN) rotational resistance W_k as a function of F_r was plotted (fig. 8b). The determined relation shows that radial load F_r has a significant effect on idler rotational resistance W_k.

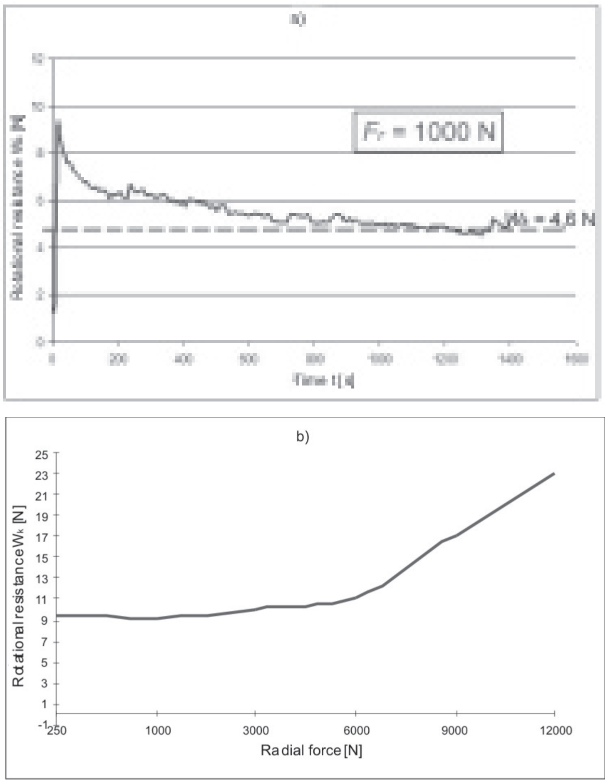

Fig.8. Dynamic rotational resistance for AKT (219 x 580mm) idler versus: time (for radial load F_r = 1kN); b) radial force F_r in range of 0.25-12 kN

The obtained measurement results for the tested five idler rollers with a steel shell and a labyrinth seal are compared in fig. 9. In addition, the arithmetic mean of $W_k(F_r)$, reflecting the character of the changes in rotational resistance, was determined for the above graphs.

The promising results yielded by this measuring method encourage the use of measuring bolts in belt conveyor operating measurements. Preparations for such measurements, with six measuring bolts installed on one set of idlers and registering idler loads and rotational resistances, are underway. These will be the first in situ idler rotational resistance measurements. They will supply data about the actual effect of the operational forces on idler rotational resistances. This, in turn, may shed new light on the energy consumption of the idler set, the optimum idler spacing and the durability of the particular idlers.

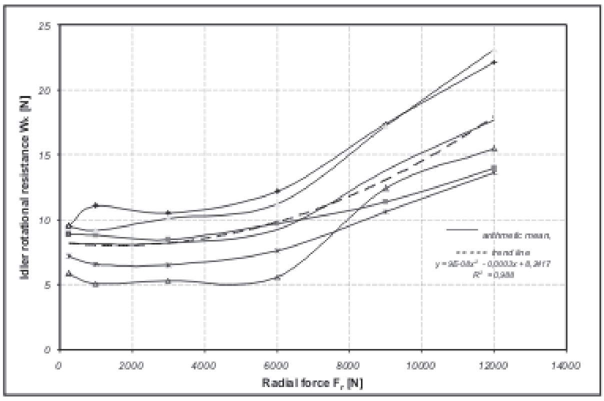

Fig. 9. Idler rotational resistance W_k versus radial force F_r for tested AKT idlers and plotted mean of all relations

4. Belt rolling resistance and idler rotational resistance tests on rig with inclined plane

Figure 1 shows that the largest component of the belt conveyor primary resistances is belt-on-idler rolling (indentation) resistance. This means that first of all this component should be analyzed when seeking optimal conveyor designs. For this purpose a special measuring rig for simulating belt-idler interaction conditions has been developed. Its main units are (fig. 10):

- a carriage with two idlers,
- an inclined section for accelerating the carriage,
- a measuring section on which the distance of idler free rolling on the belt is determined,
- a carriage braking assembly.

The measuring section for investigating carriage motion kinematics is lined with conveyor belt. The weighting carriage consists of two load-bearing idlers and a frame. The idlers are mounted in the frame which can be weighted to increase the force pressing the idlers to the belt. The carriage is accelerated to the required velocity on the inclined plane. Subsequently, on the measuring section the velocity decreases as a result of rolling resistance and idler rotational resistance. Changes in velocity are measured by three tachometric probes (Tacho1, Tacho2 and Tacho3). By analyzing the changes in the kinetic energy of the carriage rolling on the belt one can determine the rolling resistance. For this purpose one must know the rotational resistance of the idlers mounted in the carriage frame. The rotational resistance of the tested idlers is determined (using the methods presented in the previous section) prior to the measurements on the rig described above.

Knowing the times it takes the carriage to travel between the particular probes one can demarcate measuring lengths and determine the changes in kinetic energy along these lengths. For start point **E** and end point **D** of the measuring section one can determine carriage travel velocities according to the schematic shown in fig. 11.

Initial velocity $\boldsymbol{v_1}$ and end velocity $\boldsymbol{v_2}$ for carriage travel between points **D** and **E** on inclined measuring length $\boldsymbol{l_{DE}}$ are calculated from the equations:

$$v_1 = \frac{l_{AB}}{\Delta t_{AB}} \tag{6}$$

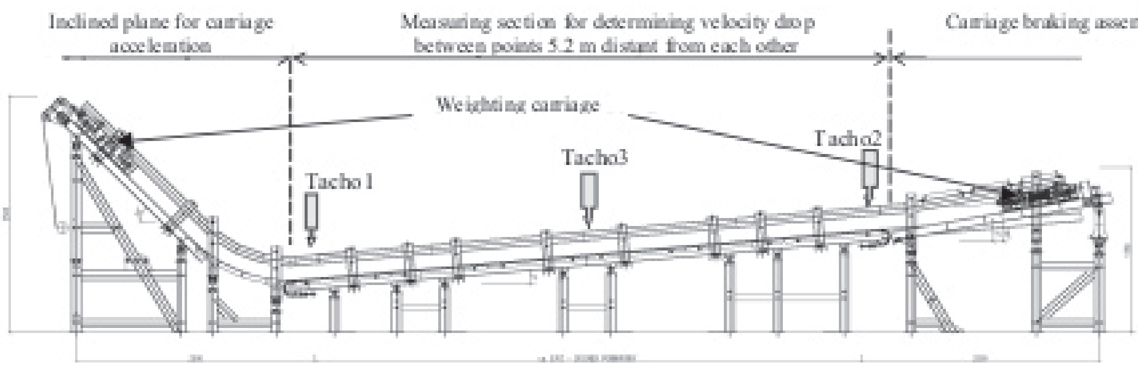

Fig. 10. Schematic of inclined-plane rig for testing belt-on-idler rolling resistance

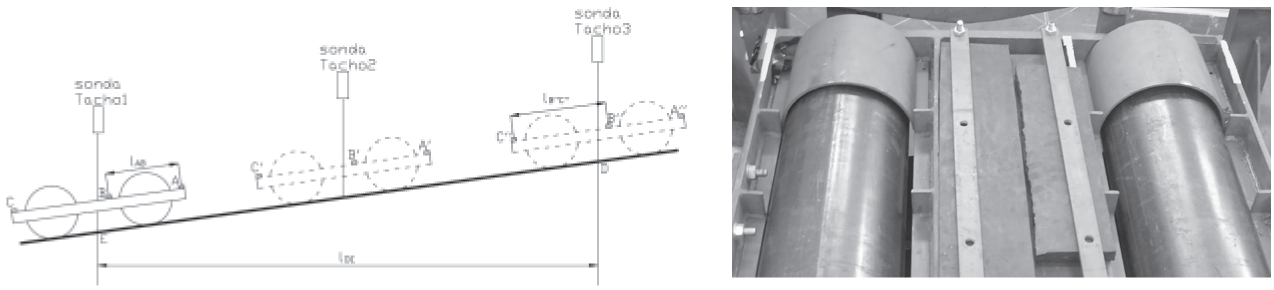

Fig. 11. Spacing of measuring points and view of measuring carriage

$$v_2 = \frac{l_{BC}}{\Delta t_{BC}} \tag{7}$$

where: l_{BC} – the distance between points B and C on the carriage, in m; Δt_{BC} – the measured time of travel between points B and C, in s; l_{AB} – the distance between points A and B on the carriage, in m; Δt_{AB} – the measured time of travel between points A and B, in s.

The drop in carriage kinetic energy during travel between points **D** and **E** amounts to:

$$\Delta E_k = \frac{1}{2}\cdot\left(m + \frac{I_r}{r^2}\right)\cdot\left(v_1^2 - v_2^2\right) \tag{8}$$

where: m – the weight of the carriage, in kg; I_r – the moment of inertia of a single idler roller, in kg·m²; r – the roller radius, in m; v_1 – the initial velocity, in m/s; v_2 – the end velocity, in m/s.

The kinetic energy changes as a result of the work of the external forces along distance l_{DE}. The sum of the external forces acting opposite to the direction of carriage travel amounts to:

$$\sum F = W_e + W_k + m\cdot g\cdot \sin\beta \tag{9}$$

The work of the external forces along the travel distance is described by the relation:

$$\Delta L = \left(W_e + W_k + m\cdot g\cdot\sin\beta\right)\cdot l_{DE} \tag{10}$$

where: W_e – indentation resistance (for two idlers in the carriage), in N; W_k – the total dynamic rotational resistance of the two rollers, in N; m – the weight of the carriage, in kg; g – gravitational acceleration, in m/s²; β – the inclination angle of the inclined plane, in °; l_{DE} – the measuring length, in m.

Since the work of the external forces and the drop in kinetic energy balance out: $\Delta E_k = \Delta L$, then taking into account equations (9) and (10) one gets this formula for the idler-on-belt rolling resistance (for the carriage with two rollers)

$$W_e = \frac{1}{2\cdot l_{DE}}\cdot\left(m + \frac{I_r}{r^2}\right)\cdot\left(v_1^2 - v_2^2\right) - W_k - m\cdot g\cdot\sin\beta \tag{11}$$

The results of tests carried out on the above rig can be used to compare the effect of belts of different type or various idler designs on rolling resistance. The unit linear belt rolling resistance determined in the way described above is compared for two types of idlers in fig. 12. The diagram clearly shows that idlers with a polyurethane shell generate greater rolling resistance, which is due to their lower stiffness and larger deformation under the radial force.

5. Tests on measuring segment of belt conveyor

Tests were carried out on specially prepared segment of a belt conveyor route in PGE KWB Bełchatów PLC to measure the total motion resistance per idler set. The total motion resistance of a single idler set is made up of the following components: the rotational resistance of three rollers, indentation resistance, flexure resistance of a belt and of a bulk material, sliding resistance of a belt on idlers (resulting from the random sideways running of the belt and the automatic deflection of the side idlers). The measuring idler set is suspended on both sides on three articulated elements (arranged in three mutually perpendicular directions). Force gauges **F1** and **F2** measuring the vertical load and the set's vertical load being the measure of the instantaneous conveyor output are installed on both sides of the idler set in the points of suspension. The total motion resistance

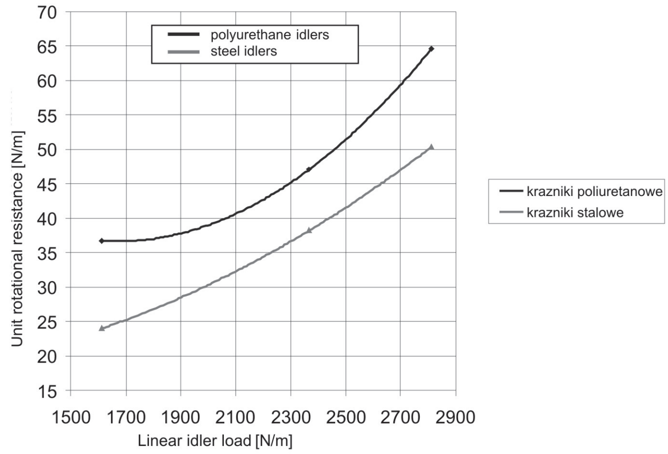

Fig. 12. Comparison of unit rolling resistance as function of linear idler load for idlers with metal shell and idlers with steel shell

per set is measured by pairs of force gauges **F3** and **F4** and **F5** and **F6** mounted on the horizontal elements on both sides of the set. Prior to starting the conveyor, initial forces F_{30}, F_{40}, F_{50} and F_{60} are set in the horizontal force gauges. As the belt moves, the initial horizontal forces registered by the gauges change. Forces F_3 and F_5 increase as follows:

$$F_3 = F_{30} + \Delta F_3 \tag{12}$$

$$F_5 = F_{50} + \Delta F_5 \tag{13}$$

Forces F_4 and F_6 decrease relative to their initial values:

$$F_4 = F_{40} - \Delta F_4 \tag{14}$$

$$F_6 = F_{60} - \Delta F_6 \tag{15}$$

In order to calculate the total motion resistance per idler set (W) one should add up all the force increments registered by the horizontal gauges during the operation of the conveyor:

$$W = \Delta F_3 + \Delta F_4 + \Delta F_5 + \Delta F_6 \tag{16}$$

It is important to properly position the idler set relative to the belt's axis and to the neighbouring idler sets. In order to eliminate any other idler loads (and so additional local motion resistance increments) it is important that the measuring idler set and the two neighbouring sets (the preceding one and the following one) are positioned in space in such a way that the axles of the idlers in the three consecutive sets lie exactly on one plane. The position of the idler sets is adjusted by means of rigging screws.

The measuring segment installed on the route of the tested overburden conveyor is shown in fig. 14.

During tests the trace of the resultant vertical force (the sum of readings from the two side force gauges **F1** and **F2)** and the trace of the resultant horizontal force (the total signal from the four force gauges **F3**, **F4**, **F5** and **F6**) are registered. The resultant vertical force is a measure of the conveyor's instantaneous output while the resultant horizontal force is the measured motion resistance per idler set.

The registered traces of instantaneous forces can be transformed into diagrams illustrating the dependence between the total idler set motion resistance and the load generated by the transported mining spoil and the belt. Figure 16 shows an exemplary overall diagram for the traces shown in fig. 15.

6. Conclusions

1. The accuracy of the computing methods is essential for analyses aimed at determining the effect of conveyor specifications on resistance to motion. In order to verify

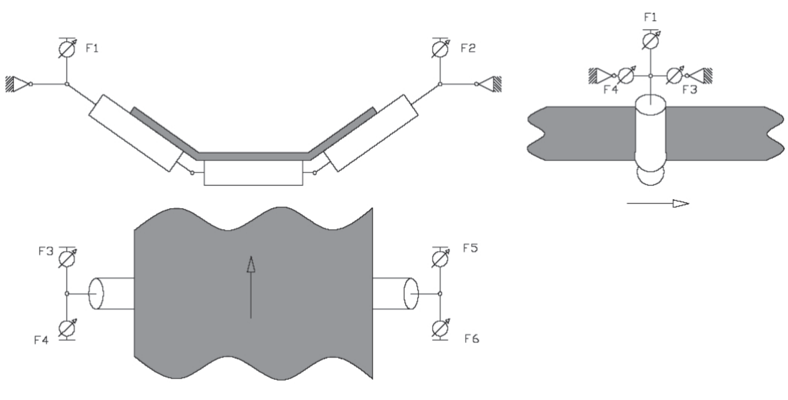

Fig. 13. Schematic of measuring idler set suspension and arrangement of force gauges

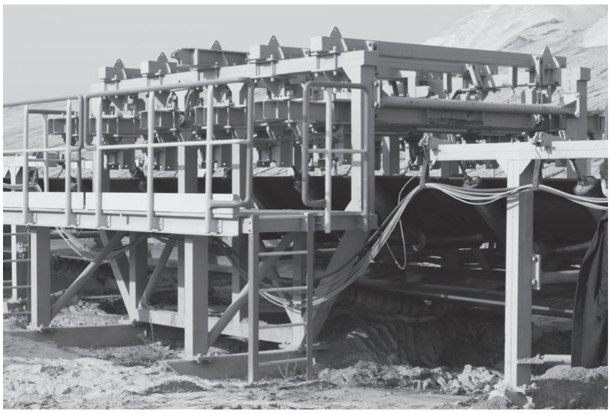

Fig. 14. Measuring segment for investigating motion resistance of single idler set

the methods it is necessary to carry out conveyor motion resistance measurements. Except for idler rotational resistance, the particular components of the primary conveyor resistances cannot be distinguished during measurements.

2. Measurements performed directly on the conveyor, during which the sum of all the components of the primary resistances is measured, supply the most data on its resistances to motion.
3. The present research aimed at reducing belt conveyor transport energy consumption focused on the two largest motion resistance components, i.e. idler rotational resistance and indentation resistance. The two components can be investigated on a special measuring rig with an inclined plane (fig. 10). Research aimed at determining the effect of the belt's parameters and different idler designs on the conveyor motion resistances is conducted on this rig.
4. Investigations of idler rotational resistance aimed at evaluating different idler designs can be conducted using the simple measuring rig shown in fig. 2 in section 3. In the case of idlers for conveyors operating in opencast lignite mines or for other high-capacity conveyors one needs to know the effect of the loads acting on the idlers on the latter's rotational resistance. For this purpose tests are conducted using a special rig with two loading wheels (fig. 5).
5. The tensometric measuring technique employing the specially designed measuring bolts has been verified in laboratory conditions and it can be successfully used for industrial measurements. Currently preparations for such measurements are underway in a brown coal mine and the technique will be used to register the forces and the rotational resistance for three roller idlers.

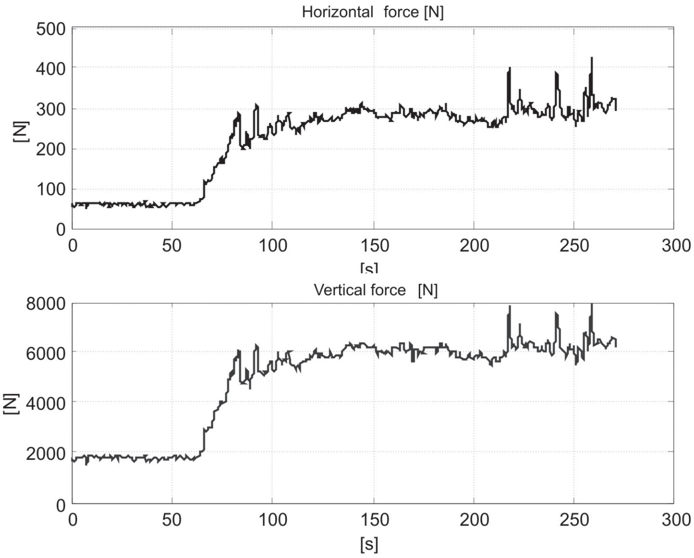

Fig. 15. Typical trace of instantaneous vertical force (mining spoil and belt load) and horizontal force (idler set motion resistance)

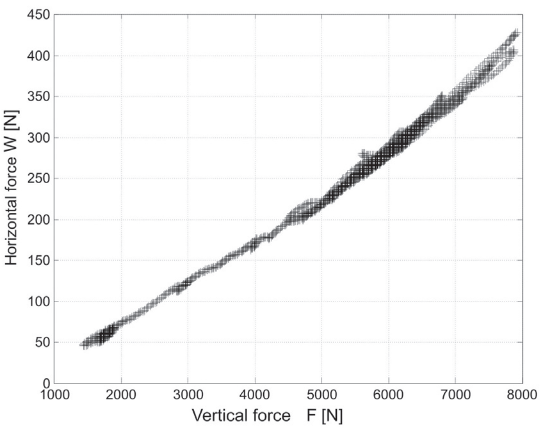

Fig. 16. Set of measuring points illustrating dependence between instantaneous horizontal force and vertical force

7. References

1. Bukowski J, Gładysiewicz L. Metoda badań oporów obracania krążników pod obciążeniem: Transport Przemysłowy i Maszyny Robocze 2010; 1: 1899-5489.
2. Furmanik K., Zarzycki J.: Badania laboratoryjne wybranych własności taśm przenośnikowych . Transport Przemysłowy i Maszyny Robocze 2009; 3: 1899-5489.
3. Geesmann F. Experimentelle and theoretischeUntersuchungen der Bewegungswiderstände von Gurtförderanlagen (Experimental and theoretical investigations of the motion resistances of belt conveyor systems). Thesis, Hanover University 2001.
4. Gładysiewicz L, Hardygóra M, Kawalec W. :Determining belt resistance. Bulk Handling Today. 2009; 5.
5. Gładysiewicz L, Król R. Badania wpływu warunków eksploatacyjnych na opory obracania krążników. Transport Przemysłowy 2003; 2: 1640-5455.
6. Gładysiewicz L, Król R. Kompleksowa ocena jakości krążników poliuretanowych stosowanych w górnictwie odkrywkowym. Prace Naukowe Instytutu Górnictwa Politechniki Wrocławskiej. Studia i Materiały 2009; 36.
7. Gładysiewicz L. Przenośniki taśmowe. Teoria i obliczenia. Oficyna Wydawnicza Politechniki Wrocławskiej. Wrocław 2003.
8. Hardygóra M, Bajda M, Gładysiewicz L. Wpływ parametrów mieszanek gumowych na energochłonność transportu przenośnikowego. Transport Przemysłowy 2007; 3: 1640-5455.
9. Kawalec W, Król R, Kubiak D. Długie przenośniki taśmowe dla kopalń rud miedzi. Nowoczesne metody eksploatacji węgla i skał zwięzłych. Kraków: Akademia Górniczo-Hutnicza im. Stanisława Staszica, 2009 (monografia).
10. Kasza P, Kulinowski P, Zarzycki J. Mobilne stanowisko do badania oporów obracania krążników. Transport Przemysłowy i Maszyny Robocze 2010; 3: 1899-5489.

Prof. Lech GŁADYSIEWICZ
Dr inż. Robert KRÓL
Mgr inż. Jędrzej BUKOWSKI
Institute of Mining
Wrocław University of Technology
Pl. Teatralny 2; 50-051 Wrocław
e-mail: lech.gladysiewicz@pwr.wroc.pl
e-mail: robert.krol@pwr.wroc.pl
e-mail: jedrzej.bukowski@pwr.wroc.pl

Sneh LATA
Amit KUMAR

MEHAR'S METHOD FOR ANALYZING THE FUZZY RELIABILITY OF PISTON MANUFACTURING SYSTEM

METODA MEHAR DO ANALIZY ROZMYTEJ NIEZAWODNOŚCI SYSTEMU PRODUKCJI TŁOKÓW

To the best of our knowledge till now there are only two analytical methods for finding the exact solution of fuzzy differential equations. In this paper, the shortcoming of one of these existing methods is pointed out. To overcome the shortcoming of the existing method, a new method, named as Mehar's method, is proposed for solving fuzzy differential equations. To show the advantage of Mehar's method over existing method the fuzzy Kolmogorov's differential equations, developed by using fuzzy Markov model of piston manufacturing system, are solved by using the existing and Mehar's method and it is shown that the results, obtained by using the existing method, may or may not be fuzzy number while the results, obtained by using Mehar's method, are always fuzzy number.

Keywords: *Fuzzy differential equations, fuzzy reliability, trapezoidal fuzzy number.*

Wedle naszej najlepszej wiedzy, do tej pory stworzono jedynie dwie metody analityczne precyzyjnego rozwiązywania rozmytych równań różniczkowych. W artykule wskazano wady jednej z istniejących metod oraz zaproponowano nową metodę rozwiązywania równań różniczkowych, nazwaną metodą Mehar, w której wady te zostały wyeliminowane. Aby wykazać przewagę metody Mehar nad istniejącą metodą, rozwiązano za pomocą obu tych metod rozmyte równania różniczkowe Kołmogorowa wyprowadzone przy użyciu rozmytego markowowskiego modelu systemu produkcji tłoków. Wykazano, że wyniki otrzymane z wykorzystaniem istniejącej metody, mogą ale nie muszą być liczbami rozmytymi, natomiast wyniki otrzymane przy pomocy metody Mehar zawsze stanowią liczbę rozmytą.

Słowa kluczowe: *rozmyte równania różniczkowe, rozmyta niezawodność, trapezoidalna liczba rozmyta.*

1. Introduction

Fuzzy differential equations are utilized for the purpose of modelling problems in science and engineering. The concept of a fuzzy derivative was first introduced by Chang and Zadeh [18] it was followed by Dubois and Prade [21], who defined and used the extension principle. Buckley and Feuring [14] introduced two analytical methods for solving n^{th} order linear differential equations with fuzzy initial conditions. Their first method of solution was to fuzzify the crisp solution and then checked to see if it satisfies the differential equation with fuzzy initial conditions and the second method was the reverse of the first method, in that they first solved the fuzzy initial value problem and then checked to see if it defines a fuzzy function.

In the last few years, lot of work has been done by several authors in theoretical and applied fields of fuzzy differential equations [1-10, 12, 13, 15-17, 19, 20, 22-24, 30-37, 39, 40].

In this paper, the shortcoming of one of these existing methods is pointed out. To overcome the shortcoming of the existing method, a new method, named as Mehar's method, is proposed for solving fuzzy differential equations. To show the advantage of Mehar's method over existing method the fuzzy Kolmogorov's differential equations, developed by using fuzzy Markov model of piston manufacturing system, are solved by using the existing and Mehar's method and it is shown that the results, obtained by using the existing method, may or may not be fuzzy number while the results, obtained by using Mehar's method, are always fuzzy number.

This paper is organized as follows: In Section 2, some basic definitions, arithmetic operations between intervals, arithmetic operations between trapezoidal fuzzy numbers and arithmetic operations between *JMD* trapezoidal fuzzy numbers are presented. In Section 3, the existing method for solving fuzzy differential equations is presented. The shortcoming of the existing method is discussed in Section 4. In Section 5, a new method, named as Mehar's method, is proposed to find the exact solution of fuzzy differential equations with the help of *JMD* representation of trapezoidal fuzzy numbers. Advantages of the proposed method over the existing method is shown in Section 6. In Section 7, advantages of *JMD* representation of trapezoidal fuzzy numbers over existing representation of trapezoidal fuzzy numbers is presented. In Section 8, fuzzy reliability of piston manufacturing system is evaluated. The conclusion is discussed in Section 9.

2. Preliminaries

In this section, some basic definitions, arithmetic operations between intervals, arithmetic operations between trapezoidal fuzzy numbers and arithmetic operations between *JMD* trapezoidal fuzzy numbers are presented.

2.1. Basic definitions

In this section, some basic definitions are presented [25].

2.1.1. *α*-cut

In this section, α-cut of a fuzzy number, zero α-cut and equality of α-cut are presented.

Definition 2.1. An α-cut of a fuzzy number $\widetilde{A}$ is defined as a crisp set $A_\alpha = \{x : \mu_{\widetilde{A}}(x) \geq \alpha, x \in X\}$, where $\alpha \in [0,1]$.

Definition 2.2. An α-cut $A_\alpha = [a,b]$ is said to be zero α-cut iff $a = 0$ and $b = 0$.

Definition 2.3. Two α-cuts $A_\alpha = [a_1,b_1]$ and $B_\alpha = [a_2,b_2]$ are said to be equal i.e., $A_\alpha = B_\alpha$ iff $a_1 = a_2$ and $b_1 = b_2$.

2.1.2. Trapezoidal fuzzy number

In this section, definitions of trapezoidal fuzzy number, zero trapezoidal fuzzy number and equality of trapezoidal fuzzy numbers are presented [25].

Definition 2.4 A fuzzy number $\widetilde{A} = (a,b,c,d)$ is said to be a trapezoidal fuzzy number if its membership function is given by

$$\mu_{\widetilde{A}}(x) = \begin{cases} 0, & -\infty < x \leq a, \\ \dfrac{(x-a)}{(b-a)}, & a \leq x < b, \\ 1, & b \leq x \leq c, \\ \dfrac{(x-d)}{(c-d)}, & c < x \leq d, \\ 0, & d \leq x < \infty. \end{cases}$$

Definition 2.5 A trapezoidal fuzzy number $\widetilde{A} = (a,b,c,d)$ is said to be zero trapezoidal fuzzy number iff $a=0$, $b=0$, $c=0$, $d=0$.

Definition 2.6 A trapezoidal fuzzy number $\widetilde{A} = (a,b,c,d)$ is said to be non-negative trapezoidal fuzzy number iff $a \geq 0$.

Definition 2.7 Two trapezoidal fuzzy numbers $\widetilde{A} = (a_1,b_1,c_1,d_1)$ and $\widetilde{B} = (a_2,b_2,c_2,d_2)$ are said to be equal i.e., $\widetilde{A} = \widetilde{B}$ iff $a_1 = a_2$, $b_1 = b_2$, $c_1 = c_2$, $d_1 = d_2$.

2.1.3. *JMD* representation of trapezoidal fuzzy number

Kumar and Kaur [28] proposed *JMD* representation of trapezoidal fuzzy number and proved that it is better to use the proposed representation of trapezoidal fuzzy numbers instead of existing representation of trapezoidal fuzzy numbers for finding the fuzzy optimal solution of fuzzy transportation problems. In this section, definitions of *JMD* trapezoidal fuzzy number, zero *JMD* trapezoidal fuzzy number and equality of *JMD* trapezoidal fuzzy numbers are presented.

Definition 2.8. Let (a,b,c,d) be a trapezoidal fuzzy number then its *JMD* representation is $(x,\alpha,\beta,\gamma)_{JMD}$, where $x = a$, $\alpha = b - a \geq 0$, $\beta = c - b \geq 0$, $\gamma = d - c \geq 0$.

Definition 2.9. A trapezoidal fuzzy number $\widetilde{A} = (x,\alpha,\beta,\gamma)_{JMD}$ is said to be zero trapezoidal fuzzy number if and only if $x=0$, $\alpha=0$, $\beta=0$, $\gamma=0$.

Definition 2.10. A trapezoidal fuzzy number $\widetilde{A} = (x,\alpha,\beta,\gamma)_{JMD}$ is said to be non-negative trapezoidal fuzzy number if and only if $x \geq 0$.

Definition 2.11. Two trapezoidal fuzzy numbers $\widetilde{A} = (x_1,\alpha_1,\beta_1,\gamma_1)_{JMD}$ and $\widetilde{B} = (x_2,\alpha_2,\beta_2,\gamma_2)_{JMD}$ are said to be equal i.e., $\widetilde{A} = \widetilde{B}$ if and only if $x_1 = x_2$, $\alpha_1 = \alpha_2$, $\beta_1 = \beta_2$, $\gamma_1 = \gamma_2$.

2.2. Arithmetic operations

In this section, arithmetic operations between intervals, trapezoidal fuzzy numbers and *JMD* trapezoidal fuzzy number are presented.

2.2.1. Arithmetic operations between intervals

In this section, some arithmetic operations between intervals are presented [25].

Let $A = [a_1, b_1]$, $B = [a_2, b_2]$ be two intervals then

(i) $A + B = [a_1 + a_2, b_1 + b_2]$

(ii) $A - B = [a_1 - b_2, b_1 - a_2]$

(iii) $\lambda A = \begin{cases} (\lambda x_1, \lambda y_1, \lambda z_1, \lambda w_1), & \lambda \geq 0 \\ (\lambda w_1, \lambda z_1, \lambda y_1, \lambda x_1), & \lambda \leq 0 \end{cases}$

(iv) $AB = [a,b]$, where, a = minimum $(a_1a_2, a_1b_2, a_2b_1, b_1b_2)$ and b = maximum $(a_1a_2, a_1b_2, a_2b_1, b_1b_2)$

2.2.2. Arithmetic operations between trapezoidal fuzzy numbers

In this section, arithmetic operations between trapezoidal fuzzy numbers are presented [25].

Let $\widetilde{A}_1 = (x_1,y_1,z_1,w_1)$ and $\widetilde{A}_2 = (x_2,y_2,z_2,w_2)$ be two trapezoidal fuzzy numbers, then

(i) $\widetilde{A}_1 \oplus \widetilde{A}_2 = (x_1 + x_2, y_1 + y_2, z_1 + z_2, w_1 + w_2)$

(ii) $\widetilde{A}_1 \ominus \widetilde{A}_2 = (x_1 - w_2, y_1 - z_2, z_1 - y_2, w_1 - x_2)$

(iii) $\lambda \widetilde{A}_1 = \begin{cases} (\lambda x_1, \lambda y_1, \lambda z_1, \lambda w_1), & \lambda \geq 0 \\ (\lambda w_1, \lambda z_1, \lambda y_1, \lambda x_1), & \lambda \leq 0 \end{cases}$

(iv) $\widetilde{A}_1 \otimes \widetilde{A}_2 \simeq$ (minimum (x), minimum (y), maximum (y), maximum (x)),
where $x = (x_1x_2, x_1w_2, w_1x_2, w_1w_2)$ and $y = (y_1y_2, y_1z_2, z_1y_2, z_1z_2)$.

2.2.3. Arithmetic operations between *JMD* trapezoidal fuzzy numbers

In this section, arithmetic operations between *JMD* trapezoidal fuzzy numbers are presented [28].

Let $\widetilde{A}_1 = (x_1,\alpha_1,\beta_1,\gamma_1)_{JMD}$ and $\widetilde{A}_2 = (x_2,\alpha_2,\beta_2,\gamma_2)_{JMD}$ be two *JMD* trapezoidal fuzzy numbers, then

(i) $\widetilde{A}_1 \oplus \widetilde{A}_2 = (x_1 + x_2, \alpha_1 + \alpha_2, \beta_1 + \beta_2, \gamma_1 + \gamma_2)_{JMD}$

(ii) $\widetilde{A}_1 \ominus \widetilde{A}_2 = (x_1 - x_2 - \alpha_2 - \beta_2 - \gamma_2, \alpha_1 + \gamma_2, \beta_1 + \beta_2, \alpha_2 + \gamma_1)_{JMD}$

(iii) $\lambda A_1 = \begin{cases} (\lambda x_1, \lambda\alpha_1, \lambda\beta_1, \lambda\gamma_1)_{JMD}, & \lambda \geq 0 \\ (\lambda x_1 + \lambda\alpha_1 + \lambda\beta_1 + \lambda\gamma_1, -\lambda\gamma_1, -\lambda\beta_1, -\lambda\alpha_1)_{JMD}, & \lambda \leq 0. \end{cases}$

(iv) $\tilde{A}_1 \otimes \tilde{A}_2 \simeq$ (minimum (x), minimum (y) − minimum (x), maximum (y) − minimum (y), maximum (x) − maximum (y)), where

$$x = (x_1x_2, x_1x_2 + x_1\alpha_2 + x_1\beta_2 + x_1\gamma_2, x_1x_2 + x_2\alpha_1 + x_2\beta_1 + x_2\gamma_1,$$
$$x_1x_2 + x_1\alpha_2 + x_1\beta_2 + x_1\gamma_2 + x_2\alpha_1 + \alpha_1\alpha_2 + \alpha_1\beta_2 + \alpha_1\gamma_2 +$$
$$+ x_2\beta_1 + \beta_1\alpha_2 + \beta_1\beta_2 + \beta_1\gamma_2 + x_2\gamma_1 + \gamma_1\alpha_2 + \gamma_1\beta_2 + \gamma_1\gamma_2)$$

and

$$y = (x_1x_2 + x_1\alpha_2 + x_2\alpha_1 + \alpha_1\alpha_2, x_1x_2 + x_1\alpha_2 + x_1\beta_2 + x_2\alpha_1 +$$
$$+ \alpha_1\alpha_2 + \alpha_1\beta_2, x_1x_2 + x_1\alpha_2 + x_2\alpha_1 + \alpha_1\alpha_2 +$$
$$x_2\beta_1 + \beta_1\alpha_2, x_1x_2 + x_1\alpha_2 + x_1\beta_2 + x_2\alpha_1 + \alpha_1\alpha_2 +$$
$$+ \alpha_1\beta_2 + x_2\beta_1 + \beta_1\alpha_2 + \beta_1\beta_2)$$

Remark 2.1. Let $\tilde{A}_1 = (x_1, y_1, z_1, w_1)$ be a *JMD* trapezoidal fuzzy number and $\tilde{A}_2 = (x_2, y_2, z_2, w_2)$ be a non-negative *JMD* trapezoidal fuzzy number, then

$$\tilde{A}_1 \otimes \tilde{A}_2 \cong \begin{cases} (x_1x_2, y_1y_2, z_1z_2, w_1w_2) & x_1 \geq 0 \\ (x_1w_2, y_1y_2, z_1z_2, w_1w_2) & x_1 < 0 \text{ and } y_1 \geq 0 \\ (x_1w_2, y_1z_2, z_1z_2, w_1w_2) & y_1 < 0 \text{ and } z_1 \geq 0 \\ (x_1w_2, y_1z_2, z_1y_2, w_1w_2) & z_1 < 0 \text{ and } w_1 \geq 0 \\ x_1w_2, y_1z_2, z_1y_2, w_1x_2) & \text{otherwise} \end{cases}$$

Remark 2.2. Let $\tilde{A}_1 = (x_1, \alpha_1, \beta_1, \gamma_1)_{JMD}$ be a *JMD* trapezoidal fuzzy number and $\tilde{A}_2 = (x_2, \alpha_2, \beta_2, \gamma_2)_{JMD}$ be a non-negative *JMD* trapezoidal fuzzy number, then

$$\tilde{A}_1 \otimes \tilde{A}_2 \cong$$

$$\begin{cases} (x_1x_2, x_1\alpha_2 + x_2\alpha_1 + \alpha_1\alpha_2, x_1\beta_2 + \alpha_1\beta_2 + x_2\beta_1 + \alpha_2\beta_1 + \\ \beta_1\beta_2, x_1\gamma_2 + \alpha_1\gamma_2 + \beta_1\gamma_2 + x_2\gamma_1 + \alpha_2\gamma_1 + \beta_2\gamma_1 + \gamma_1\gamma_2)_{JMD}, & x_1 \geq 0 \\ x_1x_2 + x_1\alpha_2 + x_1\beta_2 + x_1\gamma_2, x_2\alpha_1 + \alpha_1\alpha_2 - x_1\beta_2 - x_1\gamma_2, \\ x_1\beta_2 + \alpha_1\beta_2 + x_2\beta_1 + \beta_1\alpha_2 + \beta_1\beta_2, x_1\gamma_2 + \alpha_1\gamma_2 + \beta_1\gamma_2 + \\ x_2\gamma_1 + \gamma_1\alpha_2 + \gamma_1\beta_2 + \gamma_1\gamma_2)_{JMD}, & x_1 < 0 \text{ and } x_1 + \alpha_1 \geq 0 \\ x_1x_2 + x_1\alpha_2 + x_1\beta_2 + x_1\gamma_2, x_1\beta_2 + x_2\alpha_1 + \alpha_1\alpha_2 + \alpha_1\beta_2 - \\ x_1\beta_1 - x_1\gamma_2, x_2\beta_1 + \beta_1\alpha_2 + \beta_1\beta_2, x_1\gamma_2 + \alpha_1\gamma_2 + \beta_1\gamma_2 + \\ x_2\gamma_1 + \gamma_1\alpha_2 + \gamma_1\beta_2 + \gamma_1\gamma_2)_{JMD}, & x_1 + \alpha_1 < 0 \text{ and } x_1 + \alpha_1 + \beta_1 \geq 0 \\ x_1x_2 + x_1\alpha_2 + x_1\beta_2 + x_1\gamma_2, x_2\alpha_1 + \alpha_1\alpha_2 + \alpha_1\beta_2 - x_1\gamma_2, \\ x_2\beta_1 + \beta_1\alpha_2 - x_1\beta_2 - \alpha_1\beta_2, x_1\beta_2 + x_1\gamma_2 + \alpha_1\beta_2 + \alpha_1\gamma_2 + \\ \beta_1\beta_2 + \beta_1\gamma_2 + x_2\gamma_1 + \gamma_1\alpha_2 + \gamma_1\beta_2 + \gamma_1\gamma_2)_{JMD}, & x_1 + \alpha_1 + \beta_1 < 0 \text{ and } x_1 + \alpha_1 + \beta_1 + \gamma_1 \geq 0 \\ x_1x_2 + x_1\alpha_2 + x_1\beta_2 + x_1\gamma_2, x_2\alpha_1 + \alpha_1\alpha_2 + \alpha_1\beta_2 - x_1\gamma_2, \\ x_2\beta_1 + \beta_1\alpha_2 - x_1\beta_2 - \alpha_1\beta_2, x_2\gamma_1 - x_1\alpha_2 - \alpha_1\alpha_2 - \beta_1\alpha_2)_{JMD}, & \text{otherwise.} \end{cases}$$

3. Existing method

Buckley and Feuring [14] introduced two analytical methods for solving fuzzy initial value problem for n^{th} order linear differential equations. In this section, one of these existing methods for solving fuzzy differential equations is presented.

The solution of fuzzy initial value problem for n^{th} order fuzzy linear differential equation

$$\tilde{a}_n\tilde{y}^{(n)} \oplus \tilde{a}_{n-1}\tilde{y}^{(n-1)} \oplus ... \oplus \tilde{a}_1\tilde{y}^{(1)} \oplus \tilde{a}_0\tilde{y} =$$
$$= \tilde{g}(x), \tilde{y}(0) = \tilde{\gamma}_0, \tilde{y}^{(1)}(0) = \tilde{\gamma}_1, ..., \tilde{y}^{(n-1)}(0) = \tilde{\gamma}_{n-1} \qquad (1)$$

where, $\tilde{y}^{(i)} = \dfrac{d^i\tilde{y}}{dx^i}$ for $i = n, n\text{-}1, ..., 1$, $\tilde{a}_n$ is a non zero trapezoidal fuzzy number and $\tilde{a}_{n-1}, \tilde{a}_{n-2}, ..., \tilde{a}_1, \tilde{a}_0$ are any type of trapezoidal fuzzy numbers, can be obtained by using the following steps of the existing method:

Step 1: Find the α-cut $[a_{n(1)}(x,\alpha), a_{n(2)}(x,\alpha)]$, $[a_{n-1(1)}(x,\alpha), a_{n-1(2)}(x,\alpha)], ...,$ $[a_{1(1)}(x,\alpha), a_{1(2)}(x,\alpha)], [a_{0(1)}(x,\alpha), a_{0(2)}(x,\alpha)]$, $[y_1^{(n)}(x,\alpha), y_2^{(n)}(x,\alpha)]$, $[y_1^{(n-1)}(x,\alpha), y_2^{(n-1)}(x,\alpha)]$, ..., $[y_1^{(1)}(x,\alpha), y_2^{(1)}(x,\alpha)]$, $[y_1(x,\alpha), y_2(x,\alpha)]$ and $[\gamma_{0(1)}(0,\alpha), \gamma_{0(2)}(0,\alpha)], [\gamma_{1(1)}(0,\alpha), \gamma_{1(2)}(0,\alpha)], ...,$ $[\gamma_{n-1(1)}(0,\alpha), \gamma_{n-1(2)}(0,\alpha)]$ corresponding to fuzzy parameters $\tilde{a}_n, \tilde{a}_{n-1}, \tilde{a}_{n-2}, ..., \tilde{a}_1, \tilde{a}_0, \tilde{y}^{(n)}, \tilde{y}^{(n-1)}, ..., \tilde{y}^{(1)}, \tilde{y}$ and $\tilde{\gamma}_0, \tilde{\gamma}_1, ..., \tilde{\gamma}_{n-1}$ respectively.

Step 2: Convert the fuzzy initial value problem for n^{th} order fuzzy linear differential equation (1), into the following n^{th} order differential equation:

$$[a_{n(1)}(x,\alpha), a_{n(2)}(x,\alpha)][y_1^{(n)}(x,\alpha), y_2^{(n)}(x,\alpha)] + [a_{n-1(1)}(x,\alpha), a_{n-1(2)}(x,\alpha)]$$
$$[y_1^{(n-1)}(x,\alpha), y_2^{(n-1)}(x,\alpha)] + ... +$$
$$+ [a_{1(1)}(x,\alpha), a_{1(2)}(x,\alpha)][y_1^{(1)}(x,\alpha), y_2^{(1)}(x,\alpha)] +$$
$$+ [a_{0(1)}(x,\alpha), a_{0(2)}(x,\alpha)]\,[y_1(x,\alpha), y_2(x,\alpha)] = [g(x), g(x)],$$
$$[y_1(0,\alpha), y_2(0,\alpha)] = [\gamma_{0(1)}(0,\alpha), \gamma_{0(2)}(0,\alpha)],$$
$$[y_1^{(1)}(0,\alpha), y_2^{(1)}(0,\alpha)] = [\gamma_{1(1)}(0,\alpha), \gamma_{1(2)}(0,\alpha)] ...,$$
$$[y_1^{(n-1)}(0,\alpha), y_2^{(n-1)}(0,\alpha)] = [\gamma_{n-1(1)}(0,\alpha), \gamma_{n-1(2)}(0,\alpha)]$$

Step 3: Convert the n^{th} order differential equation, obtained from Step 2, into the following ordinary differential equations

$$b_ny^{(n)} + b_{n-1}y^{(n-1)} + ... + b_1y^{(1)} + b_0y = g(x)$$
$$y_1(0,\alpha) = \gamma_{0(1)}(0,\alpha), y_1^{(1)}(0,\alpha) = \gamma_{1(1)}(0,\alpha), ..., y_1^{(n-1)}(0,\alpha) = \gamma_{n-1(1)}(0,\alpha)$$
$$c_ny^{(n)} + c_{n-1}y^{(n-1)} + ... + c_1y^{(1)} + c_0y = g(x)$$
$$y_2(0,\alpha) = \gamma_{0(2)}(0,\alpha), y_2^{(1)}(0,\alpha) = \gamma_{2(1)}(0,\alpha), ..., y_2^{(n-1)}(0,\alpha) = \gamma_{n-1(2)}(0,\alpha)$$

where,

$$b_iy^{(i)} = \text{minimum } (a_{i(1)}(x,\alpha)y_1^{(i)}(x,\alpha), a_{i(1)}(x,\alpha)y_2^{(i)}(x,\alpha),$$
$$a_{i(2)}(x,\alpha)y_1^{(i)}(x,\alpha), a_{i(2)}(x,\alpha)y_2^{(i)}(x,\alpha))$$

and

$$c_iy^{(i)} = \text{maximum } (a_{i(1)}(x,\alpha)y_1^{(i)}(x,\alpha), a_{i(1)}(x,\alpha)y_2^{(i)}(x,\alpha),$$
$$a_{i(2)}(x,\alpha)y_1^{(i)}(x,\alpha), a_{i(2)}(x,\alpha)y_2^{(i)}(x,\alpha))$$

for $i = n, n\text{-}1, ..., 1, 0$.

Step 4: Solve the ordinary differential equations, obtained from Step 3, to find the values of $y_1(x_0, \alpha)$ and $y_2(x_0, \alpha)$ corresponding to $x = x_0$, where x_0 is any real number.

Step 5: Check that $[y_1(x_0,\alpha), y_2(x_0,\alpha)]$ defines the α-cut of a fuzzy number or not i.e., for the values of $y_1(x_0,\alpha)$ and $y_2(x_0,\alpha)$, the following conditions are satisfied or not.

(i) $y_1(x_0,\alpha)$ a monotonically increasing function for $\alpha \in [0,1]$

(ii) $y_2(x_0,\alpha)$ a monotonically decreasing function for $\alpha \in [0,1]$

(iii) $y_1(x_0,1) = y_2(x_0,1)$

Case 1: If $[y_1(x_0,\alpha)\ y_2(x_0,\alpha)]$ defines the α-cut of a fuzzy number then the fuzzy solution $\tilde{y}(x_0)$ of fuzzy differential equation (1) exist and $[y_1(x_0,\alpha), y_2(x_0,\alpha)]$ represents the α-cut corresponding to fuzzy solution $\tilde{y}(x_0)$.

Case 2: If $[y_1(x_0,\alpha)\ y_2(x_0,\alpha)]$ does not define the α-cut of a fuzzy number then the fuzzy solution $\tilde{y}(x_0)$ of fuzzy differential equation (1) does not exist.

4. Shortcoming of existing method in real life problems

Several authors have proposed different methods for analyzing the fuzzy reliability of industrial systems. One of the existing method for analyzing the fuzzy reliability is by using the fuzzy Markov model [11, 26, 27, 29, 38], in which fuzzy Kolomogorov's differential equations are developed with the help of fuzzy Markov model and the fuzzy reliability is evaluated by solving the obtained fuzzy Kolomogorov's differential equations.

In this section, the set of fuzzy Kolomogorov's differential equations, obtained by using fuzzy Markov model of a piston manufacturing system, is solved by using one of the analytical methods [14] and it is shown that the obtained solution may or may not be a fuzzy number. Due to which the solution of fuzzy differential equations, obtained by using the existing method, can not be used to analyze the fuzzy reliability of piston manufacturing system.

4.1. Fuzzy Markov modeling of piston manufacturing system

Piston manufacturing system consists of two sub-systems namely R_1 and R_2 , which are connected in series. Further the sub-system R_1 consists of six sub-systems namely *A,B,C,D,E* and *F* and similarly, six sub-systems namely *G,H,I,J,K* and *L* constitute the sub-system R_2. Markov models for the sub-systems R_1 and R_2 are shown in Figure 1 and Figure 2 respectively.

The operations that are performed on these machines or sub-systems are as follows:

1. **Sub-system** *A* **(Fixture Seat Machine):** This machine is used to clamp the piston.
2. **Sub-system** *B* **(Rough Grooving and Turning Machine):** On this machine, rough grooves are made on piston. Turning operation is performed on this machine i.e., to bring the dia of piston to proper size.
3. **Sub-system** *C* **(Rough Pin Hole Boring Machine):** Pin hole boring operation is performed using this machine i.e., proper size is given to holes.
4. **Sub-system** *D* **(Oil Hole Drilling Machine):** On this machine, one hole is made on the piston to supply the oil. The oil is used to move piston in cylinder smoothly.
5. **Sub-system** *E* **(Finishing Grooving Machine):** On this machine, the finishing is given to rough grooves which are prepared using sub-system *B*.
6. **Sub-system** *F* **(Finish Profile Turning Machine):** Oval shape is given to piston using this machine.
7. **Sub-system** *G* **(Finish Pin Hole Boring Machine):** On this machine, finishing is given to the pin hole portion which is prepared using sub-system *C*.

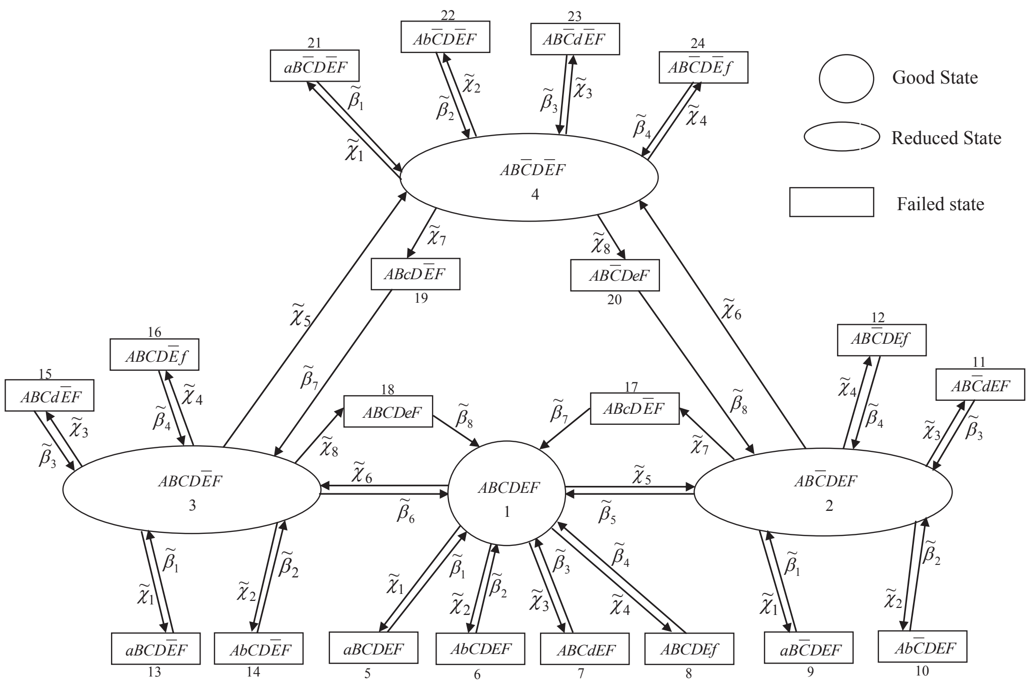

Fig. 1. Fuzzy Markov model of sub-system R_1

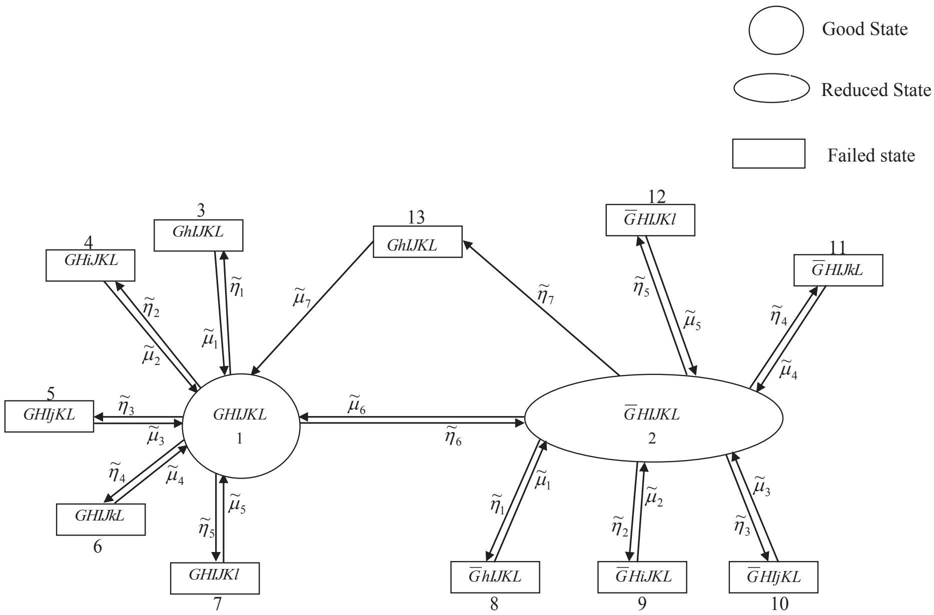

Fig. 2. Fuzzy Markov model of sub-system R_2

8. **Sub-system** H **(Finish Crown and Cavity Machine):** On this machine, finishing operation is performed on the crown of piston.
9. **Sub-system** I **(Valve Milling Machine):** On this machine, valve recess is made on the piston.
10. **Sub-system** J **(Chamfering or Radius Machine):** This machine rounds off the corners of the piston, so that it can run smoothly in the cylinder.
11. **Sub-system** K **(Circlip Grooving Machine):** On this machine, circlip grooves are made on the piston.
12. **Sub-system** L **(Piston Cleaning Machine):** This machine is used to clean the inside and outside portion of the piston.

4.2. Notation

In this section, notation that is used to analyze the fuzzy reliability of piston manufacturing system are presented:

1. A,B,C,D,E,F and G,H,I,J,K,L denote good conditions of sub-systems of R_1 and R_2 respectively.
2. The symbols a,b,c,d,e,f,g,h,i,j,k and l represent the failed state of the sub-systems A,B,C,D,E,F,G,H,I,J,K and L respectively.
3. $\overline{C},\overline{E}$ and $\overline{G}$ indicate that the sub-systems C,E and G are working in reduced state.
4. $\tilde{\chi}_i$ (i=1 to 8) represents the fuzzy failure rates of the relevant sub-systems, when the transition is from A to a, B to b, D to d, F to f, C to $\overline{C}$, E to $\overline{E}$, $\overline{C}$ to c and $\overline{E}$ to e respectively.
5. $\tilde{\beta}_i$ (i=1 to 8) represents the fuzzy repair rates of the relevant sub-systems, when the transition is from a to A, b to B, d to D, f to F, $\overline{C}$ to C, $\overline{E}$ to E, c to C and e to E respectively.
6. $\tilde{\eta}_i$ (i=1 to 7) represents the fuzzy failure rates of the relevant sub-systems, when the transition is from H to h, I to i, J to j, K to k, L to l, G to $\overline{G}$ and $\overline{G}$ to g respectively.
7. $\tilde{\mu}_i$ (i=1 to 7) represents the fuzzy repair rates of the relevant sub-systems, when the transition is from h to H, i to I, j to J, k to K, l to L, $\overline{G}$ to G and g to G respectively.
8. $\tilde{P}_j(t), j=1,2,...,n$ represents the fuzzy probability that the system is in state S_j at time t, where n is number of states. $\tilde{P}_j'(t), j=1,2,...,n$ represents derivative of $\tilde{P}_j(t)$ with respect to t.
9. $\tilde{R}_1(t)$ and $\tilde{R}_2(t)$ denote the fuzzy reliability of the sub-systems R_1 and R_2 respectively.
10. $\tilde{R}(t)$ represents the fuzzy reliability of the whole system.

4.3. Assumptions

In this section, the assumptions that are used for analyzing the fuzzy reliability of piston manufacturing system are presented:

(i) Fuzzy failure rates and fuzzy repair rates are independent with each other and their unit is per hour.
(ii) There are no simultaneous failures among the sub-systems.
(iii) Sub-systems C,E and G fails through reduced states only.

4.4. Data

On the basis of the perception of the experts, the appropriate failure rates and repair rates for the different sub-systems of R_1 and R_2, represented by trapezoidal fuzzy numbers, are shown in table 1 and table 2 respectively.

4.5. Fuzzy Kolmogorov's differential equations for the sub-systems R_1 and R_2

In this section, fuzzy Kolmogorov's differential equations are developed by using the Markov model for the sub-systems R_1 and R_2.

Fuzzy Kolmogorov's differential equations for the sub-system R_1 associated with the Markov model (Figure 1) are:

Tab. 1. Fuzzy failure rates and fuzzy repair rates for the different sub-systems of R_1

Fuzzy failure rate	Fuzzy repair rate
$\tilde{\chi}_1$=(0.00105,0.00126,0.00154,0.00175)	$\tilde{\beta}_1$=(1.026,1.0584,1.1016,1.134)
$\tilde{\chi}_2$=(0.00045,0.00054,0.00066,0.00075)	$\tilde{\beta}_2$=(0.04085,0.04214,0.04386,0.04515)
$\tilde{\chi}_3$=(0.000675,0.00081,0.00099,0.001125)	$\tilde{\beta}_3$=(0.475,0.49,0.51,0.525)
$\tilde{\chi}_4$=(0.000675,0.00081,0.00099,0.001125)	$\tilde{\beta}_4$=(0.2717,0.28028,0.29172,0.3003)
$\tilde{\chi}_5$=(0.0156,0.01872,0.02288,0.026)	$\tilde{\beta}_5$=(0.1463,0.15092,0.15702,0.1617)
$\tilde{\chi}_6$=(0.0156,0.01872,0.02288,0.026)	$\tilde{\beta}_6$=(0.2375,0.245,0.255,0.2625)
$\tilde{\chi}_7$=(0.000675,0.00081,0.00099,0.001125)	$\tilde{\beta}_7$=(0.05605,0.05782,0.06018,0.06195)
$\tilde{\chi}_8$=(0.002925,0.00351,0.00429,0.004875)	$\tilde{\beta}_8$=(0.08265,0.08526,0.08874,0.09135)

Tab. 2. Fuzzy failure rates and fuzzy repair rates for the different sub-systems of R_2

Fuzzy failure rate	Fuzzy repair rate
$\tilde{\eta}_1$=(0.00105,0.00126,0.00154,0.00175)	$\tilde{\mu}_1$=(0.3135,0.3234,0.3366,0.3465)
$\tilde{\eta}_2$=(0.00023,0.00027,0.00033,0.00038)	$\tilde{\mu}_2$=(0.475,0.49,0.51,0.525)
$\tilde{\eta}_3$=(0.00008,0.00009,0.00011,0.00013)	$\tilde{\mu}_3$=(0.6365,0.6566,0.6834,0.7035)
$\tilde{\eta}_4$=(0.00023,0.00027,0.00033,0.00038)	$\tilde{\mu}_4$=(0.03325,0.0343,0.0357,0.03675)
$\tilde{\eta}_5$=(0.00008,0.00009,0.00011,0.00013)	$\tilde{\mu}_5$=(2.8785,2.9694,3.0906,3.1815)
$\tilde{\eta}_6$=(0.0156,0.01872,0.02288,0.026)	$\tilde{\mu}_6$=(0.2109,0.21756,0.22644,0.2331)
$\tilde{\eta}_7$=(0.003,0.0036,0.0044,0.005)	$\tilde{\mu}_7$=(0.11875,0.1225,0.1275,0.13125)

$$
\begin{aligned}
&\tilde{P}_1^{(1)}(t)\oplus\tilde{\lambda}_1\tilde{P}_1(t)=\tilde{\beta}_1\tilde{P}_5(t)\oplus\tilde{\beta}_2\tilde{P}_6(t)\oplus\tilde{\beta}_3\tilde{P}_7(t)\oplus\tilde{\beta}_4\tilde{P}_8(t)\\
&\qquad\oplus\tilde{\beta}_5\tilde{P}_2(t)\oplus\tilde{\beta}_6\tilde{P}_3(t)\oplus\tilde{\beta}_7\tilde{P}_{17}(t)\oplus\tilde{\beta}_8\tilde{P}_{18}(t)\\
&\tilde{P}_2^{(1)}(t)\oplus\tilde{\lambda}_2\tilde{P}_2(t)=\tilde{\beta}_1\tilde{P}_9(t)\oplus\tilde{\beta}_2\tilde{P}_{10}(t)\oplus\tilde{\beta}_3\tilde{P}_{11}(t)\oplus\tilde{\beta}_4\tilde{P}_{12}(t)\\
&\qquad\oplus\tilde{\beta}_8\tilde{P}_{20}(t)\oplus\tilde{\chi}_5\tilde{P}_1(t)\\
&\tilde{P}_3^{(1)}(t)\oplus\tilde{\lambda}_3\tilde{P}_3(t)=\tilde{\beta}_1\tilde{P}_{13}(t)\oplus\tilde{\beta}_2\tilde{P}_{14}(t)\oplus\tilde{\beta}_3\tilde{P}_{15}(t)\oplus\tilde{\beta}_4\tilde{P}_{16}(t)\\
&\qquad\oplus\tilde{\beta}_7\tilde{P}_{19}(t)\oplus\tilde{\chi}_6\tilde{P}_1(t)\\
&\tilde{P}_4^{(1)}(t)\oplus\tilde{\lambda}_4\tilde{P}_4(t)=\tilde{\beta}_1\tilde{P}_{21}(t)\oplus\tilde{\beta}_2\tilde{P}_{22}(t)\oplus\tilde{\beta}_3\tilde{P}_{23}(t)\oplus\tilde{\beta}_4\tilde{P}_{24}(t)\\
&\qquad\oplus\tilde{\chi}_5\tilde{P}_3(t)\oplus\tilde{\chi}_6\tilde{P}_2(t)\\
&\tilde{P}_{4+i}^{(1)}(t)\oplus\tilde{\beta}_i\tilde{P}_{4+i}(t)=\tilde{\chi}_i\tilde{P}_1(t), i=1,2,3,4\\
&\tilde{P}_{8+i}^{(1)}(t)\oplus\tilde{\beta}_i\tilde{P}_{8+i}(t)=\tilde{\chi}_i\tilde{P}_2(t), i=1,2,3,4 \qquad \text{(S1)}\\
&\tilde{P}_{12+i}^{(1)}(t)\oplus\tilde{\beta}_i\tilde{P}_{12+i}(t)=\tilde{\chi}_i\tilde{P}_3(t), i=1,2,3,4\\
&\tilde{P}_{17}^{(1)}(t)\oplus\tilde{\beta}_7\tilde{P}_{17}(t)=\tilde{\chi}_7\tilde{P}_2(t)\\
&\tilde{P}_{18}^{(1)}(t)\oplus\tilde{\beta}_8\tilde{P}_{18}(t)=\tilde{\chi}_8\tilde{P}_3(t)\\
&\tilde{P}_{19}^{(1)}(t)\oplus\tilde{\beta}_7\tilde{P}_{19}(t)=\tilde{\chi}_7\tilde{P}_4(t)\\
&\tilde{P}_{20}^{(1)}(t)\oplus\tilde{\beta}_8\tilde{P}_{20}(t)=\tilde{\chi}_8\tilde{P}_4(t)\\
&\tilde{P}_{20+i}^{(1)}(t)\oplus\tilde{\beta}_i\tilde{P}_{20+i}(t)=\tilde{\chi}_i\tilde{P}_4(t), i=1,2,3,4
\end{aligned}
$$

where,

$\tilde{P}_i^{(1)}(t)=\dfrac{d\tilde{P}_i}{dt}$ for i=1 to 24

$$
\begin{aligned}
\tilde{\lambda}_1&=\tilde{\chi}_1\oplus\tilde{\chi}_2\oplus\tilde{\chi}_3\oplus\tilde{\chi}_4\oplus\tilde{\chi}_5\oplus\tilde{\chi}_6\\
\tilde{\lambda}_2&=\tilde{\chi}_1\oplus\tilde{\chi}_2\oplus\tilde{\chi}_3\oplus\tilde{\chi}_4\oplus\tilde{\chi}_6\oplus\tilde{\chi}_7\oplus\tilde{\beta}_5\\
\tilde{\lambda}_3&=\tilde{\chi}_1\oplus\tilde{\chi}_2\oplus\tilde{\chi}_3\oplus\tilde{\chi}_4\oplus\tilde{\chi}_5\oplus\tilde{\chi}_8\oplus\tilde{\beta}_6\\
\tilde{\lambda}_4&=\tilde{\chi}_1\oplus\tilde{\chi}_2\oplus\tilde{\chi}_3\oplus\tilde{\chi}_4\oplus\tilde{\chi}_7\oplus\tilde{\chi}_8
\end{aligned}
$$

with fuzzy initial conditions $\tilde{P}_1(0)$=(0.94,0.945,0.955,0.96), $\tilde{P}_2(0)$=(0.006,0.0065,0.0075,0.008), $\tilde{P}_3(0)$=(0.004,0.0045,0.0055,0.006), $\tilde{P}_4(0)$=(0.002,0.0025,0.0035,0.004) and $\tilde{P}_j(0)$=(0,0,0,0), j=4 to 24. (C1)

Fuzzy Kolmogorov's differential equations for the sub-system R_2 associated with the Markov model (Figure 2) are:

$$
\begin{aligned}
&\tilde{P}_1^{(1)}(t)\oplus\tilde{\delta}_1\tilde{P}_1(t)=\tilde{\mu}_1\tilde{P}_3(t)\oplus\tilde{\mu}_2\tilde{P}_4(t)\oplus\tilde{\mu}_3\tilde{P}_5(t)\oplus\tilde{\mu}_4\tilde{P}_6(t)\\
&\qquad\oplus\tilde{\mu}_5\tilde{P}_7(t)\oplus\tilde{\mu}_6\tilde{P}_2(t)\oplus\tilde{\mu}_7\tilde{P}_{13}(t)\\
&\tilde{P}_2^{(1)}(t)\oplus\tilde{\delta}_2\tilde{P}_2(t)=\tilde{\mu}_1\tilde{P}_8(t)\oplus\tilde{\mu}_2\tilde{P}_9(t)\oplus\tilde{\mu}_3\tilde{P}_{10}(t)\oplus\tilde{\mu}_4\tilde{P}_{11}(t)\\
&\qquad\oplus\tilde{\mu}_5\tilde{P}_{12}(t)\oplus\tilde{\eta}_6\tilde{P}_1(t)\\
&\tilde{P}_{2+i}^{(1)}(t)\oplus\tilde{\mu}_i\tilde{P}_{2+i}(t)=\tilde{\eta}_i\tilde{P}_1(t), i=1,2,3,4,5 \qquad \text{(S2)}\\
&\tilde{P}_{7+i}^{(1)}(t)\oplus\tilde{\mu}_i\tilde{P}_{7+i}(t)=\tilde{\eta}_i\tilde{P}_2(t), i=1,2,3,4,5\\
&\tilde{P}_{13}^{(1)}(t)\oplus\tilde{\mu}_7\tilde{P}_{13}(t)=\tilde{\eta}_7\tilde{P}_2(t)
\end{aligned}
$$

where,

$\tilde{P}_i^{(1)}(t)=\dfrac{d\tilde{P}_i}{dt}$ for i=1 to 13

$$
\begin{aligned}
\tilde{\delta}_1&=\tilde{\eta}_1\oplus\tilde{\eta}_2\oplus\tilde{\eta}_3\oplus\tilde{\eta}_4\oplus\tilde{\eta}_5\oplus\tilde{\eta}_6\\
\tilde{\delta}_2&=\tilde{\eta}_1\oplus\tilde{\eta}_2\oplus\tilde{\eta}_3\oplus\tilde{\eta}_4\oplus\tilde{\eta}_5\oplus\tilde{\eta}_7\oplus\tilde{\mu}_6
\end{aligned}
$$

with fuzzy initial conditions $\tilde{P}_1(0)$=(0.95,0.955,0.965,0.97), $\tilde{P}_2(0)$=(0.004,0.0045,0.0055,0.006) and $\tilde{P}_j(0)$=(0,0,0,0), j=3 to 13. (C2)

4.6. Solution of fuzzy Kolmogorov's differential equations of sub-system R_1 and R_2

The solution of fuzzy Kolmogorov's differential equations of sub-system R_1 and R_2, developed in Section 4.5, are obtained by using the existing method [14], discussed in Section 3, for

α = 0, 0.2, 0.4, 0.6, 0.8, 1 at t = 360 hours and the solution is shown in table 3 and table 4 respectively.

It is obvious from the results, shown in Table 3 and Table 4, that $[p_{j1}(t,\alpha), p_{j2}(t,\alpha)]$ does not define the α - cut of a fuzzy number $\widetilde{p}_j(t)$ for j = 1. So, the solution obtained by using the existing method [14] cannot be used to analyze the fuzzy reliability of piston manufacturing system.

Remark 4.1. In Section 4.6, it is shown that the solution obtained by using the existing method [14] can not be used to analyze the fuzzy reliability of piston manufacturing system. Similarly, several real life problems may be found for which the results of the existing method may or may not be valid.

5. Mehar's method with *JMD* representation of trapezoidal fuzzy numbers

To overcome the shortcoming of the existing method, discussed in Section 4, a new method, named as Mehar's method, is proposed to find the exact solution of fuzzy differential equations with the help of *JMD* representation of trapezoidal fuzzy numbers.

The solution of fuzzy initial value problem for n^{th} order fuzzy linear differential equation (1), where $\widetilde{a}_n$ is a non zero *JMD* trapezoidal fuzzy number and $\widetilde{a}_{n-1}, \widetilde{a}_{n-2}, \ldots, \widetilde{a}_1, \widetilde{a}_0$ are *JMD* trapezoidal fuzzy numbers, can be obtained by using the following steps of Mehar's method:

Step 1: Convert all the parameters of fuzzy differential equations, represented by trapezoidal fuzzy number (a,b,c,d), into *JMD* trapezoidal fuzzy number $(x,\alpha,\beta,\gamma)_{JMD}$, where $\alpha = b - a \geq 0$, $\beta = c - b \geq 0$, $\gamma = d - c \geq 0$. Assuming $\tilde{a}_n = (a_{n(1)}, \beta_{n(1)}, \beta_{n(2)}, \beta_{n(3)})_{JMD}$,

$$\tilde{a}_{n-1} = (a_{n-1(1)}, \beta_{n-1(1)}, \beta_{n-1(2)}, \beta_{n-1(3)})_{JMD}, \tilde{a}_{n-2} = (a_{n-2(1)}, \beta_{n-2(1)}, \beta_{n-2(2)}, \beta_{n-2(3)})_{JMD}, \ldots,$$

$$\tilde{a}_1 = (a_{1(1)}, \beta_{1(1)}, \beta_{1(2)}, \beta_{1(3)})_{JMD}, \tilde{a}_0 = (a_{0(1)}, \beta_{0(1)}, \beta_{0(2)}, \beta_{0(3)})_{JMD}, \tilde{y}^{(n)} = (y_1^{(n)}, \alpha_1^{(n)}, \alpha_2^{(n)}, \alpha_3^{(n)})_{JMD},$$

$$\tilde{y}^{(n-1)} = (y_1^{(n-1)}, \alpha_1^{(n-1)}, \alpha_2^{(n-1)}, \alpha_3^{(n-1)})_{JMD}, \ldots, \tilde{y}^{(1)} = (y_1^{(1)}, \alpha_1^{(1)}, \alpha_2^{(1)}, \alpha_3^{(1)})_{JMD}, \tilde{y} = (y_1, \alpha_1, \alpha_2, \alpha_3)_{JMD}$$

and

$$\tilde{\gamma}_0 = (\gamma_{0(1)}, \zeta_{0(1)}, \zeta_{0(2)}, \zeta_{0(3)})_{JMD}, \tilde{\gamma}_1 = (\gamma_{1(1)}, \zeta_{1(1)}, \zeta_{1(2)}, \zeta_{1(3)})_{JMD}, \ldots,$$

$$\tilde{\gamma}_{n-1} = (\gamma_{n-1(1)}, \zeta_{n-1(1)}, \zeta_{n-1(2)}, \zeta_{n-1(3)})_{JMD}$$

Tab. 3. Solution of fuzzy Kolmogorov's differential equations for sub-system R_1 obtained by using the existing method [14]

	$\widetilde{p}_j(t)$ for α = 0		$\widetilde{p}_j(t)$ for α = 0.2		$\widetilde{p}_j(t)$ for α = 0.4		$\widetilde{p}_j(t)$ for α = 0.6		$\widetilde{p}_j(t)$ for α = 0.8		$\widetilde{p}_j(t)$ for α = 1	
j	$\tilde{p}_{j1}(t,\alpha)$	$\tilde{p}_{j2}(t,\alpha)$	$\tilde{p}_{j1}(t,\alpha)$	$\tilde{p}_{j2}(t,\alpha)$	$\tilde{p}_{j1}(t,\alpha)$	$\tilde{p}_{j2}(t,\alpha)$	$\tilde{p}_{j1}(t,\alpha)$	$\tilde{p}_{j2}(t,\alpha)$	$\tilde{p}_{j1}(t,\alpha)$	$\tilde{p}_{j2}(t,\alpha)$	$\tilde{p}_{j1}(t,\alpha)$	$\tilde{p}_{j2}(t,\alpha)$
1	0.525421	0.396102	0.515146	0.401844	0.504872	0.407586	0.494597	0.413328	0.484323	0.419071	0.474049	0.424813
2	0.055996	0.065514	0.05667	0.065057	0.057344	0.064601	0.058018	0.064144	0.058692	0.063687	0.059366	0.063231
3	0.032869	0.036752	0.033158	0.036576	0.033447	0.036401	0.033737	0.036226	0.034026	0.036051	0.034316	0.035876
4	0.306812	0.424067	0.315888	0.419049	0.324964	0.414032	0.33404	0.409015	0.343116	0.403998	0.352192	0.398981
5	0.000537	0.000611	0.000542	0.000607	0.000547	0.000604	0.000553	0.000601	0.000558	0.000597	0.000564	0.000594
6	0.005867	0.006627	0.005923	0.006592	0.00598	0.006557	0.006036	0.006522	0.006093	0.006487	0.00615	0.006453
7	0.000747	0.000849	0.000754	0.000844	0.000761	0.000839	0.000769	0.000834	0.000776	0.000829	0.000784	0.000825
8	0.001307	0.001485	0.00132	0.001476	0.001333	0.001468	0.001346	0.001459	0.001359	0.001451	0.001372	0.001443
9	0.000057	0.000101	0.000059	0.000098	0.000062	0.000095	0.000065	0.000093	0.000068	0.000091	0.000071	0.000088
10	0.000623	0.001093	0.000651	0.001065	0.000681	0.001038	0.000709	0.001011	0.000738	0.000984	0.000767	0.000957
11	0.000079	0.00014	0.000082	0.000136	0.000086	0.000133	0.00009	0.000129	0.000094	0.000126	0.000098	0.000122
12	0.000139	0.000245	0.000145	0.000238	0.000151	0.000232	0.000158	0.000226	0.000164	0.00022	0.000171	0.000214
13	0.000033	0.000056	0.000034	0.000054	0.000036	0.000053	0.000037	0.000052	0.000039	0.000051	0.000041	0.00005
14	0.000366	0.000614	0.000381	0.0006	0.000397	0.000586	0.000412	0.000572	0.000428	0.000558	0.000444	0.000544
15	0.000046	0.000078	0.000048	0.000076	0.00005	0.000074	0.000052	0.000072	0.000054	0.000071	0.000056	0.000069
16	0.000081	0.000137	0.000084	0.000134	0.000088	0.000131	0.000091	0.000127	0.000095	0.000124	0.000099	0.000121
17	0.000679	0.001193	0.00071	0.001163	0.000741	0.001133	0.000773	0.001103	0.000804	0.001073	0.000836	0.001044
18	0.00117	0.001967	0.00122	0.001921	0.00127	0.001876	0.00132	0.001831	0.00137	0.001786	0.00142	0.001741
19	0.003628	0.007661	0.003876	0.007431	0.004125	0.007201	0.004373	0.006972	0.004622	0.006742	0.004871	0.006513
20	0.010731	0.022557	0.01146	0.021884	0.01219	0.021211	0.012919	0.020538	0.013649	0.019865	0.014379	0.019193
21	0.000313	0.000654	0.000334	0.000634	0.000355	0.000615	0.000376	0.000595	0.000397	0.000576	0.000419	0.000557
22	0.003293	0.006991	0.00352	0.00678	0.003748	0.006569	0.003975	0.006358	0.004203	0.006147	0.004431	0.005936
23	0.000435	0.000908	0.000464	0.000881	0.000493	0.000853	0.000522	0.000826	0.000551	0.000799	0.000581	0.000772
24	0.000759	0.001587	0.00081	0.00154	0.000861	0.001493	0.000912	0.001446	0.000963	0.001399	0.001015	0.001352

Tab. 4. Solution of fuzzy Kolmogorov's differential equations for sub-system R_2 obtained by using the existing method [14]

	$\widetilde{p}_j(t)$ for α = 0		$\widetilde{p}_j(t)$ for α = 0.2		$\widetilde{p}_j(t)$ for α = 0.4		$\widetilde{p}_j(t)$ for α = 0.6		$\widetilde{p}_j(t)$ for α = 0.8		$\widetilde{p}_j(t)$ for α = 1	
j	$\tilde{p}_{j1}(t,\alpha)$	$\tilde{p}_{j2}(t,\alpha)$	$\tilde{p}_{j1}(t,\alpha)$	$\tilde{p}_{j2}(t,\alpha)$	$\tilde{p}_{j1}(t,\alpha)$	$\tilde{p}_{j2}(t,\alpha)$	$\tilde{p}_{j1}(t,\alpha)$	$\tilde{p}_{j2}(t,\alpha)$	$\tilde{p}_{j1}(t,\alpha)$	$\tilde{p}_{j2}(t,\alpha)$	$\tilde{p}_{j1}(t,\alpha)$	$\tilde{p}_{j2}(t,\alpha)$
1	0.87807	0.862585	0.876803	0.86353	0.875536	0.864525	0.87427	0.86552	0.873003	0.866515	0.871737	0.867511
2	0.064038	0.094192	0.065987	0.092551	0.067937	0.09091	0.069887	0.08927	0.071837	0.087629	0.073787	0.085989
3	0.002941	0.004356	0.003032	0.004278	0.003123	0.004201	0.003214	0.004123	0.003305	0.004046	0.003396	0.003969
4	0.000425	0.000624	0.000436	0.000611	0.000447	0.000598	0.000458	0.000586	0.000469	0.000573	0.00048	0.000561
5	0.00011	0.000159	0.000111	0.000155	0.000113	0.000151	0.000115	0.000147	0.000117	0.000143	0.000119	0.000139
6	0.006073	0.008919	0.00623	0.008739	0.006388	0.008559	0.006546	0.008379	0.006704	0.008199	0.006862	0.008019
7	0.000024	0.000035	0.000024	0.000034	0.000024	0.000033	0.000025	0.000032	0.000025	0.000031	0.000026	0.000031
8	0.000228	0.000475	0.000229	0.000459	0.000243	0.000442	0.000257	0.000425	0.000272	0.000409	0.000287	0.000393
9	0.000031	0.000068	0.000033	0.000065	0.000035	0.000062	0.000037	0.00006	0.000039	0.000057	0.000041	0.000055
0	0.000008	0.000017	0.000008	0.000016	0.000009	0.000015	0.000009	0.000014	0.00001	0.000013	0.00001	0.000013
11	0.000442	0.000973	0.000469	0.000937	0.000497	0.000901	0.000525	0.000865	0.000553	0.000829	0.000581	0.000794
12	0.000001	0.000004	0.000001	0.000003	0.000001	0.000003	0.000002	0.000003	0.000002	0.000003	0.000002	0.000003
13	0.001617	0.003588	0.001727	0.003463	0.001837	0.003339	0.001947	0.003215	0.002057	0.003091	0.002168	0.002967

the fuzzy linear differential equation (1), can be written as

$$\begin{aligned}&(a_{n(1)},\beta_{n(1)},\beta_{n(2)},\beta_{n(3)})_{JMD}\otimes(y_1^{(n)},\alpha_1^{(n)},\alpha_2^{(n)},\alpha_3^{(n)})_{JMD}\oplus(a_{n-1(1)},\beta_{n-1(1)},\beta_{n-1(2)},\beta_{n-1(3)})_{JMD}\otimes\\&(y_1^{(n-1)},\alpha_1^{(n-1)},\alpha_2^{(n-1)},\alpha_3^{(n-1)})_{JMD}\oplus\ldots\oplus(a_{1(1)},\beta_{1(1)},\beta_{1(2)},\beta_{1(3)})_{JMD}\otimes(y_1^{(1)},\alpha_1^{(1)},\alpha_2^{(1)},\alpha_3^{(1)})_{JMD}\oplus\\&(a_{0(1)},\beta_{0(1)},\beta_{0(2)},\beta_{0(3)})_{JMD}\otimes(y_1,\alpha_1,\alpha_2,\alpha_3)_{JMD}=(g,0,0,0)_{JMD}\end{aligned}$$

$$\begin{aligned}&(y_1,\alpha_1,\alpha_2,\alpha_3)_{JMD}=(\gamma_{0(1)},\zeta_{0(1)},\zeta_{0(2)},\zeta_{0(3)})_{JMD},(y_1^{(1)},\alpha_1^{(1)},\alpha_2^{(1)},\alpha_3^{(1)})_{JMD}=(\gamma_{1(1)},\zeta_{1(1)},\zeta_{1(2)},\zeta_{1(3)})_{JMD},\ldots,\\&(y_1^{(n-1)},\alpha_1^{(n-1)},\alpha_2^{(n-1)},\alpha_3^{(n-1)})_{JMD}=(\gamma_{n-1(1)},\zeta_{n-1(1)},\zeta_{n-1(2)},\zeta_{n-1(3)})_{JMD}\end{aligned}$$

Step 2: Using Definition 2.11 and Section 2.2.3, the fuzzy differential equation, obtained from Step 1, is converted into the following four crisp linear differential equations

$$b_nz^{(n)}+b_{n-1}z^{(n-1)}+\ldots+b_1z^{(1)}+b_0z=g \qquad (2)$$

$$y_1=\gamma_{0(1)},y_1^{(1)}=\gamma_{1(1)},\ldots,y_1^{(n-1)}=\gamma_{n-1(1)}$$

$$c_nz^{(n)}+c_{n-1}z^{(n-1)}+\ldots+c_1z^{(1)}+c_0z=0 \qquad (3)$$

$$\alpha_1=\zeta_{0(1)},\alpha_1^{(1)}=\zeta_{1(1)},\ldots,\alpha_1^{(n-1)}=\zeta_{n-1(1)}$$

$$d_nz^{(n)}+d_{n-1}z^{(n-1)}+\ldots+d_1z^{(1)}+d_0z=0 \qquad (4)$$

$$\alpha_2=\zeta_{0(2)},\alpha_2^{(1)}=\zeta_{1(2)},\ldots,\alpha_2^{(n-1)}=\zeta_{n-1(2)}$$

$$e_nz^{(n)}+e_{n-1}z^{(n-1)}+\ldots+e_1z^{(1)}+e_0z=0 \qquad (5)$$

$$\alpha_3=\zeta_{0(3)},\alpha_3^{(1)}=\zeta_{1(3)},\ldots,\alpha_3^{(n-1)}=\zeta_{n-1(3)}$$

where,

$$\begin{aligned}b_iz^{(i)}=\text{minimum}\ &(a_{i(1)}y_1^{(i)},a_{i(1)}y_1^{(i)}+a_{i(1)}\alpha_1^{(i)}+a_{i(1)}\alpha_2^{(i)}+\\&+a_{i(1)}\alpha_3^{(i)},a_{i(1)}y_1^{(i)}+\beta_{i(1)}y_1^{(i)}+\beta_{i(2)}y_1^{(i)}+\beta_{i(3)}y_1^{(i)},\\&a_{i(1)}y_1^{(i)}+a_{i(1)}\alpha_1^{(i)}+a_{i(1)}\alpha_2^{(i)}+a_{i(1)}\alpha_3^{(i)}+\beta_{i(1)}y_1^{(i)}+\beta_{i(1)}\alpha_1^{(i)}+\\&+\beta_{i(1)}\alpha_2^{(i)}+\beta_{i(1)}\alpha_3^{(i)}+\beta_{i(2)}y_1^{(i)}+\beta_{i(2)}\alpha_1^{(i)}+\\&\beta_{i(2)}\alpha_2^{(i)}+\beta_{i(2)}\alpha_3^{(i)}+\beta_{i(3)}y_1^{(i)}+\beta_{i(3)}\alpha_1^{(i)}+\beta_{i(3)}\alpha_2^{(i)}+\beta_{i(3)}\alpha_3^{(i)}),\end{aligned}$$

$$\begin{aligned}c_iz^{(i)}=\text{minimum}\ &(a_{i(1)}y_1^{(i)}+a_{i(1)}\alpha_1^{(i)}+\beta_{i(1)}y_1^{(i)}+\beta_{i(1)}\alpha_1^{(i)},a_{i(1)}y_1^{(i)}\\&+a_{i(1)}\alpha_1^{(i)}+a_{i(1)}\alpha_2^{(i)}+\beta_{i(1)}y_1^{(i)}+\beta_{i(1)}\alpha_1^{(i)}+\beta_{i(1)}\alpha_2^{(i)},a_{i(1)}y_1^{(i)}+a_{i(1)}\alpha_1^{(i)}+\\&\beta_{i(1)}y_1^{(i)}+\beta_{i(1)}\alpha_1^{(i)}+\beta_{i(2)}y_1^{(i)}+\beta_{i(2)}\alpha_1^{(i)},a_{i(1)}y_1^{(i)}+a_{i(1)}\alpha_1^{(i)}+\\&a_{i(1)}\alpha_2^{(i)}+\beta_{i(1)}y_1^{(i)}+\beta_{i(1)}\alpha_1^{(i)}+\beta_{i(1)}\alpha_2^{(i)}+\\&\beta_{i(2)}y_1^{(i)}+\beta_{i(2)}\alpha_1^{(i)}+\beta_{i(2)}\alpha_2^{(i)})-b_iz^{(i)},\end{aligned}$$

$$\begin{aligned}d_iz^{(i)}=\text{maximum}\ &(a_{i(1)}y_1^{(i)}+a_{i(1)}\alpha_1^{(i)}+\beta_{i(1)}y_1^{(i)}+\beta_{i(1)}\alpha_1^{(i)},\\&a_{i(1)}y_1^{(i)}+a_{i(1)}\alpha_1^{(i)}+a_{i(1)}\alpha_2^{(i)}+\beta_{i(1)}y_1^{(i)}+\beta_{i(1)}\alpha_1^{(i)}+\\&\beta_{i(1)}\alpha_2^{(i)},a_{i(1)}y_1^{(i)}+a_{i(1)}\alpha_1^{(i)}+\beta_{i(1)}y_1^{(i)}+\beta_{i(1)}\alpha_1^{(i)}+\\&\beta_{i(2)}y_1^{(i)}+\beta_{i(2)}\alpha_1^{(i)},a_{i(1)}y_1^{(i)}+a_{i(1)}\alpha_1^{(i)}+a_{i(1)}\alpha_2^{(i)}+\beta_{i(1)}y_1^{(i)}+\\&\beta_{i(1)}\alpha_1^{(i)}+\beta_{i(1)}\alpha_2^{(i)}+\beta_{i(2)}y_1^{(i)}+\beta_{i(2)}\alpha_1^{(i)}+\beta_{i(2)}\alpha_2^{(i)})-b_iz^{(i)}-c_iz^{(i)},\end{aligned}$$

$$\begin{aligned}e_iz^{(i)}=\text{maximum}\ &(a_{i(1)}y_1^{(i)},a_{i(1)}y_1^{(i)}+a_{i(1)}\alpha_1^{(i)}+a_{i(1)}\alpha_2^{(i)}+a_{i(1)}\alpha_3^{(i)},a_{i(1)}y_1^{(i)}+\\&\beta_{i(1)}y_1^{(i)}+\beta_{i(2)}y_1^{(i)}+\beta_{i(3)}y_1^{(i)},a_{i(1)}y_1^{(i)}+a_{i(1)}\alpha_1^{(i)}+a_{i(1)}\alpha_2^{(i)}+\\&a_{i(1)}\alpha_3^{(i)}+\beta_{i(1)}y_1^{(i)}+\beta_{i(1)}\alpha_1^{(i)}+\beta_{i(1)}\alpha_2^{(i)}+\\&\beta_{i(1)}\alpha_3^{(i)}+\beta_{i(2)}y_1^{(i)}+\beta_{i(2)}\alpha_1^{(i)}+\beta_{i(2)}\alpha_2^{(i)}+\beta_{i(2)}\alpha_3^{(i)}+\beta_{i(3)}y_1^{(i)}+\\&\beta_{i(3)}\alpha_1^{(i)}+\beta_{i(3)}\alpha_2^{(i)}+\beta_{i(3)}\alpha_3^{(i)})-b_iz^{(i)}\\&-c_iz^{(i)}-d_iz^{(i)}\quad \text{for } i=n,n\text{-}1,\ldots,1,0\end{aligned}$$

Step 3. Solve the ordinary differential equations (2) to (5), obtained from Step 2, to find the values of y_1, α_1, α_2, and α_3.

Step 4. Put the values of $y_1,\alpha_1,\alpha_2,$ and α_3 in $\tilde{y}=(y_1,\alpha_1,\alpha_2,\alpha_3)_{JMD}$ to find the solution of fuzzy differential equation (1).

Step 5. Convert $\tilde{y}=(y_1,\alpha_1,\alpha_2,\alpha_3)_{JMD}$ into $\tilde{y}=(a,b,c,d)$, where, $a=y_1$, $b=y_1+\alpha_1$, $c=y_1+\alpha_1+\alpha_2$ and $d=y_1+\alpha_1+\alpha_2+\alpha_3$.

Remark 5.1. If $(y_1^{(i)},\alpha_1^{(i)},\alpha_2^{(i)},\alpha_3^{(i)})_{\text{JMD}}$ is non negative *JMD* trapezoidal fuzzy number, then the values of $b_iz^{(i)}$, $c_iz^{(i)}$, $d_iz^{(i)}$ and $e_iz^{(i)}$, defined in Step 2, can be written as

$$b_iz^{(i)}=\begin{cases}a_{i(1)}y_1^{(i)}, & a_{i(1)}\geq 0\\ a_{i(1)}y_1^{(i)}+a_{i(1)}\alpha_1^{(i)}+a_{i(1)}\alpha_2^{(i)}+a_{i(1)}\alpha_3^{(i)}, & \text{otherwise}\end{cases}$$

$$c_iz^{(i)}=\begin{cases}a_{i(1)}\alpha_1^{(i)}+\beta_{i(1)}y_1^{(i)}+\beta_{i(1)}\alpha_1^{(i)}, & a_{i(1)}\geq 0\\ \beta_{i(1)}y_1^{(i)}+\beta_{i(1)}\alpha_1^{(i)}-a_{i(1)}\alpha_2^{(i)}-a_{i(1)}\alpha_3^{(i)}, & a_{i(1)}\leq 0 \text{ and } a_{i(1)}+\beta_{i(1)}\geq 0\\ \beta_{i(1)}y_1^{(i)}+\beta_{i(1)}\alpha_1^{(i)}+\beta_{i(1)}\alpha_2^{(i)}-a_{i(1)}\alpha_3^{(i)}, & \text{otherwise.}\end{cases}$$

$$d_iz^{(i)}=\begin{cases}a_{i(1)}\alpha_2^{(i)}+\beta_{i(1)}\alpha_2^{(i)}+\beta_{i(2)}y_1^{(i)}+\beta_{i(2)}\alpha_1^{(i)}+\beta_{i(2)}\alpha_2^{(i)}, & a_{i(1)}+\beta_{i(1)}\geq 0\\ \beta_{i(2)}y_1^{(i)}+\beta_{i(2)}\alpha_1^{(i)}+\beta_{i(2)}\alpha_2^{(i)}, & a_{i(1)}+\beta_{i(1)}\leq 0 \text{ and } a_{i(1)}+\beta_{i(1)}+\beta_{i(2)}\geq 0\\ \beta_{i(2)}y_1^{(i)}+\beta_{i(2)}\alpha_1^{(i)}-a_{i(1)}\alpha_2^{(i)}-\beta_{i(1)}\alpha_2^{(i)}, & \text{otherwise.}\end{cases}$$

and

$$e_iz^{(i)}=\begin{cases}a_{i(1)}\alpha_3^{(i)}+\beta_{i(1)}\alpha_3^{(i)}+\beta_{i(2)}\alpha_3^{(i)}+\beta_{i(3)}y_1^{(i)}+\beta_{i(3)}\alpha_1^{(i)}+\\ \beta_{i(3)}\alpha_2^{(i)}+\beta_{i(3)}\alpha_3^{(i)}, & a_{i(1)}+\beta_{i(1)}+\beta_{i(2)}\geq 0\\ a_{i(1)}\alpha_2^{(i)}+a_{i(1)}\alpha_3^{(i)}+\beta_{i(1)}\alpha_2^{(i)}+\beta_{i(1)}\alpha_3^{(i)}+\\ \beta_{i(2)}\alpha_2^{(i)}+\beta_{i(2)}\alpha_3^{(i)}+\beta_{i(3)}y_1^{(i)}+\beta_{i(3)}\alpha_1^{(i)}+\\ \beta_{i(3)}\alpha_2^{(i)}+\beta_{i(3)}\alpha_3^{(i)}, & a_{i(1)}+\beta_{i(1)}+\beta_{i(2)}\leq 0 \text{ and } a_{i(1)}+\beta_{i(1)}+\beta_{i(2)}+\beta_{i(3)}\geq 0\\ a_{i(1)}\alpha_2^{(i)}+a_{i(1)}\alpha_3^{(i)}-\beta_{i(1)}y_1^{(i)}-\beta_{i(1)}\alpha_1^{(i)}-\\ \beta_{i(2)}y_1^{(i)}-\beta_{i(2)}\alpha_1^{(i)}, & \text{otherwise.}\end{cases}$$

for $i=n,n\text{-}1,\ldots,1,0$

6. Advantages of Mehar's method

The main advantages of Mehar's method over existing method [14] is that on solving the fuzzy differential equations by using the existing method, the obtained results may or may not define the α-cut of a fuzzy number while on solving the fuzzy differential equations by using Mehar's method, the obtained solution are always fuzzy number.

In this section, to show the advantages of Mehar's method over existing method, the fuzzy Kolmogorov's differential equations for the sub-systems R_1 and R_2, developed in Section 4.5, for which by using the existing method the obtained results are not appropriate, are solved by using Mehar's method, proposed in Section 5 and the obtained results, after converting the obtained *JMD* trapezoidal fuzzy number $(x,\alpha,\beta,\gamma)_{JMD}$ into existing representation of trapezoidal fuzzy number (a,b,c,d), are shown in table 5 and table 6 respectively.

It is obvious from table 5 and table 6, that $(p_{j1}(t), p_{j2}(t), p_{j3}(t), p_{j4}(t))$ defines a trapezoidal fuzzy number $\tilde{p}_j(t)$ for j = 1 to 24 and j = 1 to 13 respectively.

7. Advantages of *JMD* representation of trapezoidal fuzzy numbers over existing representation of trapezoidal fuzzy numbers

Kumar and Kaur [28] shown that it is better to use the proposed representation of trapezoidal fuzzy numbers instead of existing representation of trapezoidal fuzzy numbers for finding the fuzzy optimal solution of fuzzy transportation problems. In this section, it is shown that it is also better to use *JMD* representation of trapezoidal fuzzy numbers for solving fuzzy differential equations as compared to existing representation of trapezoidal fuzzy numbers.

To show the advantage of *JMD* representation of trapezoidal fuzzy numbers over existing representation of trapezoidal fuzzy numbers, the fuzzy Kolomorgov's differential equations, for the sub-systems R_1 and R_2 developed in Section 4.5, are solved by using Mehar's method with existing representation of trapezoidal fuzzy numbers and the obtained results are shown in table 7 and table 8 respectively.

It is obvious from table 7 and table 8, that $(p_{j1}(t), p_{j2}(t), p_{j3}(t), p_{j4}(t))$ does not define a trapezoidal fuzzy number for j = 1.

Tab. 5. Solution of fuzzy Kolmogorov's differential equations for sub-system R_1 obtained by using Mehar's method

	$\tilde{p}_j(t)$ for t=60	$\tilde{p}_j(t)$ for t=120	$\tilde{p}_j(t)$ for t=180	$\tilde{p}_j(t)$ for t=240	$\tilde{p}_j(t)$ for t=300	$\tilde{p}_j(t)$ for t=360
j	$(p_{j1}(t), p_{j2}(t), p_{j3}(t), p_{j4}(t))$	$(p_{j1}(t), p_{j2}(t), p_{j3}(t), p_{j4}(t))$	$(p_{j1}(t), p_{j2}(t), p_{j3}(t), p_{j4}(t))$	$(p_{j1}(t), p_{j2}(t), p_{j3}(t), p_{j4}(t))$	$(p_{j1}(t), p_{j2}(t), p_{j3}(t), p_{j4}(t))$	$(p_{j1}(t), p_{j2}(t), p_{j3}(t), p_{j4}(t))$
1	(0.720279,0.724095, 0.731181,0.734988)	(0.652165,0.655343, 0.66104,0.664203)	(0.603616,0.606389, 0.611232,0.613988)	(0.568691,0.571173, 0.5754,0.577863)	(0.543538,0.54602, 0.550247,0.55271)	(0.525421,0.527484, 0.530833,0.532877)
2	(0.071153,0.072092, 0.074107,0.075045)	(0.065846,0.066938, 0.069151,0.070288)	(0.062073,0.063193, 0.065337,0.066453)	(0.059359,0.060453, 0.06345,0.063539)	(0.057404,0.058498, 0.060495,0.061584)	(0.055996,0.056988, 0.058685,0.059671)
3	(0.044381,0.045198, 0.046916,0.047741)	(0.040352,0.041218, 0.042925,0.043805)	(0.037486,0.038314, 0.039853,0.040364)	(0.035423,0.036189, 0.037551,0.038333)	(0.033938,0.034704, 0.036066,0.036848)	(0.032869,0.033514, 0.034591,0.03525)
4	(0.096162,0.096893, 0.098549,0.099281)	(0.169323,0.172501, 0.174963,0.175998)	(0.221951,0.223285, 0.22648,0.227818)	(0.259851,0.261463, 0.265271,0.266889)	(0.287149,0.28731, 0.291118,0.292736)	(0.306812,0.308887, 0.313591,0.315675)
5	(0.000738,0.000761, 0.000807,0.00083)	(0.000688,0.00069, 0.000729,0.00075)	(0.000618,0.000637, 0.00067,0.000689)	(0.000582,0.000599, 0.000627,0.000643)	(0.000556,0.000573, 0.000601,0.000617)	(0.000537,0.000551, 0.000573,0.000586)
6	(0.007563,0.007585, 0.007641,0.007663)	(0.007414,0.007452, 0.007546,0.007584)	(0.006856,0.006907, 0.007028,0.007079)	(0.006417,0.006478, 0.006618,0.006679)	(0.006097,0.006158, 0.006298,0.006359)	(0.005867,0.005941, 0.006103,0.006177)
7	(0.001027,0.001049, 0.0011,0.001122)	(0.000929,0.000956, 0.00101,0.001037)	(0.000859,0.000885, 0.000933,0.000959)	(0.000809,0.000833, 0.000875,0.000899)	(0.000773,0.000797, 0.000839,0.000863)	(0.000747,0.000768, 0.000801,0.000821)
8	(0.001802,0.001829, 0.001915,0.001942)	(0.001629,0.001667, 0.001813,0.00185)	(0.001505,0.001546, 0.001737,0.001778)	(0.001417,0.001458, 0.001684,0.001725)	(0.001353,0.001394, 0.00162,0.001661)	(0.001307,0.001344, 0.001616,0.001652)
9	(0.000072,0.000076, 0.000087,0.000091)	(0.000067,0.000073, 0.000086,0.000092)	(0.000063,0.00007, 0.000084,0.000091)	(0.000061,0.000068, 0.000081,0.000088)	(0.000058,0.000065, 0.000078,0.000085)	(0.000057,0.000063, 0.000074,0.00008)
10	(0.000719,0.000722, 0.000733,0.000736)	(0.00074,0.000749, 0.000773,0.000781)	(0.000699,0.000713, 0.00075,0.000764)	(0.000665,0.000683, 0.00073,0.000748)	(0.000641,0.000659, 0.000706,0.000724)	(0.000623,0.000649, 0.000711,0.000737)
11	(0.000101,0.000105, 0.000115,0.000119)	(0.000093,0.0001, 0.000116,0.000123)	(0.000088,0.000096, 0.000114,0.000122)	(0.000084,0.000093, 0.000111,0.00012)	(0.000081,0.00009, 0.000108,0.000117)	(0.000079,0.000088, 0.000104,0.000109)
12	(0.000177,0.000181, 0.000197,0.000201)	(0.000164,0.000173, 0.000211,0.00022)	(0.000154,0.000166, 0.000224,0.000236)	(0.000147,0.000161, 0.000237,0.000251)	(0.000142,0.000156, 0.000232,0.000246)	(0.000139,0.000154, 0.000257,0.000272)
13	(0.000045,0.000049, 0.000058,0.000062)	(0.000041,0.000046, 0.000057,0.000062)	(0.000038,0.000043, 0.000053,0.000058)	(0.000036,0.000041, 0.00005,0.000055)	(0.000034,0.000039, 0.000048,0.000053)	(0.000033,0.000037, 0.000044,0.000048)
14	(0.000457,0.00046, 0.00047,0.000473)	(0.000457,0.000464, 0.000485,0.000492)	(0.000425,0.000436, 0.000466,0.000477)	(0.000399,0.000413, 0.00045,0.000465)	(0.00038,0.000394, 0.000431,0.000446)	(0.000366,0.000385, 0.00043,0.00045)
15	(0.000063,0.000066, 0.000075,0.000078)	(0.000057,0.000063, 0.000076,0.000082)	(0.000053,0.00006, 0.000074,0.000081)	(0.00005,0.000057, 0.00007,0.000077)	(0.000048,0.000055, 0.000068,0.000075)	(0.000046,0.000052, 0.000062,0.000068)
16	(0.000111,0.000115, 0.00013,0.000134)	(0.000101,0.000109, 0.000141,0.000149)	(0.000093,0.000103, 0.00015,0.00016)	(0.000088,0.000099, 0.000158,0.000169)	(0.000084,0.000095, 0.000154,0.000167)	(0.000081,0.000092, 0.000168,0.000179)
17	(0.000835,0.00084, 0.000856,0.000861)	(0.000809,0.000822, 0.000857,0.00087)	(0.00076,0.00078, 0.000833,0.000853)	(0.000723,0.000749, 0.000816,0.000842)	(0.000697,0.000705, 0.000772,0.000798)	(0.000679,0.000715, 0.0008,0.000836)
18	(0.001591,0.001613, 0.001675,0.001697)	(0.001453,0.0015, 0.001624,0.001671)	(0.001345,0.001412, 0.001581,0.001649)	(0.001266,0.00135, 0.001548,0.001633)	(0.001211,0.001295, 0.001493,0.001578)	(0.00117,0.001273, 0.001495,0.0016)
19	(0.000835,0.000839, 0.000852,0.000865)	(0.001794,0.001804, 0.001836,0.001846)	(0.002496,0.002514, 0.00257,0.002589)	(0.003002,0.00303, 0.003114,0.003142)	(0.003366,0.003394, 0.003478,0.003506)	(0.003628,0.003678, 0.003822,0.003872)
20	(0.002753,0.002772, 0.002827,0.002846)	(0.00552,0.00597, 0.00729,0.00774)	(0.007515,0.007592, 0.007819,0.007896)	(0.008951,0.009065, 0.009398,0.009512)	(0.009986,0.0101, 0.010433,0.010547)	(0.010731,0.010927, 0.011477,0.011673)
21	(0.000096,0.000099, 0.000107,0.00011)	(0.000172,0.000177, 0.00019,0.000195)	(0.000226,0.000233, 0.000251,0.000258)	(0.000265,0.000274, 0.000297,0.000306)	(0.000293,0.000302, 0.000325,0.000334)	(0.000313,0.000325, 0.000354,0.000366)
22	(0.000672,0.000675, 0.000683,0.000686)	(0.001549,0.001556, 0.001578,0.001585)	(0.002214,0.002227, 0.002266,0.002279)	(0.002696,0.002945, 0.003004,0.003023)	(0.003043,0.003062, 0.003121,0.00314)	(0.003293,0.003328, 0.003432,0.003467)
23	(0.000132,0.000135, 0.000143,0.000146)	(0.000237,0.000243, 0.000259,0.000265)	(0.000313,0.000321, 0.000344,0.000352)	(0.000367,0.000378, 0.000407,0.000418)	(0.000406,0.000417, 0.000446,0.000457)	(0.000435,0.000451, 0.00049,0.000506)
24	(0.000225,0.000228, 0.000241,0.000244)	(0.000411,0.000418, 0.000448,0.000455)	(0.000544,0.000556, 0.000617,0.000629)	(0.000641,0.000657, 0.000751,0.000767)	(0.000709,0.000725, 0.000819,0.000835)	(0.000759,0.000784, 0.000952,0.000977)

Tab. 6. Solution of fuzzy Kolmogorov's differential equations for sub-system R_2 obtained by using Mehar's method

	$\tilde{p}_j(t)$ for t=60	$\tilde{p}_j(t)$ for t=120	$\tilde{p}_j(t)$ for t=180	$\tilde{p}_j(t)$ for t=240	$\tilde{p}_j(t)$ for t=300	$\tilde{p}_j(t)$ for t=360
j	$(p_{j1}(t), p_{j2}(t), p_{j3}(t), p_{j4}(t))$	$(p_{j1}(t), p_{j2}(t), p_{j3}(t), p_{j4}(t))$	$(p_{j1}(t), p_{j2}(t), p_{j3}(t), p_{j4}(t))$	$(p_{j1}(t), p_{j2}(t), p_{j3}(t), p_{j4}(t))$	$(p_{j1}(t), p_{j2}(t), p_{j3}(t), p_{j4}(t))$	$(p_{j1}(t), p_{j2}(t), p_{j3}(t), p_{j4}(t))$
1	(0.878882,0.883263, 0.891744,0.896118)	(0.878179,0.882218, 0.890005,0.894036)	(0.878084,0.889381, 0.889381,0.893216)	(0.878072,0.881804, 0.889083,0.892803)	(0.878071,0.881734, 0.888916,0.892565)	(0.87807,0.881689, 0.888812,0.892416)
2	(0.064096,0.065113, 0.067364,0.06838)	(0.064046,0.065329, 0.068091,0.069372)	(0.064039,0.065457, 0.068421,0.069835)	(0.064038,0.065522, 0.068559,0.070038)	(0.064038,0.065554, 0.068611,0.070121)	(0.064038,0.065567, 0.068624,0.070146)
3	(0.002943,0.002986, 0.00309,0.003133)	(0.002941,0.003004, 0.003145,0.003208)	(0.002941,0.003013, 0.003164,0.003236)	(0.002941,0.003016, 0.003169,0.003244)	(0.002941,0.003018, 0.003171,0.003247)	(0.002941,0.003018, 0.00317,0.003246)
4	(0.000425,0.000432, 0.00045,0.000459)	(0.000425,0.000434, 0.000456,0.000467)	(0.000425,0.000435, 0.000457,0.000469)	(0.000425,0.000435, 0.000457,0.000469)	(0.000425,0.000434, 0.000455,0.000467)	(0.000425,0.000434, 0.000455,0.000467)
5	(0.00011,0.000111, 0.000116,0.000119)	(0.00011,0.000111, 0.000116,0.000119)	(0.00011,0.000111, 0.000116,0.000119)	(0.00011,0.000111, 0.000116,0.000119)	(0.00011,0.000111, 0.000116,0.000119)	(0.00011,0.000111, 0.000116,0.000119)
6	(0.005269,0.00528, 0.005311,0.005324)	(0.005966,0.005985, 0.006041,0.006065)	(0.006059,0.006086, 0.006164,0.006198)	(0.006071,0.006105, 0.006202,0.006206)	(0.006073,0.006114, 0.006228,0.006279)	(0.006073,0.00612, 0.00625,0.006309)
7	(0.000024,0.000025, 0.000026,0.000027)	(0.000024,0.0000244, 0.0000254,0.000026)	(0.000024,0.0000244, 0.0000245,0.0000253)	(0.000024,0.0000244, 0.0000254,0.0000262)	(0.000024,0.0000244, 0.0000254,0.000026)	(0.000024,0.0000243, 0.000025,0.000026)
8	(0.000214,0.000221, 0.000242,0.000249)	(0.000214,0.000229, 0.000268,0.000283)	(0.000214,0.000235, 0.000286,0.000307)	(0.000214,0.000239, 0.000297,0.000322)	(0.000214,0.000242, 0.000303,0.000331)	(0.000214,0.000244, 0.000307,0.000337)
9	(0.000031,0.000032, 0.000035,0.000036)	(0.000031,0.000033, 0.000039,0.000042)	(0.000031,0.000034, 0.000042,0.000045)	(0.000031,0.000034, 0.000042,0.000046)	(0.000031,0.000034, 0.000043,0.000047)	(0.000031,0.000034, 0.000043,0.000047)
10	(0.000008,0.0000082, 0.0000093,0.0000098)	(0.000008,0.0000085, 0.00001,0.000011)	(0.000008,0.0000086, 0.0000106,0.0000116)	(0.000008,0.0000086, 0.0000106,0.0000116)	(0.000008,0.000009, 0.000011,0.000012)	(0.000008,0.000009, 0.00003,0.000032)
11	(0.000373,0.000374, 0.000379,0.000381)	(0.000433,0.000437, 0.000451,0.000456)	(0.000441,0.000448, 0.000471,0.00048)	(0.000442,0.000452, 0.000483,0.000495)	(0.000442,0.000455, 0.000494,0.00051)	(0.000442,0.000457, 0.000503,0.000522)
12	(0.000001,0.0000021, 0.0000024,0.0000026)	(0.000001,0.0000011, 0.0000015,0.0000017)	(0.000001,0.0000011, 0.0000015,0.0000018)	(0.000001,0.0000011, 0.0000016,0.0000019)	(0.000001,0.0000011, 0.0000016,0.0000019)	(0.000001,0.0000011, 0.0000016,0.0000019)
13	(0.001617,0.001642, 0.001714,0.001739)	(0.001618,0.001676, 0.001835,0.001951)	(0.001617,0.001707, 0.001944,0.002034)	(0.001617,0.001736, 0.002037,0.002155)	(0.001617,0.00176, 0.002109,0.002252)	(0.001617,0.00178, 0.002165,0.002328)

Tab. 7. Solution of fuzzy Kolmogorov's differential equations for sub-system R_1 obtained by using Mehar's method with existing representation of trapezoidal fuzzy numbers

	$\tilde{p}_j(t)$ for t=60	$\tilde{p}_j(t)$ for t=120	$\tilde{p}_j(t)$ for t=180	$\tilde{p}_j(t)$ for t=240	$\tilde{p}_j(t)$ for t=300	$\tilde{p}_j(t)$ for t=360
j	$(p_{j1}(t), p_{j2}(t), p_{j3}(t), p_{j4}(t))$	$(p_{j1}(t), p_{j2}(t), p_{j3}(t), p_{j4}(t))$	$(p_{j1}(t), p_{j2}(t), p_{j3}(t), p_{j4}(t))$	$(p_{j1}(t), p_{j2}(t), p_{j3}(t), p_{j4}(t))$	$(p_{j1}(t), p_{j2}(t), p_{j3}(t), p_{j4}(t))$	$(p_{j1}(t), p_{j2}(t), p_{j3}(t), p_{j4}(t))$
1	(0.720279,0.681444, 0.635114,0.600719)	(0.652165,0.600728, 0.541703,0.501324)	(0.603616,0.547756, 0.487123,0.448286)	(0.568691,0.512688, 0.454965,0.41975)	(0.543538,0.48945, 0.436,0.404381)	(0.525421,0.474049, 0.424813,0.396102)
2	(0.071153,0.077829, 0.084789,0.088344)	(0.065846,0.070633, 0.075201,0.077243)	(0.062073,0.065921, 0.069611,0.071331)	(0.059359,0.062802, 0.066318,0.06815)	(0.057404,0.060736, 0.064376,0.066437)	(0.055996,0.059366, 0.063231,0.065514)
3	(0.044381,0.048441, 0.052512,0.054488)	(0.040352,0.042938, 0.045117,0.045866)	(0.037486,0.039332, 0.040802,0.041272)	(0.035423,0.036946, 0.038259,0.038801)	(0.033938,0.035364, 0.036761,0.037469)	(0.032869,0.034316, 0.035876,0.036752)
4	(0.096162,0.125721, 0.166747,0.196529)	(0.169323,0.213389, 0.26945,0.306637)	(0.221951,0.271397, 0.329903,0.365802)	(0.259851,0.309835, 0.365552,0.397663)	(0.287149,0.335309, 0.386578,0.414824)	(0.306812,0.352192, 0.398981,0.424067)
5	(0.000738,0.000813, 0.00089,0.00093)	(0.000688,0.000716, 0.000758,0.000775)	(0.000618,0.000652, 0.000681,0.000692)	(0.000582,0.000611, 0.000636,0.000648)	(0.000556,0.000583, 0.000609,0.000624)	(0.000537,0.000564, 0.000594,0.000611)
6	(0.007563,0.008481, 0.009508,0.010101)	(0.007414,0.008024, 0.008591,0.008833)	(0.006856,0.007273, 0.007621,0.007747)	(0.006417,0.006741, 0.007021,0.007136)	(0.006097,0.006385, 0.006663,0.006805)	(0.005867,0.00615, 0.006453,0.006627)
7	(0.001027,0.001132, 0.001241,0.001296)	(0.000929,0.000996, 0.001056,0.001079)	(0.000859,0.000907, 0.000948,0.000963)	(0.000809,0.000849, 0.000884,0.000901)	(0.000773,0.00081, 0.000847,0.000867)	(0.000747,0.000784, 0.000825,0.000849)
8	(0.001802,0.001987, 0.002179,0.002279)	(0.001629,0.001747, 0.001852,0.001893)	(0.001505,0.001591, 0.001661,0.001687)	(0.001417,0.001486, 0.001548,0.001576)	(0.001353,0.001417, 0.001482,0.001517)	(0.001307,0.001372, 0.001443,0.001485)
9	(0.000072,0.000092, 0.000118,0.000136)	(0.000067,0.000084, 0.000105,0.000119)	(0.000063,0.000078, 0.000097,0.00011)	(0.000061,0.000074, 0.000092,0.000105)	(0.000058,0.000072, 0.00009,0.000102)	(0.000057,0.000071, 0.000088,0.000101)
10	(0.000719,0.000932, 0.001221,0.001426)	(0.00074,0.000931, 0.001173,0.001335)	(0.000699,0.000867, 0.001077,0.001218)	(0.000665,0.000819, 0.001015,0.00115)	(0.000641,0.000788, 0.000979,0.001113)	(0.000623,0.000767, 0.000957,0.001093)
11	(0.000101,0.000129, 0.0001651,0.00019)	(0.000093,0.000117, 0.000146,0.000166)	(0.000088,0.000109, 0.000135,0.000153)	(0.000084,0.000103, 0.000128,0.000146)	(0.000081,0.0001, 0.000125,0.000142)	(0.000079,0.000098, 0.000122,0.00014)
12	(0.000177,0.000226, 0.00029,0.000334)	(0.000164,0.000205, 0.000256,0.000291)	(0.000154,0.000191, 0.000237,0.000268)	(0.000147,0.000181, 0.000225,0.000255)	(0.000142,0.000175, 0.000218,0.000249)	(0.000139,0.000171, 0.000214,0.000245)
13	(0.000045,0.000057, 0.000073,0.000084)	(0.000041,0.000051, 0.000063,0.000071)	(0.000038,0.000046, 0.000057,0.000063)	(0.000036,0.000044, 0.000053,0.000059)	(0.000034,0.000042, 0.000051,0.000057)	(0.000033,0.000041, 0.00005,0.000056)
14	(0.000457,0.000592, 0.000772,0.000901)	(0.000457,0.000571, 0.000712,0.000804)	(0.000425,0.000521, 0.000636,0.000711)	(0.000399,0.000485, 0.000589,0.000658)	(0.00038,0.000461, 0.000561,0.00063)	(0.000366,0.000444, 0.000544,0.000614)
15	(0.000063,0.00008, 0.000102,0.000117)	(0.000057,0.000071, 0.000087,0.000098)	(0.000053,0.000065, 0.000079,0.000088)	(0.00005,0.000061, 0.000074,0.000083)	(0.000048,0.000058, 0.000071,0.00008)	(0.000046,0.000056, 0.000069,0.000078)
16	(0.000111,0.000141, 0.00018,0.000206)	(0.000101,0.000124, 0.000154,0.000173)	(0.000093,0.000114, 0.000139,0.000155)	(0.000088,0.000107, 0.00013,0.000145)	(0.000084,0.000102, 0.000124,0.000141)	(0.000081,0.000099, 0.000121,0.000137)
17	(0.000835,0.001076, 0.001398,0.001626)	(0.000809,0.001014, 0.001274,0.001447)	(0.00076,0.000941, 0.001167,0.00132)	(0.000723,0.000891, 0.001104,0.001251)	(0.000697,0.000858, 0.001066,0.001213)	(0.000679,0.000836, 0.001044,0.001193)
18	(0.001591,0.002036, 0.002617,0.003017)	(0.001453,0.001806, 0.002237,0.002515)	(0.001345,0.001644, 0.002005,0.002238)	(0.001266,0.001537, 0.001869,0.00209)	(0.001211,0.001467, 0.001788,0.00201)	(0.00117,0.00142, 0.001741,0.001967)
19	(0.000835,0.001296, 0.002071,0.002741)	(0.001794,0.002665, 0.004017,0.005103)	(0.002496,0.003587, 0.005182,0.006392)	(0.003002,0.004198, 0.005869,0.007086)	(0.003366,0.004603, 0.006274,0.007461)	(0.003628,0.004871, 0.006513,0.007661)
20	(0.002753,0.004246, 0.006735,0.008871)	(0.00552,0.008165, 0.012241,0.015492)	(0.007515,0.010762, 0.015486,0.019052)	(0.008951,0.012483, 0.017399,0.020969)	(0.009986,0.013623, 0.018527,0.022001)	(0.010731,0.014379, 0.019193,0.022557)
21	(0.000096,0.000147, 0.00023,0.000299)	(0.000172,0.000252, 0.000375,0.000471)	(0.000226,0.000322, 0.00046,0.000563)	(0.000265,0.000368, 0.00051,0.000613)	(0.000293,0.000398, 0.00054,0.000639)	(0.000313,0.000419, 0.000557,0.000654)
22	(0.000672,0.001047, 0.001684,0.00224)	(0.001549,0.002312, 0.003506,0.004472)	(0.002214,0.003194, 0.004636,0.005737)	(0.002696,0.003782, 0.005307,0.006422)	(0.003043,0.004172, 0.005703,0.006792)	(0.003293,0.004431, 0.005936,0.006991)
23	(0.000132,0.000201, 0.000315,0.000411)	(0.000237,0.000348, 0.000518,0.000651)	(0.000313,0.000445, 0.000637,0.000781)	(0.000367,0.000510, 0.000707,0.000851)	(0.000406,0.000553, 0.000749,0.000888)	(0.000435,0.000581, 0.000773,0.000908)
24	(0.000225,0.000344, 0.000539,0.000704)	(0.000411,0.000604, 0.000898,0.001131)	(0.000544,0.000776, 0.00111,0.001361)	(0.000641,0.000889, 0.001235,0.001484)	(0.000709,0.000965, 0.001308,0.001551)	(0.000759,0.001015, 0.001352,0.001587)

Tab. 8. Solution of fuzzy Kolmogorov's differential equations for sub-system R_2 obtained by using Mehar's method with existing representation of trapezoidal fuzzy numbers

	$\widetilde{p}_j(t)$ for t=60	$\widetilde{p}_j(t)$ for t=120	$\widetilde{p}_j(t)$ for t=180	$\widetilde{p}_j(t)$ for t=240	$\widetilde{p}_j(t)$ for t=300	$\widetilde{p}_j(t)$ for t=360
j	$(p_{j1}(t), p_{j2}(t), p_{j3}(t), p_{j4}(t))$	$(p_{j1}(t), p_{j2}(t), p_{j3}(t), p_{j4}(t))$	$(p_{j1}(t), p_{j2}(t), p_{j3}(t), p_{j4}(t))$	$(p_{j1}(t), p_{j2}(t), p_{j3}(t), p_{j4}(t))$	$(p_{j1}(t), p_{j2}(t), p_{j3}(t), p_{j4}(t))$	$(p_{j1}(t), p_{j2}(t), p_{j3}(t), p_{j4}(t))$
1	(0.878882,0.872595, 0.868478,0.863537)	(0.878178,0.871845, 0.867666,0.862687)	(0.878084,0.871751, 0.867573,0.862596)	(0.878072,0.871739, 0.867563,0.862586)	(0.878071,0.871737, 0.867561,0.862585)	(0.87807,0.871737, 0.867561,0.862585)
2	(0.064096,0.073858, 0.086077,0.094293)	(0.064046,0.073796, 0.085999,0.094203)	(0.064039,0.073788, 0.085991,0.094193)	(0.064038,0.073788, 0.085989,0.094192)	(0.064038,0.073787, 0.085989,0.094192)	(0.064038,0.073787, 0.085989,0.094192)
3	(0.002943,0.0034, 0.003973,0.004361)	(0.002941,0.003396, 0.003969,0.004357)	(0.002941,0.003396, 0.003969,0.004356)	(0.002941,0.003396, 0.003969,0.004356)	(0.002941,0.003396, 0.003969,0.004356)	(0.002941,0.003396, 0.003969,0.004356)
4	(0.000425,0.000481, 0.000562,0.000625)	(0.000425,0.00048, 0.000561,0.000624)	(0.000425,0.00048, 0.000561,0.000624)	(0.000425,0.00048, 0.000561,0.000624)	(0.000425,0.00048, 0.000561,0.000624)	(0.000425,0.00048, 0.000561,0.000624)
5	(0.00011,0.000119, 0.000139,0.000159)	(0.00011,0.000119, 0.000139,0.000159)	(0.00011,0.000119, 0.000139,0.000159)	(0.00011,0.000119, 0.000139,0.000159)	(0.00011,0.000119, 0.000139,0.000159)	(0.00011,0.000119, 0.000139,0.000159)
6	(0.005369,0.006013, 0.007112,0.007977)	(0.005966,0.006755, 0.007915,0.008817)	(0.006059,0.006848, 0.008007,0.008908)	(0.006071,0.00686, 0.008018,0.008918)	(0.006073,0.006861, 0.008019,0.008919)	(0.006073,0.006862, 0.008019,0.008919)
7	(0.000024,0.000026, 0.000031,0.000035)	(0.000024,0.000026, 0.000031,0.000035)	(0.000024,0.000026, 0.000031,0.000035)	(0.000024,0.000026, 0.000031,0.000035)	(0.000024,0.000026, 0.000031,0.000035)	(0.000024,0.000026, 0.000031,0.000035)
8	(0.000214,0.000287, 0.000393,0.000476)	(0.000214,0.000287, 0.000393,0.000475)	(0.000214,0.000287, 0.000393,0.000475)	(0.000214,0.000287, 0.000393,0.000475)	(0.000214,0.000287, 0.000393,0.000475)	(0.000214,0.000287, 0.000393,0.000475)
9	(0.000031,0.000041, 0.000055,0.000068)	(0.000031,0.000041, 0.000055,0.000068)	(0.000031,0.000041, 0.000055,0.000068)	(0.000031,0.000041, 0.000055,0.000068)	(0.000031,0.000041, 0.000055,0.000068)	(0.000031,0.000041, 0.000055,0.000068)
10	(0.000008,0.00001, 0.000013,0.000017)	(0.000008,0.00001, 0.000013,0.000017)	(0.000008,0.00001, 0.000013,0.000017)	(0.000008,0.00001, 0.000013,0.000017)	(0.000008,0.00001, 0.000013,0.000017)	(0.000008,0.00001, 0.000013,0.000017)
11	(0.000373,0.000496, 0.000689,0.000852)	(0.000433,0.00057, 0.000782,0.000961)	(0.000441,0.000579, 0.000793,0.000972)	(0.000442,0.000581, 0.000794,0.000973)	(0.000442,0.000581, 0.000794,0.000973)	(0.000442,0.000581, 0.000794,0.000973)
12	(0.000001,0.000002, 0.000003,0.000004)	(0.000001,0.000002, 0.000003,0.000004)	(0.000001,0.000002, 0.000003,0.000004)	(0.000001,0.000002, 0.000003,0.000004)	(0.000001,0.000002, 0.000003,0.000004)	(0.000001,0.000002, 0.000003,0.000004)
13	(0.001617,0.002168, 0.002969,0.003591)	(0.001618,0.002168, 0.002967,0.003588)	(0.001617,0.002168, 0.002967,0.003588)	(0.001617,0.002168, 0.002967,0.003588)	(0.001617,0.002168, 0.002967,0.003588)	(0.001617,0.002168, 0.002967,0.003588)

8. Fuzzy reliability evaluation of piston manufacturing system

In Section 4.6, it is shown that the results of fuzzy Kolmogorov's differential equations, obtained by using the existing method, may or may not define the α -cut of a fuzzy number. Also, the results of fuzzy Kolmogorov's differential equations, obtained by using Mehar's method with existing representation of trapezoidal fuzzy number, shown in Table 7 and Table 8, may or may not be a fuzzy number. Due to which, the obtained results may not be used to analyze the fuzzy reliability of piston manufacturing system. But in Table 5 and Table 6, it is shown that if the same fuzzy Kolmogorov's differential equations are solved by using Mehar's method then the obtained results are fuzzy numbers. In this section, the results of fuzzy Kolmogorov's differential equations, shown in Table 5 and 6, obtained by using Mehar's method, are used to analyze the fuzzy reliability of piston manufacturing system.

Using the fuzzy probabilities for the sub-systems R_1 and R_2, shown in Table 5 and Table 6, the corresponding fuzzy reliabilities $\widetilde{R}_1(t) = \sum_{i=1}^{4} \widetilde{p}_i(t)$, $\widetilde{R}_2(t) = \sum_{i=1}^{2} \widetilde{p}_i(t)$ and $\widetilde{R}(t) = \widetilde{R}_1(t) \otimes \widetilde{R}_2(t)$ i.e., $(R_{11}(t), R_{12}(t), R_{13}(t), R_{14}(t))$, $(R_{21}(t), R_{22}(t), R_{23}(t), R_{24}(t))$ and

$$(R_1(t), R_2(t), R_3(t), R_4(t)) = \\ = (R_{11}(t), R_{12}(t), R_{13}(t), R_{14}(t)) \otimes (R_{21}(t), R_{22}(t), R_{23}(t), R_{24}(t))$$

of sub-system R_1, R_2 and the whole system are computed respectively and are shown in Table 9. The variation in reliability of sub-system R_1, R_2 and the whole system corresponding to variation in time is shown in Figure 3 to Figure 5 respectively.

9. Conclusion

The shortcoming of an existing method for finding the exact solution of fuzzy differential equations is pointed out and to overcome the shortcoming a new method, named as Mehar's method, for solving fuzzy differential equations is proposed. Also, it is shown that the solution of fuzzy Kolomorgov's differential equations, obtained by using the existing method, may or may not be fuzzy number. So, the existing method can not be used to analyze the fuzzy reliability of piston manufacturing system, while the solution of fuzzy Kolomorgov's differential equations, obtained by using Mehar's method, are always fuzzy number. So, it is better to use Mehar's method for solving fuzzy differential equations as compared to existing method.

Tab. 9. Fuzzy reliability of sub-system R_1, R_2 and the whole system obtained by using Mehar's method

Fuzzy Reliability →	$\widetilde{R}_1(t)$	$\widetilde{R}_2(t)$	$\widetilde{R}(t)$
Time (t) ↓	$(R_{11}(t), R_{12}(t), R_{13}(t), R_{14}(t))$	$(R_{21}(t), R_{22}(t), R_{23}(t), R_{24}(t))$	$(R_1(t), R_2(t), R_3(t), R_4(t))$
60	(0.931975,0.938278,0.950753,0.957055)	(0.942978,0.948376,0.959108,0.964498)	(0.878831,0.88984,0.911874,0.923077)
120	(0.927686,0.936,0.948079,0.954246)	(0.942224,0.947547,0.958096,0.963408)	(0.874088,0.886903,0.908351,0.919328)
180	(0.925126,0.931181,0.942902,0.948956)	(0.942123,0.947386,0.957802,0.960951)	(0.871582,0.882187,0.903113,0.9119)
240	(0.923384,0.929278,0.940672,0.946624)	(0.94211,0.947326,0.957642,0.962841)	(0.869929,0.880329,0.900827,0.911448)
300	(0.922029,0.926532,0.937926,0.943878)	(0.942109,0.947288,0.957527,0.962686)	(0.868651,0.877692,0.898089,0.908658)
360	(0.921098,0.926873,0.9377,0.943373)	(0.942108,0.947256,0.957436,0.962562)	(0.867773,0.877986,0.897787,0.908055)

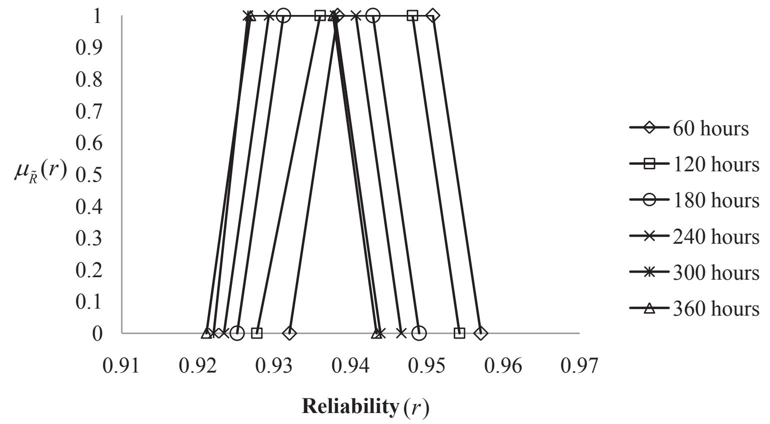

Fig. 3. Trapezoidal fuzzy number representing fuzzy reliability of sub-system R_1

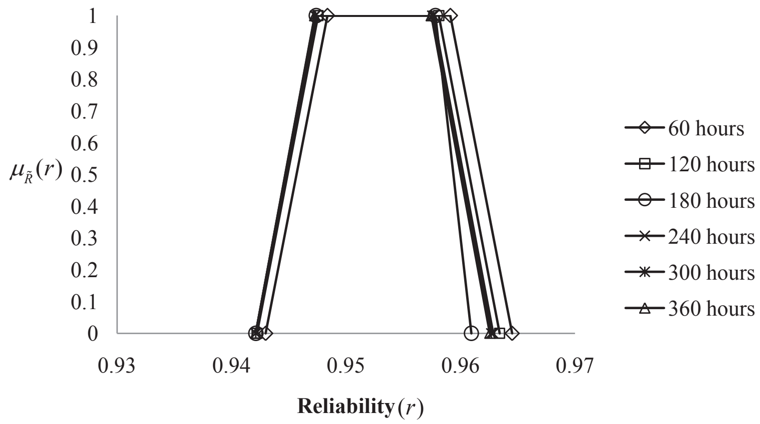

Fig. 4. Trapezoidal fuzzy number representing fuzzy reliability of sub-system R_2

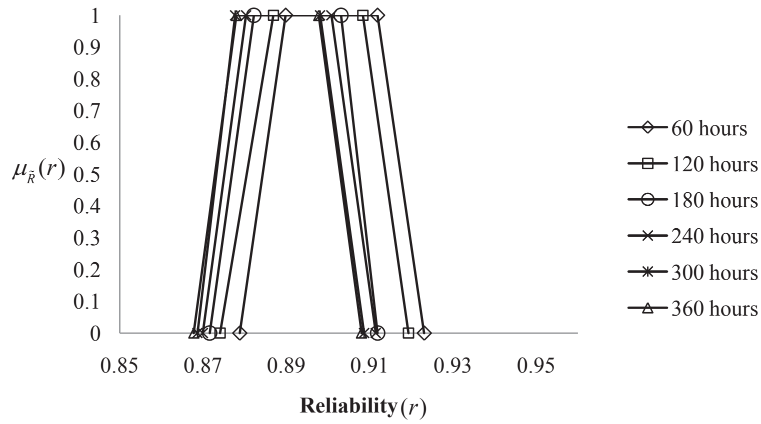

Fig. 5. Trapezoidal fuzzy number representing fuzzy reliability of whole system

****

The authors would like to thank to the editor and anonymous refeers for various suggestions which have led to an improvement in both the quality and clarity of the paper. I, Dr. Amit Kumar, want to acknowledge the adolescent inner blessings of Mehar. I believe that Mehar is an angel for me and without Mehar's blessing it was not possible to think the idea proposed in this paper. Mehar is a lovely daughter of Parampreet Kaur (Research Scholar under my supervision).

****

10. References

1. Abbasbandy S, Allahviranloo T. Numerical solutions of fuzzy differential equations by taylor method. Computational Methods in Applied Mathematics 2002; 2: 113-124.
2. Abbasbandy S, Allahviranloo T. Numerical solution of fuzzy differential equation. Mathematical and Computational Applications 2002; 7: 41-52.
3. Abbasbandy S, Allahviranloo T. Numerical solution of fuzzy differential equation by Runge-Kutta method. Nonlinear Studies 2004; 11: 117-129.
4. Abbasbandy S, Allahviranloo T, Lopez-Pouso O, Nieto J J. Numerical methods for fuzzy differential inclusions. Computer and Mathematics with Applications 2004; 48: 1633-1641.
5. Abbasbandy S, Nieto J J, Alavi M. Tuning of reachable set in one dimensional fuzzy differential equations. Chaos, Solitons and Fractals 2005; 26: 1337-1341.
6. Allahviranloo T, Ahmady N, Ahmady A. Numerical solution of fuzzy differential equations by predictor-corrector method. Information Sciences 2007; 177: 1633-1647.
7. Allahviranloo T, Ahmady v, Ahmady N. N^{th} order fuzzy linear differential equations, Information Sciences 2008; 178: 1309-1324.
8. Bede B. Note on numerical solutions of fuzzy differential equations by predictor-corrector method, Information Sciences 2008; 178: 1917-1922.
9. Bede B, Gal S G. Generalizations of the differentiability of fuzzy number valued functions with applications to fuzzy differential equation. Fuzzy Sets and Systems 2005; 151: 581-599.
10. Bede B, Rudas I J, Bencsik A L. First order linear fuzzy differential equations under generalized differentiability. Information Sciences 2007; 177: 1648-1662.
11. Binh P T T, Khoa T Q D. Application of fuzzy markov in calculating reliability of power systems. IEEE PES Transmission and Distribution Conference and Exposition Latin America, Venezuela 2006; 1-4.
12. Buckley J J, Feuring T. Introduction to fuzzy partial differential equations. Fuzzy Sets and Systems 1999; 105: 241-248.
13. Buckley J J, Feuring T. Fuzzy differential equations. Fuzzy Sets and Systems 2000; 110: 43-54.
14. Buckley J J, Feuring T. Fuzzy initial value problem for *N* th-order fuzzy linear differential equations. Fuzzy Sets and Systems 2001; 121: 247-255.
15. Buckley J J, Feuring T, HayashiY. Linear system of first order ordinary differential equations: fuzzy initial conditions. Soft Computing 2002; 6: 415-421.
16. Chalco-Cano Y, Roman-Flores H. On the new solution of fuzzy differential equations. Chaos Solitons Fractals 2008; 38: 112-119.
17. Chalco-Cano Y, Roman-Flores H. Comparison between some approaches to solve fuzzy differential equations. Fuzzy Sets and Systems 2009; 160: 1517-1527.
18. Chang S L, Zadeh L A. On fuzzy mapping and control. IEEE Transactions on Systems, Man and Cybernetics 1972; 2: 30-34.
19. Cho Y J, Lan H Y. The existence of solutions for the non linear first order fuzzy differential equations with discontinuous conditions. Dynamics Continuous Discrete Inpulsive Systems Series A: Mathematical Analysis 2007; 14: 873-884.
20. Diamond P. Brief note on the variation of constants formula for fuzzy differential equations. Fuzzy Sets and Systems 2002; 129: 65-71.
21. Dubois D, Prade H. Towards fuzzy differential calculus: Part 3, differentiation. Fuzzy Sets and Systems 1982; 8: 225-233.
22. Georgiou D N, Nieto J J, Rodriguez-Lopez R. Initial value problems for higher order fuzzy differential equations. Nonlinear Analysis 2005; 63: 587-600.
23. Gnana Bhaskar T, Lakshmikantham V, Devi V. Revisiting fuzzy differential equations. Nonlinear Analysis 2004; 58: 351-358.
24. Kaleva O. A note on fuzzy differential equations. Nonlinear Analysis 2006; 64: 895-900.
25. Kaufmann A, Gupta M M. Introduction to Fuzzy Arithmetics: Theory and Applications. Van Nostrand Reinhold, New York 1985.
26. Kleiner Y, Sadiq R, Rajani B. Modelling the deterioration of buried infrastructure as a fuzzy Markov process. Journal of Water Supply Research and Technology 2006; 55: 67-80.
27. Kumar A, Singh J, Kumar P. Fuzzy reliability and fuzzy availability of the serial process in butter oil processesing plant. Journal of Mathematics and Statistics 2009; 5: 65-71.
28. Kumar A, Kaur A. Methods for solving unblanced fuzzy transportation problems. Operational Research-An International Journal. DOI 10.1007/s 12351-010-0101-3.
29. Liu Y, Huang H Z. Reliability assessment for fuzzy multi-state systems. International Journal of Systems Science 2010; 41: 365-379.
30. Misukoshi M, Barros L C, Chalco-Cano Y, Romбn-Flores H, Bassanezi R C. Fuzzy differential equations and the extension principle. Information Sciences 2007; 177: 3627-3635.
31. Nieto J. A boundary value problem for second order fuzzy differential equations. Nonlinear Analysis 2010; 72: 3583-3593.
32. Nieto J J, Rodriguez-lopez R. Bounded solutions for fuzzy differential and integral equations. Chaos, Solitons and Fractals 2006; 27: 1376-1386.
33. Nieto J J, Rodriguez-Lypez R, Franco D. Linear first-order fuzzy differential equation, Internat Journal of Uncertainty. Fuzziness

and Knowledge-Based Systems 2006; 14: 687-709.
34. Oregan D, Lakshmikantham V, Nieto J J. Initial and boundary value problems for fuzzy differential equations. Nonlinear Analysis 2003; 54: 405-415.
35. Pederson S, Sambandham M. The Runge-Kutta method for hybrid fuzzy differential equations. Nonlinear Analysis: Hybrid Systems 2008; 2: 626-634.
36. Rodriguez-Lypez R. Comparison results for fuzzy differential equations. Information Sciences 2008; 178: 1756-1779.
37. Rodriguez-Lypez R. Monotone method fuzzy differential equations. Fuzzy Sets and Systems 2008; 159: 2047-2076.
38. Uprety I, Zaheeruddin. Fuzzy reliability of gracefully degradable computing systems. Proceedings of International Conference on Methods and Models on Computer Science 2009; 1-4.
39. Xiaoping X, Yongqiang F. On the structure of solutions for fuzzy initial value problem. Fuzzy Sets and Systems 2006; 157: 212-229.
40. Xu J, Liao Z, Hu Z. A class of linear differential dynamical systems with fuzzy initial condition. Fuzzy Sets and Systems 2007; 158: 2339-2358.

Sneh LATA, M. Sc.
Prof. Amit KUMAR
School of Mathematics and Computer Applications
Thapar University, Patiala-147004, India
e-mail: seneh.thaparian@gmail.com; amit_rs_iitr@yahoo.com

Grzegorz KOSZAŁKA

PREDICTING THE DURABILITY OF THE PISTON-RINGS-CYLINDER ASSEMBLY OF A DIESEL ENGINE USING A PISTON RING PACK MODEL

PROGNOZOWANIE TRWAŁOŚCI UKŁADU TŁOK-PIERŚCIENIE-CYLINDER SILNIKA O ZAPŁONIE SAMOCZYNNYM Z WYKORZYSTANIEM MODELU USZCZELNIENIA TPC *

The article presents a new method for predicting the durability of an internal combustion engine, which uses results of wear measurements of components of the piston-rings-cylinder system and computer simulations of the piston ring pack. In contrast to traditional methods, the method proposed here does not require previous knowledge of wear limits, which, though crucial for precise prediction, are difficult to determine reliably in modern structures. In the method presented here, wear limits are determined on the basis of an analytical model of the piston ring pack. The article shows an example of the application of the proposed method for predicting the durability of a motor-vehicle compression-ignition engine.

Keywords: *combustion engine, durability prediction, wear, blowby, cylinder liner, piston ring.*

W artykule przedstawiono nową metodę prognozowania trwałości tłokowego silnika spalinowego, wykorzystującą wyniki pomiarów zużycia elementów układu tłok-pierścienie-cylinder oraz komputerową symulację uszczelnienia TPC silnika. W przeciwieństwie do tradycyjnych metod, proponowana metoda nie wymaga wyprzedzającej znajomości zużycia granicznego, kluczowego dla dokładności prognozy, a którego wiarygodne określenie dla nowych konstrukcji jest trudne. W prezentowanej metodzie zużycie graniczne wyznaczane jest na podstawie analitycznego modelu uszczelnienia TPC. W artykule przedstawiono przykład wykorzystania metody do prognozowania trwałości samochodowego silnika o zapłonie samoczynnym.

Słowa kluczowe: *silnik spalinowy, prognozowanie trwałości, zużycie, przedmuchy spalin, tuleja cylindrowa, pierścień tłokowy.*

1. Introduction

The piston-rings-cylinder (PRC or piston) assembly is the basic functional system of an engine, and its most important function is to seal the combustion chamber in a tight and mobile manner. Due to the conditions under which they operate, the elements of the PRC assembly cannot be fitted too tightly and so there are clearances between them. Consequently, the sealing is not fully tight, allowing gas from the combustion chamber to pass into the crankcase and lubricating oil to flow into the combustion chamber. As the components of the engine wear out, the clearances grow larger and tightness decreases. Some good measures of the decrease in the tightness of the PRC assembly include increased blowby and elevated consumption of lubricating oil. Increased blowby and oil consumption have an adverse effect on the engine as they reduce engine power, increase the consumption of fuel and motor oil (resulting in elevated toxic emissions), accelerate quality wear of motor oil and wear of engine components, and decrease start-up performance of diesel engines [1, 9, 10]. Repair of a worn PRC assembly is costly and time-consuming and, if done at all, it is usually done as part of a complete overhaul. For many engine types, especially smaller ones, such repair is economically unjustified. Thus, excessive wear of the PRC system usually affects the durability of the entire engine or, in justifiable cases, may determine the necessity of carrying out a complete overhaul.

Methods used for pre-determining the durability of the piston assembly reduce the time and the costs of testing. In classic durability prediction methods, the courses of wear of selected components of the PRC assembly are assessed on the basis of shortened tests and then extrapolated to determine the time after which wear reaches a limit value (fig. 1).

To obtain reliable results when predicting durability, one has to accurately determine the courses of wear and know the value of the wear limit. The first of these conditions is usually satisfied if the operating conditions during tests do not cause

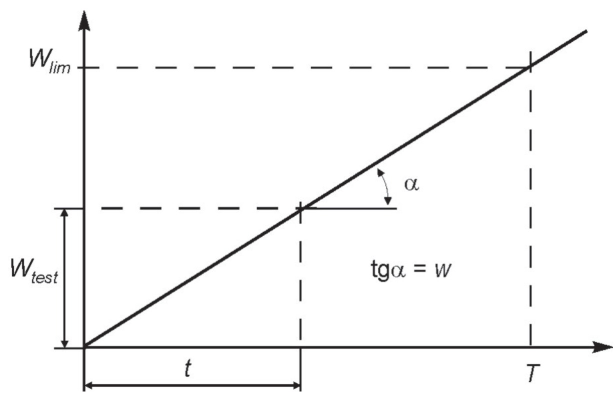

Fig. 1. The principle of predicting durability

(*) Tekst artykułu w polskiej wersji językowej dostępny w elektronicznym wydaniu kwartalnika na stronie ***www.ein.org.pl***

wear that differs qualitatively from that occurring during actual operation of the engine and if the courses of wear is determined from measurements taken on a run-in engine. Experience shows that the courses of wear after completion of run-in have a linear character (the intensity of wear *w* is constant), especially in the case of the cylinder liner [7, 11], and engines are withdrawn from operation before the period of accelerated wear of components begins.

It is more difficult to establish wear limits, because there is no linear relationship between the value of wear of components and the reduction in the tightness of the PRC assembly. That is why wear limits for engine components are most often determined using statistical methods on the basis of measurements of similar objects already withdrawn from operation. Use of such empirical models of the limit state, however, may be burdened with considerable error associated with the different impact that wear of components has on the operation of the assembly, even in similar structures. This follows from the complexity of the mechanisms governing the sealing action of the piston assembly, in which even small changes in design may cause considerable changes in efficiency. Moreover, it has to be born in mind that usually the limit state is determined in this way using engines at least one generation older than the ones for which durability is being predicted.

The article presents a new method for predicting the durability of the PRC assembly of an IC engine, in which wear limits for the components of this assembly are determined using an analytical model of the piston ring pack describing the cause-and-effect relationships between the size of the individual clearances and the rate of blowby. It should be emphasized that analytical models of the piston ring pack have already been applied for some time in the design of piston assemblies [2, 12, 13, 14, 15]. Also, the applicability of the model used in the present work for the assessment of operational changes in the tightness of the PRC assembly has been confirmed in previous studies [5, 8].

2. The piston ring pack model

The tests were carried out using an integrated model of gas flow through the clearances in the piston assembly and displacement of piston rings within piston grooves. In the gas flow model, the piston assembly was treated as a labyrinth seal comprising a series of volumes connected by choke orifices. The volumes of the labyrinth were formed by inter-ring and behind-ring volumes, while the choke orifices were created by piston ring gap clearances and clearances between the side faces of the rings and ring grooves (fig. 2). The instantaneous values of the labyrinth volumes and cross-section areas of the choke orifices were determined as a function of crank angle, taking into account thermal deformation and wear of components. The cross-section areas of the clearances between the side surfaces of a ring and a groove are most strongly dependent on the instantaneous position of the ring within the groove. Axial positions of rings within grooves were determined by taking into account the forces acting on the rings: gas pressure, inertia, and friction against the cylinder. Gas pressures and gas temperatures in the individual volumes of the labyrinth were determined using the laws of energy and mass conservation and the equation of state. Gas flow rates through the individual choke passages were calculated assuming isentropic flow and taking into account cases of subcritical and critical flow and the empirical discharge flow coefficient. The model had been described in detail in earlier articles [3, 5].

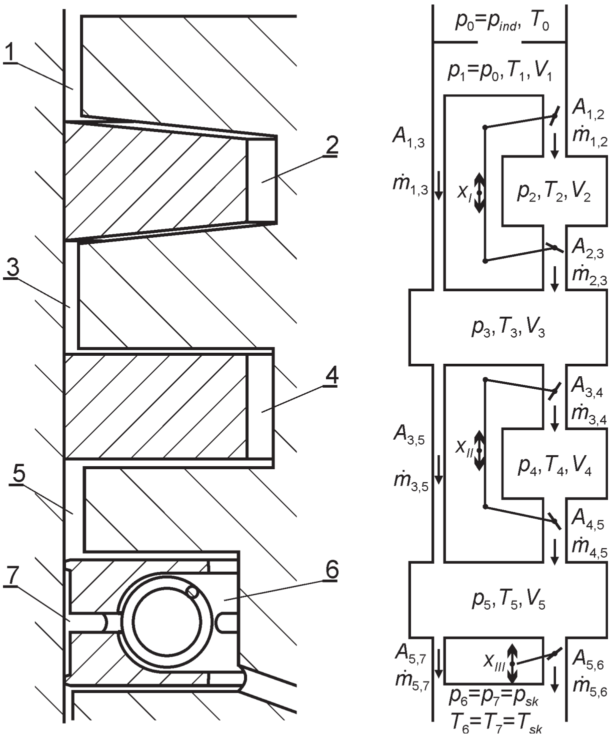

Fig. 2. Schematic diagram of the piston-ring pack and a corresponding model of a labyrinth seal (p_i, T_i – pressure and temperature of gas in the i-th volume, $m_{i,j}$ – gas flow rate from volume i to volume j, x_I, x_{II}, x_{III} – axial positions of the top, second, and oil ring, respectively) [5]

Calculations done using a numerical application of the model yield results, among others, for pressure courses in the individual volumes of the labyrinth, displacement of rings within grooves, and instantaneous rates of gas flow through the individual clearances as a function of crank angle (fig. 3). By integrating the instantaneous flow rates through the oil ring gap and the clearance between this ring and groove flank ($m_{5\text{-}7}$ and $m_{5\text{-}6}$ in figs. 2 and 3), the rate of blowby is obtained.

The input data necessary to carry out calculations using the numerical application of the model include, among others, the dimensions of engine components and pressure course in the combustion chamber as a function of crank angle. The dimensions of the components are established on the basis of technical documentation or direct measurements. In the case of key dimensions, i.e. those that determine the cross-section areas of clearances and the labyrinth volumes, the values entered into a computational software program should account for thermal deformation of the components. Thermal deformations are calculated for the given operating conditions of the engine using FEM. The deformation values determined in this way are added to the dimensions given in the documentation or those established on the basis of measurements of cold components [4]. Optimally, the course of combustion chamber pressure to be used in the calculations should be determined from measurements done on an actual engine.

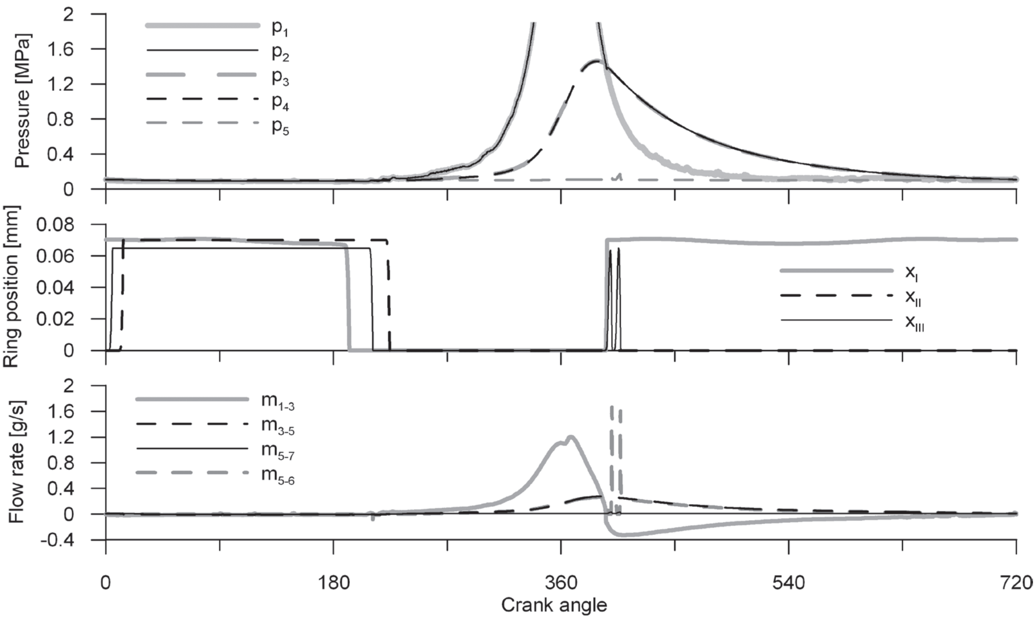

Fig. 3. Pressures in the volumes between and behind the rings, axial displacements of rings within piston grooves, and gas flow rates through ring gaps and the clearance between oil ring side face and groove as a function of crank angle, determined using the piston ring pack model

The geometrical dimensions entered into the calculations can consider the wear of the individual elements of the piston assembly, analogically to the way thermal deformations are taken into account. This allows one to estimate how an increase in wear affects the tightness of the piston assembly. The possibility of using the presented model for the assessment of the effect of wear on blowby was confirmed earlier by comparing results of numerical calculations with blowby measured in actual engines [5, 6, 8].

3. The durability prediction method

According to the proposed method, an engine should be run in before the durability of its PRC assembly is assessed. The time of engine operation in that period (t_0 in fig. 4) should be such that the unstabilized tribological processes associated with run-in have definitely been completed.

The principal part of the experimental tests starts with an assessment of the initial tightness of the PRC assembly done by measuring blowby flow rate B_1 and by determining initial engine wear W_1. Wear is estimated through measurements of the components of the PRC system after prior disassembly of the engine.

As a next step, the engine should be allowed to operate for time t to enable assessment of the rate of wear of its components, having in mind that a longer operation time allows obtaining more precise results. The engine in that period may be run either in a vehicle or on a test bed. The operating conditions, however, should not diverge too far from those intended for its normal operation. Once this testing stage is completed, measurements of blowby flow rate B_2 and engine wear W_2 have to be done analogically to the way in which blowby flow rate B_1 and initial engine wear W_1 have been measured.

The wear rate w of components is determined on the basis of the measurements of W_1 and W_2 in accordance with the following relationship:

$$w = \frac{W_2 - W_1}{t} \tag{1}$$

A second area of work on durability assessment using the proposed method is associated with investigations of the model of the piston ring pack. Working in this area, one should first determine all the input data necessary for the calculations, including the results of the earlier measurements of wear of components of the piston assembly. Next, tightness calculations should be done for input data corresponding to the initial engine wear W_1 and for input data corresponding to the final wear W_2 measured after the engine durability tests. A comparison of the calculated and observed increases in the blowby flow rate caused by wear allows one to assess the adequacy of the model. If the results of simulations concur with the results of measurements, further simulations should be done for higher values of wear of the PRC assembly, assuming that the wear rates for the individual components are those determined in the experimental tests. The aim of those calculations is to find such a value of wear W_{lim} for which the increase in blowby rate will reach an assumed limit value B_{lim}. The value of wear W_{lim} determined in this way is the wear limit. The limit blowby flow rate is determined taking into account the negative effects of blowby on engine operation and previous experiences from engine durability tests.

The predicted engine durability t_{lim} at a given wear rate w and the limit value of wear W_{lim} is

$$t_{\text{lim}} = \frac{W_{\text{lim}} - W_1}{w} + t_0 \tag{2}$$

A schematic diagram for predicting engine durability on the basis of measurements of blowby flow rate and wear of the components of the PRC assembly is shown in fig. 4.

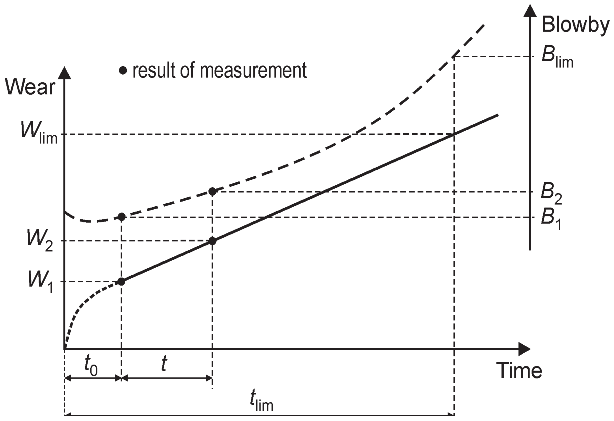

Fig. 4. The durability prediction method

4. A computational example

4.1. Determination of the courses of wear

The test object was a six-cylinder compression ignition engine with a capacity of 6.8 dm^3 and rated power of 110 kW at the speed of 2800 rpm. The engine was equipped with wet, cast iron cylinder liners with the nominal inside diameter of 110 mm. The piston travel was 120 mm.

To avoid errors related to the deviation of a single engine from the average of a population, the tests were conducted on 5 engines mounted in trucks of medium loading capacity and a gross vehicle weight of 12 Mg. All the vehicles were the property of one transport provider and were used under similar conditions, with an average monthly mileage of 10 000 km. The engines were lubricated with the same CE/SF SAE 15W/40 class oil.

The tightness and wear of the PRC assembly were measured after 50 000 km of travel. This amount of travel guaranteed full run-in of the engines. The blowby flow rate was measured at idle run. Next, the engine was partially disassembled to measure the wear of its components. After removal of the heads the cylinder diameters were measured by the micrometric method using a Carl Zeiss two-point bore gauge with the minimum graduation of 0.002 mm. The cylinder diameters were measured in two directions, parallel (A-A) and perpendicular (B-B) to the main axis of the engine, at four levels: 20 (top dead center TDC of the top ring), 35 (TDC of the second compression ring), 50, and 95 mm from the head face. Then the assembled engines were operated under pre-disassembly conditions. Once the engines had reached a mileage of 150 000 km, blowby flow rate and engine wear were measured again in the same manner as at 50 000 km.

The results provided a basis for determining mean values of wear of the components of the PRC assembly for all five test vehicles. Since the piston ring pack model does not provide for deviations from circularity of the components of the PRC assembly, the results for directions A-A and B-B, i.e. parallel and perpendicular to the main axis of the engine, respectively, were averaged. The results are shown in fig. 5a. Next, the wear courses were extrapolated on the assumption that they were linear (constant wear rate *w*, fig. 5b).

4.2. Determination of the limit state and durability of the engine

Input data for the calculations with the use of the piston ring pack model were established. Geometrical data were established on the basis of technical documentation and measurements. Thermal deformations were determined using FEM and added to the dimensions established for a cold engine. Measurements of indicated pressure were carried out on an engine test bench.

Calculations were done for dimensions of the components corresponding to the mileages of 50 000 km and then 150 000 km. The input data for the calculations at the different mileages differed only in the dimensions of the components which had been changed by wear. The calculations took into account wear of the cylinder liner (fig. 5a), wear of the running faces of rings, and wear of the side faces of rings and piston grooves. The value of blowby determined in the numerical calculations at 150 000 km of travel was 22% higher than at 50 000 km. Because the simulated change in blowby matched the actual one, further numerical calculations were done for higher mileages. Wear values (dimensions) of the individual components at higher mileages were established on the basis of the previously determined courses of wear (an example for a liner is shown in fig. 5). The calculations were done with a view to finding a mileage at which blowby would reach a limit value. Since the investigated engine was not a new model, specimens withdrawn from opera-

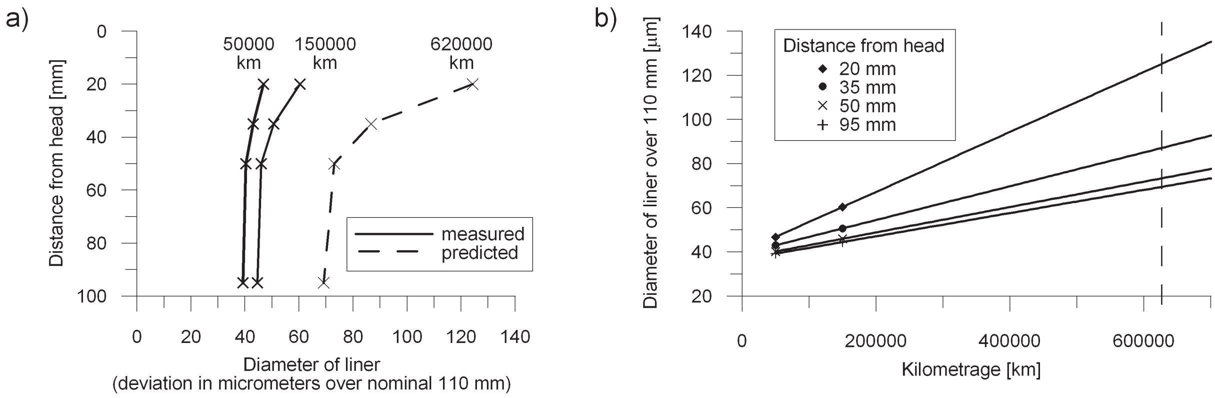

Fig. 5. Experimentally determined diameters of cylinder liners at different distances from head (a), assumed courses of cylinder liner wear at different distances from head (b), and predicted limit state of the cylinder liner –liner diameters at 620 000 km of travel – determined as described in section 4.2 (a)

tion could be used to establish limit blowby values. They turned out to be 2.5 times higher than the values obtained in the test engines at 50 000 km of travel. Hence this increase in blowby was assumed to be the limit increase. In numerical calculations, a 2.5-fold increase in blowby rate was obtained for predicted wear at mileages of over 620 000 km. This mileage defines the durability of the engine as predicted by the proposed method. The predicted liner wear profile for this mileage, which is at the same time the predicted wear limit, is shown in fig. 5a. The actual mileages achieved by engines of the investigated type have been in the range between 500 and 800 thousand km.

5. Conclusions

The proposed durability assessment method is based on experimentally determined wear rates for the components of the PRC assembly and on results of numerical studies of an analytical model of the piston ring pack. Wear rates can be determined from measurements of engines tested either on a test-stand or in a vehicle [9-10]. The proposed method has the advantage of not requiring prior knowledge of the wear limit. In traditional durability prediction methods, the adopted wear limit determines the adequacy of the obtained results. Unfortunately, this value is difficult to specify reliably in modern engine structures. By contrast, the new method described in this article does not require previous knowledge of the wear limit because wear limits are determined here on the basis of an analytical model of the piston ring pack. This, however, requires the knowledge of the permissible decrease in the tightness of the PRC assembly. The permissible decrease in tightness may be adopted on the basis of assumed permissible decrease in the efficiency and eco-friendliness of an engine.

The applicability of the proposed method for predicting the durability of a motor-vehicle compression-ignition engine has been verified in the study reported here. An additional merit of the discussed analytical model is that it can be directly used in work on improving the design of the PRC assembly.

6. References

1. Andersson P, Tamminen J, Sandstrom C-E. Piston ring tribology. A literature survey. VTT Tiedotteita - Research Notes 2178, Espoo (Finland), 2002.
2. Keribar R, Dursunkaya Z, Flemming M F. An Integrated Model of Ring Pack Performance. Journal of Engineering for Gas Turbines and Power 1991; 113: 382-389.
3. Koszałka G. Modelling the blowby in internal combustion engine, Part 1: A mathematical model. The Archive of Mechanical Engineering 2004; 2(LI): 245-257.
4. Koszałka G. Modelling the blowby in internal combustion engine, Part 2: Primary calculations and verification of the model. The Archive of Mechanical Engineering 2004; 4(LI): 595-607.
5. Koszałka G. Application of the piston-rings-cylinder kit model in the evaluation of operational changes in blowby flow rate. Eksploatacja i Niezawodnosc – Maintenance and Reliability 2010, 4(48): 72-81.
6. Koszałka G, Niewczas A. The Influence of Compression Ring Clearances on the Blowby in a Diesel Engine. SAE Paper 2006-01-3356, 2006.
7. Koszałka G, Niewczas A. Wear profile of the cylinder liner in a motor truck diesel engine. Journal of KONES Powertrain and Transport 2007; 4(14); 183-190.
8. Koszałka G, Niewczas A, Guzik M. Predicted and Actual Effect of Cylinder Liner Wear on the Blowby in a Truck Diesel Engine. SAE Paper 2008-01-1717, 2008.
9. Merkisz J, Tomaszewski F, Ignatow O. Trwałość i diagnostyka węzła tłokowego silników spalinowych – wybrane zagadnienia [Durability and diagnostic testing of the combustion engine piston junction – selected issues]. Poznań: Wyd. Politechniki Poznańskiej, 1995.
10. Niewczas A. Trwałość zespołu tłok-pierścienie tłokowe-cylinder silnika spalinowego [Durability of the piston-ring-cylinder assembly of a combustion engine]. Warszawa: WNT, 1998.
11. Niewczas A, Koszałka G, Droździel P. Stochastic model of truck engine wear with regard to discontinuity of operation. Eksploatacja i Niezawodnosc – Maintenance and Reliability 2006; 2(30): 52-55.
12. Tian T. Dynamic behaviours of piston rings and their practical impact. Part 1: ring flutter and ring collapse and their effects on gas flow and oil transport. Journal of Engineering Tribology 2005; 4(216): 209-227.
13. Tian T, Noordzij L B, Wong V W, Heywood J B. Modeling Piston-Ring Dynamics, Blowby and Ring-Twist Effects. Journal of Engineering for Gas Turbines and Power 1998; 120: 843-854.
14. Wolff A. Numerical analysis of piston ring pack operation. Combustion Engines – Silniki Spalinowe 2009; 2(137): 128-141.
15. Wolff A. Experimental verification of the model of piston ring pack operation of an internal combustion engine. The Archive of Mechanical Engineering 2009; 1(LVI): 73-90.

Grzegorz KOSZAŁKA, Ph.D., Eng.
Department of Internal Combustion Engines and Transport
Lublin University of Technology
ul. Nadbystrzycka 36, 20-618 Lublin, Poland
e-mail: g.koszalka@pollub.pl

Jacek MUCHA

THE ANALYSIS OF RECTANGULAR CLINCHING JOINT IN THE SHEARING TEST

ANALIZA ZNISZCZENIA PROSTOKĄTNEGO ZŁĄCZA PRZETŁOCZENIOWEGO W PRÓBIE ŚCINANIA*

This paper presents the results of experimental researches on effect of clinching joint's load direction change on its characteristics and the maximum shearing force value. The single-folded clinching joints made of aluminum sheet AW1050A have been the subject of researches. Properly prepared specimens of rectangle clinching joints with material notch have been shear tested on the tensile testing machine UTS 100. The extreme joint destruction have been analyzed for the layout angle β = 0°, 90°. The separation mechanism has been described for all angle values β = 0°, 30°, 45°, 90°. The total separation work by joint shearing has also been mentioned.

Keywords: *clinching joints, shearing, joint separation.*

W pracy zawarto wyniki badań eksperymentalnych dotyczących wpływu zmiany kierunku obciążenia przetłoczeniowego złącza na przebieg charakterystyki i maksymalną wartość siły ścinania. Przedmiotem badań były jednozakładkowe połączenia przetłoczeniowe blach z aluminium AW1050A. Odpowiednio wykonane próbki prostokątnych połączeń przetłoczeniowych z nacięciem materiału poddano testom ścinania na maszynie wytrzymałościowej UTS 100. Przeanalizowano skrajne przypadki zniszczenia złącza dla kąta ułożenia β = 0°, 90°. Opisano mechanizm rozdzielenia połączenia dla wszystkich wartości kąta β = 0°, 30°, 45°, 90°. Zwrócono również uwagę na wielkość całkowitej pracy rozdzielenia przez ścinanie złącza.

Słowa kluczowe: *połączenia przetłoczeniowe, ścinanie, rozdzielenie złącza.*

1. Introduction

When using the rectangle clinching joints, the awareness of their static strength is extremely important. This enables e.g. to determine load values and types, for which the joint can be used. The most frequently considered parameter is the shearing resistance [4, 5, 6, 7, 11, 12].

The strength (and resistance) of rectangular joint on externally applied shearing load is not identical due to a merging area shape [2, 3, 8, 13, 14]. This depends on its location in relation to the main load direction (see fig. 1).

When mounting sheet elements, the line of locally cut material may be parallel (fig. 2a) or lateral (fig. 2b) to the merging seam line. It is preferred that the main joint load direction coincides with the direction of the highest joint load-carrying ability. In practical conditions, usually it is not possible to locate the direction in that way. The use of clinching joint technology is justified by the capability of its adaptation that the tool access is guaranteed to achieve the tool adequate support rigidity and its retraction after the process [15].

The awareness of rectangular clinching joint strength and related issues enables selecting proper forming process parameters and determining correct operating conditions. The knowledge on destruction mechanism plays a crucial role when designing and using these joints [10].

Most of available papers is related to clinching joint issue. Only some of them deal with rectangular joints. Recently only some researches, including joint load direction change, have been conducted [2, 3, 8, 13, 14]. One of a few papers [2], related to clinching joint strength analysis, presents the description

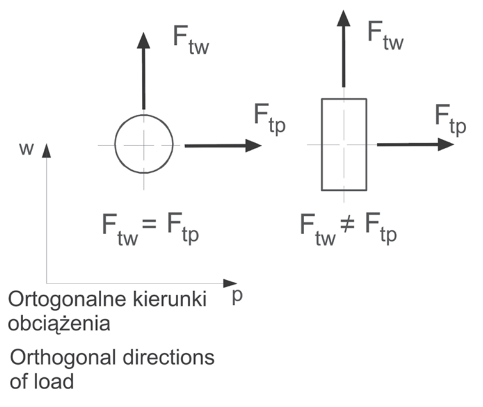

Fig. 1. The cases of rectangle and circular shearing of clinching joint

a)

b)

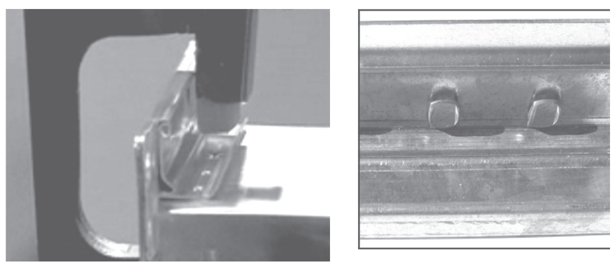

Fig. 2. Overpress joining of HVAC pipe elements made of a steel sheet: a) with a longitudinal seam layout, b) with a perpendicular seam layout

(*) Tekst artykułu w polskiej wersji językowej dostępny w elektronicznym wydaniu kwartalnika na stronie ***www.ein.org.pl***

of clinching joint static shearing test. Other publications [13, 14], also interesting from this point of view, present the difference of work to be made when destruction testing circular and rectangular joints of various layouts in relation to the principal direction of joint strain. On the other hand, the authors in another publication [8] have presented the effect of joint layout change in nodes of spatial design made of thin sheet profiles on value and characteristics of a force that forces the design deformation. The paper describing the rectangular clinching joint with various layouts in the sheet construction of a controlled crush zone [1] is also worth of interest. The specified joint layout in such components also effects their separation [2].

In this paper, the author has presented the analysis of effect of the joint layout angle (in relation to the load) on the critical value of force separating the joint. Moreover, the author has performed the analysis of destruction of correspondingly loaded joints.

2. The matter of joint forming

The joining process (along with material notching) is performed using tools specifically designed for this method, i.e. the punch of desired shape and the die with segments. These segments may be pressed using the sleeve made of high strength elastomer or flat or coil springs [6].

The joint forming process may be divided into three main phases: I – notching (notching along with prestamping); II – stamping; III – pressing (restriking the overpress bottom) – see fig. 3.

When the punch is being immersed, the material is cut in the point of sheet and die cutting edge and the material fractures and separates in the end of stamping – phase I. The achieved material notches occur along the die cutting edges and facilitate the further stamping process. Then the sheet stamping occurs – phase II. This phase has a short duration and occurs right after the complete material cut and before the overpress bottom pressing. The further punch displacement presses the bottom material and its pressing - phase III. The material cutting, but on quite a lower level, accompanies also the bottom pressing. The radial material flow (fig. 3a) and die segment displacement is caused by the punch pressure on the overpress bottom. This is how the „lock" is created, i.e. seizing the upper sheet material in the lower one. Once the desired sheet merging effect is achieved, the joint forming punch is retracted.

The rectangular clinching joint technology enables joining two (fig. 4a), three (fig. 4b) and even more material layers.

3. The scope and methodology of experimental researches

The commonly available aluminum sheet AW1050A has been used to examine the effect of merging area layout angle in relation to the displacement deforming the joint on its critical load values. The experimental researches have been conducted on the specimens prepared as follows: sheet strips, width of 40 mm and length of 110 mm, cut from the sheet of thickness 1.00±0.05 mm. The material properties are as follows: the agreed yield stress $R_{p0.2}$ = 25 MPa; strength limit R_m = 75 MPa; Young module E = 69 000 MPa; relative elongation A_{50} = 25 mm.

The sheet strips have been joined using tools of specified geometry (fig. 5), mounted on the hydraulic jaw device, while maintaining specified dimensions of finished specimen (fig. 6).

Depending on the punch and die geometry, various maximum pressure force to temporary shearing strength ratios may be achieved. However, single set of tools and single final over-

a) b)

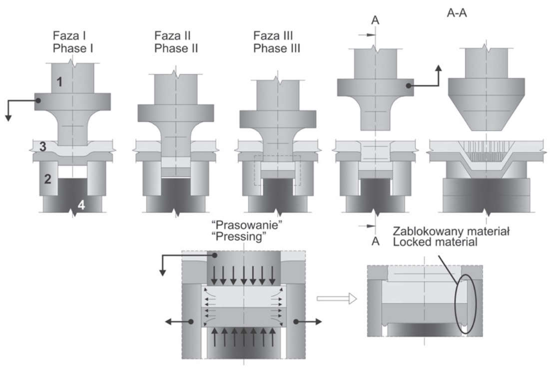

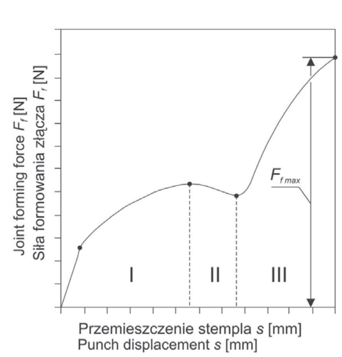

Fig. 3. Forming the rectangular clinching joint with material notch: a) diagram, b) forming force characteristics

a) b)

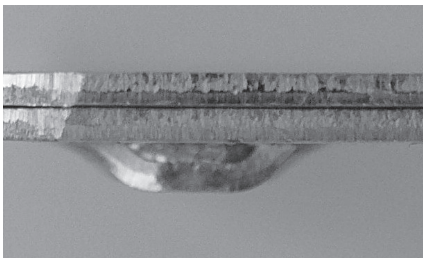

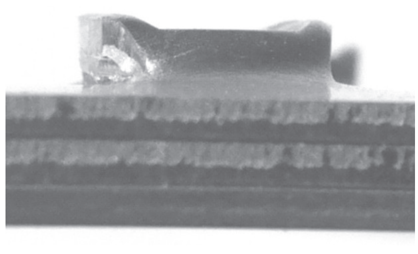

Fig. 4. Merging: a) two material layers, b) three material layers

press thickness (X) have been used in the initial experimental analysis.

When preparing the joint specimens, the merging area geometry layout angle β (fig. 6) has been the only variable parameter, others have been constant. For all cases, the overpress bottom thickness (X) has been of 0.85±0.02 mm.

The key differentiator of clinching joints is the occurrence of specified sheet material seizing in form of lock. The achieved specimens had the characteristic overpress (fig. 7a) and the flash in the merging point (fig. 7b). The specific form of joined material layers (fig. 7c, d) has been achieved thanks using the 2-segment flexible die.

The sheet joints for shearing tests have been properly marked. Such prepared joints have been subjected the shearing strength tests until complete separation. Three specimen series have been examined for four layout angles β. For each one, the force and displacement parameters have been recorded on the tensile testing machine UTS 100. The cross sections of joint have been cut using the wire erosion machine. This enabled to eliminate additional joint deformations, which occur for other cutting methods.

a)

b)

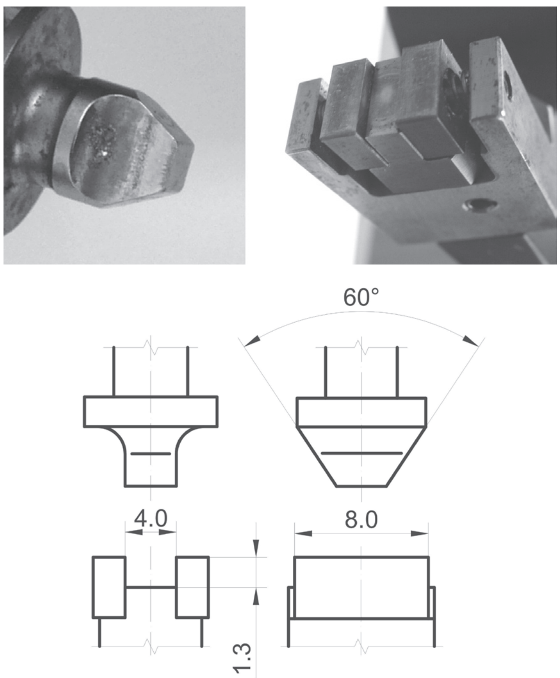

Fig. 5. Joint forming tools: a) appearance of a forming punch and segment flexible die, b) basic geometry

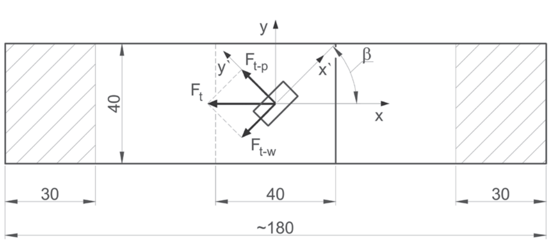

Fig. 6. The characteristics of merging area layout and shearing test specimen geometry

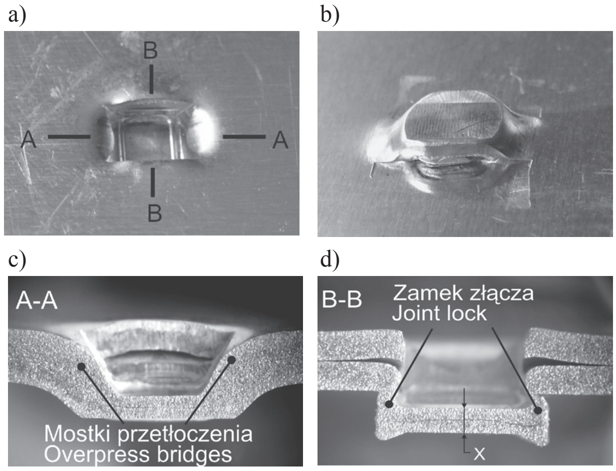

Fig. 7. Joint view: a) the overpress side, b) the flash side, and c) and d) specified cross sections

4. Results and analysis

For circular joints, the load-carrying ability is an isotropic feature. Slight differences in the shearing force characteristics are achieved for highly anisotropic sheets [9]. On the other hand, the rectangular joints feature the anisotropy for load carrying depending on its direction (fig. 8).

For examined cases of joint layout angle $\beta = 0^o, 30^o, 45^o, 90^o$ different force characteristics have been achieved (fig. 9).

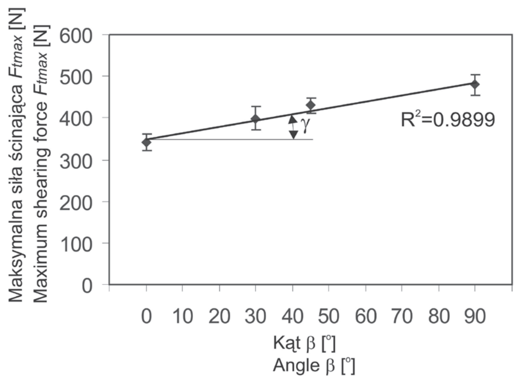

Fig. 8. The effect of layout angle β in relation to applied load direction on maximum shearing force value

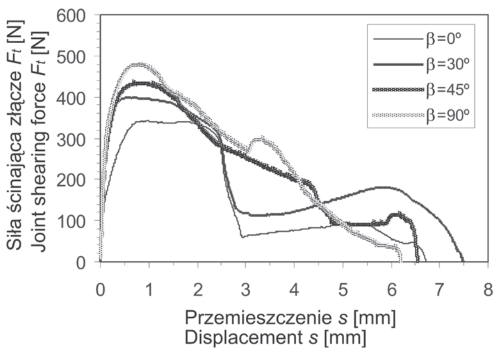

Fig. 9. The effect of layout angle β in relation to applied load direction on shearing force characteristics

The shearing force curve is a joint reaction to displacement that forces the joint element deformation. This reflects the order of joint lock degradation and energy demand until complete sheet separation.

If we know the shearing force characteristics (fig. 10) for considered layout angle, the work value may be determined by the following formula:

$$W = \int_0^{s_e} F_t(\beta)ds \tag{1}$$

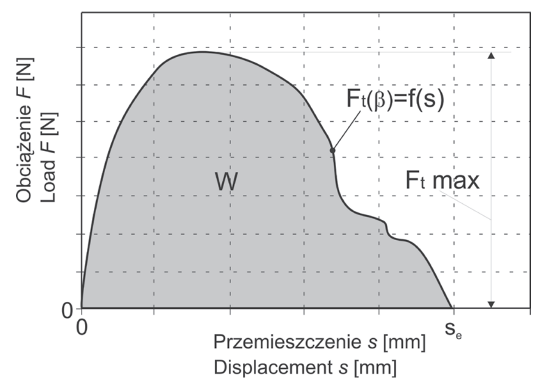

Fig. 10. The graphical interpretation of work made until joint separation

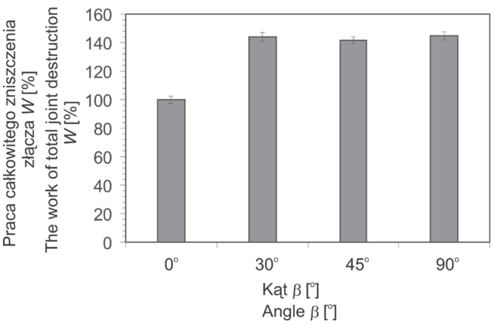

Fig. 11. Relation of joint destruction work and layout angle β

For tests with diametrically different joint layout angles in relation to applied load direction, the highest work value differences during the shearing test have been observed. The dissipation of an energy for complete sheet separation for $\beta = 90^o$ has been almost by 50% higher in relation to the shearing test for $\beta=0^o$ (fig. 11). For angles $\beta = 30^o$ and 45^o the work made had a value similar to the one for 90^o. The last two cases are accompanied by the mixed destruction mechanism, which was explained further in this paper.

For all cases, the complete joined sheet separation has occurred due to an overpress material decohesion. The separation method has depended on the shearing force components (fig. 12), which have been influenced by the joint layout angle.

The joined aluminum sheet strips have featured such a rigidity that generally all the applied load has been carried by the merging area during the test. Thus separated sheets for all specimens have not been deformed.

The individual shearing force curves along with the final appearance of specimens enable describing the joint separation mechanism.

When loading the joint for $\beta=0^o$ the separation has occurred due to a partial lock tear-up in area „1" along with an overpress material cohesion loss in areas „2" and „3" (fig. 13a). Basically, the longitudinal load of joint ($F_t=F_{t-w}$) has firstly resulted in bridge „I" stretching with force F^r_{t-w} and bridge „II" bending with torques M_{g1} i M_{g2} (fig. 14). The friction forces (T) have ac-

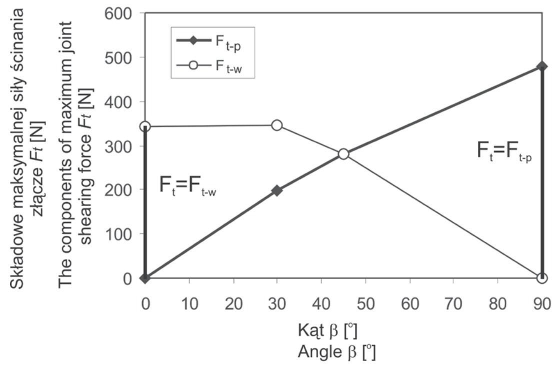

Fig. 12. The effect of layout angle β in relation to applied load direction on corresponding shearing force components

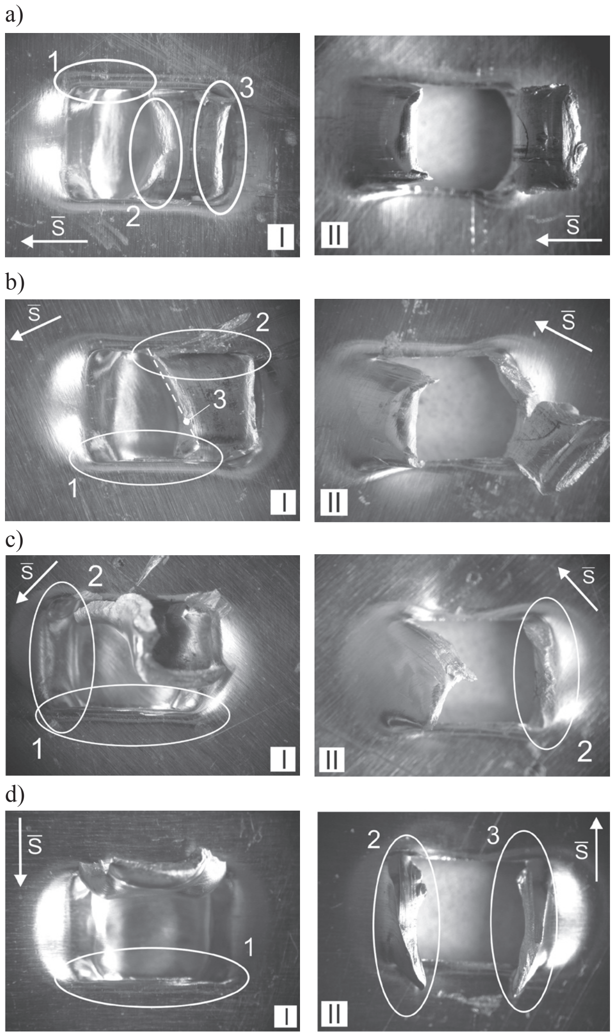

Fig. 13. The form of sheet merging area destruction achieved after the shearing test of rectangular clinching joint for layout angle β (I – lower sheet, II – upper sheet): a) 0^o, b) 30^o, c) 45^o, d) 90^o

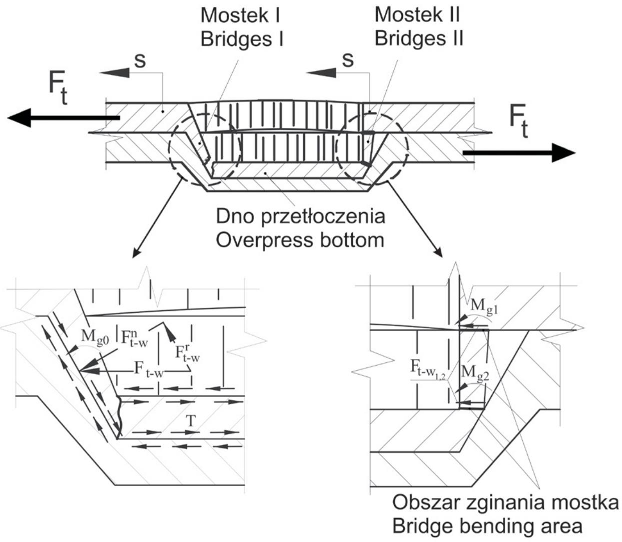

Fig. 14. Simplified description of joint bridge load during the shearing test for β=0º

companied the lock element displacement. For such a located joint during the strength test, the force firstly has risen, and then the force value has stabilized at 340 N (fig. 9). The further joint deformation has caused the bridge I breaking (area "3") and decreasing the shearing force to about 60 N. Then the gradual lock tear-up has been occurring in area "1" (fig. 13a) along with bridge II stretching. Since then the force has been increasing until the displacement of s≈6.75 mm (fig. 9), and the critical necking and bridge II material breaking (area "2" on fig. 13a).

In turn, lateral joint location (the line of cut material is perpendicular to an applied load direction) when shear testing (F_t=F_{t-p}) has resulted in a different force characteristics, comparing to the longitudinal location (fig. 9). The peak shearing force was 480 N and by 40% higher than for an angle of 0°.

When strength testing for *β* = 90° the joint has been destructed by lock tear-up in area „1" (fig. 13d), and bridge material cohesion loss in cross sections (areas "2" and "3" on fig. 13d). The application of shearing force F_t to joint has resulted in loading the overpress with resultant bending moment (M_{g1}) and shearing force (F_{t-p}). As a result the lock has been torn up in an overpress bottom area "b", and the bridge material cut off in cross section II_p (fig. 15).

The "I_p" cross section of joint has featured higher load-carrying ability than "II_p" cross section due to a larger area and lower strains during the joint forming. In the "a" area, the bottom material interference and its gradual rotation has been observed, thus the final position of an overpress bottom (fig. 13d). In the end of separation phase in the II_p cross section, only the shearing force and stretching force have accompanied the material cohesion loss.

When looking at the photos of destructed joints for intermediate β angle values (30°, 45°), it can be stated that the mixed destruction mechanism has occurred. When loading the joint for β=30°, firstly the lock tear-up has occurred in area "1" (fig. 13b). The slight loosing of seized material has accompanied the loading the sheet merging area, on the side of sheet cut in area "1". On the other hand, on the opposite side (in area "2") the gradual interference of joined layer material has occurred along with an increasing sheet displacement. Thus we have the layout

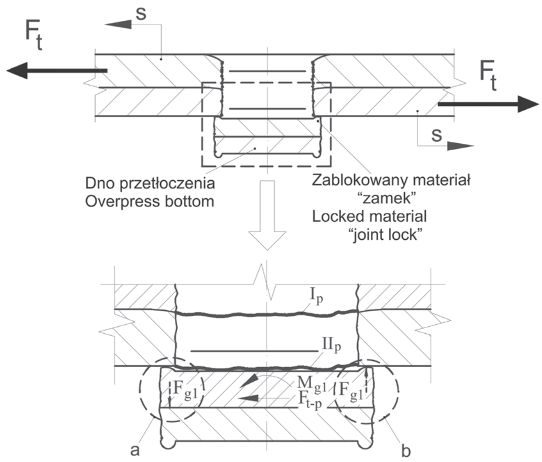

Fig. 15. Simplified description of joint load during the shearing test for β=90º

of an overpress material separation line (detail "3") with an angle of 90° in relation to sheet displacement.

Increasing the joint layout angle (β) in relation to displacement direction up to 45° has intensified the phenomena occurring just like for angle of 30°. As a result of the strength test, the turning out of the overpress bottom (fig. 13c) has accompanied the complete material tear-up in area "1". One of the bridges has been separated in the point of transition into the overpress bottom (area "2"). In previous cases the overpress bridges has been left along with the upper sheet.

5. Summary

Based on the presented experimental analysis we can state as follows:

- For a longitudinal joint load, the material cohesion loss firstly occurs in one bridge, and then all load is carried out by the rest of the lock created by pressing.

- The energy dissipation when destructing the sheet strips for $\beta=90^o$ has been by around 50% higher in relation to $\beta=0^o$ test case, but the maximum shearing force has been higher by about 40%.
- For all cases of joint layout, the diversified maximum shearing force has been achieved, and when considering the destruction work value, the similar value level has been achieved for three layout angles (30°, 45° and 90°).
- For lateral joint load, the important factor is creating possibly large material lock, which plays the significant role in joint rigidity.
- When designing the joint layout in the seam, the mounting easiness and its further operation in relation to load have to be considered.

The performed researches have revealed that such an experimental analysis might be a supplement and extension of the knowledge on rectangular clinching joint behavior for various load directions.

The specified merging area location may improve locally the load-carrying ability of single joints and balance the elastic effort of a sheet construction.

6. References

1. Bartczak B, Gierczycka-Zbrożek D, Gronostajski Z, Polak S. The use of thin-walled sections for energy absorbing components: a review. Archives of Civil and Mechanical Engineering 2010; 4(10): 5-19.
2. Gronostajski Z, Polak S. Quasi-static and dynamic deformation of double-hat thinwalled elements of vehicle controlled body crushing zones joined by clinching, Archives of Civil and Mechanical Engineering 2008; 2(8): 57-65.
3. Lennon R, Pedreschi R, Sinha B P. Comparative study of some mechanical connections in cold formed steel. Construction and Building Materials 1999; 3(13): 109-116.
4. Mucha J. The characteristics of H320LA steel sheet clinching joints. Advances in Manufacturing Science and Technology 2010; 4(34): 47-61.
5. Mucha J, Bartczak B. Thoughts on the effective modeling of the process of joining thin sheets using the clinching method. Obróbka Plastyczna Metali 2010; 2(21): 105-117.
6. Mucha J, Kaščák Ľ. Wybrane aspekty kształtowania okrągłych połączeń przetłoczeniowych. Problemy eksploatacji - Maintenance Problems 2010; 4(79): 29-38.
7. Mucha J, Kaščák L, Spišák E. Joining the car-body sheets using clinching process with various thickness and mechanical property arrangements. Archives of Civil and Mechanical Engineering 2011; 1(11): 135-148.
8. Pedreschi R F, Sinha B P. An experimental study of cold formed steel trusses using mechanical clinching. Construction and Building Materials 2008; 5(22): 921-931.
9. Saberi S, Enzinger N, Vallant R, Cerjak1 H, Hinterdorfer J, Rauch R. Influence of plastic anisotropy on the mechanical behavior of clinched joint of different coated thin steel sheets. International Journal of Material Forming 2008; 1(1): 273-276.
10. Shiming G, Lothar B. Mechanism of mechanical press joining. International Journal of Machine Tools and Manufacture 1994; 5(34): 641-657.
11. Tubielewicz K, Turczyński K. Kształtowanie połączeń blach metodą prasowania na zimno. Technologia i Automatyzacja Montażu 2001; 2(52): 66-70.
12. Tubielewicz K, Turczyński K, Tubielewicz M. Wskaźniki wytrzymałościowe połączeń kształtowych prasowanych na zimno. Technologia i Automatyzacja Montażu 2004; 3(55): 67-72.
13. Varis J P. The suitability of round clinching tools for high strength structural steel. Thin-Walled Structures 2002; 3(40): 225-238.
14. Varis J P. The suitability of clinching as a joining method for high-strength structural steel. Journal of Materials Processing Technology 2003; 1-3(132): 242-249.
15. Varis J P. Ensuring the integrity in clinching process. Journal of Materials Processing Technology 2006;1-3(174): 277-285.

Jacek MUCHA, Ph. D., Eng.
Faculty of Mechanical Engineering and Aeronautics
Rzeszow University of Technology
al. Powstańców Warszawy 8
35-959 Rzeszów, Poland
e-mail: j_mucha@prz.edu.pl

Bożena SKOTNICKA-ZASADZIEŃ
Witold BIAŁY

AN ANALYSIS OF POSSIBILITIES TO USE A PARETO CHART FOR EVALUATING MINING MACHINES' FAILURE FREQUENCY

ANALIZA MOŻLIWOŚCI WYKORZYSTANIA NARZĘDZIA PARETO-LORENZA DO OCENY AWARYJNOŚCI URZĄDZEŃ GÓRNICZYCH*

The article presents a general classification of quality management tools applied in different industry branches. From among these tools the authors have chosen a pareto chart to present an analysis of mining machines participating in the mining process. The analysis covers mining machines such as: a roadheader, chain conveyor, belt conveyer, crusher and a support.

***Keywords**: quality management, Pareto chart, failure frequency.*

W artykule przedstawiono ogólną klasyfikację narzędzi zarządzania jakością stosowanych w różnych gałęziach przemysłu. Spośród tych narzędzi został wybrany diagram Pareto-Lorenza, za pomocą którego przestawiono analizę awaryjności urządzeń górniczych biorących udział w procesie wydobywczym kopalni. Analizie poddano kombajn, przenośnik zgrzebłowy, przenośnik taśmowy, kruszarkę oraz obudowę.

***Słowa kluczowe**: zarządzanie jakością, diagram Pareto-Lorenza, awaryjność urządzeń.*

1. Introduction

Most hard coal mines have an Integrated Quality Management System and only sometimes management tools imposed by the documentation are applied as part of the system evaluation in order to assess the improvement of quality in an enterprise. The changing economic situation in the state, competition as well as ever-growing requirements of coal-mine recipients (clients) make the managers search for new ways of improving the production (mining) process [10]. In the process of hard coal mining it is very important to monitor mining machines as well as to analyse the failure frequency of machines and equipment taking part in this process.

2. Characteristics of quality management tools

Quality management tools are used to collect and process data related to various quality aspects. Most frequently they are used to supervise (monitor) the whole production cycle, starting with a design, through manufacturing and finishing with the completed production process. Quality management tools fall into two categories: traditional (old) and new ones. tables 1 and 2 present the range of use for traditional and new quality management tools.

Table 1 presents traditional quality management tools and their range of use, while table 2 shows new quality management tools and their range of use.

In this article one of traditional quality management tools – a Pareto chart has been used to evaluate mining equipment failure frequency. A Pareto chart is a tool which enables factors influencing a particular phenomenon to be organised. By means of this graphic picture it is possible to present both relative and absolute distribution of the types of errors, problems and their causes (fig. 1) [5].

The field under the Pareto chart has been divided into three areas:

- Area A – in case of 20% of populations containing 80% of cumulatve feature values.
- Area B – in case of another 30% of populations containing another 10% of cumulative feature values
- Area C – in case of the remaining 50% of populations which contain 10% of cumulative feature values.

In practice a Pareto chart is used to group particular problems and their causes in order to solve crucial problems in a given enterprise [11].

3. Problem analysis

In the mining industry a Pareto chart is used to monitor and control mining machines (a cutter-loader, chain conveyor, belt conveyor, crushers as well as power supply and control equipment) which are an important element of the mining process. It is important to evaluate these machines' failure frequency and reliability as well as to find which of the discovered causes responsible for the high failure rate may be eliminated in the first place [4,16].

The construction of a Pareto chart for mining equipment control and monitoring is divided into the following stages:

- Information collection (collecting data on mining equipment failure frequency at particular stages of the mining process),
- Putting the collected data in order (assigning particular failures to particular mining equipment, such as a cutter-loader, chain conveyor, belt conveyor, crusher, mechanised support),
- Calculation of cumulative percentage values (establishing the cumulative percentage values for particular failures),
- Preparating a Pareto chart,
- Interpretation of the Pareto chart.

(*) Tekst artykułu w polskiej wersji językowej dostępny w elektronicznym wydaniu kwartalnika na stronie ***www.ein.org.pl***

Tab. 1. Range of use for old quality management tools

Tool	Range of use
Cause-and-effect diagram of Ishikawa (fish bone diagram)	• To solve quality-related problems which involve an extended chain of causes • It is a method of recording ideas • Discovers unrevealed connections between causes • Helps to find the source of a problem
Check sheets	• Used when collecting date on the frequency of problems and defects during a production process and other processes • Used in data collection process • Used when standardising a list of activities
Histogram	• Pictorial presentation of processes and economic phenomena versus time • Visual presentation of information on the course of procesess • Shows the changeability of phenomena and states
Pareto chart	• Eliminating the most frequent phenomena • Eliminating the biggest cost sources • Analysis of a problem importance and frequency
Correlation diagrams	• Enables a graphic presentation of relationships between variables • For identifying potential sources of incosistence • Used to find whether the two effects may result from the same cause
Check cards	• To evaluate process stability over long periods of time • To assess whether the process is under control at a particular period of time • To identify areas of possible improvement • To prevent manufacture of defective products • To ensure systematic control over the process
Block diagram	• To illustrate the sequence of activities in a process • To find relations between activities • To easily specify the effects of undertaken activities • Provides a possibility of facilitating the analysis of the process course and eliminating unnecessary activities

Source: a study based on [9].

Tab. 2. Range of use for new quality management tools

Tool	Range of use
Relationship diagram	• Solving problems connected with determining the cause and effect dependence. • Showing the co-dependence between causes leading to a particular effect. • Attempts to find dependences between causes outlined in a relation diagram.
Relation diagram	• Issues subjected to analysis are too thorough or to chaotic to be defined in a simple way. • It is necessary to support a particular solution, concept, design. • The aim is to explain and justify a stance. • A useful tool after a brainstorming session is sought.
Systematic diagram	• We want to solve a specific problem (then it resembles the diagram of Ishikawa). • We present subsequent stages of activities in the process subjected to analysis.
Matrix diagram	• Helps to understand the relationships between particular groups in the diagram. • Is used to communicate these relationships.
Matrix data analysis	• Searching for market niches. • Marketing analyses. • Shows important dependencies with regard to selected features of a product.
Process Decision Programme Chart (PDPC)	• To evaluate any situations which may occur after implementing a new plan of activities which involves a risk of failure. • When implementing complicated plans of action. • When implementing plans with deadlines.
Arrow diagram	• Comprehensive planning of a project or process, taking the tasks and resources into consideration. • Project implementation time analysis. • Project implementation monitoring. • Re-planning the course of a project while taking the changes into account.

Source: a study based on [9].

3.1. Characteristics of mining equipment failure frequency

Breakdowns in hard coal mines may be divided according to their causes as follows:

- mining causes, where the main causes include: rock mass shocks, roof collapse (odpad stropu), water pumping, lump crushing, exceeding the level of CH_4 etc. In general these causes are not man-made.
- technical causes occur when the equipment and machines used in the mining process are damaged. Such equipment includes: heading machines, conveyors, mechanised supports and crushers;
- organisational causes which are independent from the mining conditions and conditions of machine operation. Such failures include: lack of water supply or lack of power supply.

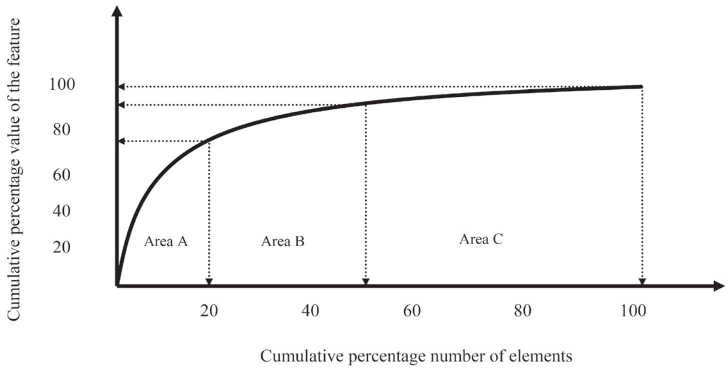

Fig. 1. Pareto chart

According to the type of failure, we distinguish the following:
- mechanical,
- electrical,
- hydraulic causes.

In order to obtain a more detailed analysis, mining equipment failures may be further divided according to the area of their occurrence, e.g..: arms and cutting heads, traction systems, hydraulic systems, electrical system or the body [3].

In Polish coal mining industry, coal beds are mined using the longwall method by means of winning equipment which works on a machine cutting basis [1,7,8]. For this reason, one of major areas of a coal-mine activity is the use of equipment (machines) [6]. Among others this should involve control over rational and effective use of equipment in the mining process [14].

Technical systems used in a hard coal mine are characterised by:
- considerable scattering,
- complexity,
- working area limitation by the size of underground excavations.

The main task for maintenance teams is to ensure continuous work of machines and equipment (at a given moment). As a result of such actions, the costs of machines and equipment maintenance, and thus production costs, i.e. the costs of a mining plant functioning are reduced. If this process is disturbed, huge losses are generated [13].

The main element in the mining process is the sequence of getting, which consists of the following stages [2,3]:
- the process of getting,
- horizontal transport,
- vertical transport.

When following the sequence of getting we may find that it is a series system. A failure of one of the above listed links results in "switching off" the remaining elements of this sequence.

As the sequence of getting in the process of coal mining (the mining of useful minerals) is a basic element influencing the size of output, and in consequence the costs related to this process, the failure frequency of this basic element has been subjected to analysis [2,3]. The failure frequency of all the faces working in one of the hard coal mines belonging to Kompania Węglowa S.A. in 2009 has been analysed. More than 400 types of failures have been found. Table 3 presents examples of mining machine failures.

3.2. Practical use of a Pareto chart for evaluating mining equipment failure frequency

Mining equipment failure frequency has benn analysed using one of the traditional quality management tools – a Pareto chart.

A Pareto chart has been constructed according to the following stages:
1. Data on the type of failures of the following mining equipment has been collected: cutter-loaders, chain conveyors, belt conveyors, curshers and mechanised supports,
2. Particular failures have been assigned to particular mining machines,
3. Cumulative percentage values have been calculated (cumulative percentage values for particular failures) by means of the following formulas:

$$PIE_j = \frac{100}{IE} \tag{1}$$

$$SPIE_j = PIE_j + PIE_{j-1} \tag{2}$$

$$\frac{100 \cdot IA_j}{\sum_{i=1}^{IE} IA_j} \tag{3}$$

$$SPIA_j = PIA_j + PIA_{j-1} \tag{4}$$

where: PIE_j – percentage number of elements, $SPIE_j$ – cumulative percentage number of elements, IE – number of elements, PIA_j – percentage number of failures, $SPIA_j$ – cumulative percentage number of failures, IA – number of failures.

Table 4 presents data on the type of mining equipment, a cumulative percantage number of particular machines, a number of failures in a particular machine, a percentage number of failures and a cumulative percentage number of failures.

Figure 2 presents a Pareto chart for the failure frequency of the sequence of getting in one of the mines belonging to Kompania Węglowa S.A.

Tab. 3. Examples of the types of failures and their causes

Type of failure	Machine	Examples of damage
Mechanical failures	Cutter-loader	Damaged cutter-loader cable
		Damaged cable layer
		Protection system exchange
		Damaged cooler of the cutter-loader lower arm
		Damaged water cable
Electrical failures	Cutter-loader	No control
		Electrical damage of the cutter-loader cable
		Burnt fuse of the hydraulic pump
Hydraulic failures	Cutter-loader	Damaged cutter-loader water hose
		Damaged sealing of the cutter-loader upper head
		Water hose exchange
Organisational failures	Cutter-loader	No water for the cutter-loader
		No power supply on the face
		No pressure on the face
Mechanical failures	Chain conveyor	No control
		Damaged coupling insert
		Seized bearing of the right gear
Electrical failures	Chain conveyor	Damaged set of chokes on the upper drive contactor
		Damaged control panel
		No control – damaged fuse
Organisational failures	Chain conveyor	No water
		No power supply
Mechanical failures	Belt conveyor	Damaged coupling
		Gear exchange
Electrical failures	Belt conveyor	No control
		Fuse exchange
		No brake control
Organisational failures	Belt conveyor	No power supply on transport equipemnt
		No power supply
Mechanical failures	Crushers	Flux exchange
		Broken ram
Electrical failures	Crushers	No control
		No power supply
Mechanical failures	Support	Exchange of hose in pressure conduit
		Damaged hose
Electrical failures	Support	No pump control
Organisational failures	Support	Pipeline sealing

Tab. 4. Mining equipment failure frequency

Number of equipment	Type of equip-ment	Cumulative percentage number of elements	Number of failures	Percentage number of failures	Cumulative percentage number of failures
j		SPIE	IA	PIA	SPIA
1	Cutter-loader	20	193	43	43
2	Chain conveyor	40	110	24	67
3	Belt conveyor	60	94	21	88
4	Crusher	80	28	6	94
5	Support	100	27	6	100

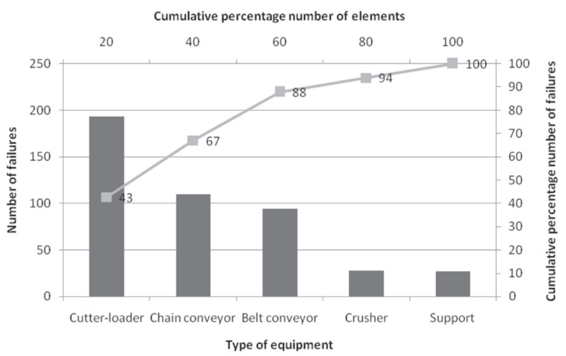

Fig. 2. Pareto chart

4. Summary

The Pareto chart indicates that the highest number of failures (88%) are caused by three mining machines:
- cutter-loaders,
- chain conveyors,
- belt conveyors.

The remaining machines, such as crushers and mechanised supports cause only 12% of failures.

Taking into consideration the percentage share of the three important mining machines (cutter-loaders, chain conveyors and belt conveyors) it may be concluded that the total of 60% of machines cause as much as 88% of failures.

Longwall equipment failures affect the effectiveness and concentration of output and in consequence, translate into the financial result of a mine.

Preliminary analyses (table 3) and studies [2, 3] indicate that most failures found in the above mentioned three types of machines are mechanical ones. This leads to the conclusion that the above mentioned three types of mining machines should be subjected to thorough analysis. Such analysis should specify the main causes of failures, methods and preventive measures which should be taken in order to drastically reduce the failure frequency of these elements of mining equipment. Persons monitoring and controlling the work of cutter-loaders, chain conveyors, belt conveyors should take special care of these machines' technical condition and try to prevent any failures.

In their further studies, the authors will present the causes and effects of these machines' failures which have the biggest impact on the mining sequence delays, i.e. winning machines (cutter-loaders) and transport equipment (chain and belt conveyors).

5. References

1. Biały W. Wybrane metody badania urabialności węgla. Eksploatacja i Niezawodnosc - Miantenance and Reliability, 2001; 5: 36-40.
2. Biały W, Bobkowski G. Możliwości wykorzystania narzędzi komputerowych w gospodarce remontowej kopalń węgla kamiennego. Mechanizacja i Automatyzacja Górnictwa 2005; 4: 42-51.
3. Biały W. Awaryjność górniczych urządzeń technicznych w procesie wydobywczym. Problemy Bezpieczeństwa w Budowie i Eksploatacji Maszyn i Urządzeń Górnictwa Podziemnego. Praca zbior. pod red. K. Krauze. Lędziny: Centrum Badań i Dozoru Górnictwa Podziemnego Sp. z o. o., 2010: 73-85.
4. Duży S. Elementy zarządzania jakością w procesie drążenia wyrobisk korytarzowych w kopalni węgla kamiennego. Gospodarka Surowcami Mineralnymi 2007; 23(Zeszyt Specjalny nr 2): 71-80.
5. Franik T. Monitorowanie podstawowych parametrów procesów produkcyjnych w kopalni węgla kamiennego. Komputerowo zintegrowane zarządzanie. Praca zbior. pod red. R. Knosali, Opole: Oficyna Wydawnicza Polskiego Towarzystwa Zarządzania Produkcją, 2009: 286-295.
6. Jonak J. Use of artificial intelligence automation of rock cutting. Journal of Mining Science 2002; 3(38): 270-277.
7. Jonak J, Gajewski J. Wybrane problemy diagnostyki i monitorowania pracy górniczych przenośników taśmowych. Eksploatacja i Niezawodnosc – Maintenance and Reliability, 2006; 4: 74-79.
8. Krauze K. Urabianie skał kombajnami ścianowymi. „Śląsk" sp. z o.o. Katowice: Wydawnictwo Naukowe, 2000.
9. Krzemień E. Zintegrowane zarządzanie – aspekty towaroznawcze: jakość, środowisko, technologia, bezpieczeństwo. Katowice: Wydawnictwo Śląsk, 2003.
10. Łucki Z. Zarządzanie w górnictwie naftowym i gazownictwie. Kraków: Wydawnictwo UNIVERSITAS, 2005.
11. Łuczak J, Matuszak-Flejszman A. Metody i techniki zarządzania jakością. Kompendium wiedzy. Poznań: Quality Progress, 2007.
12. Uzgören N, Elevli S, Elevil B, Önder U. Reliability analysis of draglines' mechanical failures. Eksploatacja i Niezawodnosc – Maintenance and Reliability, 2010; 4: 23-29.
13. Orlacz J.: Wprowadzenie do zagadnień niezawodności i trwałości maszyn i urządzeń górniczych. Gliwice: Wydawnictwo Politechniki Śląskiej, 1999.
14. Peter F. Rethinking Pareto analysis maintenance applications of logarithmic scatterplots. Journal of Quality i Maintenance Engineering, 2001; 4(7): 252-263.
15. Wang Z, Huang H-Z, Du X. Reliability - based design incorporating several maintenance policies. Eksploatacja i Niezawodnosc – Maintenance and Reliability, 2009; 4: 37-44.
16. Wolniak R, Skotnicka B. Metody i narzędzia zarządzania jakością – teoria i praktyka. Gliwice: Wydawnictwo Politechniki Śląskiej, 2007.

Dr inż. Bożena SKOTNICKA-ZASADZIEŃ
Dr hab. inż. Witold BIAŁY, prof. nzw. w Pol. Śl.
Institute of the Production Engineering
Silesian University of Technology
Ul. Roosevelta nr 26, 41-800 Zabrze, Polska
e-mail: bozena.skotnicka@polsl.pl; wbialy@polsl.pl

Yu PANG
Hong-Zhong HUANG
Liping HE
Zhonglai WANG
Ning-Cong XIAO

CONVEX SUBLATTICE BASED RELIABILITY THEORY

TEORIA NIEZAWODNOŚCI OPARTA NA POJĘCIU PODKRATY WYPUKŁEJ

Classical probability theory has been widely used in reliability analysis; however, it is hard to handle when the system is lack of adequate and sufficient data. Nowadays, alternative approaches such as possibility theory and fuzzy set theory have also been proposed to analyze vagueness and epistemic uncertainty regarding reliability aspects of complex and large systems. The model presented in this paper is based upon possibility theory and multistate assumption. Convex sublattice is addressed on congruence relation regarding the complete lattice of structure functions. The relations between the equivalence classes on the congruence relation and the set of all structure functions are established. Furthermore, important reliability bounds can be derived under the notion of convex sublattice. Finally, a numerical example is given to illustrate the results.

Keywords: *congruence relation, convex sublattice, lattice theory, multistate structure function, possibility theory, upper bound set.*

Klasyczna teoria prawdopodobieństwa ma szerokie zastosowanie w analizie niezawodności, jednak trudno jest się nią posługiwać, kiedy brak jest wystarczających i odpowiednich danych na temat systemu. Obecnie, proponuje się alternatywne podejścia, takie jak teoria możliwości czy teoria zbiorów rozmytych, za pomocą których można analizować niepewność epistemiczną oraz nieostrość w odniesieniu do aspektów niezawodności złożonych i dużych systemów. Model przedstawiony w niniejszym artykule oparto na teorii możliwości oraz na założeniu wielostanowości. Podkratę wklęsłą opisano na relacji kongruencji, odnoszącej się do całej kraty funkcji struktury. Ustalono relacje pomiędzy klasami równoważności na relacji kongruencji a zbiorem wszystkich funkcji struktury. Ponadto posługując się pojęciem podkraty wypukłej można wyprowadzać istotne kresy niezawodności. Wyniki zilustrowano przykładem numerycznym.

Słowa kluczowe: *relacja kongruencji, podkrata wypukła, teoria krat, wielostanowa funkcja struktury, teoria możliwości, górny kres zbioru.*

1. Introduction

The classical reliability theory is based upon binary structure functions and probability theory [19, 21]. In the binary probabilistic approach, the component state and system state may be assumed to be either perfectly functioning or completely failed, which is an oversimplification of reality [6]. The increasing complexity of real systems has brought the emergent need of intermediate states. With this background, the theory of multistate structure functions was proposed to overcome the problem [14, 15]. Moreover, in many real life cases, adequate statistical data is unavailable to obtain due to the limitation of experimental conditions [13]. Probability theory is shown not the only possible way of representing imprecision and uncertainty [7]. In fact, possibility theory has played a vital role in analyzing system uncertainty [8, 12, 17]. The models for reliability estimation studied from a non-probabilistic point of view are proposed to overcome the problems of approach in past literatures [1, 9, 10, 18, 20].

In order to better represent the system or component state space, lattice theory is essential in mathematical modelling using non-classical reliability theory [16]. By considering the complete lattice of a structure function, a general framework has given us a better foundation of reliability analysis [2, 4]. Cappelle [3] presented a theory of multistate structure functions on partially ordered sets (in casu complete lattices), which is able to solve several problems arising from the dichotomous model. Based on a combination of multistate structure functions and possibility theory, Cappelle and Kerre [7] derived a congruence relation on the complete lattice of structure functions which links several concepts and provides powerful tools to model physical systems. Based upon the congruence relation proposed by Cappelle and Kerre, the concept of convex sublattice is presented in reliability analysis in this paper. According to the convex sublattice properties, the upper (lower) bound set of structure functions on equivalence relations regarding the congruence relation is addressed to go along with the practical engineering. Given an equivalence class on structure functions, it can be verified that the upper (lower) bound set of the equivalence class is a convex lattice. Thus, several important boundaries of the structure function set are employed. Furthermore, the significance of the definitions and properties are explained, both from theoretical and practical point of view.

This paper is organized as follows. In the next section, preliminary definitions such as structure functions and congruence relations are briefly reviewed. In Section 3, the notion of a convex sublattice is applied to reliability theory, along with the explanation of how the theorems and properties can be used in practical engineering. Afterwards, a numerical example is addressed in Section 4 to exemplify the usefulness of the introduced concepts. As a result, some conclusions are employed in Section 5.

2. Preliminary definitions

In this section, three useful notions regarding the theory of multistate structure functions on complete lattices are introduced. Considering that systems are with a finite number of components, we first give the concept of structure function, which can reflect the functional relationship between components states and system state.

Definition 1 [3] Let $(L_i,\leq)$, $1\leq i\leq n$, and $(L,\leq)$ be $n+1$ complete lattices. An $L_1\times...\times L_n - L$-mapping ϕ, satisfying

(i) $\phi(0,...,0) = 0$ and $\phi(1,...,1) = 1$ (1)

(ii) ϕ is isotone, that is

$$\left(\forall(\mathbf{x},\mathbf{y})\in(L_1\times\cdots\times L_n)^2\right)\left(\mathbf{x}\leq\mathbf{y}\Rightarrow\phi(\mathbf{x})\leq\phi(\mathbf{y})\right) \quad (2)$$

is called to be a *structure function* from $(L_1\times...\times L_n, \leq)$ to $(L,\leq)$.

$\mathcal{M}(L_1\times...\times L_n, L)$ denotes the set of all the structure functions from complete lattice $(L_1\times...\times L_n,\leq)$ to complete lattice $(L,\leq)$. The order relationship $\preceq$ is defined as follows: for any two $L_1\times...\times L_n - L$ structure functions ϕ_1 and ϕ_2,

$$\phi_1 \preceq \phi_2 \Leftrightarrow (\forall\mathbf{x}\in L_1\times\cdots\times L_n)(\phi_1(\mathbf{x})\leq\phi_2(\mathbf{x})) \quad (3)$$

More properties of the complete lattice of structure functions will not be introduced here. For more details, the readers are referred to [3]. In the sequel, a core notion of congruence relation is addressed. All the equivalence classes employed in this paper are based upon the congruence relation.

Definition 2 [11] Let $(L,\leq)$ be a lattice and θ a binary relation on L; θ is a *congruence relation* if and only if

(i) θ is an equivalence relation on L,

(ii) for any elements x_1, x_2, y_1 and y_2 of L

$$x_1\in[y_1]_\theta \text{ and } x_2\in[y_2]_\theta \Rightarrow$$

$$\Rightarrow x_1\wedge x_2\in[y_1\wedge y_2]_\theta \text{ and } x_1\vee x_2\in[y_1\vee y_2]_\theta \quad (4)$$

In this definition, $[x]_\theta$ is the equivalence class of θ which is generated by x. The infimum (supremum) operator is denoted by $\wedge(\vee)$ on the lattice $(L,\leq)$, meanwhile denoted by $\cap(\cup)$ on the set of structure functions, that is, for any two structure functions ϕ_1 and ϕ_2,

$$\phi_1\cap\phi_2 : L_1\times\cdots\times L_n\to L : \mathbf{x}\mapsto\phi_1(\mathbf{x})\wedge\phi_2(\mathbf{x}) \quad (5)$$

The operation $\cup$ can be defined analogously. The subset S of the lattice L is called convex iff $a,b\in S$, $c\in L$, and $a\leq c\leq b$ imply that $c\in S$. Since the intersection of any number of convex sublattice is a convex sublattice unless void, the definition of convex sublattice is generated by a subset [11].

Definition 3 [11] Let $(L,\leq)$ be a lattice and S a subset of L, S is a convex sublattice of L if and only if

$$(\forall a,b\in S)([a\wedge b, a\vee b]\subseteq S) \quad (6)$$

For $a,b\in L$, $a\leq b$, the interval $[a,b]=\{x|a\leq x\leq b\}$ is an important example of a convex sublattice. For a chain C, $a,b\in C$, $a\leq b$, the half-open intervals: $(a,b]=\{x|a<x\leq b\}$ and $[a,b)=\{x|a\leq x<b\}$, and the open interval: $(a,b)=\{x|a<x<b\}$, whenever nonvoid, are examples of convex sublattices.

3. Convex sublattice concept applied in reliability theory

Regarding the definition of convex sublattice, some interesting results are proposed to show how the convex sublattice concept is related to reliability theory in this section. First, two preliminary results, which are proposed by Cappelle and Kerre [7], are employed as lemmas. Then, three main theorems and one property are addressed with detailed proof. As a result, the significance of theoretic concepts applied in practical reliability engineering is addressed.

3.1. Preliminary results

The lemmas presented in this part are as a foundation of the main theoretical results. A typical equivalence class of structure functions is addressed in Lemma 1. On the basis of this equivalence class, different subsets result in different observations.

Lemma 1 [7] Let A be a subset of $L_1\times...\times L_n$, ϕ and φ two arbitrary structure functions from $(L_1\times...\times L_n,\leq)$ to $(L,\leq)$, then

$$\varphi\in[\phi]_{\theta_A}\Leftrightarrow(\forall\mathbf{x}\in A)(\varphi(\mathbf{x})=\phi(\mathbf{x})) \quad (7)$$

Lemma 2 [7] Let A and B be two subsets of $L_1\times...\times L_n$ and ϕ a structure function from $(L_1\times...\times L_n,\leq)$ to $(L,\leq)$, then

$$A\subseteq B\Rightarrow[\phi]_{\theta_B}\subseteq[\phi]_{\theta_A} \quad (8)$$

Lemma 2 can be intuitively understood from fig.1. That is, more observation will result in a smaller number of appropriate structure functions that meet with given information.

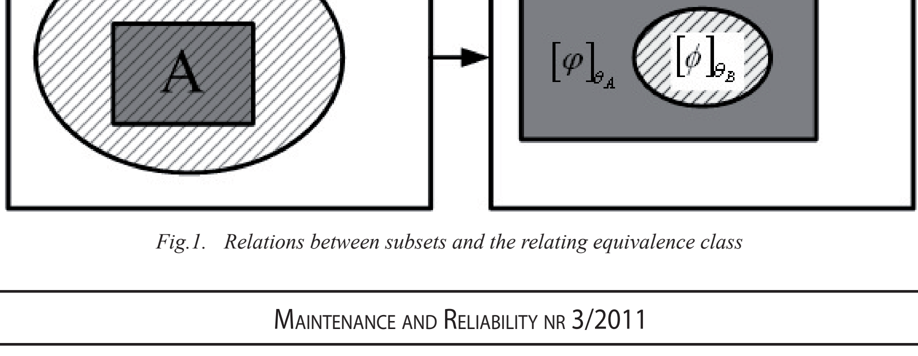

Fig.1. Relations between subsets and the relating equivalence class

3.2. Main theoretical results

All the theorems addressed in this part will provide us with several typical convex sublattices of ($\mathcal{M}(L_1\times...\times L_n,\ ),\preceq$), which are with significant meaning in engineering application.

Theorem 1 Let A be a subset of $L_1\times...\times L_n$ and ϕ a structure function from $(L_1\times...\times L_n,\leq)$ to $(L,\leq)$, then $\left([\phi]_{\theta_A},\prec\right)$ is a convex sublattice of ($\mathcal{M}(L_1\times...\times L_n,L),\preceq$).

Proof: Let ϕ_i and ϕ_j be two arbitrary elements of $[\phi]_{\theta_A}$, it can be addressed from Lemma 1 that

$$(\forall \mathbf{x}\in A)\left(\phi_i(\mathbf{x})=\phi(\mathbf{x})=\phi_j(\mathbf{x})\right) \tag{9}$$

Thus,

$$(\forall \mathbf{x}\in A)\left((\phi_i\cap\phi_j)(\mathbf{x})=\phi(\mathbf{x})=(\phi_i\cup\phi_j)(\mathbf{x})\right) \tag{10}$$

Let ϕ' be any element belongs to $\left[\phi_i\cap\phi_j,\phi_i\cup\phi_j\right]$, then

$$\phi_i\cap\phi_j\preceq\phi'\preceq\phi_i\cup\phi_j \tag{11}$$

Hence,

$$(\forall \mathbf{x}\in L_1\times\cdots\times L_n)\left((\phi_i\cap\phi_j)(\mathbf{x})\leq\phi'(\mathbf{x})\leq(\phi_i\cup\phi_j)(\mathbf{x})\right) \tag{12}$$

which leads to

$$(\forall \mathbf{x}\in A)\left(\phi'(\mathbf{x})=\phi(\mathbf{x})\right) \tag{13}$$

or equivalently

$$\left(\forall\phi'\in\left[\phi_i\cap\phi_j,\phi_i\cup\phi_j\right]\right)\left(\phi'(\mathbf{x})\in[\phi]_{\theta_A}\right) \tag{14}$$

Then, we can get

$$\left(\forall\phi_i,\phi_j\in[\phi]_{\theta_A}\right)\left(\left[\phi_i\cap\phi_j,\phi_i\cup\phi_j\right]\subseteq[\phi]_{\theta_A}\right) \tag{15}$$

Taking Definition 3 into account, the theorem is deduced. $\left([\phi]_{\theta_A},\prec\right)$ is a convex sublattice of ($\mathcal{M}(L_1\times...\times L_n,L),\preceq$) based on the equivalence relation θ_A. The lattices which are presented in the following two theorems are on the basis of equivalence class $[\phi]_{\theta_A}$.

Theorem 2 Let A be a subset of $L_1\times...\times L_n$, ϕ a structure function from $(L_1\times...\times L_n,\leq)$ to $(L,\leq)$ and M_aA (M_iA) denote the upper (lower) bound set of $[\phi]_{\theta_A}$ within $\mathcal{M}$, then $(M_aA,\leq)$ ($(M_iA,\leq)$) is a complete sublattice of ($\mathcal{M}(L_1\times...\times L_n,L),\preceq$).

Proof: Only the proof of upper bound set M_aA a complete sublattice of ($\mathcal{M}(L_1\times...\times L_n,L),\preceq$) is given here. The results about the lower bound set M_iA can be proved analogously.

Let $(\phi_i|i\in I)$ be a non-empty family in M_aA, then

$$(\forall i\in I)(\forall\mathbf{x}\in A)\left(\phi_i(\mathbf{x})\geq\phi(\mathbf{x})\right) \tag{16}$$

Thus,

$$(\forall\mathbf{x}\in A)\left(\inf_{i\in I}\phi_i(\mathbf{x})\geq\phi(\mathbf{x})\right)\text{ and }(\forall\mathbf{x}\in A)\left(\sup_{i\in I}\phi_i(\mathbf{x})\geq\phi(\mathbf{x})\right) \tag{17}$$

Since both $\inf_{i\in I}\phi_i(\mathbf{x})$ and $\sup_{i\in I}\phi_i(\mathbf{x})$ are belonged to M_aA, $(M_aA,\leq)$ is a complete sublattice of ($\mathcal{M}(L_1\times...\times L_n,L),\preceq$).

Theorem 3 Let A be a subset of $L_1\times...\times L_n$, ϕ a structure function from $(L_1\times...\times L_n,\leq)$ to $(L,\leq)$ and M_aA (M_iA) denote the upper (lower) bound set of $[\phi]_{\theta_A}$ within $\mathcal{M}$, then $(M_aA,\leq)$ ($(M_iA,\leq)$) is a convex sublattice of ($\mathcal{M}(L_1\times...\times L_n,L),\preceq$).

Proof: As is proved in theorem 2, only the proof of upper bound set M_aA a convex sublattice of ($\mathcal{M}(L_1\times...\times L_n,L),\preceq$) is addressed here.

According to Definition 3, we must prove that

$$\left(\forall\phi_i,\phi_j\in M_aA\right)\left(\left[\phi_i\cap\phi_j,\phi_i\cup\phi_j\right]\subseteq M_aA\right) \tag{18}$$

Since for any structure function $\phi_m\in[\phi]_{\theta_A}$,

$$(\forall\mathbf{x}\in A)\left(\phi_m(\mathbf{x})=\phi(\mathbf{x})\right) \tag{19}$$

Furthermore, for any $\phi_i,\phi_j\in M_aA$ and any $\mathrm{x}\in L_1\times...\times L_n$,

$$\phi_i(\mathbf{x})\geq\phi_m(\mathbf{x}),\quad\phi_j(\mathbf{x})\geq\phi_m(\mathbf{x}) \tag{20}$$

Hence,

$$(\forall\mathbf{x}\in L_1\times\cdots\times L_n)\left((\phi_i\cap\phi_j)(\mathbf{x})\geq\phi_m(\mathbf{x}),\ (\phi_i\cup\phi_j)(\mathbf{x})\geq\phi_m(\mathbf{x})\right) \tag{21}$$

which leads to that for any $\phi'\in\left[\phi_i\cap\phi_j,\phi_i\cup\phi_j\right]$,

$$(\forall\mathbf{x}\in L_1\times\cdots\times L_n)\left(\phi'(\mathbf{x})\geq\phi_m(\mathbf{x})\right) \tag{22}$$

It is obvious that ϕ' is an upper bound of $[\phi]_{\theta_A}$, that is $\phi'\in M_aA$.

Thus, it can be obtained that (1) holds from the selection of ϕ'.

It turns out that $(M_aA,\leq)$ ($(M_iA,\leq)$) is a convex sublattice of ($\mathcal{M}(L_1\times...\times L_n,L),\preceq$), and complete sublattice at the meantime. That is to say, the upper (lower) bound set of $[\phi]_{\theta_A}$ within $\mathcal{M}$ exists and can be figured out. Adding subset B of $L_1\times...\times L_n$, more interesting results can be figured out in the following.

Corollary 1 Let A and B be two subsets of $L_1\times...\times L_n$ ($A\subseteq B$) and ϕ a structure function from $(L_1\times...\times L_n,\leq)$ to $(L,\leq)$, then the upper (lower) bound set of $[\phi]_{\theta_B}$ within $[\phi]_{\theta_A}$ is a convex sublattice of $\left([\phi]_{\theta_A},\preceq\right)$.

Proof: Immediate from Theorem 3 and Lemma 2.

Property 1 Let A be a subset of $L_1\times...\times L_n$, ϕ a structure function from $(L_1\times...\times L_n,\leq)$ to $(L,\leq)$ and M_aA(M_iA) denote the upper (lower) bound set of $[\phi]_{\theta_A}$ within $\mathcal{M}$, then (i) the maximum and minimum of $(M_aA,\leq)$ is the supremum of $(\mathcal{M},\leq)$ and $\left([\phi]_{\theta_A},\leq\right)$, respectively; (ii) the maximum and minimum of $(M_iA,\leq)$ is the infimum of $(\mathcal{M},\leq)$ and $\left([\phi]_{\theta_A},\leq\right)$, respectively.

Proof: There are two parts in statement (i):

1) The maximum of $(M_aA,\leq)$ is the supremum of $(\mathcal{M},\leq)$;
2) The minimum of $(M_aA,\leq)$ is the supremum of $\left([\phi]_{\theta_A},\leq\right)$

Let φ denote the supremum of $(\mathcal{M},\leq)$. According to $[\phi]_{\theta_A}\subseteq\mathcal{M}$, it can be immediately obtained that φ is an upper bound of $\left([\phi]_{\theta_A},\leq\right)$, that is $\varphi\in M_aA$. For $\forall\eta\in M_aA$, η is an upper bound of $\left([\phi]_{\theta_A},\leq\right)$ within $(\mathcal{M},\leq)$, then $\eta\in(\mathcal{M},\leq)$. Based on the denotation of φ, $\varphi(\mathbf{x})\geq\eta(\mathbf{x})$ holds for $\forall\ \mathbf{x}\in L_1\times\cdots\times L_n$. Thus, φ is an upper bound of $(M_aA,\leq)$. It can be deduced that φ is the maximum of $(M_aA,\leq)$.

The other statements can be addressed in a similar way.

Corollary 2 Let A and B be two subsets of $L_1\times\ldots\times L_n$ ($A\subseteq B$), ϕ a structure function from($L_1\times\ldots\times L_n,\leq$) to ($L,\leq$) and $M_aB(M_iB)$ denote the upper (lower) bound set of $[\phi]_{\theta_B}$ within $[\phi]_{\theta_A}$, then (i) maximum and minimum of $(M_aB,\leq)$ is the supremum of $([\phi]_{\theta_A},\leq)$ and $([\phi]_{\theta_B},\leq)$, respectively; (ii) maximum and minimum of $(M_iB,\leq)$ is the infimum of $([\phi]_{\theta_B},\leq)$ and $([\phi]_{\theta_A},\leq)$, respectively.

Proof: Immediate from Property 1 and Lemma 2.

In the preceding paragraphs, main theoretical results have been addressed, together with the boundary of bound set. It will be shown how to apply these results of convex sublattices to actual problems.

3.3. Explanations and discussions

In real life situations, it is necessary to estimate structure functions. How can we narrow the scope of appropriate structure functions from a set of observation? Mathematically, considering a subset A of $L_1\times\ldots\times L_n$, set $A_\phi=\{(\mathbf{x},y)|\mathbf{x}\in A\}$ is called an observation set of ϕ in which $\phi(\mathbf{x})=y$. Thus, an ordered couple $(\mathbf{x},y)$ is called an observation, which is an element of A_ϕ [5]. As a matter of fact, it is rarely possible to investigate all the observations. Suppose that system state space is presented as a limited amount of elements of $L_1\times\ldots\times L_n$, denoted by A, thus the set of observation A_ϕ is determined. Additionally, given the observation A_ϕ, $[\phi]_{\theta_A}$ represents the equivalence class of structure functions which satisfy Equation (7). Hence, the bounds of set $[\phi]_{\theta_A}$ can be figured out. Based on the determined observations, engineers are always fond of the structure functions superior to any in $[\phi]_{\theta_A}$. In fact, for any $\mathbf{x}\in A$, $\mathbf{x}$ denotes the state vector of n subsystems (components) and different structure function corresponds to a different system structure. As for the same state vector of n subsystems (components), for instance, parallel and series system may lead to different results of system state. This system structure can be represented by the structure function. Undoubtedly, people are willing to find structure for system which can be under better state based on the same subsystem (component) state. This is why it is essential to study the upper bound set of $[\phi]_{\theta_A}$. According to the order relation within the set of all the structure functions, those are superior to any in $[\phi]_{\theta_A}$ should be superior to any element of the upper bound set of $[\phi]_{\theta_A}$.

It can be proven from Theorem 2 that both the supremum and the infimum of the upper bound set of $[\phi]_{\theta_A}$ exist. It is indicated in Theorem 3 that any structure function situated between the supremum and the infimum is an upper bound of $[\phi]_{\theta_A}$. Furthermore, the lower and upper bound of M_aA can be substituted and transformed through Property 1, which will result in useful bounds. Given a data of subsystem (component) state, good structure function is capable of leading to a good system state. Engineers are able to compare the characteristics between the examining structure function and those within $[\phi]_{\theta_A}$. Comparison of the examining structure function and those within $[\phi]_{\theta_A}$ is directly converted to the comparison of the examining structure function and the infimum of the upper bound of $[\phi]_{\theta_A}$ or the supremum of the lower bound of $[\phi]_{\theta_A}$. Consider a structure function ϕ from ($[0,1]^2,\leq$) to ($[0,1],\leq$), $\phi:[0,1]^2\to[0,1]:(x_1,x_2)\mapsto$ $\mapsto\frac{x_1+x_2}{2}$, Let A be the set of $\left\{(0,0),\left(\frac{1}{2},\frac{1}{2}\right),(1,1)\right\}$, it can be figured out that $\varphi_1(x_1,x_2)=\min(x_1,x_2)$ and $\varphi_2(x_1,x_2)=\max(x_1,x_2)$ is the supremum of the lower bound of $[\phi]_{\theta_A}$ and the infimum of the upper bound of $[\phi]_{\theta_A}$, respectively. Thus, given the examining structure function $\varphi(x_1,x_2)=x_1\cdot x_2$, it is easy to find out that both φ_1 and φ_2 are superior to φ. Therefore, comparison of the examining structure function and those within $[\phi]_{\theta_A}$ is given.

4. Numerical example

In this section, the numerical example in Ref. [4] is used to illustrate the results in Section 3.

Consider a structure function ϕ from ($[0,1]^2,\leq$) to ($[0,1],\leq$),

$$\phi:[0,1]^2\to[0,1]:(x_1,x_2)\mapsto\frac{x_1+x_2}{2} \tag{23}$$

It is easy to know the value of ϕ in some specific points, such as,

$$\phi\left(\frac{1}{5},\frac{4}{5}\right)=\frac{1}{2}\ ,\ \phi\left(\frac{1}{4},\frac{3}{4}\right)=\frac{1}{2}\ \text{ and }\ \phi\left(\frac{1}{3},\frac{2}{3}\right)=\frac{1}{2} \tag{24}$$

For the sake of simplicity, set $\left\{(0,0),\left(\frac{1}{4},\frac{3}{4}\right),\left(\frac{1}{3},\frac{2}{3}\right),(1,1)\right\}$ is denoted by A and set $\left\{(0,0),\left(\frac{1}{5},\frac{4}{5}\right),\left(\frac{1}{4},\frac{3}{4}\right),\left(\frac{1}{3},\frac{2}{3}\right),(1,1)\right\}$ is denoted by B. It is indicated that $[\phi]_{\theta_A}$ and $[\phi]_{\theta_B}$ are presented as closed intervals denoted by $[l(A,\phi),u(A,\phi)]$ and $[l(B,\phi),u(B,\phi)]$, respectively [7]. The denotations in the intervals are expressed as follows,

$$l(A,\phi)(\mathbf{x})=\sup_{\mathbf{y}\in[0,\mathbf{x}]\cap A}\phi(\mathbf{y})\ ,\quad u(A,\phi)(\mathbf{x})=\inf_{\mathbf{y}\in[\mathbf{x},1]\cap A}\phi(\mathbf{y}) \tag{25}$$

$$l(B,\phi)(\mathbf{x})=\sup_{\mathbf{y}\in[0,\mathbf{x}]\cap B}\phi(\mathbf{y})\ ,\quad u(B,\phi)(\mathbf{x})=\inf_{\mathbf{y}\in[\mathbf{x},1]\cap B}\phi(\mathbf{y}) \tag{26}$$

Hence, the following expressions are obtained after some calculations:

$$l(A,\phi):[0,1]^2\to[0,1]:(x_1,x_2)\mapsto$$

$$\mapsto\begin{cases}1 & ; \quad x_1=x_2=1\\ \frac{1}{2} & ; \quad (x_1,x_2)\in\left[\frac{1}{4},1\right]\times\left[\frac{3}{4},1\right]\bigcup\left[\frac{1}{3},1\right]\times\left[\frac{2}{3},1\right]\ \backslash\{(1,1)\}\\ 0 & ; \quad \text{elsewhere}\end{cases} \tag{27}$$

$$u(A,\phi):[0,1]^2\to[0,1]:(x_1,x_2)\mapsto$$

$$\mapsto\begin{cases}0 & ; \quad x_1=x_2=0\\ \frac{1}{2} & ; \quad (x_1,x_2)\in\left[0,\frac{1}{4}\right]\times\left[0,\frac{3}{4}\right]\bigcup\left[0,\frac{1}{3}\right]\times\left[0,\frac{2}{3}\right]\ \backslash\{(0,0)\}\\ 1 & ; \quad \text{elsewhere}\end{cases} \tag{28}$$

$$l(B,\phi):[0,1]^2 \to [0,1]:(x_1,x_2)\mapsto$$

$$\mapsto \begin{cases} 1 \quad ; \quad x_1 = x_2 = 1 \\ \dfrac{1}{2} \quad ; \quad (x_1,x_2) \in \left[\dfrac{1}{5},1\right]\times\left[\dfrac{4}{5},1\right] \bigcup \left[\dfrac{1}{4},1\right]\times\left[\dfrac{3}{4},1\right] \\ \qquad\qquad \bigcup \left[\dfrac{1}{3},1\right]\times\left[\dfrac{2}{3},1\right] \setminus\{(1,1)\} \\ 0 \quad ; \quad \text{elsewhere} \end{cases} \tag{29}$$

$$u(B,\phi):[0,1]^2 \to [0,1]:(x_1,x_2)\mapsto$$

$$\mapsto \begin{cases} 0 \quad ; \quad x_1 = x_2 = 0 \\ \dfrac{1}{2} \quad ; \quad (x_1,x_2) \in \left[0,\dfrac{1}{5}\right]\times\left[0,\dfrac{4}{5}\right] \bigcup \left[0,\dfrac{1}{4}\right]\times\left[0,\dfrac{3}{4}\right] \\ \qquad\qquad \bigcup \left[0,\dfrac{1}{3}\right]\times\left[0,\dfrac{2}{3}\right] \setminus\{(0,0)\} \\ 1 \quad ; \quad \text{elsewhere} \end{cases} \tag{30}$$

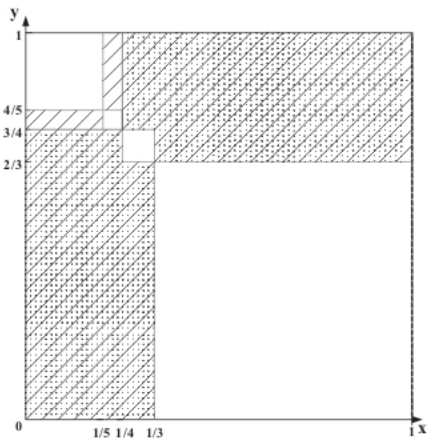

Fig.2 comparison of the domains regarding A and B

The virtual and hatched part in Fig.2 states the domain related to A and B, respectively, in the calculation of boundary structure functions. From this figure, it can be found out that $l(A,\phi) \prec l(B,\phi)$ and $u(A,\phi) \succ u(B,\phi)$. Thus, it is obvious that $[\phi]_{\theta_B} \subset [\phi]_{\theta_A}$, which can be obtained from $A \subset B$ and Lemma 2.

Furthermore, it is easily deduced that if $M_a B$ ($M_l B$) (the upper (lower) bound set of $[\phi]_{\theta_B}$ within $[\phi]_{\theta_A}$) is the closed interval $[u(B,\phi),u(A,\phi)]$ ($[l(A,\phi),l(B,\phi)]$), then the following statements can be seen in this numerical example:

1) The maximum of $(M_a B,\le)$ is the supremum of $\left([\phi]_{\theta_A},\le\right)$;
2) The minimum of $(M_a B,\le)$ is the supremum of $\left([\phi]_{\theta_B},\le\right)$;
3) The maximum of $(M_l B,\le)$ is the infimum of $\left([\phi]_{\theta_B},\le\right)$;
4) The minimum of $(M_l B,\le)$ is the infimum of $\left([\phi]_{\theta_A},\le\right)$.

These results meet with the theoretical results in the previous sections. It is stated in a practical point of view that lower and upper bound of the bound set can be substituted and transformed, which will lead to some useful reliability bounds.

4. Conclusion

Based on the notion of congruence relationship, a convex sublattice on the complete lattice of structure functions is presented in this paper. It is indicated that the relationship between lattices of equivalence classes and set of all the structure functions gives a better comprehension in system reliability, from both theoretical and practical point of view. The upper bound set of equivalence class regarding congruence relation presented in this paper has been shown to be a vital notion in engineering applications. Finally, theoretic properties are testified in the numerical example.

****

This research is partially supported by the National Natural Science Foundation of China under the contract number 51075061, and the Research Fund for the Doctoral Program of Higher Education of China (New Faculty) under the contract number 20100185120029.

****

5. References

1. Adduri P R, Penmetsa R C. System reliability analysis for mixed uncertain variables. Structural Safety 2009; 31(5): 375-382.
2. Cappelle B, Kerre E E. Computer assisted reliability analysis: an application of possibilistic reliability theory to a subsystem of a nuclear power plant. Fuzzy Sets and Systems 1995; 74: 103-113.
3. Cappelle B. Multistate structure functions and possibility theory: an alternative approach to reliability. Kerre E E, ed. Introduction to the Basic Principle of Fuzzy Set Theory and Some of its Applications, Gent: Communication and Cognition, 1991: 252-293.
4. Cappelle B, Kerre E E. On a Possibilistic Approach to Reliability Theory. In: Proceeding 2nd Int. Symposium on Uncertainty Modeling and Analysis (ISUMA 93). Maryland M. D., 1993: 415-418.
5. Cappelle B, Kerre E E. An algorithm to compute possibilistic reliability. In: ISUMA-NAFIPS, 1995: 350-354.
6. Cappelle B. Structure functions and reliability mappings, a lattice theoretic approach to reliability. Doctoral Dissertation, University Gent, 1994.
7. Cappelle B, Kerre E E. Issues in possibilistic reliability theory. Reliability and Safety Analyses under Fuzziness 1994; 4: 61-80.
8. Delmotte F, Borne P. Modeling of reliability with possibility theory. IEEE Transactions on Systems, Man, and Cybernetics Part A: Systems and Humans 1998; 28(1): 78-88.
9. Dubois D, Prade H. Possibility theory, probability theory and multiple-valued logics: A clarification. Annals of Mathematics and Artificial Intelligence 2001; 32: 35–66.
10. Dubois D, Prade H. Possibility theory and its applications a retrospective and prospective view. The IEEE International Conference on Fuzzy Systems, 2003: 3-11.

11. Gratzer G. General Lattice Theory, Birkhauser Verlag, Basel, 1978.
12. He L P, Huang H Z, Du L, Zhang X D, Miao Q. A review of possibilistic approaches to reliability analysis and optimization in engineering design. Lecture Notes in Computer Science 4553, 2007; Part IV: 1075-1084.
13. Huang H-Z, Zhang X. Design optimization with discrete and continuous variables of aleatory and epistemic uncertainties. Journal of Mechanical Design, Transactions of the ASME, 2009, 131: 031006-1-031006-8.
14. Li A J, Wu Y, Lai K K, Liu K. Reliability estimation and prediction of multi-state components and coherent systems. Reliability Engineering and System Safety 2005; 88(1): 93-98.
15. Lisnianski A, Levitin G. Multi-state system reliability assessment, optimization and applications. Series on Quality Reliability and Engineering Statistics, Vol.6, Singapore: World Scientific, 2003.
16. Montero J, Cappelle B, Kerre E E. The usefulness of complete lattices in reliability theory. Reliability and Safety Analyses under Fuzziness 1994; 4: 95-110.
17. Mourelatos Z P, Zhou J. Reliability estimation and design with insufficient data based on possibility theory. Collection of Technical Papers - 10th AIAA/ISSMO Multidisciplinary Analysis and Optimization Conference 2004; 5: 3147-3162.
18. Singer D. A fuzzy set approach to fault tree and reliability analysis. Fuzzy Sets and Systems 1990; 34: 145-155.
19. Wang Z L, Huang H-Z, Du X. Optimal design accounting for reliability, maintenance, and warranty. Journal of Mechanical Design, Transactions of the ASME, 2010, 132: 011007.1-011007.8.
20. Wang Z L, Huang H-Z, Du L. Reliability analysis on competitive failure processes under fuzzy degradation data. Applied Soft Computing, 2011, 11: 2964-2973.
21. Zuo M J, Huang J S, Kuo W. Multi-state k-out-of-n systems. Pham H, ed. Handbook of Reliability Engineering. London: Springer-Verlag, 2003: 3-17.

Yu PANG, M. Sc.
Prof. Hong-Zhong HUANG, Ph.D.
Prof. Liping HE, Ph.D.
Zhonglai WANG, Ph.D.
Ning-Cong XIAO, M. Sc.
School of Mechanical, Electronic, and Industrial Engineering
University of Electronic Science and Technology of China
Chengdu, Sichuan, 611731, P. R. China
E-mail: hzhuang@uestc.edu.cn

Zbigniew GRONOSTAJSKI
Marek HAWRYLUK
Marcin KASZUBA
Przemysław SADOWSKI
Slawomir WALCZAK
Dariusz JABŁOŃSKI

MEASURING & CONTROL SYSTEMS IN INDUSTRIAL DIE FORGING PROCESSES

SYSTEMY KONTROLNO-POMIAROWE W PRZEMYSŁOWYCH PROCESACH KUCIA MATRYCOWEGO*

The paper presents portable measuring & control systems, designed and built by the authors, and their application to the analysis of two industrial processes: the precision hot forging of CV universal joint casings in closed dies in the crank press (GKN Driveline Oleśnica) and the forging of concrete slab carrying handles in a TR device in the eccentric press (INOP Poznań). The systems enable the measurement, archiving and analysis of forging force-time/displacement traces correlated with tool temperature, as well as the measurement of production speed and the quantity of produced forgings. Recently an acoustic emission (AE) signal registration capacity has been incorporated into the system to investigate the changes occurring during the forging process, especially progressive tool wear. The information obtained in this way is to be used to improve the operating conditions of the forging presses and to optimize the whole forging process by means of CAD/CAM/CAE software based on FEM. The measuring & control systems consist of an industrial computer (comprising a real-time controller, a multi-speed measurement card, RAM memory, large capacity hard disks and a set of amplifiers and transducers) and sensors (force, displacement, pyrometers, thermocouples, linear and angular encoders, accelerometers and AE). Two applications (based on LabView) have been developed for each of the systems. One of the applications is installed on the industrial computer and is used to control the system as well as to record and process the voltage signals received from the individual sensors. The other application enables the analysis of the processed signals.

Keywords: *portable measuring and control systems, industrial forging processes.*

W pracy przedstawiono zastosowania autorskich, przenośnych systemów pomiarowo-kontrolnych do analizy dwóch przemysłowych procesów: kucia na ciepło obudowy przegubów homokinetycznych na prasie korbowej w matrycach zamkniętych (GKN Driveline Oleśnica) oraz kucia zaczepów do przenoszenia płyt betonowych na prasie mimośrodowej w przyrządzie TR (INOP Poznań). Zbudowane przez autorów systemy pozwalają na pomiar, archiwizację i analizę przebiegów sił kucia w funkcji czasu/przemieszczenia skorelowane z pomiarem temperatury narzędzi, pomiary prędkości procesu oraz ilości wykutych odkuwek. Ostatnio wzbogacono je o rejestrację sygnału akustycznego AE w celu określenia zachodzących zamian podczas procesu a szczególnie postępującego zużycia narzędzi. Uzyskane informacje mają posłużyć również do poprawy warunków eksploatacji pras oraz do optymalizacji całego procesu kucia wykorzystując narzędzia CAD/CAM/CAE oparte o MES. Prezentowane systemy zbudowane są z komputera przemysłowego (kontrolera czasu rzeczywistego, wielokanałowej szybkiej karty pomiarowej, kości pamięci operacyjnej, dysków twardych o dużej pojemności, zestawu wzmacniaczy i przetworników) oraz odpowiednich czujników pomiarowych (siły, przemieszczenia, pirometrów, termopar, enkoderów liniowych i kątowych, akcelerometrów, czujników AE). Do każdego z systemów opracowano po 2 aplikacje (na bazie programu LabView). Pierwsza aplikacja jest zainstalowana w komputerze przemysłowym i służy do sterowania systemem oraz zapisem i przetwarzaniem sygnałów napięciowych uzyskiwanych z poszczególnych czujników. Druga przeznaczona jest do analizy zarejestrowanych sygnałów.

Słowa kluczowe: *przenośmy system pomiarowo kontrolny, przemysłowy proces kucia.*

1. Introduction

Because of their advantages, such as high productivity, small finishing allowances and the very good service properties of the finished products, forging processes belong to the most commonly used product manufacturing technologies [6, 11, 16, 18].

Industrial forging processes are conducted using powerful forming machines, usually presses and hammers. Today most forging shops use their own (often "old") machines, adapting them for the current production [1, 7]. It is seldom that they decide to purchase a new machine dedicated to a specific production. Forging machines and equipment usually have simple

(*) Tekst artykułu w polskiej wersji językowej dostępny w elektronicznym wydaniu kwartalnika na stronie ***www.ein.org.pl***

measuring & control systems capable of controlling only the maximum forging force, the machine running speed, the number of forgings and the initial temperature of the preforms.

The great number and variety of factors affecting forging process correctness, and their interaction make die forging processes very difficult to analyze. For this reason FEM based CAD/CAM/CAE tools are increasingly often employed to design, analyze and optimize forging processes [4, 8, 9, 13, 14, 15, 17]. For a comprehensive analysis and verification of the results obtained in this way it is often necessary to measure many additional quantities which for various reasons are difficult to measure in the course of forging. In order to improve productivity and the quality of the forgings more precise control of process parameters than the one of which the current control systems are capable is needed [10, 12].

The authors have developed mobile systems for measuring and controlling the principal forging process parameters. The data acquired by the systems will be used to improve the operating conditions of forging presses, to increase the life of forging tools and to optimize the forging process by means of FEM based CAD/CAM/CAE software.

The measuring & control systems were employed in two forging processes: the hot forging of the CV universal joint casing in closed dies in the crank press (GKN Driveline Oleśnica) and the forging of concrete slab carrying handles in a TR device in the eccentric press (INOP Poznań).

2. Multioperation forging of CV universal joint casing

2.1. Process description

The industrial forging of the CV universal joint casing in the GKN Driveline Forge consists of four hot forging operations and one cold forging operation (fig. 1). The forging process has many stages and it proceeds as follows. From a storehouse bundles of metal bars are delivered to a cutting machine where they are cut into proper lengths. Then the preforms are heated in an induction heater to a temperature of about 900°C. It is critical that the process temperature remains constant in order to ensure the proper quality of the forgings. The preforms heated up to the proper temperature are fed into the press where they are deformed in four operations. The high quality of the forging is assured thanks to process stability and on-time control. After leaving the press the forgings are subjected to controlled cooling. Then they go to a shot-blasting machine where they are cleaned of graphite. Subsequently they are transferred to the mechanical working room and to the half-shaft assembly lines.

2.2. Description of measuring & control system

The system was to measure and record the forging forces versus punch path length or time (for the four operations), the temperature of the tools and the preforms. Another aim of the recording was to verify the numerical modelling of the forging process, being run in parallel. The measuring system, designed and built by the authors, was installed on a Shuler industrial press with a maximum press load of 20000kN. The system consists of a real-time controller based on the MPC5200 400MHz processor using the CompactRIO platform. An industrial computer, a reconfigurable chassis with FPGA circuits, and analog and digital input/output measuring cards (fig. 2a) form the whole setup working in tandem with a 1 terabyte hard disk. This configuration enables the high-rate recording of data from the sensors, offering many signal processing possibilities. The computer records data coming from four MP55 extensometer amplifiers (fig. 2b), a ZE-115-M encoder mounted on the press crankshaft and four 5B47 thermocouple amplifiers. The thermocouples are installed in four dies. Thanks to the FPGA circuits the computer can analyze the recorded signals in real time and control the production process. In response to an improper value of one (or several) of the process parameters the other parameters can be changed in order to bring the process back on course.

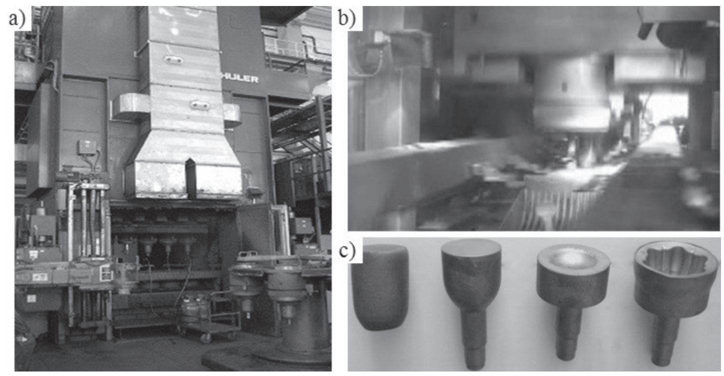

Fig. 1. Forging process: a) crank press, b) side view of press working chamber, c) forgings after successive operations

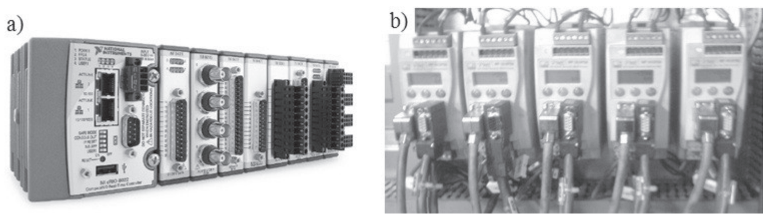

Fig. 2. Measuring system: a) Industrial computer CompactRIO with installed input/output modules, b) MP55 amplifiers

The special system data processing application has filters (whose settings are fixed by the operator) and tools for searching the saved files whereby characteristics fragments of force waveforms or defined events (e.g. an exceedance of a critical force or temperature value in a particular operation) can be easily and quickly found and compared for the particular operations. The program allows one to save the results to text file and to plot graphs in Excel (fig. 3).

2.3. Application of measuring & control system

The measuring & control system was used to analyze the forging forces during the particular operations and at the beginning and end of the forging process (after between 10-20 hours of work) and to compare them with the force waveforms obtained from FEM simulations (fig. 4).

One can notice close similarity between the FEM waveforms and the recorded traces, especially for the characteristic points corresponding to the successive degrees of cross section reduction. Some of the differences may stem from the imperfect tuning of the numerical model due to the different tribological conditions: constant friction coefficient values were assumed in the FEM model whereas in the industrial process the friction forces undergo changes. Research is underway to bring the numerical model as close as possible to the real industrial process, e.g. by increasing the precision with which the friction coefficient is calculated and taking into account the variation of the friction coefficient in the course of the process.

When one examines the traces for the particular operations, recorded over 10-20 hours, it becomes apparent that the maximum "parabolas" occur at the beginning of the process (the steady state after 20 minutes of forging) while the minimum force

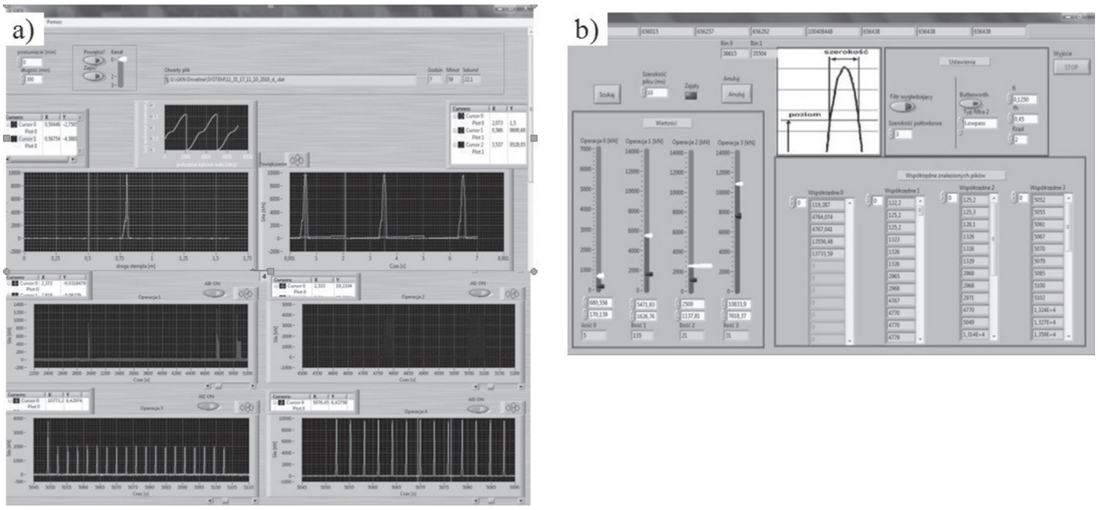

Fig. 3. Measuring system panels: a) main menu, b) menu with filters

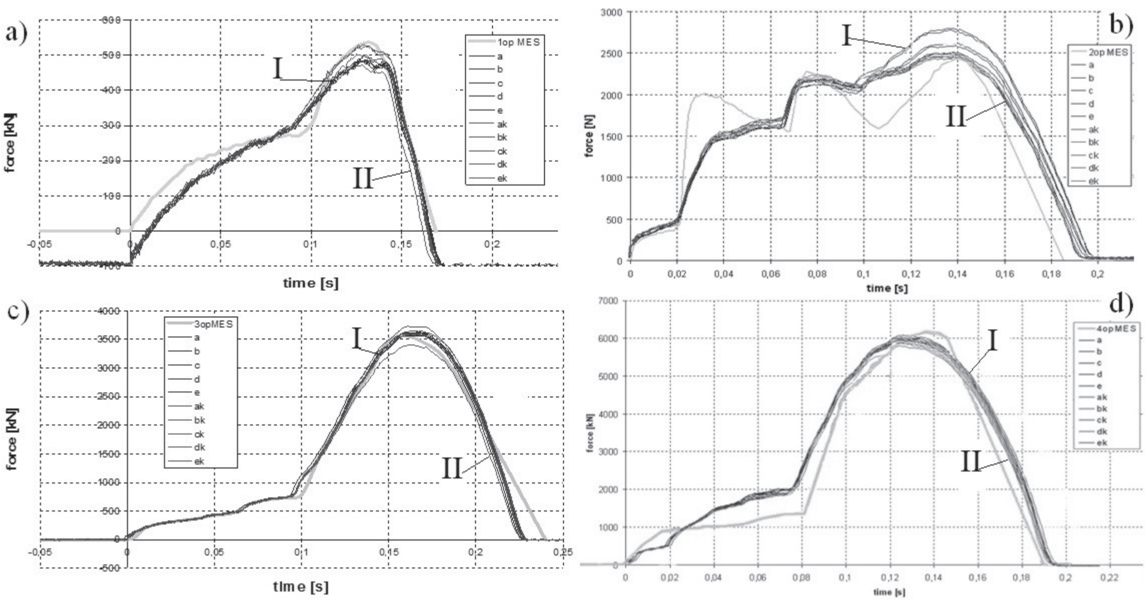

Fig. 4. Comparison of recorded force traces (I – at beginning and II – after 10-20 hours of continuous operation) and waveforms obtained from numerical modelling for: a) 1st forging operation, b) 2nd forging operation, c) 3rd forging operation and d) 4th forging operation

values occur towards the end of the forging process. Assuming that the whole process proceeded without disturbance, the reduction in the force may indicate progressive wear of the tools. This was confirmed by measurements of the post-forging die impressions by means of an optical scanner, statistical analyses of the tool life and microstructural examinations.

The results relating to the influence of the amount of the lubricating medium on tool temperature were found to be interesting, particularly for the industrial press operators. A water-graphite mixture was used in the forging of CV universal joint casings. Special sets of tools each with a hole into which a thermocouple would be inserted (4 mm below the tool surface) had been constructed to measure the temperature of the tools during the forging process.

In this way the real tool temperature during forging was measured. The measurements of real tool temperature by means of the measuring system and the thermocouples inserted through the special groove into the dies shows that many factors affect the temperature of the tools during the forging process (fig. 5a). When the flow rate of the lubricating mixture was doubly increased, the temperature dropped by about 100°C. Stopping the press for twenty seconds resulted in a further drop in temperature by about 100°C. A break lasting for the time needed to produce two forgings resulted in a temperature decrease of 20°C. On the basis of the obtained results the press operators were able to select the optimum lubricant amount and feeding time for the forging process in order to minimize the thermal shock causing the thermal-mechanical fatigue of the tools. The rationalization of the cooling and lubrication conditions ultimately resulted in increased durability of the dies. The measurements made with the thermocouples also served to verify the Finite Element Model of heat exchange for the die in the second operation in the forging of the CV universal joint (fig. 5b). The temperature of the preforms and forgings was also recorded by means of pyrometers and a thermovision camera (fig. 6). Thanks to the investigations also the temperature of rejected preforms was determined.

2.4. Expansion of measuring & control system

The system is to be expanded to include wireless operator panels displaying the actual process parameters and traces of the signals coming from the sensors. Moreover, a system for the remote configuring and control of the computer via a mobile phone and text messages and the Internet is to be added. Two-way communication with the user will make it possible to immediately notify the persons responsible for the proper running of the forging press about any irregularities and to send reports for particular periods.

3. Forging of concrete slab carrying handles

3.1. Description of forging process

The P1.3T carrying handle (an element fixed to concrete slabs for carrying the latter on construction sites) is hot forged from a bar (the temperature of the erforms was about 1100°C) in three operations in a PMS 160B eccentric press (fig. 7a) using a TR device (fig. 7b). Figure 7c shows the final product and the erforms. Figure 8 shows the tools used in the 2nd and 3rd forging operation. The punches and the die inserts are made of steel WCL and ORVAR SUPREME (WCLV).

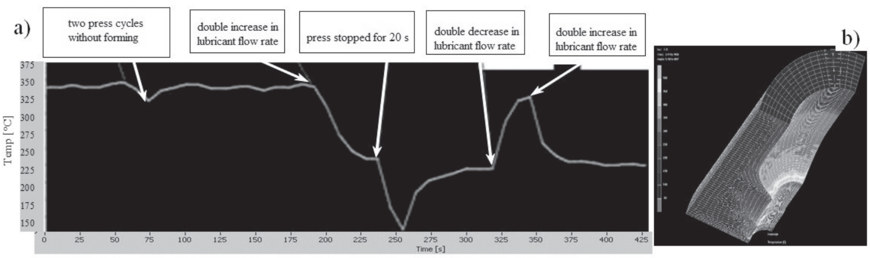

Fig. 5. Variation in temperature during analyzed forging process: a) variation in temperature during forging of CV universal joints , b) thermomechanical FEM model for two operations

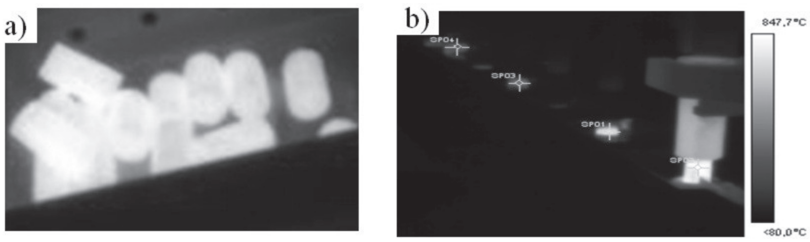

Fig. 6. Temperature measurement: a) rejected preforms, b) thermal photograph featuring heated up die impressions and preform

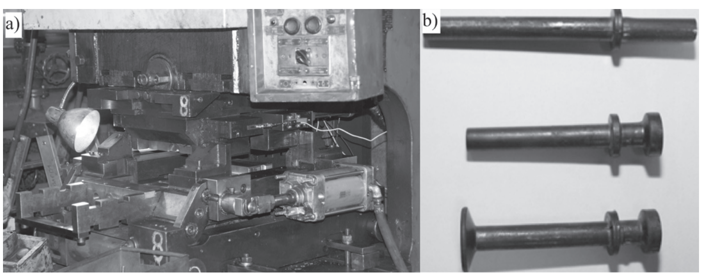

Fig. 7 Stand for forging carrying handles: a) TR device, c) final product with erforms

Fig. 8. Tools for forging carrying handles: a) dies for 2nd operation, b) matrices for 3rd operation, c)2nd and 3rd operation punch with AE sensor

3.2. Description of measuring & control system

The measuring & control system was designed in order to fully monitor the forging of the carrying handle (the measurement of the force versus time and displacement in conjunction with the measurement of the temperature of the tools and the AE signal). The system, designed and built by the authors, was installed on a special laboratory stand (in INOP in Poznań) which made it possible to conduct forging in semi-industrial conditions. The authors decided to use the system for pioneering acoustic emission investigations of tool wear (punches for the 2nd and 3rd operation were fitted with AE probes, fig. 8c). An industrial computer was designed and optimized for such investigations. The computer has a four-core processor, a 2GB fast operating memory, hard disks with a capacity of 2 TB and analog modules working directly with sensors. Four sensors are connected to the computer: a temperature sensor (a type K sheathed thermocouple, d = 0.5 mm) placed in the punch, a position sensor (mounted on the forging device), a sensor (K Nordic Transducer) registering the upsetting force and a broadband acoustic emission sensor (VS45-H Vallene) registering acoustic emission in a band of 20-450 kHz. The latter sensor is connected to an AEP3 preamplifier (Vallene, fig. 9b) with a configurable amplification of 35-49 dB and a band-pass filter with selectable characteristics.

The acoustic emission phenomenon is commonly used in on-destructive testing. The elastic wave generated as a result of a local dynamic change in the energy state, caused by, for example, a breach in the structure of the material can be registered on its surface by an acoustic emission sensor. The range of the generated frequencies is quite wide, extending from tens of kilohertz to megahertz [2, 3, 5, 10]. Piezoelectric AE sensors can register elastic waves and convert them into electrical signals. By using several AE sensors and analyzing the time of arrival of the elastic wave at the successive sensors one can determine the place from which the wave was emitted (fig. 10).

The computer supervising application analyzes the acoustic emission signal in real time. Recording on the hard disks starts when the voltage received from the AE circuit exceeds the set threshold and ends when the voltage falls below this threshold. Also a certain time before and after the event is included. Thanks to this solution the whole available information can be recorded and disk space saved. The duration of each AE event (since the moment the system is activated) is remembered whereby one can later correlate the AE events with the force, temperature and position traces. Thanks to the high computing power it is possible to analyze AE signals and those from the other sensors and make decisions contributing to longer machine life and preventing low quality products from being produced [3].

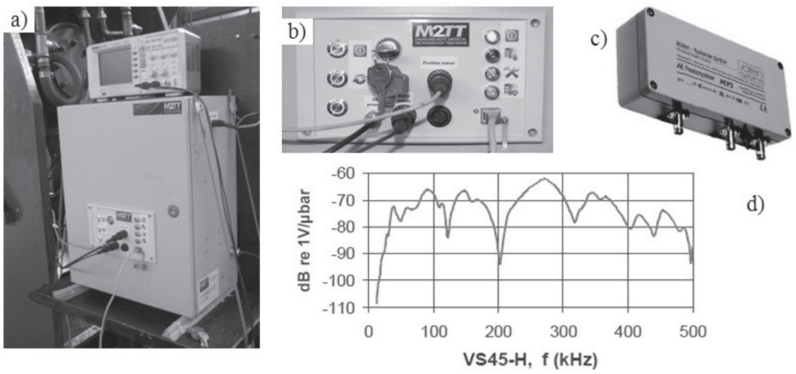

Fig. 9. Industrial computer: a) view of setup, b) front panel, c) AEP3 amplifier and d) characteristic of AE sensor VS45-H shown in fig. 7c

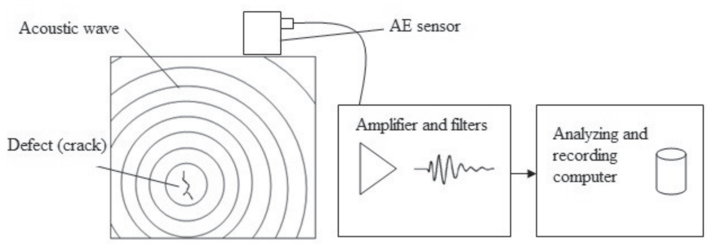

Fig. 10. Dynamically arising defect (microcrack) generating elastic wave which is registered by AE sensor. After it is amplified signal from sensor gets to recording computer

A special application (for system data handling) based on LabVIEW was also developed for the forging of carrying handles. Using its specialist filters one can search the whole saved file and easily and quickly find the defined events (an exceedance of the force in a given operation or a temperature exceedance). The results can be saved to text file. This virtual tool is operated by changing the particular user panels and the positions of the adjusters and switches by means of a keyboard or a computer mouse (fig. 11).

The application offers the possibility to select AE events correlated with force and temperature (fig. 12).

In order to enable a more in-depth analysis of the AE signal, the possibility of determining (for three selected AE events) two highly valuable parameters, i.e. the power spectrum (fig. 13a) and the Wigner-Ville transform, and filtering individual signals was included in the application.

The *power spectrum* allows one to determine the frequency of AE event occurrence for the maximum RMS signal amplitudes while the *Wigner-Ville transform* can be used to estimate the duration of an AE event for specified signal frequencies (e.g. the duration of wave propagation in a fractured tool).

3.3. Application of measuring & control system

Currently research is underway to explore the possibility of applying the measuring & control system to the AE analysis of the punches for the 2nd and 3rd operation since it is for these tools that thermal-mechanical fatigue is observed (fig. 14). The average life of the punches used in these operations is 10-12 thousand units, after which they are renovated (subjected to facing to a depth of 2 mm).

An analysis of the AE signal is difficult and arduous since each production process in real conditions is accompanied by events which may generate an elastic wave in the surroundings of the sensor. Such events are various tool impacts, fluid flows in the machine, vibrations of machine components and so on. In real systems, there are also many other acoustic emission sources besides the above interfering signals. Elastic waves originating in other machine parts and in the workpiece reach the sensor mounted on the surface of the punch. Therefore it is necessary to explore the machine and it surroundings with regard to acoustics. Various solutions, such as band-pass filtration making it possible to register AE signals with a specified frequency range and threshold registration consisting in registering the AE sensor signal only when the voltage exceeds a certain threshold, are used to eliminate interference. For this reason first the AE events (fig. 13) originating from known phenomena and elements (e.g. the interference generated by the operation of the press, the putting of a erform into the die, the closing and opening of the device, etc.) should be identified. After most of the AE events have been identified one can search the signal for new events. Then the broadband sensor is replaced with a resonance sensor. Thanks to the narrowing of signal frequency it is possible to increase the measurement sensitivity and identify the events being symptomatic of microcracs in the punch or of its wear.

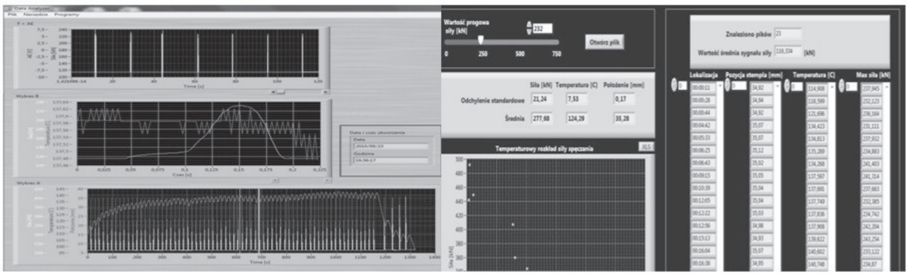

Fig. 11. Front panel of application for monitoring force versus time/displacement and panel for analysis of selected quantities, using signal filtration

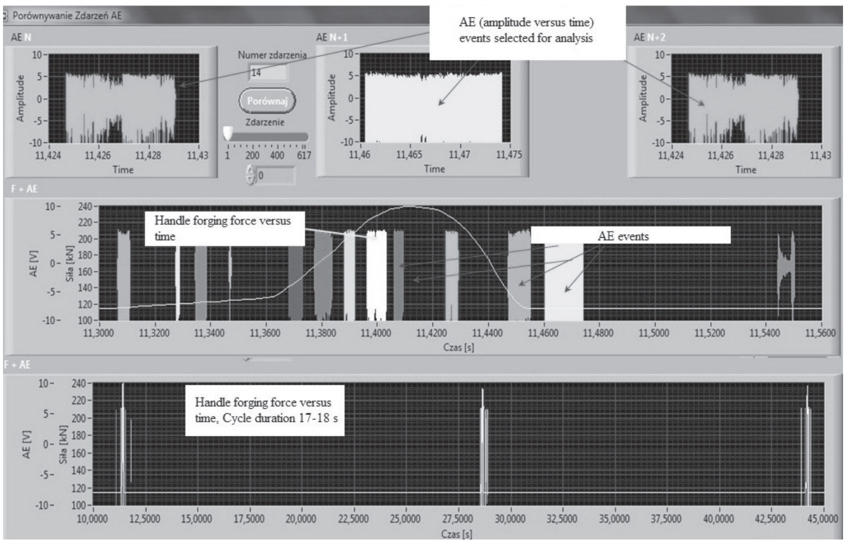

Fig. 12. Main panel for analysis and selection of AE events

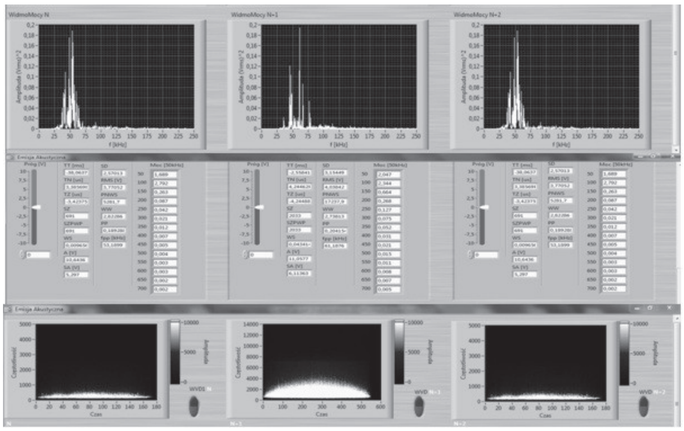

Fig. 13. a) Main application panel for determining signal power spectrum, b) panel for Wigner-Ville transform comparisons using signal filtration

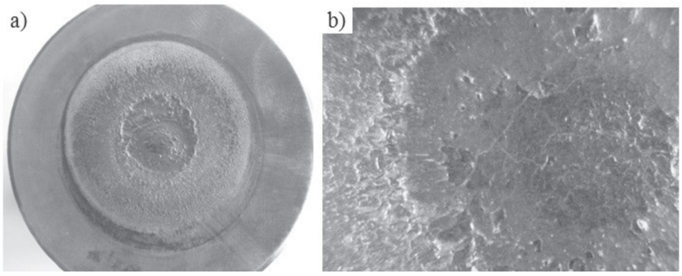

Fig. 14. Worn out punch for taper forging after 14 thousand forgings: a) macro view, b) magnification showing thermal-mechanical wear of most degraded front part of tool

4. Conclusions

The measuring & control systems presented in this paper enable the monitoring of selected parameters of industrial manufacturing processes. In the case of industrial forging the principal parameters are the forging forces as a function of time/displacement, and the temperature of the tools and the preforms. The systems, designed and built by the authors, enable the measurement, archiving and advanced analysis of the above (mutually correlated) quantities. In addition, one of the systems uses AE signal measurement to determine tool wear, which is an innovative solution. The setup consist of an industrial computer and proper sensors. The systems could be created thorough precise study of industrial forging processes (the forging forces, the distribution of strains, the temperature of the tools and the preforms). Their application will contribute to an improvement in the operating conditions of the presses and to a longer life of the tools. A comparison of AE signal measurements and the operating conditions will make it possible to more fully exploit the possibilities of tool materials for specific applications.

This research was done as part project WND-POIG.01.03.01-02-161/09: "Comprehensive expert system for the optimization of tool life in forging processes" within The Innovative Economy Programme. Wrocław Supercomputing Centre's MARC and ProEngineer programs were used in the research.

5. References

1. ASM Metals Handbook volume 14, Forming and forging, 337-338.
2. Bertrand J. Emisja akustyczna źródła metody zastosowania. Wydawnictwo Pascal Warszawa, 1994.
3. Christian U. Grosse, Masayasu O. Acoustic emission testing basics for research. Applications and Civil Engineering, Springer; 1 edition, 2008.
4. Doege E. Bohnsack R. Closed die technologies for hot forging. Journal of Materials Processing Technology 2000; Vol. 98: 165-170.
5. Głowacz A. Głowacz Z. Diagnostics of Induction Motor Based on Analysis of Acoustic Signals with Application of FFT and Classifier Based on Words. Archives of Metallurgy and Materials 2010; Vol. 55; No. 3: 707-712.
6. Gontarz A. Myszak R. Forming of External Steps of Shafts in Three Slide Forging Press. Archives of Metallurgy and Materials 2010; Vol. 55; No. 3: 659-664.
7. Gronostajski Z. Hawryluk M. The main aspects of precision forging. Archives of Civil and Mechanical Engineering 2008; Vol. 8, No. 2: 39-56.
8. Hojny M. Application of an integrated CAD/CAM/CAE/IBC system in the stamping process of a bathtub 1200 S. Archives of Metallurgy and Materials 2010; Vol. 55; No. 3: 713–723.
9. Hyrcza-Michalska M, Rojek J, Fruitos O. Numerical simulation of car body elements pressing applying tailor welded blanks -

practical verification of results. Archives of Civil and Mechanical Engineering 2010; Vol. 10; No. 4: 31-44.
10. Islam El-galy, Bernd-Arno B. Online monitoring of hot die forging processes using acoustic emission (part i). J. Acoustic Emission 2008; Vol. 26: 208-218.
11. Kocańda A, Czyżewski P, Khedheyer H. Mehdi. Numerical analysis of lateral forces in a die for turbine blade forging. Archives of Civil and Mechanical Engineering 2009; Vol. 9; No. 2: 49-54.
12. Neugebauer R, Bräunlich H, Scheffler S. Process monitoring and closed loop controlled process. Archives of Civil and Mechanical Engineering 2009; Vol. 9; No. 2: 105-126.
13. Pietrzyk M, Madej Ł, Rauch Ł, Gołąb R. Multiscale modeling of microstructure evolution during laminar cooling of hot rolled DP steels. Archives of Civil and Mechanical Engineering 2010; Vol. 10; No. 4: 57-67.
14. Presz W. Cacko R. Analysis of the influence of a rivet stress distribution on the micro-SPR joint – initial approach. Archives of Civil and Mechanical Engineering 2010; Vol. 10; No. 4: 69-75.
15. Trzepieciński T. 3D Elasto-plastic fem analysis of the sheet drawing of anisotropic steel sheet metals. Archives of Civil and Mechanical Engineering 2010; Vol. 10; No. 4: 95-106.
16. Vazquez V, Altan T. Die design for flashless forging of complex parts. Journal of Materials Processing Technology 2000; Vol. 98; No. 2: 81-89.
17. Vazquez V, Altan T. New concepts in die design — physical and computer modeling applications. Journal of Materials Processing Technology 2000; Vol. 98; No. 2: 212-223.
18. Yoshimura H, Tanaka K. Precision forging of aluminum and steel. Journal of Materials Processing Technology 2000; Vol. 98; No. 2: 196-204.

Prof. dr hab. inż. Zbigniew GRONOSTAJSKI
Dr inż. Marek HAWRYLUK
Mgr inż. Marcin KASZUBA
Mgr inż. Przemysław SADOWSKI
Instytutu Technologii Maszyn i Automatyzacji
Politechnika Wrocławska
ul. Ignacego Łukasiewicza 5
50-371 Wrocław, Poland
e-mail: zbigniew.gronostajski@pwr.wroc.pl
e-mail: marek.hawryluk@pwr.wroc.pl
e-mail: marcin.kaszuba@pwr.wroc.pl
e-mail: przemyslaw.sadowski@pwr.wroc.pl

Mgr inż. Sławomir WALCZAK
Dariusz JABŁOŃSKI
GKN Driveline Oleśnica
ul. Południowa 18
56-400 Oleśnica, Poland
e-mail: slawomir.walczak@gkndriveline.com
e-mail: dariusz.jablonski@gkndriveline.com

Zdzisław MAZUR
Alejandro HERNANDEZ-ROSSETTE

SERVICE PROBLEMS OF AN AXIAL COMPRESSORS OF A LAND BASED, HIGH POWER, REACTION GAS TURBINES

PROBLEMY EKSPLOATACYJNE OSIOWYCH SPRĘŻAREK REAKCYJNYCH STACJONARNYCH SILNIKÓW TURBINOWYCH DUŻYCH MOCY

A compressor blade failure was experienced at the 69 MW gas turbine of a combined cycle (C.C.) unit after four years operation since the last overhaul. Three unit failure events occurred at small periods, which caused forced outage. Visual examination carried out after the failure events indicated that the compressor vanes (diaphragms) had cracks in their airfoils initiating at blade tenons welded to the diaphragm outer shroud at some stages. Also, many stationary vanes and moving blades showed foreign object damage (FOD), rubbing and bending. A compressor failure evaluation was completed including cracked vane metallographic analysis, unit operation parameter analysis, history-of-events analysis, and crack initiation and propagation analysis. This paper provides an overview of the compressor failure investigation, which led to identification of the vane high cycle fatigue (HCF) failure mechanism generated by rotating stall during unit start-ups, highly accelerated by corrosion generated by the fogging system and influenced by high stationary vane and moving blade brittleness as the primary contribution to the observed failure. They are provided recommendations to avoid similar failure of the compressor blades in the future.

Keywords: *fogging, blades failure, high cycle fatigue, rotating stall, vibratory stresses, corrosion.*

W sprężarce turbiny gazowej o mocy 69 MW, pracującej w cyklu kombinowanym wystąpiły uszkodzenia łopatek po czterech latach eksploatacji od ostatniego remontu głównego. Zarejestrowano trzy przypadki uszkodzeń w krótkim odstępie czasu, które spowodowały potrzebę zatrzymania i remontu turbiny. Badania wzrokowe przeprowadzone po każdym stwierdzeniu uszkodzeń, ujawniły pęknięcia w łopatkach niektórych stopni palisad kierowniczych zlokalizowane w piórach łopatek. Pęknięcia zaczynały sie w stopach łopatek spawanych do bandaża zewnętrznego palisad kierowniczych. Znaczna liczba łopatek kierowniczych i wirnikowych miała również uszkodzenia spowodowane przez obce ciała, przytarcia i były pogięte. Przeprowadzono badania i analizę uszkodzeń sprężarki włączając w to badania metalograficzne pękniętych łopatek, analizę parametrów operacyjnych turbiny, analizę historii zarejestrowanych przypadków uszkodzeń i analizę inicjacji i propagacji pęknięć. W niniejszym artykule opisuje sie badania uszkodzeń palisad łopatkowych sprężarki, które doprowadziły do konkluzji końcowej, ze pęknięcia łopatek palisad kierowniczych były rezultatem zmęczenia wysokocyklicznego materiału łopatek, spowodowanego przez oderwania wirow w czasie uruchomienia turbiny, przyspieszone przez korozje wywołaną chłodzeniem mieszankowym. Uszkodzenia ułatwiła znaczna kruchość materiału łopatek sprężarki. Zostały sformułowane zalecenia, aby uniknąć podobnych uszkodzeń łopatek sprężarki w przyszłości.

Słowa kluczowe*: chłodzenie mieszankowe, uszkodzenia łopatek sprężarki, zmęczenie wysokocykliczne, oderwanie wirujące, naprężenia spowodowane drganiami, korozja.*

1. Introduction

Inlet cooling systems are a popular choice worldwide to add power to gas turbines, especially during peak demand periods in summer time when high ambient temperatures reduce output [5]. Increased power output is achieved by injecting a water-droplet ‘fog’ into the turbine air inlet. Evaporation of water droplets within the inlet stream causes the air to be cooled, increasing mass flow through the turbine and turbine power output by up to ten per cent, depending on environmental conditions. As a rule of thumb, one per cent of injected water (relative to the intake airflow) boosts turbine power by 5-7 per cent [2, 5-6]. However, the main pre-requisite for proper fogging system performance is that the water droplets must be small enough to evaporate in their path through a compressor [5]. If the water droplets are larger than required, evaporation occurs within the compressor outlet, rather than at the early compressor stages. This reduces inter-cooling process efficiency and therefore the degree of power augmentation obtained [6]. The presence of large particles can also increase the risk of compressor blade erosion and corrosion [1]. Fogging presents additional technological challenges such as the proper adjustment and modification of gas turbine air-cooling, combustion, control and protection systems [2]. Caution must also be taken to maintain compressor stability and blade mechanical integrity. Of prime importance are droplet size and water droplet distribution and concentration within the fog, as this defines how rapidly the droplets evaporate in the compressor system [2]. Inlet fogging is very common for combustion turbines in all cycle configurations. For all classes of turbines there are two types, one which applies just enough fog to evaporate all the water prior to any moisture coming in contact with rotating turbine parts and another that actually allows the first several stages of compression to run wetted. For complete evaporation from typical high pressure fog nozzles, a residence time of around 3s is required [1, 4]. No fog nozzle produces homogeneous droplet size, but rather droplets are produced over a range of sizes. Larger droplets are unlikely to evaporate in time and will impinge on IGV's and compressor blades, causing erosion and corrosion [2]. A significant amount of water will also impinge on duct surfaces, silencers etc, requiring an extremely effective drain system and a lined duct since demineralized water is quite aggressive. If the drain system is ineffective and/or fails, a slug of water could be ingested into the compressor causing catastrophic failure [2]. In some cases water injection into the compressor (overspray) will cause mismatching of successive stages as flow coefficients will increase and design temperature rises will not be met. This will cause points on the compressor map to move towards the surge line and increase stage loading, possibly pushing the later stages nearer to stall [2]. Excessive water injection, along with off-design operating conditions, non-standard fuels, combustion dilution and compressor blade degradation can lead to aerodynamic instabilities and subsequent high-cycle fatigue failures [1, 4]. This paper provides an overview of the compressor stationary vane (diaphragm) failure investigation, which led to an identification of the HCF failure mechanism generated by rotating stall during unit start-ups, highly accelerated by corrosion generated due to the fogging system.

2. Compressor blades failure analysis

2.1. Background

The gas turbine under evaluation is a 69-MW Combined Cycle (C.C.) unit operated at 3600 rpm, which consists of 19 compressor stages and 4 gas turbine stages and had accumulated approximately 200,000 operation hours [3]. During the last main overhaul in 2005, all compressor moving and stationary blades were replaced. In 2006, the unit was equipped with a fogging system at the compressor air inlet duct to increment unit power output during high ambient temperature days (hot days) as is shown in fig. 1

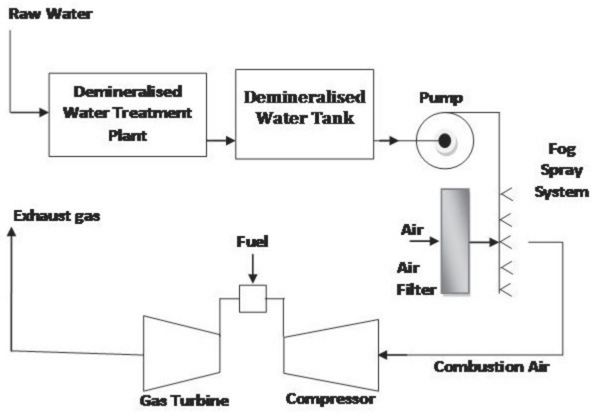

Fig. 1. Outline of the fog inlet air cooling system

Fog water nozzles were installed upstream of the compressor inlet air filter without any water filter/catcher before the water spray nozzles. Since the last overhaul up to the date of the first failure event in December 2008, the unit had accumulated 27,000 operation hours and 97 start-ups in total, and 740 hours operation and 4 start-ups with a fogging system [3]. Three failure events of the unit occurred at small periods. The first failure occurred in December 2008, a second event in March 2009 and a third event in May 2009. The compressor damage distribution during the three failure events is shown in fig. 2.

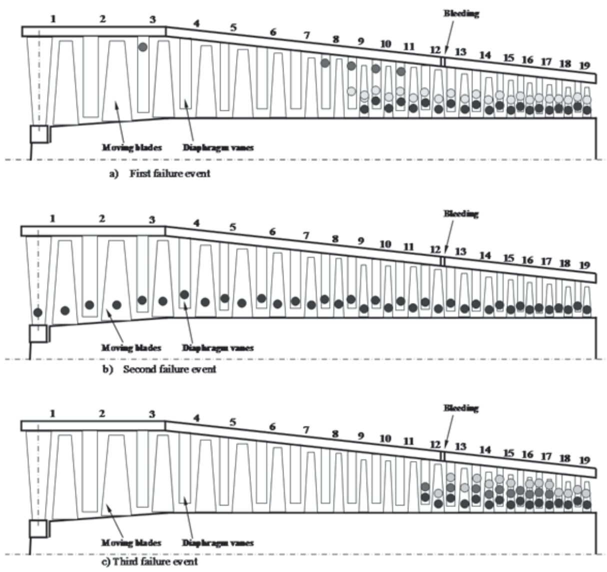

Fig. 2. Compressor damage distribution during the three failure events

Legend: 1-19 – Compressor stages

- FOD of moving blades and vanes

- Rubbing of moving blades and vanes

- Fracture of moving blades and vanes

During the first failure event in December 2008, there was FOD and rubbing of compressor moving blades (see fig. 3) and FOD, rubbing, bending and fracture of compressor stationary vanes (diaphragms) as shown in fig. 4. There were also vane fractures at the vane union diaphragm shrouds, stages 8 to 10 as shown in fig. 5.

Fig. 3. Compressor moving blade damage

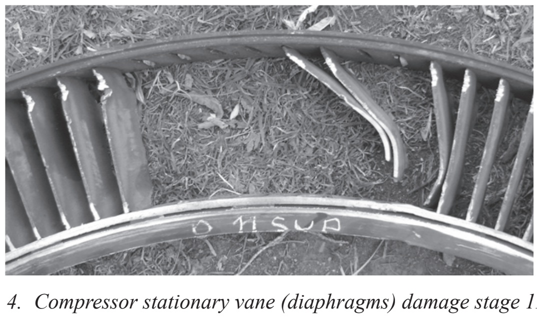

Fig. 4. Compressor stationary vane (diaphragms) damage stage 11

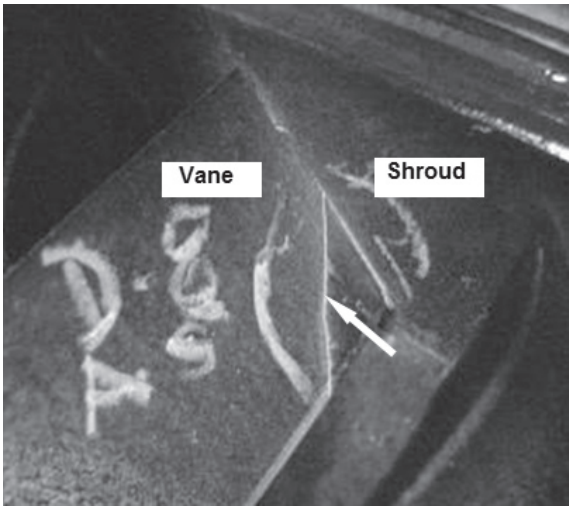

Fig. 5. Vane fractures at the union of vanes with diaphragm shrouds stages 8 to 10.

During the second failure event in March 2009, there occurred FOD of compressor moving blades and stationary vanes (diaphragms) stages 1 to 19 as shown in figs. 6 and 7. The failure was attributed to the fogging system water spray nozzle, which broke and was separated from the nozzle support structure and then introduced in the compressor flow path channel at high velocity causing FOD in the compressor. During the third failure event in May 2009, there occurred FOD of compressor moving blades and stationary vanes (diaphragms) stages 12 to 19 as shown in figs. 8 and 9.

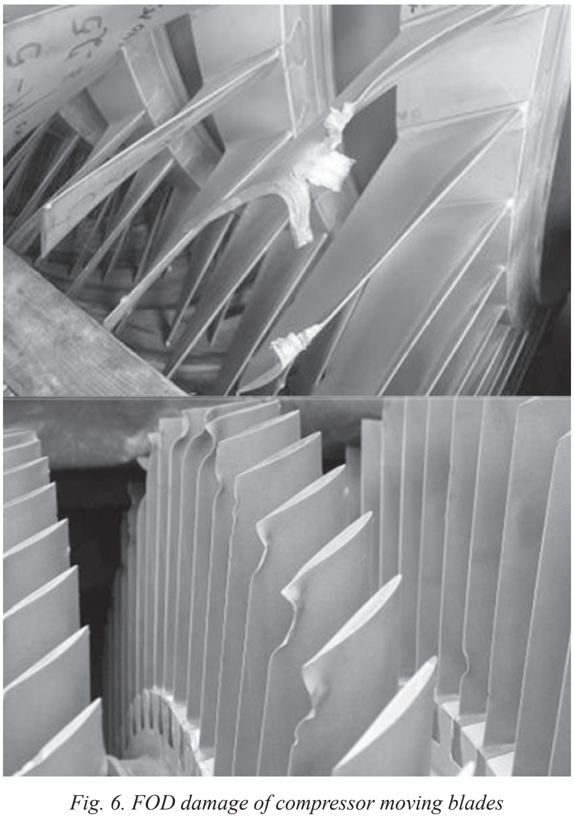

Fig. 6. FOD damage of compressor moving blades

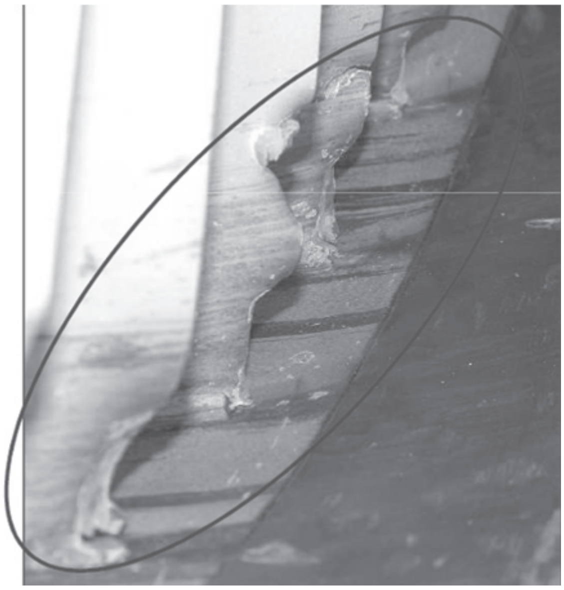

Fig. 7. FOD damage of compressor vanes (diaphragms)

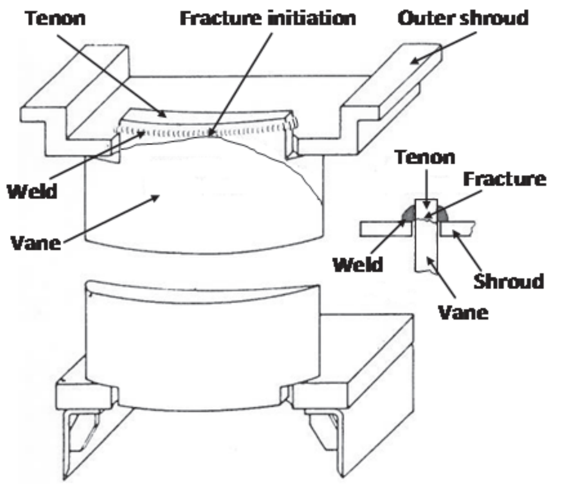

Fig. 8. General view of compressor damage in the bleeding zone between stages 12 y 13

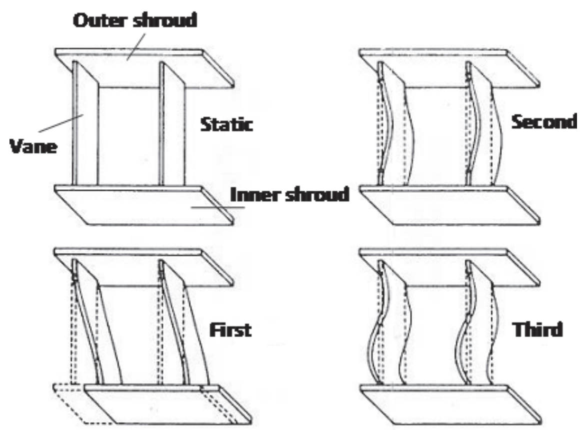

Fig. 9. Damage of stationary vanes of stage 13

Many blades/vanes were heavily impacted and deformed; some moving blades and stationary vanes were fractured. An apparently fatigued type fracture surface was found in the union of vane tenons with diaphragm outer shrouds, stage 13, as shown in fig. 10. It can be seen from fig. 10 that fracture was initiated at the vane tenon weld heat affected zone and the presence of fatigue beach marks can be observed. Also, there were corrosion deposits on the compressor vanes and casing as shown in fig. 9. Among the three compressor failure events presented, the third one is the root cause analysis in this paper.

Fig. 10. Fracture surface of compressor diaphragm vane tenons, stage 13 with appearance of HCF

2.2. Analysis of the compressor vane cracking mechanism

Vane cracks were developed in the vane tenons at the outer shroud of the diaphragm (fig. 11). As mentioned before, these cracks were of the high cycle fatigue type (fig. 10) and initiated in the heat affected zone adjacent to the tenon weld. They were caused by vibratory stresses which occurred during start-up acceleration as a result of diaphragm resonance in one of its first three natural frequencies [7] with local air flow disruptions associated with the presence of rotating stall cells, as explained before, and upstream rotating blade wakes. The first three diaphragms vibratory mode shapes corresponding to mentioned previously diaphragms natural frequencies are shown in fig. 12 [7]. The manufacturer reported that the stress concentration factor due to the weld heat affected zone of diaphragm tenons is 3.5 approximately [7]. Due to this fact and the presence of corrosion pits on the vane/tenon, local stresses rise significantly in this zone, leading to fatigue failure initiation and propagation.

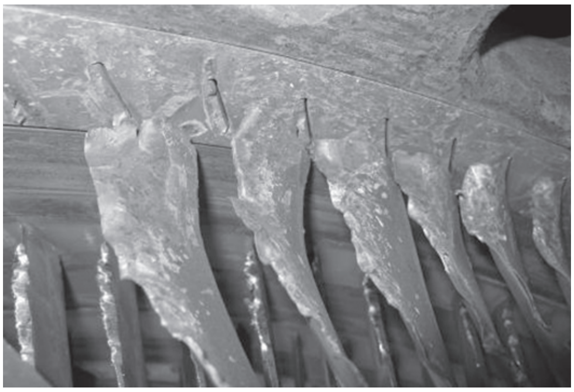

Fig. 11. Fracture localization at compressor vanes of diaphragms

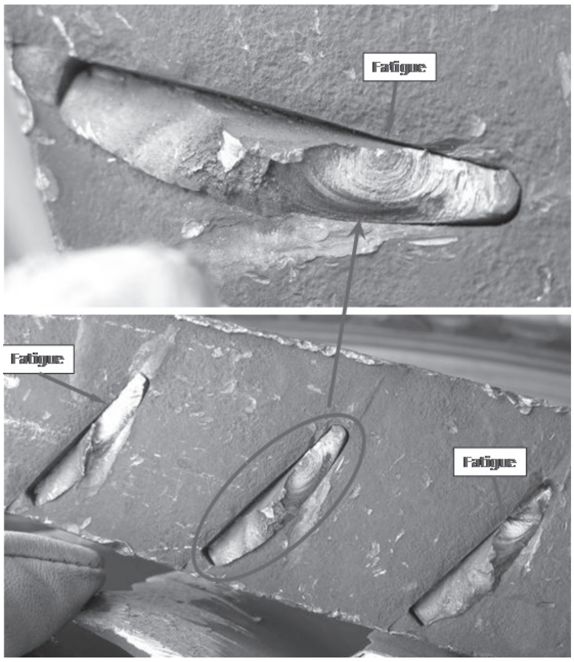

Fig. 12. Diaphragm first three vibratory mode shapes

2.3. Analysis of compressor "Rotating Stall"

The rotating stall phenomenon is generic to all axial flow compressors and can be explained as follows. The throat area and vane and blade angles at each compressor stage are designed to operate with maximum efficiency at full speed. In the low speed range, the air is not sufficiently compressed in the front stages to allow it to flow readily through the smaller throat areas in the rear stages. This choking in the rear stages reduces incoming air flow and, hence, velocity. This reduction in velocity in turn causes an increase in the incidence angle of air impinging on blades in the front stages. When this incidence angle exceeds a given amount, the blade in question stalls; i.e., the air flow separates from the suction side of the blade causing turbulence and low velocity flow (fig. 13).

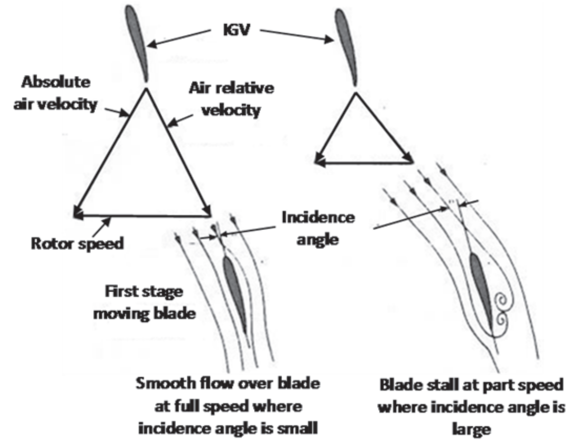

Fig. 13. Stall diagram in compressor blades when the incidence angle exceeds a boundary angle

This stalling does not occur simultaneously over all the blades in the stage but instead occurs as one or more pockets, called stall cells, distributed around the stage circumference (fig. 14). By a somewhat involved mechanism these cells rotate, hence, the term “rotating stall”. The speed range over which rotating stall can occur in the analyzed unit identified by the O.E.M. referring to the same frame is between 1500 rpm and 2600 rpm [7]. The manufacturer reported some similar cases of diaphragm failures in other units of the same frame caused by rotating stall [7].

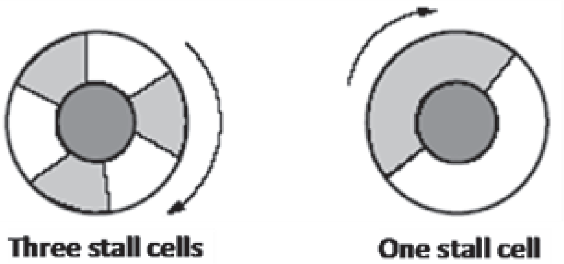

Fig. 14. Typical stall cell patterns.

There may be one to four cells present, with the number of cells decreasing with increasing speed, and they rotate at 50 % to 65 % of rotor speed [7]. Each time a stall cell passes over a rotating blade or stationary vane, the aerodynamic load on that component is sharply reduced as a result of low velocity flow in the cell. Hence, the effect of rotating stall cells is to induce vibratory stresses on vanes and blades. These stresses reach their maximum when the rotating stall excitation frequency or one of its harmonics is coincident with the blade natural frequency. The stall excitation frequency is relatively low even when compared to the blade first mode resonance frequency; thus only the higher harmonics will cause resonance and only to the first blade mode. However, due to the number of cells which can occur and their irregular shape and spacing, many harmonics of the fundamental stall excitation frequency can be present. Although rotating stall during start-up cannot be eliminated, its effects are minimized by modulating the inlet guide vanes (IGV) and increasing inter-stage bleeding. Normally the vibratory stresses generated at blades/vanes are low, but the presence of corrosion pits on blade/vane surfaces can dramatically reduce material fatigue strength, causing small surface cracks which propagate due to stress concentration at the crack front. Since rotating stall only exists in the low speed range, cracking is related to the number of startups rather than operating hours at full speed.

2.4. Metallurgical investigation

A metallurgical investigation of the failed vanes was carried out, including metallography, SEM (scanning electronic microscopy), fractography and chemical analysis. The vane airfoil zone microstructure is shown in fig. 15. The microstructure consists of tempered homogenous martensite typical for forged stainless steel according to specification AISI 410. Chemical composition and hardness tests of the failed vanes confirmed concordance of the blade material used to the design specification. The average blade material hardness was 24 HRC, which falls within design limits. Also, a hardness test was performed on the fracture surface of vane/tenon stage 13. The hardness falls within the range 40–56 HRC. This value is very high (brittle material) and means that, after vane-to-shroud welding, no stress relieving process of the diaphragms was executed. Fractography evaluation was achieved on the exposed vane/tenon crack surface using scanning electronic microscopy (SEM) to determine the origin of the fracture. Fig. 16 shows a general view of the vane/tenon fracture surface. Two different zones were found: a dark zone with appearance of sudden fracture and a shiny zone with beach marks typical of a HCF failure mechanism.

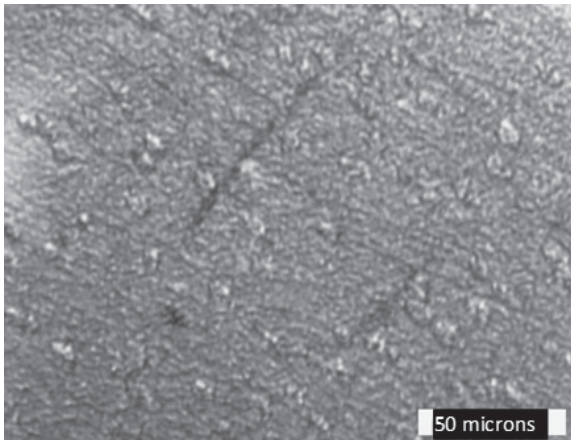

Fig. 15. Microstructure of AISI 410 alloy obtained by SEM

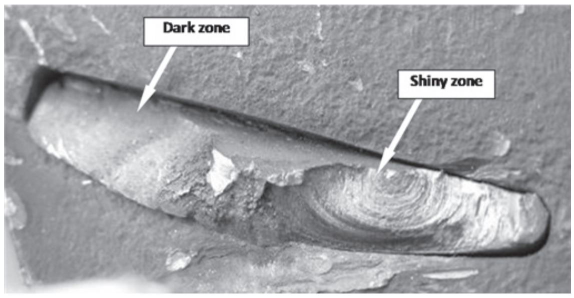

Fig. 16. General view of the vane/tenon fracture surface, stage 13

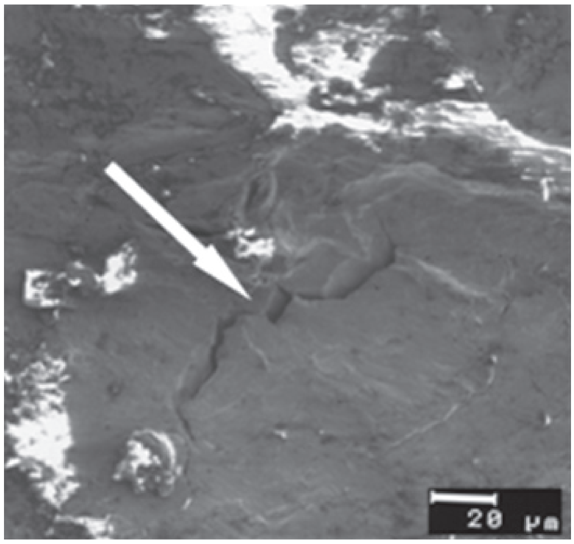

Fig. 17. Detail of the vane/tenon fracture initiation zone, stage 13

Fig. 17 shows a detail of the fracture initiation zone of the vane/tenon stage 13. It can be appreciated that fracture initiation was trans-granular which is typical for an HCF mechanism and the presence of micro cracks on the fracture surface close to the fracture initiation zone. Blade fracture initiated in corrosion pits (Fig. 18 b). The presence of beach marks on the fracture surface is noticeable (fig. 18a) as well as a high quantity and density of corrosion pits, which indicates severe corrosion attack (fig. 18b). Twelve (12) beach marks were counted on the fracture surface, and no visible striation lines were detected. The shiny appearance of this fracture surface zone suggests that it is a recent fracture. Fig. 19 shows an Energy Dispersion Spectrum (EDS) of deposits found on the vane fracture surface in two zones: the dark zone and the shiny zone shown in fig. 16. It may be concluded from fig. 19, that the dark zone/surface has more oxygen concentration than the shiny one has, which means it was exposed more time to a corrosive ambient than the latter. Deposits of Na, Al, S and Zn were also found on the fracture surface, among which Na and S are principal corrosive agents in reaction with water.

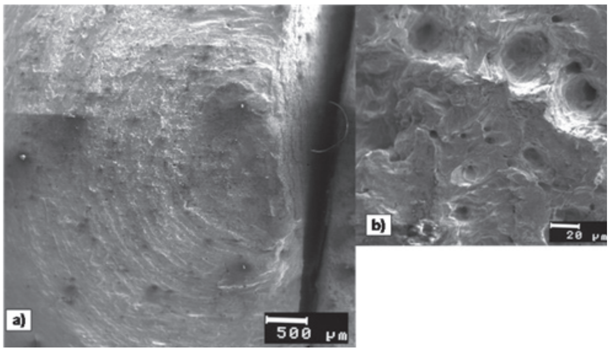

Fig. 18. Details of the fracture surface shiny zone from figure 16. Beach marks a) and corrosion pits b) on the fracture surface of vane/tenon stage 13

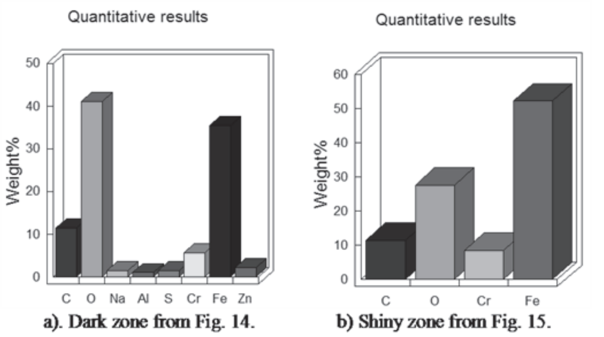

Fig. 19. Deposits found on the vane/tenon fracture surface, diaphragm stage 13: a) Dark zone frome fig. 16, b) Shiny zone from figure 16

2.5. Compressor vane failure analysis

Analyzing details of the features recorded in compressor vanes/diaphragms (stage 13) and the failure mechanism presented above, it may be concluded that failure origin/initiation and propagation can be attributed to high cycle fatigue (HCF) generated by the rotating stall phenomenon during unit start-ups with very important corrosion contribution. Metallurgical investigation results revealed that fracture initiation points were localized in corrosion pits that raise local stresses compared to the original unaltered surface. Corrosion products (deposits) were also found in the same zone. The fog water nozzles had been installed upstream of the compressor inlet air filter without any water filter/catcher before the water spray nozzles. Because of this, many compressor stages operated with humid air which, in contact with corrosive agents, developed a corrosion process. These findings lead to the conclusion that blade high cycle fatigue failure initiation and propagation were highly influenced by corrosion processes. From fig. 20 it can be appreciated that the existence of assembly clearances between the vane and outer diaphragm shroud is an open way for corrosive agents to deposit on the vane/tenon heat affected zone (weakest zone), causing corrosion pits that lead to accelerated fatigue initiation of the vane/tenon.

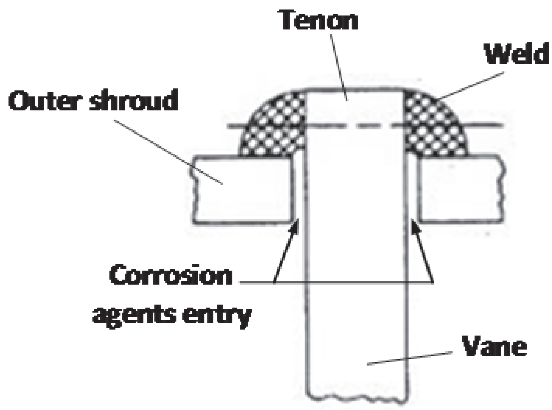

Fig. 20. Scheme of the union of diaphragm vanes with the outer shroud

Severe FOD impacts on the vanes close to the diaphragm outer shroud during the first failure event (December 2008) could generate sudden partial fractures of the vanes/tenons due to their high hardness and related brittleness, as appears in the dark zone in fig. 16. Diaphragm stages 13 and 14 in which vanes/tenons fatigue fractures occurred during the third failure event (fig. 10, May 2009) operated continuously since the overhaul in 2005 and were present during all unit failure events. These vanes were probably fractured partially during the first failure event by FOD and not detected by non destructive examination. As can be seen in fig. 11, if tenon fracture is localized within the diaphragm outer shroud width (not propagated to the vane airfoil), this fracture is covered by the weld and outer diaphragm shroud, making it impossible to detect by the magnetic particle examination commonly used for diaphragm non-destructive testing. It supports the conclusion mentioned above that tenon partial fractures (dark zone in fig. 16) were developed during the first failure event. This conclusion is supported also by the chemical analysis of the vane/tenon fracture surface presented in fig. 19, which indicates that the fracture dark zone (fig. 16, sudden fracture) is more oxidized than the shiny zone (fatigue fracture), meaning that sudden fracture was developed some time before fatigue fracture. A pre-existence of initial sudden fractures at the vanes/tenons before the unit third failure event is also supported by the fact that vane fatigue failure soon developed during the third failure event after only two unit start-up attempts. Diaphragm vanes are joined to the shrouds by one weld in the case of stages 12 to 19 (fig. 21a) and by two welds in the case of stages 1 to 11 (fig. 21b). It may be seen from fig. 21 that the joint with two welds (fig. 21b) provides a better distribution of flexural moments (M) because each weld is loaded by half of the moment (M/2). In the case of joints with only one weld (fig. 21a) the load is twice as high, and the probable failure of this joint is much greater. During the first and third failure events, vane fatigue fracture is related to rotating stall initiated at vanes of the front stages, before air bleeding, see fig. 2a) and fig. 2c) which is consistent with the rotating stall mechanism described in previous sections. Fatigue fracture of the rear stage vanes, after air bleeding during the third failure event (fig. 2c) is related to upstream rotating blade wakes associated with rotating stall. Also, the weaker vane-to-shroud weld joint design of the rear stages (fig. 21a) accelerated the fatigue fracture of these vanes. Other possible causes of vane failure were verified including IGV angles and IGV schedule control logic, excessive water injection by fogging (water overspray), possible off-design operating conditions and compressor blades/vanes degradation, but no related irregularities were found.

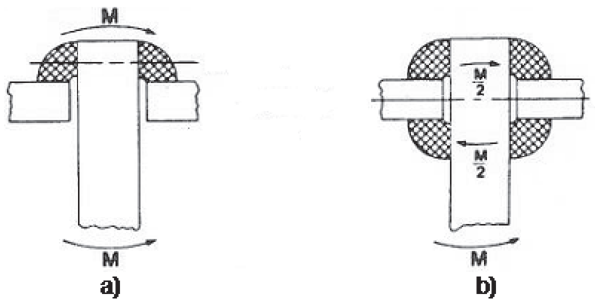

Fig. 21. Design of the diaphragm vane-to-shroud weld joint: a) Stages 12-19; b) Stages 1-11.

It may be concluded that compressor diaphragm failure origin/initiation and propagation can be attributed to high cycle fatigue (HCF) generated by a rotating stall phenomenon during unit start-ups. Vanes/tenon HCF during the third failure event was very high, accelerated by the pre-existence of sudden vane fractures and corrosion pits caused by the humid ambient generated by the fogging system. Also, vane fatigue failure was accelerated by the high brittleness of vane tenons (heat affected zone) generated by the welding process without any stress relieving process. The stress concentration factor for the weld heat affected zone in the analyzed case was 3.5 [7].

3. Conclusions

Based on an analysis of the results from compressor vane metallographic examination, unit operational parameters, rotating stall phenomenon, fogging system, compressor vane cracking mechanism, and chemical analysis of deposits, it may be concluded that compressor diaphragm failure initiation and propagation was driven by a high cycle fatigue mechanism accelerated to a high degree by corrosion processes in the vane tenon heat affected zone. The rotating stall phenomenon is generic to all axial flow compressors during startup and was identified by the O.E.M. referring to the same frame. The vibratory stresses generated at blades/vanes are low, but the presence of corrosion pits on the blade/vane surface dramatically reduced material fatigue strength, causing small surface cracks which propagated due to stress concentration at the crack front. Conditions for the corrosion process were generated by fogging (humid air), assembly union geometry between vanes and diaphragm outer shrouds and the presence of corrosive agents in the compressor flow. Vane fatigue failure was accelerated by the high brittleness of vane tenons (heat affected zone) generated by the welding process without any stress relieving process and weak design of vane-to-shroud weld joints in some stages.

4. References

1. Bhargava R. K, Meher-Homji C. B, Chaker M. A, Bianchi M, Melino F, Peretto A, Ingistov S. Gas turbine Fogging Technology: A state-of-the-art review, Part III: Practical considerations and operational experience. Journal of Engineering of Gas Turbines and Power, 2007; 129: 461-472.
2. Fogging state of the art, 2009, www.meefog.com.
3. Mazur Z, Hernandez-Rossette A, Porcayo-Calderón J, Mariño-López C. 2009 Diagnóstico de la causa raíz de la falla de la U2 de la central de Ciclo Combinado Tula (In Spanish), Report IIE/43/I/2827/002/2009, Instituto de Investigaciones Electricas, Cuernavaca, 2009.
4. Mercer M. Hot Times For Turbine Cooling", Diesel & Gas Turbine Worldwide, 2002; 62: 5-13.
5. Savic S, Kippax P. Fogging dynamics solved. (Advanced Gas Turbines). Power Engineering International, 2003; 11: 264-272.
6. Savic S, Mitsis G, Härtel C, Khaidarov S, Pfeiffer P. (2002) Spray Interaction and Droplet Coalescence In Turbulent Air-Flow, an Experimental Study With Application To Gas Turbine High Fogging, Proceedings of Institute for Liquid Atomisation and Spray Systems-Europe, Zaragoza, Spain, 2002; 221-226.
7. Westinghouse: Proceedings of Gas Turbine User Association Conference, Pittsburgh, USA, 1978; 68-76.

Dr inż. Zdzislaw MAZUR
Mgr inż. Alejandro HERNANDEZ-ROSSETTE
Gerencia de Turbomaquinaria
Instituto de Investigaciones Electricas
Av. Reforma nr 113, Col. Palmira,
62-490 Cuernavaca, Morelos, Mexico
e-mail: mazur@iie.org.mx; ahr@iie.org.mx

Ning HUANG
Dong HOU
Yang CHEN
Liudong XING
Rui KANG

A NETWORK RELIABILITY EVALUATION METHOD BASED ON APPLICATIONS AND TOPOLOGICAL STRUCTURE

METODA OCENY NIEZAWODNOŚCI SIECI OPARTA NA APLIKACJACH I STRUKTURZE TOPOLOGICZNEJ

Applications play an important role in the reliability evaluation of communication networks. In other words, the reliability of a network can be totally different when different applications are considered for the same network. However existing reliability evaluation methods, which are mostly based on the graph theory, give no or little consideration to applications. This paper proposes a concept of network application reliability and a Markov-based method for analyzing the proposed network application reliability measure. Furthermore, based on the reliability of each individual application, a method is proposed to evaluate the overall network reliability that incorporates effects of different applications running on the network. Both a case study and experiments are performed to illustrate the proposed concept and methods.

Keywords: *application, Markov model, network, reliability.*

Aplikacje odgrywają ważną rolę w ocenie niezawodności sieci komunikacyjnych. Innymi słowy, niezawodność sieci może być całkowicie różna dla różnych aplikacji tej samej sieci. Niestety, istniejące metody oceny niezawodności, w większości oparte na teorii grafów, poświęcają niewiele lub nie poświęcają wcale uwagi aplikacjom. W niniejszym artykule przedstawiono koncepcję niezawodności aplikacji sieciowych oraz opartą na modelu Markowa metodę analizy proponowanej miary niezawodności aplikacji sieciowych. Ponadto, na podstawie niezawodności poszczególnych aplikacji, zaproponowano metodę oceny ogólnej niezawodności sieci, która łączy efekty różnych aplikacji działających w danej sieci. Zaproponowaną koncepcję i metody omówiono na podstawie studium przypadku oraz badań eksperymentalnych.

Słowa kluczowe: *aplikacja, model Markowa, sieć, niezawodność.*

1. Introduction

Reliability analysis has become an essential step in the design, operation, and tuning of network systems [4, 24]. Considerable research efforts have been expended in the network reliability analysis. As a pioneer, Lee first defined and evaluated the network reliability mainly based on network connectivity [6]. Following the similar idea, a series of network reliability evaluation algorithms and optimization methods have been proposed [1, 3, 7, 8, 9, 12, 13, 19, 20, 21, 23, 28, 30, 32]. All these studies are based on the graph theory and the network topology. Among these works, synthesis evaluation methods are especially discussed in [1, 7, 8, 28, 30]. Later on other more advanced synthesis evaluation methods have been proposed, including but not limited to AHP (Analytic Hierarchy Process) [14, 27], fuzzy reliability evaluation [17], and ANN (Artificial Neural Network) [5]. Since 1980s, network congestion and traffic delay have become noticeable factors in the network reliability research. For example, Barberis and Park investigated network availability considering throughput and delay [10, 25]. Tao and Chen considered routing dynamics and congestion into the network reliability computation [33]. In general, the existing network reliability research can be classified into two types [29]: *inherent reliability* considering topology connectivity and *applicable reliability* considering network traffic. The former focuses on topology structure, and has been analyzed using probability theory and graph theory. The latter focuses on how the network works and what is in the network, and examines performance reliability of the network [11, 15, 22].

Those research works on network reliability, however, gave little or no consideration to the effects of applications, though the network reliability and performance can be different when different applications run on the network. Recently studies on application-layer network performance testing [18, 26] have started. The performance of application layer is quite different from and not directly related to the performance of the other layers in the OSI model. And end users are usually concerned with the performance of specific applications [2, 31]. It is worth noting that the Internet Engineering Task Force (IETF) proposed a performance testing methodology and some metrics on the application layer in RFC 3511 [16]. And the influence of applications for network reliability has also been noticed in [34, 35].

To the best of our knowledge, there is no work considering various applications and incorporating the effects of them in the evaluation of the network reliability. In this paper, a concept of network application reliability is proposed and a Markov-based method for analyzing the proposed application reliability measure is discussed. Furthermore, based on the reliability of each individual application, a method is proposed to evaluate the overall network reliability that considers the effects of different applications running on the network. Both a case study and experiments are performed to illustrate the proposed concept and methods.

2. Concept and model

The following concepts are defined and used in the latter discussions:

A network: is a group of hardware devices and services. It has the transportation ability to support applications for users.

A service: is a function that a network provides to users. Usually a function is supported by a software system or a group of cooperating software systems.

An application: is the usage of services by a group of users with some demanded performance requirements.

Application profile: represents the information of an application, including information of the users involved and a set of operation probabilities of the application;

Usage profile: contains a set of application profiles and their occurrence probabilities.

The proposed application-centric model for communication network reliability is shown in fig.1.

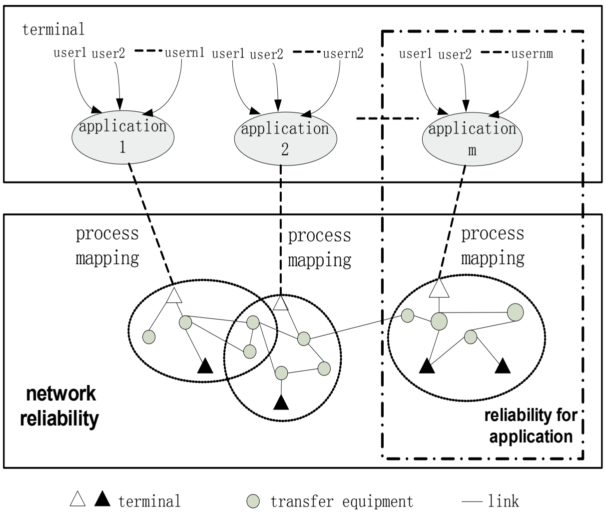

Fig.1. Network reliability model

Let R represent the overall network reliability, and R_i represent reliability for application A_i. R is a function of R_i and usage-profile. Namely R is a function of reliabilities for all applications, and the relationship among all the applications in the network. Let H_i be the set of hardware that application A_i involves. $\{Feature_j\}_i$ means a set of reliability of each element in H_i. Before evaluating the application reliability, each application should be mapped to its topology. The main idea of this mapping is to separate devices into groups according to the usage of the application, as illustrated in fig.1. We use $topo\log y_i$ to indicate the mapped topology of H_i, namely how the hardware components involved in A_i are connected. $Deploy_i$ represents how application A_i is deployed in the network. $App - profile_i$ shows the application profile of application A_i. The application reliability R_i is a function of $\{Feature_j\}_i$, $topo\log y_i$, $deploy_i$ and $App - profile_i$.

3. Proposed algorithms

Algorithms for computing the application reliability and the overall network reliability are explained in this section. Two assumptions are made in the proposed algorithms: 1) All the network components (nodes or links) fail statistically-independently; and 2) The transfer of data flow in the network is a Markov process, meaning that the determination of the next node to transfer the flow depends on the present node, not the past path.

As briefed in Section 2, R_i is a function of $\{Feature_j\}_i$, $topo\log y_i$, $deploy_i$, and $app - profile_i$, and R is the function of $\{R_i\}$ and usage-profile. The substances of the parameters in this algorithm are:

1) $Feature\}_i$: reliabilities of the components.
2) $Topo\log y_i$: the transfer matrix.
3) $Deploy_i$: mapping to the network components according to the deployment of the services.
4) $App - profile_i$: the transfer probability of the application when it is running.
5) $Usage - profile$: the number and importance of the applications.

The general algorithm can be described as the following process:

Step 1: prepare $\{Feature_j\}_i$ and $Usage - profile$: Analyze the network, and prepare the static parameters including the reliabilities of nodes and links from the history usage data (they usually can be obtained from devices providers). Assign the weight for each application according to its importance in the network.

Step 2: analyze applications on the network. For each application A_i, determine its concerned services as a set S_i, and its process (data flow) for the network reliability.

Step 3: analyze $deploy_i$ for each application A_i. Based on the information obtained in step2, analyze where each service is installed and what nodes and links its process concerns. Because the data flow has direction, every application A_i is mapped to two diagrams, request diagram and response diagram, corresponding to request data flow and response data flow, respectively.

Step 4: analyze $App - profile_i$. Acquire the multi-branch transfer probabilities of the nodes for each application A_i using history data or statistic methods for both request diagram and response diagram.

The transfer probability of a link is computed as the ratio of the size of the data flow through the link to the total size of data flows through all the links involved in the application. For example, a node used in a specific application connects with three links which are named as *a*, *b*, and *c*, respectively. The sizes of the data flows going through the three links are respectively 20KB, 30KB and 50KB. Thus the transfer probabilities of the three links are respectively 0.2, 0.3, and 0.5.

Step 5: calculate reliability R_i for each individual application A_i using the method presented in Section 3.1.

Step 6: evaluate the overall network reliability using the method described in Section 3.2.

3.1. Reliability evaluation for an application

Let H_i^s and H_i^t respectively represent the set of nodes for request diagram and response diagram of application A_i, R_i^s

and R_i^t respectively represent reliability corresponding request diagram and response diagram. There are six steps to compute the reliability of application A_i.

Step 1: obtain the transfer matrix Q based on the request diagram of application A_i.

Let n_i and n_j represent network nodes, namely $n_i, n_j \in H_i^s$. Represent a link from n_i to n_j with l_{ij}, the reliability of n_i with N_i, the reliability of l_{ij} with L_{ij}, and the transfer probability from n_i to n_j with P_{ij}. We regard every node in the network as a state of the Markov model. The model also includes states C and F that represent the application request is completed successfully (N_C=1) and the request is failed (N_F=1) respectively. Thus the complete state space for the Markov model is $\{n_1, n_2, \ldots, n_n, C, F\}$. The state transition matrix is named T:

$$T = \begin{array}{c} \\ n_1 \\ \vdots \\ n_i \\ \vdots \\ n_{n-1} \\ n_n \\ C \\ F \end{array} \begin{array}{c} \begin{array}{cccccccc} n_1 & n_2 & \cdots & n_j & \cdots & n_n & C & F \end{array} \\ \left[\begin{array}{cccccccc} 0 & N_1L_{12}P_{12} & \cdots & N_1L_{1j}P_{1j} & \cdots & N_1L_{1n}P_{1n} & N_1L_{1C}P_{1C} & 1-F_1 \\ \vdots & \vdots & & \vdots & & \vdots & \vdots & \vdots \\ 0 & N_iL_{i2}P_{i2} & \cdots & N_iL_{ij}P_{ij} & \cdots & N_iL_{in}P_{in} & N_iL_{iC}P_{iC} & 1-F_i \\ \vdots & \vdots & & \vdots & & \vdots & \vdots & \vdots \\ 0 & N_{n-1}L_{(n-1)2}P_{(n-1)2} & \cdots & N_{n-1}L_{(n-1)j}P_{(n-1)j} & \cdots & N_{n-1}L_{(n-1)n}P_{(n-1)n} & N_{n-1}L_{(n-1)C}P_{(n-1)C} & 1-F_{n-1} \\ 0 & N_nL_{n2}P_{n2} & \cdots & N_nL_{nj}P_{nj} & \cdots & 0 & N_nL_{nC}P_{nC} & 1-F_n \\ 0 & 0 & \cdots & 0 & \cdots & 0 & 0 & 0 \\ 0 & 0 & \cdots & 0 & \cdots & 0 & 0 & 0 \end{array}\right] \end{array} \quad (1)$$

Where,

$$F_i = \sum_{j=2}^{n} N_i L_{ij} P_{ij} + N_i L_{iC} P_{iC}, L_{iC} = 1, P_{iC} = 0 or 1 \quad (2)$$

Every element $T(a,b)$ in matrix T represents the probability of successful transfer of a flow from node n_a to node n_b. The value of $T(a,b)$ is the product of N_a, L_{ab} and P_{ab}. For instance, the element $T(i,2)$ in row n_i and column n_2 is the product of the reliability of n_i, the reliability of l_{i2} and the transfer probability from n_i to n_2, namely the product of N_i, L_{i2} and P_{i2}. n_1 represents the requester of the application whose in-degree is 0. C represents the completion state and F represents the failure state. Both of them are absorbing states with out-degrees of 0. Therefore, elements in the first column and the last two rows in T are 0.

The matrix Q is obtained by removing the row and column of F from matrix T.

$$Q = \begin{array}{c} \\ n_1 \\ \vdots \\ n_i \\ \vdots \\ n_{n-1} \\ n_n \\ C \end{array} \begin{array}{c} \begin{array}{ccccccc} n_1 & n_2 & \cdots & n_j & \cdots & n_n & C \end{array} \\ \left[\begin{array}{ccccccc} 0 & N_1L_{12}P_{12} & \cdots & N_1L_{1j}P_{1j} & \cdots & N_1L_{1n}P_{1n} & N_1L_{1C}P_{1C} \\ \vdots & \vdots & & \vdots & & \vdots & \vdots \\ 0 & N_iL_{i2}P_{i2} & \cdots & N_iL_{ij}P_{ij} & \cdots & N_iL_{in}P_{in} & N_iL_{iC}P_{iC} \\ \vdots & \vdots & & \vdots & & \vdots & \vdots \\ 0 & N_{n-1}L_{(n-1)2}P_{(n-1)2} & \cdots & N_{n-1}L_{(n-1)j}P_{(n-1)j} & \cdots & N_{n-1}L_{(n-1)n}P_{(n-1)n} & N_{n-1}L_{(n-1)C}P_{(n-1)C} \\ 0 & N_nL_{n2}P_{n2} & \cdots & N_nL_{nj}P_{nj} & \cdots & 0 & N_nL_{nC}P_{nC} \\ 0 & 0 & \cdots & 0 & \cdots & 0 & 0 \end{array}\right] \end{array} \quad (3)$$

Step 2: derive matrix W, and calculate the determinant of W denoted as $|W|$.

For any integer m (m>0), $Q^m(i,j)$ is the probability that the data packet is transferred from n_i to n_j within m steps. It is supposed that S is a matrix with the order of n+1, and:

$$S = I + Q + Q^2 + \cdots = \sum_{k=0}^{\infty} Q^k \quad (4)$$

where, I is an identity matrix.

The application reliability is thus the transfer probability from n_1 to C, that is, $R_i^s = S(n_1, C)$. When $W = I - Q$, we have:

$$S = W^{-1} = (I - Q)^{-1} \quad (5)$$

Then the value of $|W|$ can be computed.

Step 3: remove the first column and the last row of W, name the remaining matrix as M, and calculate $|M|$.

Step 4: calculate R_i^s as the reliability for request diagram of application A_i with the formula:

$$R_i^s = (-1)^n \frac{|M|}{|W|} \quad (6)$$

where, n is the number of nodes in the application request diagram.

Proof:

$$R_i^s = S(n_1, C) = W^{-1}(n_1, C) = \frac{W^*(n_1, C)}{|W|} = \frac{(-1)^{n+1+1}|M|}{|W|} = (-1)^n \frac{|M|}{|W|} \quad (7)$$

where, W^* is the adjoint matrix of W.

Step 5: using the above similar steps, calculate R_i^t based on the response diagram for application A_i.

Step6: computed reliability for application A_i using the following formula:

$$R_i = R_i^s \times R_i^t \quad (8)$$

3.2. Reliability evaluation for the entire network

There is typically more than one application existing in the network. Therefore a method is needed to integrate the single application reliabilities to obtain the entire network reliability. In this work, the overall network reliability is evaluated as a weighted sum of reliabilities of all applications running on the network, as shown in (9).

$$R = \sum_{i=1}^{n} \omega_i R_i, \sum_{i=1}^{n} \omega_i = 1 \quad (9)$$

Where ω_i represents the weight of application A_i, which indicates the number of users or the significance of the application. Consider an example where there are three applications of three groups of users called Lan1, Lan2 and Lan3 with the same significance level. The topology reliabilities of these applications are respectively R_1 = 0.9, R_2 = 0.8, R_3 = 0.9, and the number of users of Lan1, Lan2 and Lan3 are respectively 6, 7 and 7. The weights of these applications are computed as ω_1= 6/(6+7+7)=0.3, ω_2=0.35, ω_3=0.35. Thus, the overall network reliability is $R = \sum_{i=1}^{3} \omega_i R_i = 0.865$.

4. Case study

In this section, a case study is performed to show how a network reliability can be evaluated using the method described in Section 3.

4.1. System description

Figure 2 illustrates a small campus network with teaching VOD (Video on Demand) applications running on it. Reliabilities of nodes and links in this network are given in table 1 and table 2, respectively. Lan1, Lan2 and Lan3 are three different groups of users. There are 10 users in Lan1, 15 in Lan2, and 25 in Lan3. Lan 1 is a LAN of student dormitories and faculty apartments; Lan 2 is a LAN of the teaching zone, and Lan 3 is a LAN of the teaching showcase area.

Service1 and Service2 are grouped together to support a VOD providing application where users can watch part of the teaching videos and TVs (referred to as application1 hereafter), and they are installed separately on Server1 and Server3. Service3 itself also supports the same VOD providing application as a main server for all the video sources (application2) and it is installed on Server2. Service4 supports a HTTP application where users access to the Internet or other communication networks (application3), and is installed on Server2 too. These three applications run on the network: users can visit application1 through Lan1, application2 through Lan2, and application3 through Lan3.

4.2. Network Reliability Evaluation

Using the method of Section 3, the reliability of this example network reliability can be evaluated using the following steps:

Step 1: prepare data, including reliabilities of the nodes and links, shown in tables 1 &2.

Step 2: analyze applications. For example, for application1, users request Service1 (on Server1) for a special video by a browser. If this video can be provided by Service1, it can be downloaded by the users. Otherwise, the request will be transferred to Service2 (on Server3) to find the video.

For application1, S_1={browser, Service1, Service2}. In this step, only services are analyzed without consideration of hardware, namely, these services can be installed on different servers involving different transform devices.

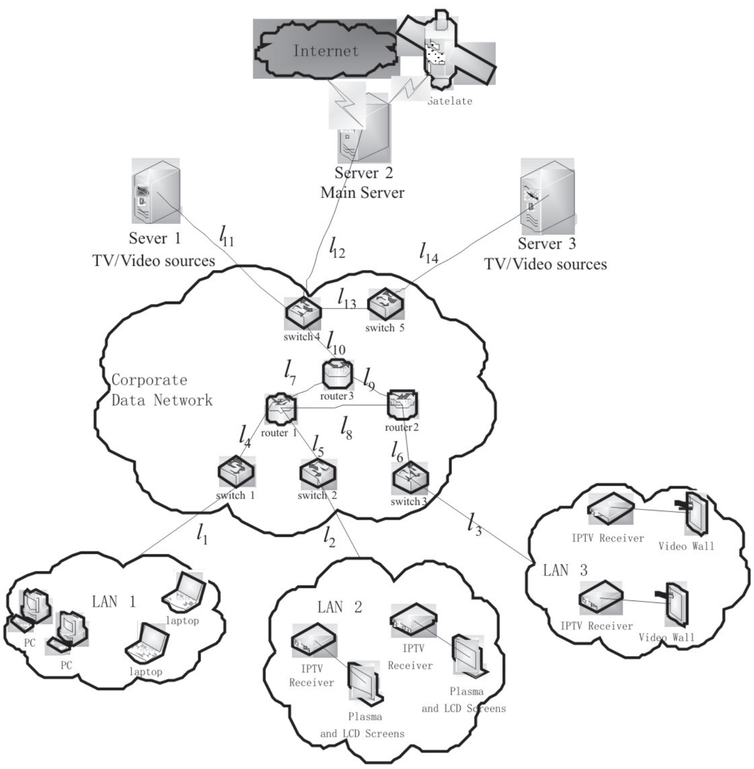

Fig. 2 Network structure of the case

Tab. 1. Reliability of the Nodes

Node	R_i	Node	R_i
lan1	1	router2	0.97
lan2	1	router3	0.99
lan3	1	switch4	0.98
switch1	0.98	switch5	0.98

Tab. 2. Reliability of the Links

Link	L_i	Link	L_i
l_1	0.99	l_8	0.98
l_2	0.98	l_9	1
l_3	0.98	l_{10}	0.99
l_4	1	l_{11}	0.99

Step 3: figure out the request diagram for applicaiton1. Based on S_1 obtained in Step2, servers, switches, and routers are figured out based on the actual network configuration, shown in figure 3. Note that if Service1 and Service2 are installed on different servers or the different routing rules are involved, then the diagram will be different.

In this case, request diagram concerns all the devices to support application1. But if the routing rules in Router1 are changed to deliver its data packages only to Router3, then the request diagram will be changed to another one without Router2.

Step 4: establish the transfer probabilities of the multi-branch nodes for request diagram for application1.

In this example system, the requests of application1 are sent to server1 with a probability of 0.8, and to server 3 with a probability of 0.2 (when the object file is not found on server1). That is, the transfer probabilities of l_{11} and l_{13} are 0.8 and 0.2, respectively. Similarly, the transfer probabilities of l_7 and l_8 are 0.6 and 0.4, respectively. For the nodes with only one outgoing link, the transfer probability of the link is simply 1.

Step 5: calculate R_1^s and R_1^t for application1. Here the evaluation of R_1^s is explained in detail:

1) Add a state C for application1 indicating that this application request is completed successfully. Derive matrix Q_1 from the reliabilities of correlative nodes and links as well as the transfer probabilities.
2) Compute the matrix $W_1=I-Q_1$, and the value of its determinant $|W_1|$. W_1 is an upper triangular matrix here, and $|W_1|=1$.
3) Remove the first column and the last row from W_1 to get a new matrix M_1, then obtain the result $|M_1|\approx-0.86852$.
4) The request reliability of application1 can be calculated as:

$$R_1^s = (-1)^n \frac{|M_1|}{|W_1|} \approx (-1) * \frac{-0.86852}{1} = 0.86852$$

where, n represents the number of nodes in the topology of figure 3, which is 9.

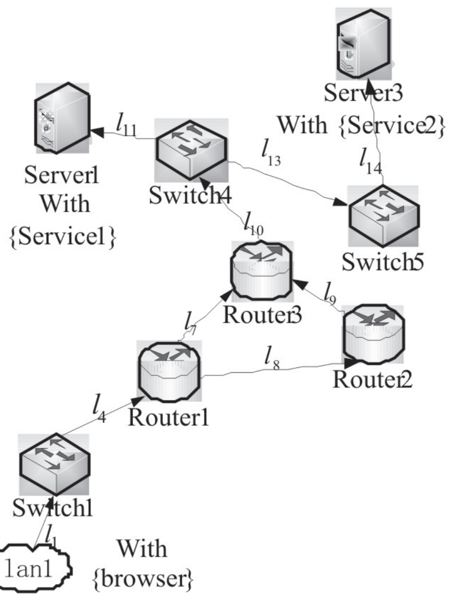

Fig. 3 Request Diagram of application1

Calculate reliability R_1^t in the similar way. In this example, response diagram is the same as the request diagram with opposite directions. So we have $R_1^t = R_1^s = 0.86852$. Thus, $R_1 = R_1^s \times R_1^t = 0.86852^2 = 0.75433$.

Step 6: Similarly, following step 2 to step 5, reliabilities of application2 and application3 can be evaluated as: $R_2\approx0.68800$, $R_3\approx0.69499$.

Step 7: calculate the network reliability as a weighted sum of all the single application reliabilities. The weights of the three applications are calculated as the proportion of their users. Thus the entire network application is calculated as: $R = \sum_{i=1}^{3} \omega_i R_i = 0.2*0.75433 + 0.3*0.68800 + 0.5*0.69499 = 0.704761$.

5. Experiments and analysis

Further experiments are performed on the example network under different conditions to study the effects of component reliability and applications on the network reliability.

5.1. Experiment 1: Influence of component reliability on network reliability

Fig. 4. shows the change of the application reliability R_1, R_2 and R_3, and network reliability R, when the reliability value of switch4, N_{s4} changes. Similarly, fig. 5. shows the effect of the change of reliability of switch5 N_{s5} on the reliabilities of single applications and the entire network.

Based on fig. 4 and fig. 5, we can see that R_1, R_2, R_3, and R decrease as N_{s4} or N_{s5} decreases. In addition, switch4 is more important than switch5 to application 1 and application 2, because R_1 and R_2 reduce more rapidly in fig. 4 than in fig. 5. As shown through this example, our algorithm can facilitate the study of sensitivity or importance of different components to the network reliabilities.

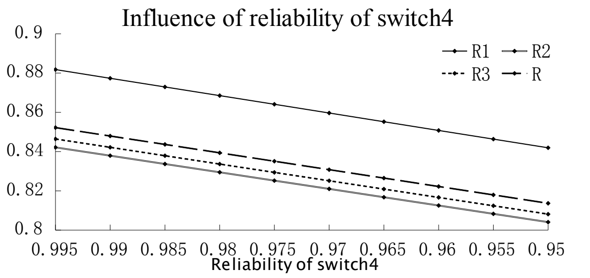

Fig. 4 Reliabilities decrease as the reliability of switch4 is reduced

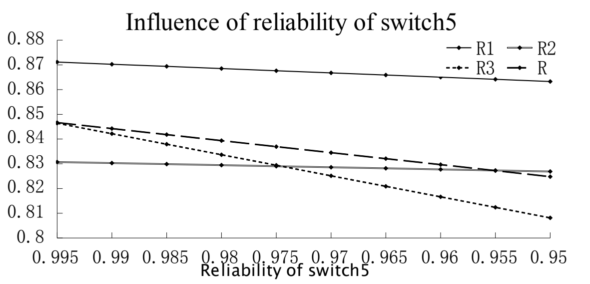

Fig. 5 Reliabilities decrease as the reliability of switch5 is reduced

5.2. Experiment 2: Influence of applications on network reliability

Experiments are performed on the example network to study the effects of applications on the network reliability.

When the proportion of the requests sent to Server1 and Server3 in applications changes, the changes of network reliability are shown in figure. 6. In particular, as the portion of requests sent to Server 1 decreases and portion sent to Server 3 increases, both the reliability of application1R_1, and the overall network reliability R decrease. This is reasonable because the branch to Server1 has a greater reliability than the branch to Server3.

The influence of component reliability on the overall network reliability has been studied and widely acknowledged. Meanwhile, the reliability of a network can be totally different when different applications are considered for the same network. Experiments performed in Sections 5.1 and 5.2 show that our evaluation method reflects the influence of not only components but also applications on the network reliability. This research is our first step for studying application-oriented reliability for communication networks with deterministic routings. It has provided another view of network reliability, which can reflect the users' requirements better.

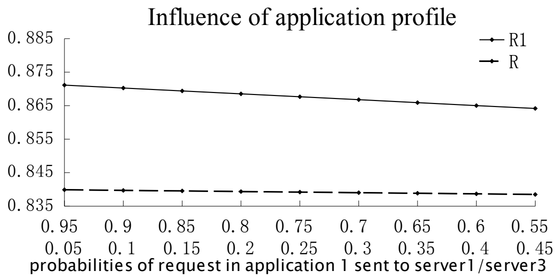

Fig. 6. The influence of applications on network reliability

6. Conclusions and future work

Traditional network reliability algorithms mainly focus on network topology/connectivity while giving little or no consideration to applications running on the network. Thus results obtained using the traditional methods are not convincing enough for practical projects in enterprises because applications can affect the performance/reliability of a network greatly. A new application-centric network reliability concept and corresponding evaluation algorithm have been proposed in this paper. As shown through the case study and experiments, the algorithm considers the effects of both component reliabilities and applications in the network reliability evaluation.

Our future work will focus on (1) how to classify applications to reduce the computational overhead when the number of service is large; (2) how to optimize the algorithm to avoid the computational complexity caused by the excessive matrix order when the number of nodes related to a specific application is enormous; and (3) how to abstract more useful information about applications and components and incorporate it into the algorithm.

7. References

1. A. R. Abdelaziz. A New Approach to Power Network Synthesis. Proc. Of the 8th International Conference on Harmonics and Quality of Power, 1998:495.
2. A. Avritzer, E. J. Weyuker. The Role of Modeling in the Performance Testing of E-Commerce Applications. IEEE Transactions on Software Engineering, 2004, 30(12): 1072-1083.
3. A. M. Shooman. Algorithms for Network Reliability and Connection Availability Analysis. IEEE Transactions on Reliability, 1995, 44(10): 309-333.
4. A. P. Snow. Network Reliability: The Concurrent Challenges of Innovation, Competition and Complexity. IEEE Transactions on Reliability, 2001, 50(1): 3 8-40.
5. Chat Srivaree-ratana, Abdullah Konak and Alice E. Smith. Estimation of all-terminal network reliability using an artificial neural network. Computers & Operations Research, 2002, 29(7): 849-868.
6. C. Y. Lee. Analysis of Switching Networks. Bell Syst. Tech.J., 1955, 34: 1287-1315.
7. F. T. Boesch. Synthesis of Reliable Networks-A Survey. IEEE Transactions on Reliability, 1986, 35(3): 240-246.
8. F. T. Boesch. On Unreliability Polynomials and Graph Connectivity in Reliable Network Synthesis. Journal of Graph Theory, 1986, 10(3): 339-352.
9. Fu-Min Yeh, Hung-Yau Lin, Sy-Yen Kuo. Analyzing Network Reliability With Imperfect Nodes Using OBDD. Proc. of the 2002 Pacific Rim International Symposium on Dependable Computing, Tsukuba, Japan, 2002: 89-96.
10. G. Barberis and U. Mazzei. Traffic-based Criteria for Reliability and Availability Analysis of Computer Networks. Proc. IEEE ICC'77, Chicago, IL, Vol.1 session 22.6, June 1977.
11. Gao Zhuqing, Fan Hehong, Zhang Mingde, Sun Xiaohan. Connectivity Reliability Evaluation for Optical Layer in IP Over WDM Networks Based on Minimal Path Sets. Proceedings of the 7th International Conference of Advanced Communication Technology, Phoenix Park, Korea, 2005: 131-136.
12. Ghasemzadeh M., Meinel C., Khanji S.. K-terminal Network Reliability Evaluation Using Binary Decision Diagram. 3rd International Conference on Information and Communication Technologies: From Theory to Applications, Umayyad Palace, Damascus, Syria, 2008: 1-5.
13. Héctor Cancela, Mohamed El Khadiri. The Recursive Variance-Reduction Simulation Algorithm for Network Reliability Evaluation. IEEE Transactions on Reliability, 2003, 52(2): 207-212.
14. Hossam Mahmoud Ahmad Fahmy. Reliability Evaluation in Distributed Computing Environments Using the AHP. Computer Networks, 2001, 36(5-6): 597-615.
15. Hui-Ling Liu, Shooman M.L.. Simulation of Computer Network Reliability with Congestion. Proceedings of Reliability and Maintainability Symposium, Washington D.C., USA, 1999: 208-213.

16. B. Hickman, D. Newman, S. Tadjudin, T. Martin, Benchmarking Methodology for Firewall Performance. RFC3511, April 2003
17. James Dunyak, Ihab W. Saad, Donald Wunsch. A Theory of Independent Fuzzy Probability for System Reliability. IEEE Transactions on Fuzzy Systems, 1999, 7(2): 286-294.
18. Jens Grabowski, Dieter Hogrefe, Gyorgy Rethy, Ina Schiferdecker, Anthony Wiles, Colin Willcock. An Introduction to the Testing and Test Control Notation (TTCN-3). Computer Networks, 2003, 42(3):3 75-403.
19. Jintao Xiong, Weibo Gong. A Novel Algorithm on Network Reliability Analysis. 10th International Conference on Telecommunications, Papeete, Tahiti (French Polynesia), 2003: 1407-1411.
20. J. M. Wilson. An Improved Minimizing Algorithm for Sum of Disjoint Products. IEEE Transactions on Reliability, 1990, 39(1): 42-45.
21. Johannes U.Herrmann and Sieteng Soh. A Memory Efficient Algorithm for Network Reliability. Proceedings of the 15th Asia-Pacific Conference on Communications (APCC 2009), Shanghai, China, 2009: 703-707.
22. Li Xiao, Nahrstedt.k. Reliability Models and Evaluation of Internal BGP Networks. INFOCOM 2004. Proceedings of the 23th Annual Joint Conference of the IEEE Computer and Communications Societies, Hong Kong, China, 2004: 1593-1604.
23. L. Xing. An Efficient Binary Decision Diagrams Based Approach for Network Reliability and Sensitivity Analysis. IEEE Transactions on Systems, Man, and Cybernetics, Part A: Systems and Humans, 2008, 38(1): 105-115.
24. M. O. Ball, C. J. Colbourn, J. S. Provan. Network Reliability. System Research Center, 1992.
25. Park Y J, Tanaka S. Reliability Evaluation of a Network with Delay. IEEE Trans. on Reliability, Vol. R-28, No. 4, 1979.
26. Peter James Schwaller, John Quillian Walker, Steven Thomas Joyce, Timothy Scott Huntley. Endpoint Node Systems Computer Program Products for Application Traffic Based Communications Network Performance Testing, U. S. Patent 6,061,725, May 9, 2000.
27. Qingyang Song, Jamalipour, A.. Network Selection in an Integrated Wireless LAN and UMTS Environment Using Mathematical Modeling and Computing Techniques. Wireless Communications, IEEE, 2005, 12(3): 42-48.
28. Rong-Hong Jan. Design of Reliable Networks. Computers & Operations Research, 1993, 20(1): 25-34.
29. Ruiying Li, Rui Kang, Ning Huang, Weiwei Chen, Yang Chen. A Practical Approach for Network Application Reliability Assessment. Eksploatacja i Niezawodnosc - Maintenance and Reliability, 2009, 43(4): 17-27.
30. Sawionek, B., Wojciechowski, J., Arabas, J.. Synthesis of Reliable Networks in the Presence of Line Failures. Circuits and Systems, 2000. Proceedings. ISCAS 2000 Geneva. The 2000 IEEE International Symposium, 2000: 649.
31. Siddhartha Dalal, Yu-Yun Ho, Ashish Jain, Allen McIntosh. Application Performance Assurance Using End-to-End User Level Monitoring. International Conference on Dependable Systems and Networks, 2002: 694-703.
32. Sy-Yen Kuo, Fu-Min Yeh and Hung-Yau Lin. Efficient and Exact Reliability Evaluation for Networks With Imperfect Vertices. IEEE Transactions on Reliability, 2007, 56(2): 288-300.
33. Tao Yu,Shanzhi Chen,Ming Ai. A Framework for Reliability Computation of the IP Network. Proceeding of the 8th ACIS International Conference on Software Engineering, Artificial Intelligence, Networking, and Parallel/Distributed Computing, Qingdao, China, 2007: 323-327.
34. Tatsuya Matsukwa, Hiroyuki Funakoshi. Analyzing Failure Frequency and Severity in Communication Networks, Reliability and Maintainability Symposium, San Jose, CA, 2010: 1-6.
35. Watanabe H, Kudo M, Kawanishi K, Yamasaki K. A Reliability Design Method for Private Networks. Reliability and Maintainability Symposium, 2003: 237-243.

Prof. Ning HUANG
Dong HOU
Yang CHEN
Prof. Rui KANG
School of Reliability and Systems Engineering
Beihang University, Beijing, P.R. China
e-mail: hn@buaa.edu.cn; houdong163@163.com
e-mail: chenyangjenny@126.com; kangrui@buaa.edu.cn

Dr. Liudong XING
Department of Electrical and Computer Engineering
University of Massachusetts, Dartmouth, MA 02747, USA
e-mail: lxing@umassd.edu

Rafał S. JURECKI
Tomasz L. STAŃCZYK

THE TEST METHODS AND THE REACTION TIME OF DRIVERS

METODY BADAŃ A CZAS REAKCJI KIEROWCÓW*

The paper presents issues related to determination of the driver's reaction time. A brief review of methods for determining the reaction time of drivers has been conducted. The results of own researches on the reaction time of drivers in pre-accident situations have been presented. The scenario of an accident situation according to which they were conducted has been presented. The presentation includes results of measurements of the reaction time set in the three test environments: on a test track, in a driving simulator and on the psychological aptitude test stand. A comparison of the obtained reaction time values has been conducted and the correlation between them has been determined.

***Keywords:** drivers' tests, the reaction time of drivers, test methods.*

W artykule przedstawiono zagadnienia związane z wyznaczaniem czasu reakcji kierowcy. Przeprowadzono krótki przegląd metod wyznaczania czasu reakcji kierowców. Zaprezentowano wyniki własnych badań dotyczących czasu reakcji kierowców w sytuacjach przedwypadkowych. Omówiono scenariusz sytuacji wypadkowej, według którego zostały one przeprowadzone. Przedstawiono wyniki pomiarów czasu reakcji wyznaczone w trzech środowiskach badawczych: na torze badawczym, w symulatorze jazdy samochodem oraz na stanowisku do badań psychotechnicznych. Dokonano porównania otrzymanych wartości czasu reakcji i wyznaczono korelacje pomiędzy nimi.

***Słowa kluczowe**: badania kierowców, czas reakcji kierowców, metody badań.*

1. Introduction

Motor vehicle accidents are inherent in traffic and are usually the result of many different reasons that occur in an emergency situation (including human error).

In different countries the risk to participate in road accidents is different, and differences between countries are quite significant. Therefore, periodic analysis of accidents are made for both quantitative and qualitative assessment of their causes [11, 14]. But in order to determine how a particular driver's performance could affect the course of a road accident, it is very often necessary reconstruct an accident in detail. For such reconstruction usually carried out using specialized computer programmes, it is necessary to use multiple parameters characterizing both a vehicle, a driver behaviour and environmental conditions. While the vehicle parameters and environmental conditions are relatively easy to determine, however in case of a driver it is generally difficult to estimate the rules. The action of the driver is dependent on many factors: fatigue, stress, experience in driving a motor vehicle, etc. One of the parameters characterizing driver's behaviour that is necessary for reconstruction is the reaction time. It is worth mentioning that the driver's reaction time is one of the basic parameters which have a very strong influence on the final outcome in the analysis of the course of the accident, and their recommended values are given in the manuals and training materials for court experts.

Depending on the value of a driver reaction time an expert takes for analysis of the accident may depend on the extent of any fault of a driver.

Most of literature report values of reaction time obtained in the tests on the so-called reaction on a simple stimulus (single beep or light) - in which a driver during the study is to react on one of the control elements of a car (brake pedal, handbrake lever, steering wheel). Examples of such studies are very well known and widely used until recently with the results of M. Burckhardt, and H. Burg [1]. In these studies, which were made on the actual way involved two cars driving behind each other. A test driver of a second car was to react to brake lights that light up of the car in front. A total of 41 persons have been examined in this way during these studies. During 1 hour (time for the test of 1 participant) was recorded about 100 reaction time values, which means that subsequent reactions of the driver followed on average every 40 seconds. Reaction time values determined by this method have been adopted by resolution of the symposium of the German forensic experts (20 Deutsche Verkehrsgerichtstag in Goslar, 1982 [4]) and have been widely used in Germany in the 80's and 90's. According to this recommendation, but also because of much more careful, than in other cases, a statistical processing of results carried out, they were widely regarded as one of the most correct and reliable. This is confirmed by the fact of their citation in the major publications of books on the dynamics of braking [2] or the reconstruction of road accidents [26].

A similar method of measurement Nishida [18] used in his study. The literature is full of other descriptions of test methods of drivers' reaction time to a single stimulus, such as the special ring tone [25], or a single light pulse of a stimulator, stuck on the windscreen [5, 15].

In real road situations (except driving in a column), the driver reacts to complex stimuli and the behaviour of the driver trying to avoid an accident involves both braking and (or) turning a steering wheel.

In the literature 10 - 15 years ago it is difficult to find data on the reaction time in which both the stimulus and the driver's reactions are complex. In many studies of reactions to complex

(*) Tekst artykułu w polskiej wersji językowej dostępny w elektronicznym wydaniu kwartalnika na stronie ***www.ein.org.pl***

stimuli carried out frequently simulated situations were highly simplified. For example, in papers [5, 16], tests of reactions to stimuli were the tests using the lights stuck on the windscreen of the car before the driver. The driver had to react both to a colour and light system, which have a manoeuvre assigned to them – for example weak or strong braking, turn left or turn right, etc.

In recent years, studies on the roads or tracks increasingly rely on the implementation of certain selected, recognized as representative, contract accident scenarios. Examples are the tests described in paper [17], in which on a track was simulated a perpendicular car intrusion to the crossroads. The authors of this work carried out a similar scenario in the tests described in [10, 22, 23]. Another example might be testing the driver's reaction to a small children's bike [15] pushed out (from behind a parked car in the right lane).

In studies aimed at introducing an assistant system, in the recent period, it became popular to use air-filled dummies made of a thick foil in the shape and dimensions of the vehicle [9, 20, 21] to support different research scenarios such as „sudden braking" 'sudden bypassing", etc.

In summary, it can be concluded that the number of this type of research available in the literature is small and covers only some specific cases. In addition to the lack of data for certain situations, other important drawbacks of the data obtained in this way are:

- their obsolete for the present population of drivers (grown-up and adjusted to the environment with a large variety of complex technical equipment);
- lack of data on high-risk groups, particularly young drivers aged 18 to 25 years (in this group, road accidents in the European Union countries, including Poland, are the main causes of death);
- their origin countries (e.g. Germany or the USA) with significantly differing levels of development of the motorization and the conditions under which it operates (the density and organization of traffic, condition of roads and markings, the share of motorways in the overall road network, the method of driver training, etc.).

In view of the above conclusions, the authors focused on one indicator of driver's performance, which is the reaction time and have decided to carry out research designed to extend knowledge in this field. They were to help find answers to questions about the possible correlation between drivers' reaction time obtained with different testing methods.

2. Test methods of drivers' reaction time

Despite years of research, yet has not been developed a method that most professionals in the field of accident reconstruction would be considered by far the best one for determining the reaction time of drivers. Generally, you can specify the following ways to implement this type of research:

1. Tests on psychological aptitude test stands for drivers (or similar).
2. Experiments on roads or testing tracks.
3. Research in driving simulators.
4. Study (observation types) in the actual road conditions.

The authors of this publication, in a study of driver behaviour in pre-accident situations determined drivers' reaction times in the first three research environments for the same group of 30 drivers.

2.1. Studies on simple testing stands

The study aimed to determine the reaction time of drivers conducted on simple stands historically have been used first. Currently, such tests can be encountered only occasionally but they are generally regarded as a complementary test. These studies, however, have been applied commonly by psychologists to evaluate its suitability for the profession of the driver, and many publications appear the values obtained in this way the reaction time.

In the studies that use this method by the authors the times of simple and complex reactions have been determined [10]. Determination of a simple reaction time was based on the driver's reaction to a single simple stimulus - light or sound. Driver's reaction was to press a key at the time of the appearance of a stimulus. The research of a complex reaction consisted in a specific type of stimulus - the light colour or sound, has been assigned with a specific manipulator on which the driver should press with a hand or foot

2.2. Experiments on roads or test tracks

Studies on roads or test tracks are recognized by majority of professionals as the best way to simulate traffic situations [16], to perform various vehicle dynamics studies [19], as well as determining the reaction time. Opportunity to reflect actual conditions of vehicle motion, the parameters of the road, as well as the ability to measure the reaction time in a real car are undeniable advantages of such studies. However, the value of results obtained in this way and their usefulness for the analysis of certain types of accidents, strongly depends on way the experiment is conducted. In recent years, the tests of the behaviour of drivers tests based on certain scenarios of accidents are performed on test tracks. These include generally a very specific road situation, and therefore the value of reaction time obtained in this way are also limited in their scope of use.

The study conducted by the authors, widely described in [10, 12, 22, 23] include a scenario in which on the track was simulated a perpendicular intrusion of car at the crossroads. Schematic test scenario is given in figure 1.

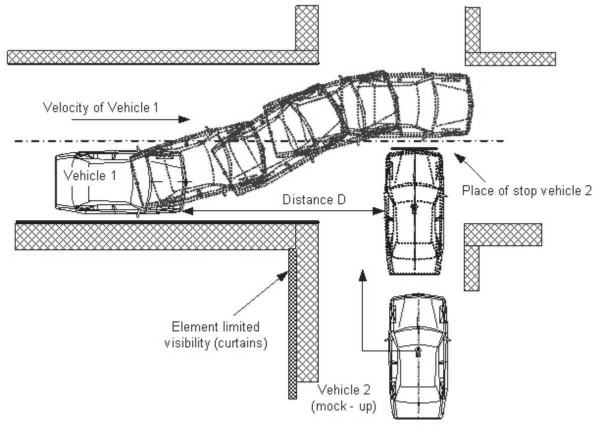

Fig. 1. Schematic scenario of an accident situation

The driver of the "Vehicle 1" moving at a speed V1 is forced to react to avoid collision with vehicle 2 which enters the crossroads without giving it priority – fig. 1. This scenario was based on observation of the actual situation at the crossroads located in Kielce (fig. 2).

Fig. 2. Real crossroads

Picture of the implementation of research conducted by the authors shown in fig. 3.

A detailed description of the tests carried out on the track is given in [12].

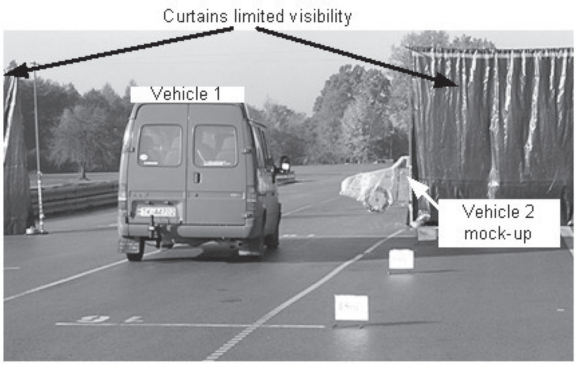

Fig. 3. Realisation of a scenario during research on a track

2.3. Research in driving simulators

The development of computer technology influenced significantly propagate research in simulators. Driving simulators are devices in which the driver directs the car using the same control elements, like in a real car (the accelerator pedal, brake, steering wheel), but the car traffic is implemented in a virtual environment [3]. Simulators can be divided into: dynamic simulators, which in addition to mapping the traffic situation on the big screen, inertial forces acting on the driver are mapped, for example during braking or in a curvilinear motion and static simulators in which these forces are not mapped.

One of the indisputable advantages of simulators is the possibility of an exact match to the environment and to perform such scenarios which implementation of the road conditions would be impossible or would involve danger. During the research carried out by the authors in the simulator [13] a selected, the same to tests on the track scenario has been realised (fig. 4).

Fig. 4. View of imitation the crossroads in the simulator

3. The analysis of the obtained values of reaction time

In this analysis, the influence of research methods on the reaction time values obtained are presented on the basis of authors' own research. The advantage of such a comparison is that during research an identical accident situation has been carried out (fig. 1). In order to obtain a high degree of surprise of drivers, the studies strongly reduced the visibility of the driver by installing curtains on the track, for example, in the simulator by mapping a high hedge and used so-called "empty runs" in which the obstacle does not appear. The same group of drivers was tested in various research environments. Were also consistent for the whole research of results' analysis.. A detailed description of these studies can be found in the works: [7, 8, 12].

Basic studies were carried out on Kielce Track and in the AutoPW driving simulator [10] at Warsaw University of Technology. The task of the drivers was aiming to avoid a collision with an obstacle, the driver himself decided whether only to brake or carry out only avoidance manoeuvre or perform both of these manoeuvres simultaneously. This feature, according to the authors, makes conditions similar to the real situation, in which the driver is not imposed on his behaviour. The results obtained have been confronted with the results of tests on a test psychological aptitude stand of drivers.

The analysis of research results used the concept of risk time. **Risk time** is defined as the time period allowed to the driver after noticing the obstacle to a possible collision with it. It is used by the driver for actions to avoid any accident or its consequences. Risk time used by the driver to perform defensive actions was calculated as the ratio of the car distance from the obstacle at the time of accident risk appearance (fig. 5) to its speed. This parameter, as shown by the analysis carried out in the work of authors [9, 24], is a very important parameter characterizing a pre-accident situation and driver behaviour. Tests were conducted for 15 different time values of risk time for three speeds 40, 50 and 60 km/h and five distances from an obstacle 10, 20, 30, 40, 50m.

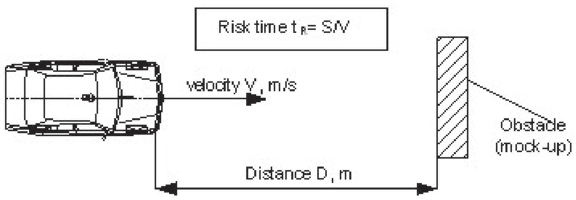

Fig. 5. Determination of risk time

Detailed results of the analysis of drivers' reaction time in the event of accident risk based on research carried out on Tor Kielce have been presented in the article [9].

In the present study the reaction times are as follows:

- mental reaction time, understood as the time since the appearance of an obstacle to the start of leg from the accelerator, hereinafter referred to briefly: "the accelerator pedal" reaction time;
- psycho-motor reaction time when braking, determined as the time from emergence of an obstacle to the onset of the brake pedal force, hereinafter referred to briefly: "brake" reaction time;
- psycho-motor reaction time during a turn, determined as the time from emergence of an obstacle to the onset reaction to the steering wheel, hereinafter referred to as: "turn" reaction time.

Dependence of reaction time for particular emergency braking manoeuvres, i.e., braking with a foot brake, engine braking and steering have been shown in fig. 6. For all the manoeuvres of the dependence of the risk time function is linear. The average reaction time value and standard deviation (value in parentheses) for selected values of risk time has been presented in table 1.

Similarly, the values of the reaction time of drivers during testing in the simulator have been determined. Graphical comparison of results has been shown in fig. 7. In the case of reaction time results obtained in the simulator, presented dependent on risk time, we can say that they also have a linear character. Examples of reaction time values obtained in the simulator are shown in table 2.

Psycho-technical research has been conducted on the same group of drivers. Each of the drivers was examined twice. Obtained results are presented in fig. 8. The average values of simple reaction time have been compared with the reaction time obtained during the experimental tests, both on the track and in the simulator.

Determination has been made of the R correlation coefficient of simple reaction time compared to the reaction time set for the turning manoeuvre and braking with a foot brake for all

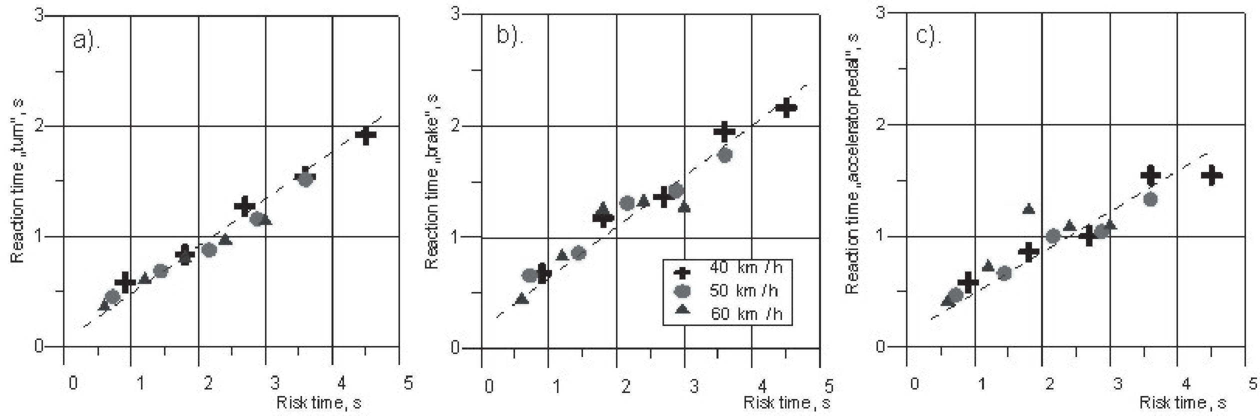

Fig. 6. The reaction time of drivers in the risk time function obtained during testing on the track; a) "turn" reaction time , b) "brake" reaction time , c) "accelerator pedal" reaction time

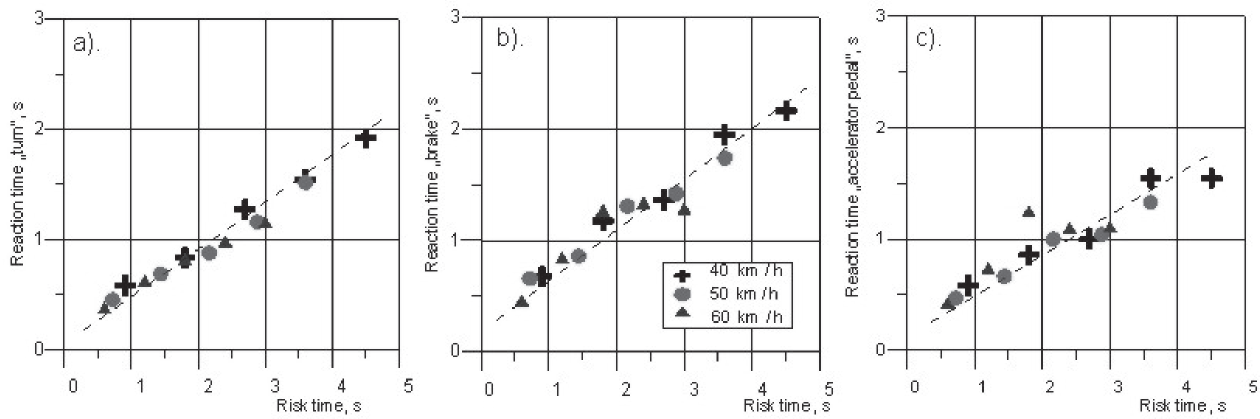

Fig. 7. The reaction time of drivers in risk time function obtained in a simulator a) „turn" reaction time, b) „brake" reaction time , c) „accelerator pedal" reaction time

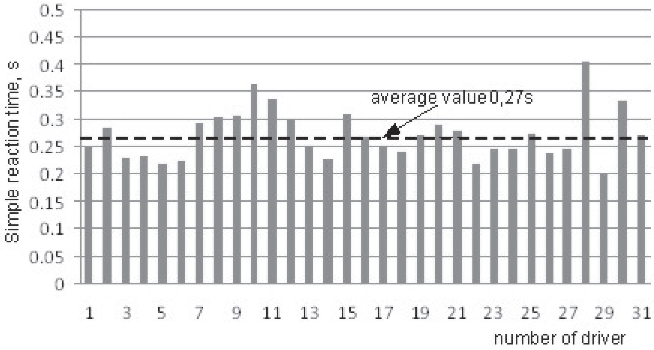

Fig. 8. Simple reaction time

Tab. 1. Summary of sample values of reaction time obtained on the track

Reaction time	Risk time, s				
	0,72	1,44	2,16	2,88	3,6
Mental "Accelerator pedal"	0,47 (0,10)	0,66 (0,16)	0,99 (0,15)	1,04 (0,37)	1,5 (0,56)
Psycho - motor performance during braking,„Brake"	0,65 (0,08)	0,85 (0,15)	1,31 (0,20)	1,42 (0,31)	1,85 (0,48)
Psycho - motor during a turn,„Turn"	0,45 (0,09)	0,68 (0,16)	0,87 (0,29)	1,15 (0,21)	1,54 (0,56)

Tab. 2. Summary of sample values of reaction time obtained in the simulator

Reaction time	Risk time, s				
	0,72	1,44	2,16	2,88	3,6
Mental "Accelerator pedal"	0,35 (0,19)	0,45 (0,11)	0,51 (0,17)	0,66 (0,19)	0,81 (0,36)
Psycho-motor performance during braking„Brake"	Brak reakcji	0,64 (0,15)	0,73 (0,18)	0,92 (0,33)	0,96 (0,22)
Psycho-motor during a turn,„Turn"	0,43 (0,06)	0,49 (0,13)	0,62 (0,21)	0,81 (0,39)	1,23 (0,58)

the samples (with different values of initial risk time). Correlation coefficients values for simple reaction time and reaction time - „brake" is shown in table 3 and for the simple reaction time and reaction time - „turn" (table 4). These correlations were determined for the results obtained on the track and in the simulator.

Obtained low and even negative correlation coefficient values indicate that there is no correlation between simple reaction time determined at the stand and the time determined in the research on track and in the simulator, both the turning reaction and braking.

The second study was to examine complex reaction time values. The results obtained are presented in fig. 9.

According to the authors there was a trial to determine the inter-relationship between the values of reaction time. Correlation coefficients were determined for the complex reaction time, and brake reaction time (table 5) and turning of wheels (table 6) obtained in studies on the track and in the simulator. In this case, also low or even negative correlation coefficient values have been obtained.

Tab. 3. The correlation coefficients between simple reaction time and the values of "brake" reaction time (time for different values of risk time)

Risk time, s		0,6	0,72	0,9	1,2	1,44	1,8	1,8	2,16	2,4	2,7	2,88	3,0	3,6	3,6	4,5
Truck	R	-0.124	-0.037	-0.348	-0.470	-0.141	0.446	-0.184	-0.034	-0.468	-0.620	-0.487	-0.395	-0.193	-0.461	-0.106
simulator		-	-	-	-0.104	-0.004	-0.085	-0.129	0.236	0.133	0.213	0.155	0.199	0.126	0.222	0.145

Tab. 4. The correlation coefficients between simple reaction time and values „turn" reaction time (for different values of risk time)

Risk time, s		0,6	0,72	0,9	1,2	1,44	1,8	1,8	2,16	2,4	2,7	2,88	3,0	3,6	3,6	4,5
Truck	R	0.277	-0.354	-0.017	-0.318	-0.307	-0.319	-0.092	-0.188	0.068	0.008	-0.014	0.120	-0.154	0.141	-0.200
simulator		-0.466	-0.771	-0.219	0.209	0.054	0.364	0.446	0.576	0.094	0.395	0.520	0.203	0.220	0.461	0.117

Tab. 5. The correlation coefficients between complex reaction time and the values "brake" reaction time (time for different values of risk time)

Risk time, s		0,6	0,72	0,9	1,2	1,44	1,8	1,8	2,16	2,4	2,7	2,88	3,0	3,6	3,6	4,5
Truck	R	0.324	-0.289	-0.163	-0.023	-0.074	0.192	-0.093	-0.050	0.007	-0.083	-0.180	-0.095	0.055	0.031	0.134
Simulator		-	-	-	0.062	0.145	-0.213	-0.204	-0.020	-0.034	-0.371	-0.148	0.066	0.075	-0.276	-0.118

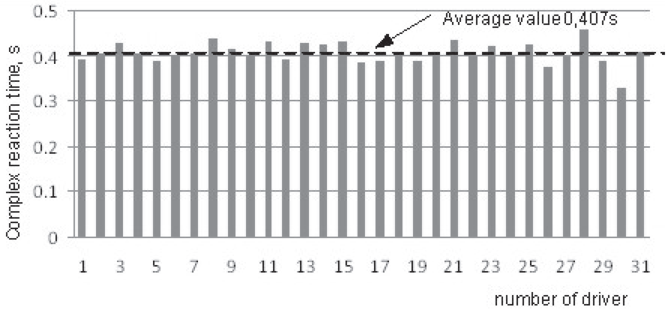

Fig. 9. Comparison of the complex reaction time

Tab. 6. The correlation coefficients between complex reaction time and values of „turn" reaction time (for different values of the time risk)

Risk time, s		0,6	0,72	0,9	1,2	1,44	1,8	1,8	2,16	2,4	2,7	2,88	3,0	3,6	3,6	4,5
Truck	**R**	0.128	0.030	0.001	-0.207	-0.311	-0.177	-0.027	-0.092	0.162	-0.085	-0.120	-0.220	-0.064	-0.049	-0.191
simulator		-0.304	-0.971	-0.144	0.133	0.211	0.302	0.077	0.158	-0.071	0.473	0.159	0.016	0.194	-0.176	-0.075

4. Conclusions

The values of the reaction time of drivers assigned to each set of manoeuvres on the track and in the simulator is characterized by a linear dependence of risk time. Both of these values are closely correlated. Through the results can be seen, however, that the reaction time of drivers obtained in the simulator for all tested manoeuvres achieves smaller values in relation to the measured values on the track.

The reason is that drivers are aware that they driver a car in a virtual environment, so even very violent manoeuvres are safe. You can "with impunity", without any consequences to perform rapid turns, leave off a road, drive through fences, gates, etc. During the test on the track the drivers act in a way not to lead to a dangerous situation of rapid overloading the car, the roll-over, etc.

The resulting accuracy has been also indicated in the literature [6]. The difference between the published opinions and the results in the present study lies in the fact that in the cited works a fixed value time difference obtained on the track and in the simulator has been given. According to [6] reaction times on the track are longer by 0.3 s for the brake and did not differ for the reaction with a turning. According to Mc Gehee and others [17] the reaction times on the track are longer by 0.1 seconds for the braking and 0.03 s with a turning. The research presented in this paper shows that this difference is not constant, but varies depending on the risk time characterizing of a given trial (see figure 10).

The obtained values of the measured reaction time as a psychological aptitude test stand have been compared with those obtained on the track and in the simulator (fig. 11). The figure contains lines corresponding to the simple and complex reaction times, even though it is a constant, not depending on risk time.

While analogizing graphs of fig. 10, we can say that simple and complex reaction time is significantly shorter than obtained for the same drivers during testing on the track or in the simulator. Only in the case of a determined reaction time for trials with very small values of risk time (0.5-1.0 s), they are similar. It is worth noting that only for "turn" reaction time, the difference in values between the track and simulator weakly depends on risk time, so it is close to a constant value. When we analyse "brake" and "accelerator pedal" reaction time, it then was can notice, that them the greater the risk time value, the greater the difference between the results obtained on the track and in the simulator.

When you present the obtained results of reaction time for each maneuver in a single graph (fig. 11), one can say that in the case of testing on the track, the reaction time for "accelerator" is less since the "turn" one. The highest values of reaction time have been obtained for "brake".

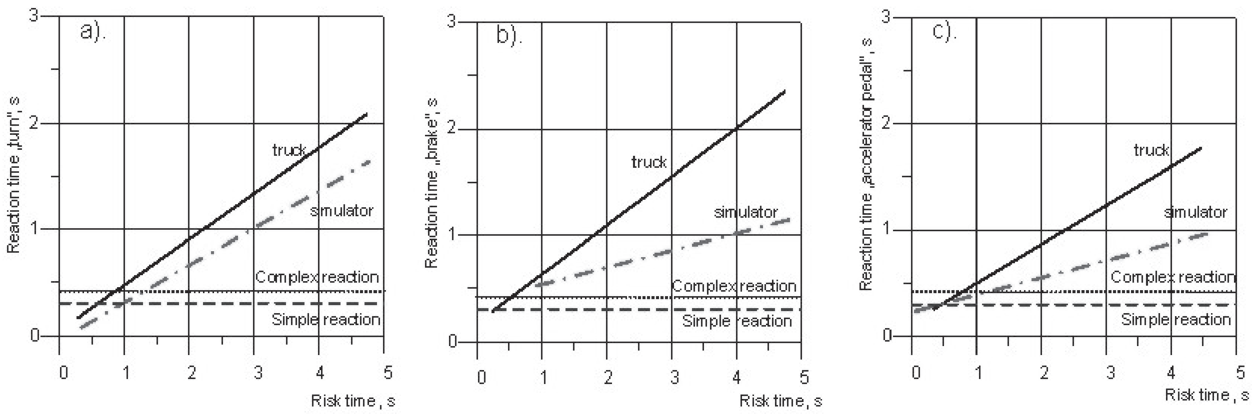

Fig. 10. Comparison of the time for considered manoeuvres: a) "turn" reaction time, b) "brake" reaction time , c) "accelerator pedal" reaction time

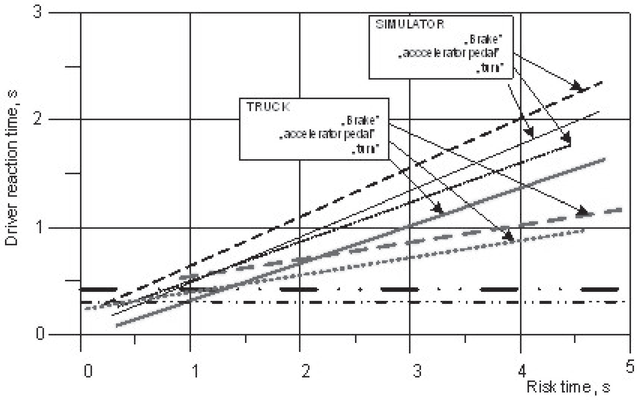

Fig. 11. Comparison of the reaction time

If the average reaction time of drivers in the simulator generated the lowest values have been determined for the "accelerator" reaction time and the highest for the "turn".

You need to be aware, however, that the above-mentioned behaviour of drivers, each sequence of manoeuvre has been determined for a particular scenario of a pre-accident situation. For other scenarios, the situation of the driver's mode of action may vary. Therefore, the authors in their attempt for further work is to determine the impact of different scenarios on obtained reaction time of drivers.

Determined correlation coefficients between "brake" and "turn" reaction time in relation to the simple and complex reaction time are very small, and in many cases even negative. In total, 120 studies conducted correlation only in 4 cases the absolute value of the correlation coefficient was greater than 0.5.

No correlation has been found with the results of the experiment on the track and the simulator shows that the reaction time obtained in studies on simple psychological stand can not be treated as the actual reaction time of drivers in traffic situations and can not be used in the reconstruction of road accidents.

This conclusion is very important because in some publications the reaction time determined in similar stands is taken as the actual reaction time of drivers in the analysis of the accident.

5. References

1. Burckhardt M, Burg H. Die Brems-Reaktionsdauer von Pkw-Fahrer. Der Ferkehrsunfall 1981; 12: 224-235.
2. Burckhardt M. Fahrwerktechnik: Bremsdynamik und Pkw-Bremsanlagen. Würzburg: Vogel Verl., 1991.
3. Chodnicki P, Guzek M, Lozia Z, Mackiewicz W, Stegienka I. Static autoPW driving simulator, version 2003. Zeszyty Naukowe Politechniki Świętokrzyskiej seria Mechanika, Kielce 2004; 79: 157-164.
4. Dannert G. Grundprobleme der Reaktionzeit des Kraftfahrers. Ferkehrsunfall und Fahrzeugtechnik 1998; 12: 328-334.
5. Fröming R. Assesment of Integrated Pedestrian Protection System. PhD thesis. Fortschritt-Berichte VDI. Reihe 12. Verkehrstechnik/Fahrzeugtechnik 2008; 681.
6. Green M. How long does it take to stop? Methodological analysis of driver perception-brake times. Transportation Human Factors 2000; 2(3): 195-216.
7. Guzek M, Jurecki R, Lozia Z, Stańczyk T. L. Comparative analyses of driver behaviour on the track and in virtual environment. Driving Simulation Conference Europe DSC 2006 Europe, Paris 2006: 221-232.
8. Hillenbrand J. Fahrerassistenz zur Kollisionsvermeidung. PhD thesis. Fortschritt-Berichte VDI, Reihe 12, Verkehrstechnik/Fahrzeugtechnik 2008; 669.
9. Jansson J, Johansson J, Gustafsson F. Decision Making for collision avoidance systems. SAE Paper 2002-01-0403.
10. Jurecki R.S. Modelowanie zachowania kierowcy w sytuacjach przedwypadkowych.. Rozprawa doktorska. Modeling driver behavior in pre-crashes situations. Doctoral dissertation. Politechnika Świętokrzyska, Wydział Mechatroniki i Budowy Maszyn, Kielce, 2005.
11. Jurecki R. Wypadki drogowe w Polsce, skutki i przyczyny. Road accidents in Poland, the consequences and causes. III Konferencja naukowo- Techniczna "Problemy bezpieczeństwa w pojazdach samochodowych". Wydawnictwo Politechniki Świętokrzyskiej. Zeszyty Naukowe Politechniki Świętokrzyskiej seria Mechanika 2002; 79: 223-232.
12. Jurecki R, Stańczyk T.L. Driver model for the analysis of pre-accident situations. Vehicle System Dynamics 2009; 47 (5): 589-612.
13. Jurecki R. S, Stańczyk T. L, Lozia Z. Badania manewru omijania pojawiającej się przeszkody w warunkach badań na torze oraz w symulatorze jazdy. Zeszyty Naukowe Instytutu Pojazdów Politechniki Warszawskiej, Warszawa 2005; 1(56): 65-78.
14. Kisilowski J, Zalewski J. Wybrane problemy analizy przyczyn wypadków drogowych w Polsce w latach 1995-2004. Eksploatacja i Niezawodnosc - Maintenance and Reliability 2008; 1: 37-43.
15. Krause R, de Vries N, Friebel W.-Ch. Mensch und Bremse in Notbremssituationen mit Pkw – neue Erkenntnise zu Prozesszeiten beim Bremsen. Teil 1. Ferkehrsunfall und Fahrzeugtechnik 2007; 6: 164-171.
16. Magister T, Krulec R, Batista M, Bogdanović L. The driver reaction time measurement experiences. Innovative Automotive Technology – IAT'05. Bled, 21^{st}-22^{nd} April 2005.

17. McGehee D.V, Mazzae E.N, Baldwin G.H.S. Driver reaction time in crash avoidance research: validation of a driving simulator study on a test track. Proceedings of the 14th Triennial Congress of the International Ergonomics Association and the 44th Annual Meeting of the Human Factors and Ergonomics Society (IEA 2000). San Diego/USA 2000; 6.
18. Nishida Y. Driving characteristics of the elderly: risk compensation of the elderly driver from the viewpoint of reaction behavior. JSAE Review 1999; 20: 375-380.
19. Parczewski K. Wnęk H. Wykorzystanie modelu samochodu do analizy ruchu pojazdu po torze krzywoliniowym. Eksploatacja i Niezawodnosc - Maintenance and Reliability 2010; 4: 37-46.
20. Schorn M. Quer-und Längsregelung eines Personenkraftwagens für ein Fahrerassistenzsystem zur Unfallvermeidung. PhD thesis. Fortschritt-Berichte VDI, Reihe 12, Verkehrstechnik/Fahrzeugtechnik 2007; 651.
21. Stählin U. Eingriffsentscheidung für ein Fahrerassistenzsystem zur Unfallvermeidung. PhD thesis. Fortschritt-Berichte VDI. Reihe 12. Verkehrstechnik/Fahrzeugtechnik 2008; 683.
22. Stańczyk T. L, Jurecki R. Czasy reakcji kierowców w stanach zagrożenia wypadkowego. Materiały III Konferencji "Rozwój techniki samochodowej a ubezpieczenia komunikacyjne" Radom, 2006. Wyd. WSB im. J. Chrapka: 321-348.
23. Stańczyk T. L, Jurecki R. Fahrereaktionszeiten in Unfallrisikosituationen – neue Fahrbahn- und Fahrsimulatorversuche. Verkehrsunfall und Fahrzeugtechnik 2008; 07-08: 235 – 246.
24. Stańczyk T., Jurecki R. O przyczynach różnic w publikowanych wartościach czasów reakcji kierowców. Materiały X Konferencji „Problemy rekonstrukcji wypadków drogowych". Kraków – Szczyrk 2006. Kraków: Wydawnictwo Instytutu Ekspertyz Sądowych: 157-171.
25. Törnros J. Effect of driving speed on reaction time during motorway driving. Accident Analysis and Prevention 1995; 27 (4): 435-442.
26. Wypadki drogowe. Vademecum biegłego sądowego. Pr. zbiorowa. Kraków: Wyd. IES, 2002.

Dr inż. Rafał S. JURECKI
Dr hab. inż. Tomasz L. STAŃCZYK prof. PŚK
Department of Motor Vehicles and Transport
Kielce University of Technology
Faculty of Mechatronics and Mechanical Engineering
7 Aleja Tysiąclecia Państwa Polskiego, 25-143 Kielce, Poland
e-mail: rjurecki@tu.kielce.pl
e-mail: stanczyk@tu.kielce.pl

MANUFUTURE 2011 CONFERENCE WITH MEDIA PATRONAGE OF EKSPLOATACJA I NIEZAWODNOŚĆ - MAINTENANCE AND RELIABILITY

www.manufuture2011.eu

Within the second half of the year 2011 Poland will take over the Presidency of the EU Council. One of the event which is planned to be organized in Poland during that time is Manufuture 2011 conference on **24-25 October 2011 in Wroclaw**.

For the first time the Manufuture conference will be organized in the country, which is placed in Central Europe and is recognized as a new EU member state. It offers a unique opportunity to present the potential of this EU region in manufacturing research, as well as to invoke discussion on the future of product development and manufacturing in view of unique internal market with an idea of elimination exclusion zones.

The main objective of the conference is to present the vision of future manufacturing and its role in further growth of Europe - building smarter, greener and more competitive European industry based on partnership between EU, EECA region, Balkan countries and Turkey.

The conference is organized under the auspices of European Commission and Polish Presidency of the EU Council 2011, with local academic and governmental institutions.

At the Manufuture 2011 conference the following main areas will be discussed:

- Cooperation West-East Europe in global manufacturing
- Cooperation and partnership of EU member states with Balkan countries as well as EECA region and Turkey
- Cooperation between old and new EU member states
- Current stage of research and innovations in advanced manufacturing
- SMEs in transforming European economies
- Public engagement activities
- Effective models of academia-research-industry cooperation
- Industrial education.

Manufuture 2011 conference is organized in coherence with Fumat 2011 conference (www.fumat2011.eu) and has received funding from the European Union's Seventh Framework Programme. It will be forum of exchanging views, ideas and opinions on further development of industrial manufacturing in Europe. Engagement of crucial decision makers, representatives of industrial organizations, academic area and social organizations will assure a significant role on European and national field.

Conference will be accompanied with **a wide range of activities towards youth and young people**, including primary school and secondary school pupils. In the frame of those activities cooperation with Festival of Science is considered. During the Festival the NMP theme would be agitated and all could consist of at least 10 thematic lectures with 200 pupils and students. The action **'NMP for school'** requires at least 20 parallel meetings at schools, accompanied with a media campaign.

Wroclaw city and Manufuture 2011 conference venue

Wroclaw is the main academic and industrial **centre of the Lower Silesia Region and one of the most important in Poland**. It is the fourth largest city in the country and the largest one in the west side of the country. Wroclaw is inhabited by over 630 000 citizens and offers place for incubating companies through establishing Wroclaw Technology Park, Wroclaw Industrial Park and Lower Silesian Innovation and Science Park.

Manufuture 2011 conference will take place in perfectly located **The Regional Center for Business Tourism**. This center is a new high capacity meeting facility being developed at the complex one of the finest and interesting building in Wroclaw, inscribed on the World Heritage List of UNESCO - **the Centennial Hall**. The Regional Center for Business Tourism offers flexible meeting spaces of the highest quality.

INFORMATION FOR AUTHORS

Terms and Conditions of Publication:

- The quarterly „Maintenance and Reliability" publishes original papers written in Polish with an English translation.
- Translation into English is done by the Authors after they have received information from the Editorial Office about the outcome of the review process and have introduced the necessary modifications in accordance with the suggestions of the referees!
- Acceptance of papers for publication is based on two independent reviews commissioned by the Editor.

Fees:

- Pursuant to a resolution of the Board of PNTTE, as of 2009 the publication fee for one text is 600 zloty + VAT.
- Coloured graphical elements in the submitted text require agreement from the Editor and are charged extra.

Technical requirements:

- After receiving positive reviews and after acceptance of the paper for publication, the text must be submitted in a Microsoft Word document format.
- Drawings and photos should be additionally submitted in the form of graphical files in the *.tif, *.jpg or *.cdr (v. X3) formats.
- A manuscript should include (in accordance with the enclosed correct manuscript format: *.pdf, *.doc):
- names of authors, title, abstract, and key words that should complement the title and abstract (in Polish and in English)
- the text in Polish and in English with a clear division into sections (please, do not divide words in the text);
- tables, drawings, graphs, and photos included in the text should have descriptive two-language captions,
- if this can be avoided, no formulae and symbols should be inserted into text paragraphs by means of a formula editor
- references (written in accordance with the required reference format)
- author data – first names and surnames along with scientific titles, affiliation, address, phone number, fax, and e-mail address
- The Editor reserves the right to abridge and adjust the manuscripts.
- All submissions should be accompanied by a submission form.

Editor contact info: (Submissions should be sent to the Editor's address)

Editorial Office of „Eksploatacja i Niezawodność - Maintenance and Reliability"
Nadbystrzycka 36, 20-618 Lublin, Poland
e-mail: office@ein.org.pl

INFORMATION FOR SUBSCRIBERS

Fees

Yearly subscription fee (four issues) is 100 zloty and includes delivery costs.
Subscribers receive any additional special issues published during their year of subscription free of charge.

Orders

Subscription orders along with authorization to issue a VAT invoice without receiver's signature should be sent to the Editor's address.

Note

In accordance with the requirements of citation databases, proper citation of publications appearing in our Quarterly should include the full name of the journal in Polish and English without Polish diacritical marks, i.e.,

Eksploatacja i Niezawodnosc – Maintenance and Reliability.

Wydawca:

Polskie Naukowo-Techniczne Towarzystwo Eksploatacyjne
(Warszawa)

Publisher:

Polish Maintenance Society
(Warsaw)

członek:

Europejskiej Federacji Narodowych Towarzystw Eksploatacyjnych

member of:

European Federation of National Maintenance Societies

patronat naukowy:

Polska Akademia Nauk Oddział Lublin

scientific supervision:

Polish Academy of Sciences Branch in Lublin